Physico-Chemical Characterisation and Functionality of the Polysaccharide Extracted from the New Zealand Black Tree Fern, *Cyathea medullaris* (Mamaku)

A thesis presented in partial fulfilment of the requirements for the degree of

Doctor of Philosophy

in

Food Technology

At Massey University, Palmerston North, New Zealand

May Wee Sui Mei

2015

Preface

What do the New Zealand black tree fern and the Russian Matroyshka doll have in common?

The Matroyshka doll is a doll in a doll in a doll. And the tree fern? It is but a fern in a fern in a fern. The fronds make up the fern tree, which is made up of smaller frond representations called the primary pinna, which is made of up the secondary pinna, which is, (you guessed it) made of up the tertiary pinna. Looking at the tertiary pinna is no different from looking at the secondary, or the primary pinna. In other words, the fern is constructed of self-similar shapes. The figure below is an actual tertiary pinna of the black tree fern scanned as an image. It looks just like an entire fern leaf blade doesn't it?

This self-similarity or macrocosmic characteristic of nature is seemingly random and sometimes oblivious to the human mind trained by classical geometry. To Benoit Mandelbrot, the recursive nature of the tree fern is what he came to describe as ***fractals*** *in 1977. Fractals are a family of shapes, characterised by irregularities and self-similarity which are still statistical in nature. Triangles, squares and circles are shapes, as much as flowers, snowflakes, clouds, waves and even Brownian motion can be.*

Keeping in mind that fractals are the underlying fundamentals of nature can prepare us to recognise the order within the disorder, and not be bound by current knowledge. For every researcher dealing with nature, there is always one thing to remember: God might not play dice, but it will most certainly play hide-and-seek. It is now for us to embark on a journey to seek out what wonders might lie within the polysaccharide extracted from the New Zealand black tree fern in this thesis.

May 2014

“I don’t know what I’m looking for.”

“Why not?”

“Because … because … I think it might be because if I knew
I wouldn’t be able to look for them.”

- Douglas Adams, Hitchhiker’s Guide to the Galaxy

Abstract

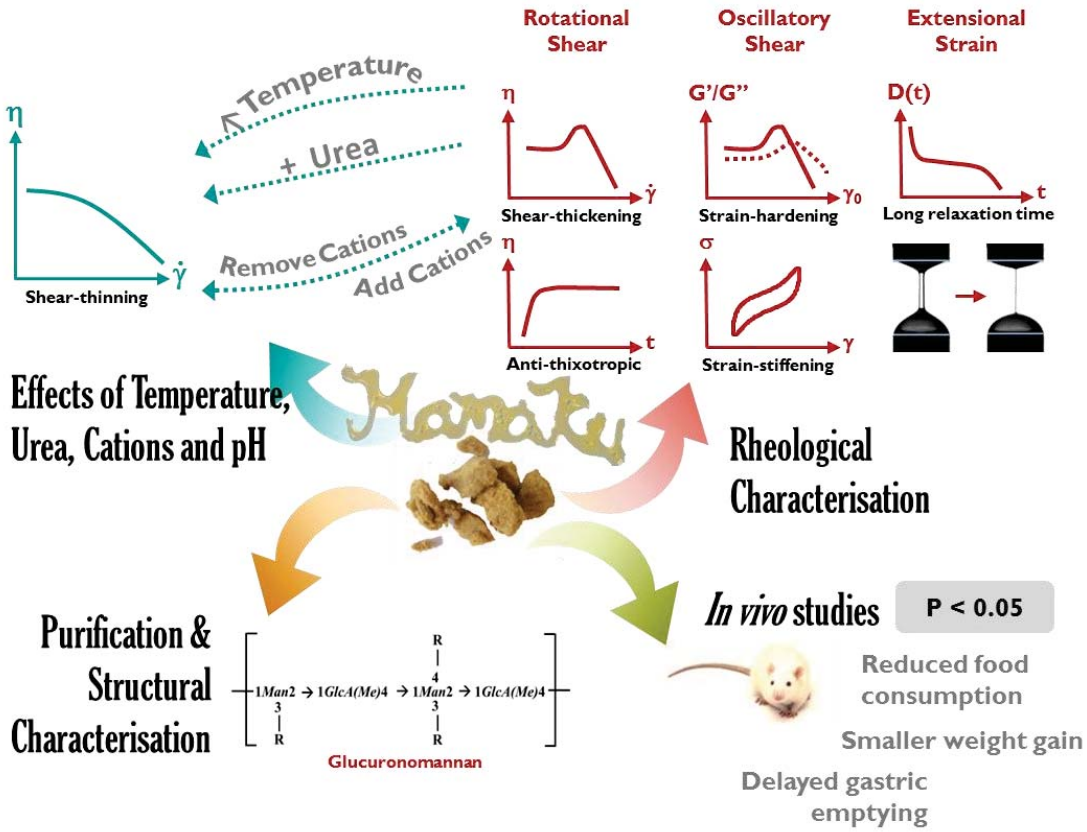

The aim of this thesis was to characterise the polysaccharide extracted from the New Zealand black tree fern, *Cyathea medullaris*, or mamaku in Māori using a combination of rheological, structural and *in vivo* research techniques. Polysaccharides are biopolymers with diverse functionalities that have found their way into many applications in the food, cosmetic or pharmaceutical industries. Novel sources of polysaccharides may have promising functional properties for new or existing applications, therefore it is essential to have fundamental knowledge of their properties. The native and endemic New Zealand black tree fern produces mucilage (containing the polysaccharide) which is extracted from the thick fleshy stem pith of the frond.

Rheological properties of the polysaccharide were characterised using rotational shear, oscillatory shear, and extensional rheology. The combination of these techniques provided information on how the polysaccharide deformed under shear, strain and extension. Rotational shear was further classified into tests for shear-dependent viscosity/normal stresses, time-dependent viscosity, and shear-history dependent viscosity. The polysaccharide (5% w/w) exhibited shear-thickening (4-10s^{-1}), positive first normal stress differences coinciding with shear-thickening, anti-thixotropy (under constant shear with time at shear rates between 4-10s^{-1}), and thixotropy (at 1s^{-1}, pre-sheared at 10s^{-1}) or rheopexy (at 10s^{-1}, pre-sheared at 1000s^{-1}) depending on shear-history. Oscillatory shear was classified into linear and nonlinear rheology, *i.e.* small amplitude (SAOS) and large amplitude oscillatory shear (LAOS) respectively. Under linear strain deformation, the polysaccharide displayed viscoelasticity and a power-law dependence on concentration for relaxation time ($\lambda_s \sim c^{3.6}$). Complex viscosity did not superimpose on shear viscosity at higher shear rates/angular frequency (nonlinear region),

therefore not complying with the Cox-Merz rule. The LAOS response in the nonlinear region was characterised by new large-strain and minimum-strain moduli parameters (G'_L and G'_M), as well as the traditional first-harmonic storage modulus G'. The polysaccharide (10% w/w mamaku) was found to exhibit first a linear viscoelastic region (0.1-20% γ_0), followed by strain-softening (20-800% γ_0), then strain hardening (800-2000% γ_0) and finally a second strain-softening region due to viscous flow (>2000% γ_0) for all three elastic moduli measurements. Closer examination of Lissajous plots in the intercycle strain-hardening region revealed deviation from ellipsoidality *i.e.* sigmoidal shapes, which were representative of intracycle strain-stiffening. Finally, the evolution of filament diameter with time and extensional relaxation time were characterised using a capillary breakup extensional rheometer (CaBER). The polysaccharide exhibited long extensional relaxation times (4.6s), high extensional viscosities (~10^4) and large Trouton ratios (~10^4).

Factors *i.e.* temperature, urea concentration, cations (ionic strength) and pH were tested to investigate how changes in the environment would affect the rheological properties of the polysaccharide. These factors are also intrinsically related to intermolecular interactions which may be present in the polysaccharide e.g. hydrogen bonding, hydrophobic interaction and electrostatic attractions. Thus the molecular origin of its rheological behaviour could also be elucidated through these effects. Shear-thickening was lost at higher temperatures (≥50°C) but enhanced at low temperatures. The peak viscosity during shear-thickening exhibited an Arrhenius' Law dependency with an activation energy of flow of ~90 kJ/mol (5% w/w). Hydrogen bonds are sensitive to temperature and inversely proportion to temperature in the order of kT, which indicated that hydrogen bonds are likely to be involved in shear-thickening of the polysaccharide. The addition of urea, a hydrogen-bond disruptor (chaotropic agent) suppressed shear-thickening completely in 5% w/w mamaku solution at a concentration of 5M. Urea molecules compete for hydrogen bonding sites with the polysaccharide and lower the lifetime of polymer-polymer associations. Removal of salts from the native mamaku solution via dialysis resulted in loss of shear-thickening as well. However, shear-thickening was reinstated upon addition of salts (NaCl, KCl, $N(CH_3)_4Cl$, $CaCl_2$, $MgCl_2$, $LaCl_3{\cdot}7H_2O$, $AlCl_3{\cdot}6H_2O$) back. Mono-, di- and trivalent cations screen the electrostatic charges on the polysaccharide thus lowering the viscosity as the polysaccharide adopts a more compact configuration. In addition, trivalent cations also cause chain collapse (precipitation) and re-dissolution of the polysaccharide, a phenomenon known as re-entrant condensation in polyelectrolytes. Lastly, shear-thickening was also recovered in the dialysed extract at pH 2-4. Similarly, the protons (H^+) screen the electrostatic charges which lowered the viscosity of the polysaccharide. Screening of electrostatic repulsion appeared to promote shear-thickening rather than ionic cross-linking, since monovalent cations and protons were able to recover shear-thickening.

Chemical structure is an important identity for any polysaccharide. In addition, the chemical structure can provide insight as to how the polysaccharide may have participated in shear-thickening. The native mamaku extract was further purified prior to structural characterisation via ultracentrifugation, starch hydrolysis, de-proteinisation and ethanol (80% w/v) precipitation. This method of purification yielded approximately 15% of purified material, removing most of the starch, minerals and simple sugars from the native extract. The purified fraction retained its shear-thickening character and had a molecular weight of 1.94 x 10^6 Da. Structural characterisation determining monosaccharide composition and glycosyl linkages were carried out using methylation, HPLC/GC, GC-MS and NMR techniques. The structure of the mamaku polysaccharide was

suggested to be a glucuronomannan backbone (methylesterified 4-Glc*p*A (27.9 mol%) with 2,3- (9.2 mol%) and 2,3,4-linked Man*p* (10.9 mol%)) with branched sugar side-chains of galactose, arabinose, xylose, non-methylesterified glucuronic acid (8.2 mol%) and other simple sugars at the O-3 and O-4 of the mannose residues.

Piecing the information obtained from the various characterisation techniques together helped to elucidate the molecular origin of shear-thickening, anti-thixotropy, strain-hardening and extensional-hardening. They were postulated to be of the same event, *i.e.* intra- to intermolecular association between polysaccharide chains during shear, strain or extension via hydrogen bonding. Stretching the polysaccharide exposed associative groups within the long chain, which interacted in a cooperative zip-like manner. The hydrogen bonds were suggested to take place via the hydroxyl (-OH) groups of mannose or carbonyl/carboxyl groups (-C=O/-COOH) of the glucuronic acids.

Finally, the satiety effects of the mamaku gum were tested *in vivo* in rats. The functional ability of the polysaccharide to confer satiety was postulated to arise from its high viscosity as well as its shear-thickening behaviour, which alters gastric antrocorporal contractions and delays gastric emptying. Oral gavage of the rats with mamaku gum (15% w/w) showed a significant reduction in short term food consumption ($p<0.05$), smaller weight gains ($p<0.05$), as well as prolonged gastric emptying ($p<0.05$) as compared to rats gavaged with water. Therefore the polysaccharide could potentially be used as a satiety aid in food products.

Biopolymers which exhibit such complex rheological properties that can be easily controlled by manipulating environmental factors are rarely or never before encountered. Clearly, the mamaku polysaccharide would find its way into novel applications, starting with satiety enhancers.

Acknowledgements

A big, big thank you and a hug to my chief supervisor, Lara, (who cringes when called Dr. Lara Matia-Merino), for her mentorship, her guidance, her support and encouragement when skies are gloomy, and for keeping me in shape with BodyStep classes (one will be surprised at the number of cookies and cups of coffee one consumes while doing a PhD). I am very lucky to have her as a supervisor! The acknowledgements page does not do enough justice to my gratitude towards her, perhaps the only supervisor who would accompany a student on a trip to the dentist.

Another ~~gargantuan~~ big ('use simple English!', as he always says) thank you to my co-supervisor, Kelvin Goh, for being my mentor for the last six years ever since I was an undergraduate student. For all the constructive criticisms sandwiched between compliments, for the patience with putting up my occasional defiance, and for encouraging me to take up a PhD in the first place. Likewise, this acknowledgements page does not do enough justice to my gratitude towards him. I will be showing up in his office with an hour long speech one of these days (… did I just hear him groan 'oh no..' again?).

I would also like to thank Massey University for financially supporting me with the Massey University Doctoral Scholarship and Universities New Zealand for awarding me with the Claude McCarthy Fellowship which made my trip to MIT possible.

Thank You To my favourite lab managers who have been like friends to me, for coming to my rescue when I land myself in yet another mess, and for forgiving when my experiments start growing mould in their labs: Garry Radford, Warwick Johnson (Papa Warwick), Michelle Tamehana, Chris Hall (Edwardo) and Janiene (Flossy).

Thank You To all Massey staff who has provided so much help in the laboratories, technical issues, administrative work and the occasional chit-chat: Steve Glasgow, Julia Good, John Edwards, Michelle McGrath, Richard Haverkamp, Graham Freeman, Mark Waterland, Shane Telfer, Fliss Jackson, Gary Mack, Pat Edwards, Matt Levin, Peter Jeffery, Yvonne Parkes, Denise Mist and Eteta Trueman.

Thank You To the carbohydrate chemistry team at Industrial Research Limited (IRL) for accommodating me at your laboratory, and guiding me through the highly complicated structural analysis work in 2011 and 2012: Ian Sims, Susie Carnachan and Tracy Bell.

Thank You To the Hatsopoulos Microfluidics Laboratory team at Massachusetts Institute of Technology for inspiring me with so much more than just rheology, for opening my eyes to a world and culture I never thought I would be part of. I would like to express my sincerest thanks to Gareth McKinley for collaborating with us and his warm hospitality during my stay in Boston, to Aditya Jaishankar for being such an amazing friend who constantly fascinates me with fractals and philosophy, and the rest of the HML group Sean Buhrmester, Bavand Keshavarz, Chris Dimitriou, Divya Panchanathan, Thomas Ober, Kenneth Park, Setareh Shahsavari, and Michelle.

Thank You To the rat studies team for supporting and encouraging me in spite of all the adversities faced during execution of the trial: Roger Lentle, Kim Wylie, Anne Broomfield, Corrin Hulls, Aimee Hamlin, Juliet Cayzer, and to the animal ethics committee for approving the research.

Thank You To all Massey University lecturers for their guidance, most of whom since my undergraduate days: Alistair Carr, Allan Hardacre, Brian Wilkinson, Heather McClean, Janet Weber, Jason Hindmarsh, Matt Golding, Nigel Grigg, Owen McCarthy, Richard Archer, Richard Love, Steve Flint, Michael Parker and Tuoc Trinh.

Thank You To all my friends, office mates and flatmates who contributed to what used to be a non-existential social life: Ivana (Commando Sequeira), Hayley (Bro), Jeremy (Chest Hair), Yen, Visaka, Lakshmi, Mehak, Khaizura, Bob (Boobies), Naila, Shazla, Irene, Esther, Sandra, Chalida, Ian, Jerry, Melody, Samantha, Pamela, Matthew, Anges (High Class), Wensheng, Siang Wee, Anne, Bryan, Evgeniy (Geniy), Li Mo (Momo), Grace (Ahbuji), Faith (Ah ma), Justin, Soffalina, Daisy, Seng Guan, Jordon, Anynda (Amoeba), Tian Wen, Ling Li, Qing Ping, Sheryl, Celia, Eileen, Massey University Singapore graduates and Singapore Polytechnic internship students of years 2011-2014 who were here in Palmy.

And finally,

Thank You to my family, to God, to the universe, to the rheometer for going through shear-thickening and shear-thinning with me (it was *shear* torture!), and to life, for all the bitter-sweetness so that I shall have stories to tell

Table of Contents

PREFACE ..... **III**

ABSTRACT ..... **VII**

ACKNOWLEDGEMENTS ..... **XI**

TABLE OF CONTENTS ..... **XIII**

LIST OF FIGURES ..... **XIX**

LIST OF TABLES ..... **XXVII**

LIST OF PUBLICATIONS ..... **XXIX**

CHAPTER 1 INTRODUCTION **1**

CHAPTER 2 LITERATURE REVIEW **3**

2.1 Polysaccharides 3

2.1.1 Plant Polysaccharides 4

2.2 Structural Properties of Polysaccharides 9

2.2.1 Monosaccharides 10

2.2.2 Glycosidic Linkages 11

2.2.3 Conformation 12

2.3 Physical and Molecular Properties of Polysaccharides 13

2.3.1 Molecular Weight and Distribution 13

2.3.2 Intrinsic Viscosity 14

2.3.3 Solubility 15

2.3.4 Concentration 15

2.4 Rheological Properties of Polysaccharides 16

2.4.1 Shear-dependent Viscosity 16

2.4.2 Viscoelasticity 18

2.4.3 Extensional Viscosity 19
2.5 Shear-Thickening Rheology 21
2.5.1 Associative Polymers 22
2.5.2 Shear-Thickening Mechanisms 22
2.6 Intermolecular Interactions in Polysaccharides 26
2.6.1 Hydrogen Bonds 26
2.6.2 Hydrophobic Interactions 27
2.6.3 Electrostatic Attractions 27
2.7 Applications of Polysaccharides 28
2.7.1 Satiety Effects of Polysaccharides 29

CHAPTER 3 EXPERIMENTAL TECHNIQUES 33
3.1 Mamaku Gum Extraction 33
3.2 Rheological Characterisation 34
3.2.1 Rotational Shear Rheology 34
3.2.2 Small Amplitude Oscillatory Shear Rheology 41
3.2.3 Large Amplitude Oscillatory Shear Rheology 43
3.2.4 Extensional Rheology 47
3.3 Structural Characterisation 50
3.3.1 Monosaccharide Composition 50
3.3.2 Linkage Analysis 51
3.3.3 Nuclear Magnetic Resonance (NMR) 52
3.4 Animal Studies 53
3.4.1 Rats 53
3.4.2 Oral Gavage 54
3.4.3 Statistical Analysis 55

CHAPTER 4 RHEOLOGICAL CHARACTERISATION OF MAMAKU POLYSACCHARIDE 57
4.1 Introduction 57
4.2 Materials and Methods 58
4.2.1 Rotational Shear Rheology 58

4.2.2 Oscillatory Shear Rheology 58
4.2.3 Extensional Rheology (CaBER) 59
4.3 Results and Discussion 60
4.3.1 Shear-Dependent Rotational Shear Rheology 60
4.3.2 Time-Dependent Rotational Shear Rheology 61
4.3.3 Small Amplitude Oscillatory Shear Rheology 69
4.3.4 Large Amplitude Oscillatory Shear Rheology 71
4.3.5 Extensional Rheology 80
4.4 Conclusion 86

CHAPTER 5 EFFECTS OF TEMPERATURE, UREA, IONIC STRENGTH AND PH 87
5.1 Introduction 87
5.2 Materials and Methods 89
5.2.1 Sample Preparation 89
5.2.2 Rheological Measurements 90
5.2.3 Relative Viscosity 91
5.2.4 Zeta-Potential 91
5.2.5 Mineral Analysis 91
5.3 Results and Discussion 92
5.3.1 Effect of Temperature 92
5.3.2 Effect of Urea 98
5.3.3 Effect of Ionic Strength 102
5.3.4 Effect of pH 114
5.3.5 Overall Discussion 115
5.4 Conclusion 116

CHAPTER 6 PURIFICATION AND STRUCTURAL CHARACTERISATION OF MAMAKU POLYSACCHARIDE 117
6.1 Introduction 117
6.2 Materials and Methods 119
6.2.1 Purification 119
6.2.2 Chemical Analysis 121

6.2.3 Structural Analysis 123
6.2.4 Size-Exclusion Chromatography-Multi-Angle Laser Light Scattering (SEC-MALLS) 126
6.2.5 Rheological Measurements 127
6.3 Results and Discussion 128
6.3.1 Purification 128
6.3.2 Composition Analysis 134
6.3.3 Size-Exclusion Chromatography-Multi-Angle Laser Light Scattering (SEC-MALLS) of Purified Mamaku Polysaccharide 135
6.3.4 Rheological Properties of Purified Mamaku Polysaccharide 135
6.3.5 Structural Analysis 137
6.4 Conclusion 142

CHAPTER 7 PILOT STUDY ON SATIETY EFFECTS OF MAMAKU GUM IN RATS 143

7.1 Introduction 143
7.2 Materials and Methods 144
7.2.1 Animal Ethics 144
7.2.2 Preparation of Mamaku Solution 144
7.2.3 Animals and Experimental Design 144
7.2.4 Statistical Analysis 145
7.2.5 Pathology 146
7.2.6 Rheological Measurements 146
7.2.7 Bomb Calorimetry 146
7.3 Results 147
7.3.1 Gastric Emptying 147
7.3.2 Food Consumption 148
7.3.3 Body Weight 149
7.4 Discussion 151
7.4.1 Gastric Emptying 151
7.4.2 Food Consumption 154
7.4.3 Body Weight Gain 155
7.4.4 Toxicity 155
7.5 Conclusion 155

CHAPTER 8 OVERALL CONCLUSIONS AND RECOMMENDATIONS..... 157

8.1 Overall Conclusions.....157

8.2 Recommendations.....164

8.2.1 Future Work.....164

8.2.2 Applications.....166

REFERENCES..... 169

APPENDIX..... 181

List of Figures

Figure 1.1 – Flow diagram of thesis overview 2
Figure 2.1 – Picture of the New Zealand black tree fern plant (*Cyathea medullaris*) 6
Figure 2.2 – Botanical parts of the New Zealand black tree fern plant (*Cyathea medullaris*) 7
Figure 2.3 – Chemical structures of some monosaccharides commonly found in plant polysaccharides (adapted from Izydorczyk, 2005) 10
Figure 2.4 – Comparison of structures between L- and D-glucose (adapted from Oakenfull, 1998) 10
Figure 2.5 – Comparison of structures between α-D and β-D-glucose 11
Figure 2.6 – Torsion angles of glycosidic bond (Izydorczyk, 2005) 11
Figure 2.7 – Geometrical representation of various glycosidic linkage types in D-glucose; a) zig-zag β(1→4), b) U-turn β(1→3), c) twisted β(1→2), d) zig-zag α(1→3), e) zig-zag α(1→4)-D-galactose, f) U-turn α(1→4) (adapted from Oakenfull, 1998) 13
Figure 2.8 – Comparison between molecular weight measurement types (M_n, M_v, M_w, M_z) for a heterogeneous polysaccharide (adapted from Steve & Qi, 2005b) 14
Figure 2.9 – Concentration regimes of polysaccharide solutions. From left: dilute, semi-dilute and concentrated (adapted from Pieter, 2003) 16
Figure 2.10 – Typical flow curve exhibited by a shear-thinning polysaccharide(Jacques & Jean-Louis, 2004) 17
Figure 2.11 – Typical mechanical spectrum *i.e.* storage (G', —) and loss (G", ---) moduli with angular frequency of an entangled polymer system; τ_d: relaxation time at crossover frequency (adapted from Jacques & Jean-Louis, 2004) 19
Figure 2.12 – Illustration of molecule under shear (weak) and extensional (strong) deformation (adapted from Padmanabhan, 2010) 20
Figure 2.13 – Schematic viscosity curves of different shear-thickening behaviour in materials 21
Figure 2.14 – a) polymers with a single associative block b) polymers with two associative end blocks c) polymers with many associative groups (red: associating blocks, blue: solvophilic blocks) (adapted from Chassenieux, et al., 2011) 22
Figure 2.15 – Schematic mechanism of shear-thickening due to cross-linking during shear (adapted from Ballard, et al., 1988) 24
Figure 2.16 – Schematic illustration of effective (●--●), free (○--○) and dangling (●--○) chains in a transient network model (adapted fromS. Q. Wang, 1992) 25
Figure 2.17 – Gaussian chain (adapted from Doi & Edwards, 1988) 25
Figure 2.18 – Functional properties and applications of polysaccharides based on their rheological, structural and physiological properties 29
Figure 3.1 – Pictorial representation of Mamaku extraction procedure and materials 33
Figure 3.2 – Two-step model demonstrating relationship between shear stress and shear rate 34
Figure 3.3 – Typical viscosity curves for a Newtonian, shear-thickening and shear-thinning fluid 35
Figure 3.4 – Typical viscosity curves for a thixotropic, anti-thixotropic and time-independent fluid at a constant shear rate 35

Figure 3.5 – Three-dimensional deformation of viscoelastic material in the x, y and z-direction 36
Figure 3.6 – Weissenberg (or rod-climbing) effect of 7% w/w mamaku solution with rod rotating at ~120 rev/min (Goh, et al., 2007) 36
Figure 3.7 – Comparison between stress responses of an elastic solid, viscous liquid and viscoelastic fluid under constant strain (adapted from Trinh & Trinh, 2009) 38
Figure 3.8 – Kelvin/Voigt mechanical spring and dashpot mechanical model for viscoelastic fluid 38
Figure 3.9 - Centrifugal expulsion of 5% w/w mamaku sample during viscosity measurements at approximately 50s^{-1} 40
Figure 3.10 - Viscosity curves of 5% w/w mamaku obtained using the parallel plate, cone and plate and double gap geometries 40
Figure 3.11 - Viscosity curves of 5% w/w mamaku obtained using the parallel plate with sandpaper, without sandpaper, and with serrated plates 40
Figure 3.12 – Stress vs. strain response (left) and Lissajous plots (right) of elastic solid, Newtonian fluid and viscoelastic fluids under small oscillatory shear 41
Figure 3.13 – Comparison of stress waveforms in the linear and nonlinear viscoelastic regions as represented on an amplitude sweep 43
Figure 3.14 – Classification of materials into type I) strain-thinning, II) strain-hardening, III) weak strain overshoot and IV) strong strain overshoot 44
Figure 3.15 – Quantification of G'_M and G'_L from Lissajous plots in a) linear and b) nonlinear viscoelastic regions 45
Figure 3.16 – a) Elastic and b) viscous Lissajous curves (solid lines) with contributions from elastic and viscous stress components (dotted lines) 46
Figure 3.17 – Example of LAOS data analysed using MITlaos 46
Figure 3.18 – Uniaxial deformation of material 47
Figure 3.19 – Typical transient extensional and shear viscosity of polymer solutions with time 48
Figure 3.20 – Schematic illustration of capillary breakup extensional rheometer 48
Figure 3.21 – Derivatisation of neutral monosaccharides into alditol acetates and TMS derivatives (adapted from Cui, 2005) 51
Figure 3.22 – Illustration of a rat stomach (adapted from DeSesso & Jacobson, 2001) 54
Figure 3.23 – Oral gavaging rats with mamaku gum 55
Figure 4.1 – Flow diagram of rheological techniques (shear and extensional) used to characterise the mamaku polysaccharide 57
Figure 4.2 – a) Viscosity curves of 2.5 (■), 3.5 (○), 5 (▲), 7 (▽) and 9% (◆) w/w native mamaku polysaccharide; b) representation of Newtonian, shear-thickening and shear-thinning regions on a viscosity curve 60
Figure 4.3 – Viscosity curves of 5% w/w mamaku obtained with various data collection time settings at 20°C 61
Figure 4.4– a) Viscosity of 5% w/w mamaku as a function of time at various shear rates at 20°C; b) magnified at 4 (●), 6 (○), 8 (▲) and 10s^{-1} (◇) during the first two minutes of the measurement 61
Figure 4.5 – Viscosity and first normal stress difference vs. shear rate for 2 and 10% w/w mamaku solutions at 20°C 63

Figure 4.6 – First normal stress difference (N_1) of 5% w/w mamaku with time at constant shear rates 4, 6, 8 and 10s-1 at 20°C 64

Figure 4.7 – Viscosity curves of 5% w/w mamaku on increasing (filled symbols) and decreasing (unfilled symbols) shear rates at 20°C; a) 0.1 to 1s^{-1}; b) 0.1 to 5s^{-1}; c) 0.1 to 10s^{-1} (additional ▲/△ symbols indicate viscosity with 5 minutes rest after the up-curve); d) 0.1 to 1000s^{-1} 65

Figure 4.8 – Viscosity changes with time as a function of shear history of 1 (+), 10 (○) or 1000s^{-1} (△) of 5% w/w mamaku at 20°C; each symbol represents one data series sheared for a total of 80 minutes. For example, to test the effects of shear history at 1000s^{-1} (△/black symbols), the sample was sheared at 1000s^{-1}, followed by 1s^{-1}, and subsequently back to 1000s^{-1}, and then followed by 10s^{-1}, and again back to 1000s^{-1} then followed by 100s^{-1} 66

Figure 4.9 – Viscosity changes with time as a function of pre-shear at 10s^{-1} for 5% w/w mamaku at 20°C; solid line represents viscosity of 5% w/w mamaku at 1s^{-1} from rest 66

Figure 4.10 – a) Frequency sweep (γ_0 = 5%) and b) concentration dependence of relaxation time for 2.5, 5 and 7% w/w mamaku polysaccharide 69

Figure 4.11 – Superposition of apparent viscosity (η, filled symbols) obtained by steady-shear measurements and complex viscosity (η^*, unfilled symbols) obtained by oscillatory measurements for 2.5 (■), 5 (▲) and 7% (●) w/w mamaku solutions 70

Figure 4.12 – Amplitude sweep (G' (■), G'' (□) and δ (▲) as a function of % strain) of 10% w/w mamaku at ω = 10rad/s, 20°C. 71

Figure 4.13 – a) Three-dimensional and b) two-dimensional Lissajous-Bowditch plots of stress vs. strain and c) stress vs. strain rate of 10% w/w mamaku at ω=10 rad/s from 0.1 to 3,000% strain, 20°C; The linear viscoelastic, strain-softening, strain-hardening and strain-softening regions are coloured green, yellow, red and brown respectively. 73

Figure 4.14 – Elastic (stress vs. strain) Lissajous-Bowditch plots of 10% mamaku at ω=10 rad/s for a) LVER (region I, 0.6-10% γ_0, green, dotted lines outline the overall ellipsoidal shape of the Lissajous plots); b) strain softening (region II, 20-800% γ_0, yellow, clockwise arrow indicate inter-cycle strain-softening) ; c) strain-hardening (region III, 800-2000% γ_0, red, anti-clockwise arrow indicates inter-cycle strain-hardening) and d) strain-softening (region IV, 2000-5010% γ_0, brown); Examples of determining G'_M (minimum strain modulus, gradient of tangent at γ_0=0, solid line) and G'_L (maximum strain modulus, gradient of secant at γ_{max}, dashed line) are shown for each region. 74

Figure 4.15 – Normalised elastic Lissajous curves (stress vs. strain) for 10% w/w mamaku solution arranged in a Pipkin space at ω = 1, 2.5, 5, 10rad/s and γ_0 = 10, 631, 1580 and 2510%. Maximum stress values are indicated at the top left corner of each Lissajous plot. The linear viscoelastic, strain-softening, strain-hardening and strain-softening regions are coloured green, yellow, red and brown respectively. 76

Figure 4.16 – a) Comparison of new LAOS parameters with original first-harmonic moduli; b) strain-stiffening and shear-thickening ratio of 10% w/w mamaku at 1-6000% strain amplitude 77

Figure 4.17 – Superposition of oscillatory measurements (G' vs. strain rate) on rotational measurements (η vs. shear rate) for a) 2.5% and b) 5% w/w mamaku 79

Figure 4.18 – Evolution of fluid filament diameter with time for a) 2.5, b) 5.0 and c) 7.0% w/w using CaBER; initial aspect ratio $\Lambda_0 = L_0/D_0 = 1.6/6 = 0.27$ and final aspect ratio $\Lambda = 7.4/6 = 1.23$; solid lines represent fitted data in the elasto-capillary regime using Equation 4.8; d) comparison between 2.5, 5.0 and 7.0% w/w on a log-scale with their respective relaxation times at 25°C 80

Figure 4.19 – Still frames of fluid filament during CaBER experiment at 25°C for a) 2.5% w/w (breakup time, t_b=0.80s) and b) 5.0% w/w (t_b=55.3s) at various times normalised by breakup time, $\underline{t}$, where $\underline{t}=t/t_b$ 80

Figure 4.20 – Normalised diameter $D(t)/D_0$ plotted against non-dimensional time $t^* = t/\lambda$ where λ is the corresponding relaxation time of the three mamaku gum solutions 81

Figure 4.21 – a) Extensional viscosity and b) Trouton ratio of 2.5 (■) and 5% (●) w/w mamaku as a function of accumulated Hencky strain at 25°C 84

Figure 5.1 – Flow diagram for probing stability and intermolecular associations in mamaku polysaccharide 88

Figure 5.2 – Viscosity curves of a) 2.5% and b) 5 %w/w mamaku polysaccharide at 5 (■), 10 (●), 15 (▲), 20 (▼), 25 (◆), 30 (◀), 35 (▶), 40 (⬢), 45 (⬟) & 50°C (★) 92

Figure 5.3 – a) Dependence of peak viscosity, η_{max} (■) and characteristic time scale, $1/\boldsymbol{\gamma max}$ (●)on temperature for 5% w/w mamaku; b) characteristic time scale normalised by concentration (2.5 (■), 5 (○), 7 (▲) & 9% w/w (▽)) with temperature 93

Figure 5.4 – Reduced viscosity ($\eta_r=b_T\cdot\eta$) vs. reduced shear rate ($\boldsymbol{\gamma r}=a_T\cdot\boldsymbol{\gamma}$) of 5% w/w mamaku at various temperatures; inset: horizontal (a_T) and vertical (b_T) shift factors with temperature, T_{ref}=20°C 94

Figure 5.5 – Time-temperature superposition of reduced storage modulus (G'_r) vs. reduced angular frequency ($\omega_r=a_T\cdot\omega$) of 5% w/w mamaku at various temperatures (γ_0=5%); inset: horizontal shift factor (a_T) with temperature, T_{ref}=20°C 94

Figure 5.6 – Arrhenius plots of critical (squares) and maximum (circles) viscosities (filled) and shear rates (unfilled) of 2.5% w/w mamaku 96

Figure 5.7 – Activation energies based on viscosity at critical (■), maximum (□), 0.1s^{-1} (●) and 1000s^{-1} (○) shear rates at different mamaku concentations (% w/w) 96

Figure 5.8 – Viscosity curves of a) 2.5 and b) 5% w/w mamaku polysaccharide with 0 (■), 1 (●), 2 (▲), 3 (▼), 4 (◆) & 5M (◀) urea at 20°C 98

Figure 5.9 – a) Dependence of peak viscosity (η_{max}) (■) and characteristic time scale ($1/\boldsymbol{\gamma max}$) (●) on urea concentration for 5% w/w mamaku; b) inverse of maximum shear rate normalised by mamaku concentration (2.5 (■), 5 (○), 7% w/w (▲)) at 20°C 99

Figure 5.10 – Reduced viscosity ($\eta_r=b_C\cdot\eta$) vs. reduced shear rate ($\boldsymbol{\gamma r}=a_C\cdot\boldsymbol{\gamma}$) of 5% w/w mamaku with 0 (■), 1 (●), 2 (▲), 3 (▼), 4 (◆) and 5M (◀) urea; inset: horizontal (a_C; ●) and vertical (b_C; ○) shift factors with urea concentration, C_{ref}=0M and 20°C 100

Figure 5.11 – Time-urea concentration superposition of frequency sweeps of 5% w/w mamaku with 0 (■), 1 (●), 2 (▲), 3 (▼), 4 (◆) and 5M (◀) urea by shifting along x-axis with shift factor, a_c; inset: shift factor values with urea concentration, C_{ref}=0M at 20°C 101

Figure 5.12 – Viscosity curves of 5% w/w native mamaku extract before (■) and after (▲) dialysis (MWCO 12-14,000 Da), and addition of 0.05M NaCl (●) for increasing (filled) and decreasing shear rates (unfilled symbols) at 20°C 102

Figure 5.13 – a) Effect of NaCl concentration (0.001 (×), 0.005 (+), 0.01 (✱), 0.05 (●), 0.1 (▲), 0.25 (▼), 0.5 (◆) & 1.0M (◀) on shear-thickening of 5% w/w dialysed mamaku at 20°C; b) Zero-shear viscosity (■) estimated using a modified Cross' equation for shear-thickening fluids and viscosity at 100s-1 (○) at various NaCl concentrations 104
Figure 5.14 – a) Frequency sweeps G' (filled) and G" (unfilled) of 5% w/w dialysed mamaku at 0 (■), 0.001 (●) & 0.05M (▶) NaCl at 1% strain and 20°C; b) relaxation time of dialysed mamaku with NaCl concentration (0.001-0.5M) 106
Figure 5.15 – Effect of CaCl2 concentration (0.001 (×), 0.005 (●), 0.01 (▲), 0.05 (▼), 0.1 (◆), 0.25 (◀), 0.5 (▶) & 1.0M (●)) on shear-thickening of 5% w/w dialysed mamaku at 20°C 107
Figure 5.16 – Dialysed mamaku extract in (from left to right) 0.001-0.1M $LaCl_3 \bullet 7H_2O$ 108
Figure 5.17 – Effect of $LaCl_3 \bullet 7H_2O$ concentration (0.001 (×), 0.1 (+), 0.25 (●), 0.5 (▼), 0.75 (■) & 1.0M (◆)) on shear-thickening of 5% w/w dialysed mamaku; sample precipitation occurs with 0.005, 0.01, 0.05M $LaCl_3 \bullet 7H_2O$ at 20°C 108
Figure 5.18 – Effect of $AlCl_3 \bullet 6H_2O$ concentration (0.001 (×), 0.005 (+), 0.01 (✱), 0.05 (▼), 0.1 (◆), 0.25 (◀), 0.5 (▶) & 1.0M (●)) on shear-thickening of 5% w/w dialysed mamaku at 20°C 109
Figure 5.19 – Effect of $LaCl_3 \bullet 7H_2O$ concentration on relative viscosity (■) of 1% w/w dialysed mamaku and zeta-potential (○) of 5% w/w dialysed mamaku at 20°C 109
Figure 5.20 – Viscosity curves of native (☐) and dialysed (☒) mamaku extract with salts of different cation valencies i.e. monovalent (NaCl (⊕), KCl (○), TMAC (◑)), divalent (CaCl2 (◆), MgCl2 (◩)) and trivalent (AlCl3 (△) (also at 0.01M (◭)), LaCl3 (▲)) at 0.1M concentration and 20°C 111
Figure 5.21 – Comparison of a) viscosity at critical shear rate, b) critical shear rate & c) extent of shear-thickening with various mono- (NaCl (⊞), KCl (☐) , di- (CaCl2 (●), MgCl2 (○)) and trivalent (AlCl3 (▲), LaCl3 (△)) cations at equivalent ionic strengths (lines serve as visual guides) 113
Figure 5.22 – a) Viscosity curves of 5% w/w dialysed mamaku under various pH conditions (pH 1-11) and b) magnified in pH region from 2.0-5.0 114
Figure 5.23 – pKa titration curve of dialysed mamaku solution (5% w/w) 114
Figure 6.1 – Flow diagram of overall purification scheme of mamaku extract 121
Figure 6.2 – Carboxyl reduction of methylesterified and non-methylesterified uronic acids (adapted from Pettolino, Walsh, Fincher, & Bacic, 2012) 125
Figure 6.3 – Summary of glycosyl linkage analysis based on methylation, hydrolysis, reduction and acetylation reactions (adapted from Pettolino, et al., 2012) 126
Figure 6.4 – Appearance of native mamaku solution before (left) and after (right) ultracentrifugation at 250,000g for 1 hour at 20°C 128
Figure 6.5 – Yield of solid material before and after ultracentrifugation (UC) and ethanol precipitation (EtOH) 128
Figure 6.6 – Protein removal using Sevag reagent; top brown layer: aqueous polysaccharide phase; water-chloroform interface: denatured protein gel; bottom clear layer: chloroform phase 129
Figure 6.7 – Extraction scheme for multiple ethanol precipitation of native mamaku polysaccharide solution 131
Figure 6.8 – Appearance of polysaccharide residue after first and second ethanol precipitations 132

Figure 6.9 – Viscosity curves of purified mamaku solutions (0.8% w/w) with one (EtOH x 1, ■) or two (EtOH x 2, ●) ethanol precipitations, and the alcohol-soluble fraction after two precipitations (E2, ○).....133
Figure 6.10 - Molecular weight analysis by size-exclusion coupled with multi-angle laser light scattering (SEC-MALLS) of purified mamaku polysaccharide.....135
Figure 6.11 – a) Viscosity curves of purified mamaku at concentrations of 0.2-1.4% w/w; dashed lines represent viscosity of a 5% w/w native mamaku solution before purification; b) Concentration dependence of zero-shear viscosity; Unfilled symbols (□) represent viscosities measured using an Ubbelohde dilution capillary viscometer; filled symbols (■) are zero-shear viscosities in the dilute regime estimated by fitting the Cross equation to the complex viscosity curves.....136
Figure 6.12 – Selected regions of the a) ^{13}C-NMR and b) ^{1}H-NMR spectra of purified mamaku polysaccharide 140
Figure 6.13 – Possible structure of mamaku polysaccharide; R = T-Xyl*p*, T-Gal*p* or T-Glc*p*A and other more complex oligosaccharides containing sugars with linkages shown in Table 6.4.....141
Figure 7.1 – Summary of experimental design in a flow diagram 144
Figure 7.2 – Boxplot of stomach contents two hours after gavaging with 4ml mamaku or water; a significant difference (*) was found in the weight of contents remaining in the stomach of rats gavaged with mamaku compared with those gavaged with water; horizontal line represents the median and the box represents the interquartile ranges.....147
Figure 7.3 – Mamaku gum removed from the stomach two hours post-gavage.....147
Figure 7.4 – Mean quantity of food consumed by each treatment group from day 16 to day 24; red arrows indicate days which the rats have been gavaged; significant difference (*) between groups gavaged with mamaku and water on day 22 (3rd gavage) and for all gavaging days (****) based on repeated measures ANOVA; bars represent standard error (SE) of the mean 148
Figure 7.5 – a) Cumulative average weight gain of mamaku and water group during gavaging week (day 17-26); error bars represent SE of the mean; red arrows indicate days which the rats have been gavaged; b) Average weight gain of mamaku and water group during acclimation (day 1-16), gavaging (day 17-25), and for the entire experiment (day 1-25).....149
Figure 7.6 – Average weight gain after gavage (total weight change 24 hours after gavage e.g. weight difference between days 17 and 18) and between gavage (total weight change in 24 hours without gavage e.g. weight difference between days 18 and 19) gavages for mamaku and water group; significant difference (****) between groups gavaged with mamaku and water 24 hours after gavage based on repeated measures ANOVA error bars represent SE of the mean.....149
Figure 7.7 – Illustration of the gastric emptying process (adapted from Sherwood, 1993) 151
Figure 7.8 – Viscosity curve of 15% w/w mamaku solution at 37°C.....152
Figure 7.9 – Viscosity curves of 17% w/w mamaku gum and 1.5% w/w guar gum at 20°C.....153
Figure 8.1 – Schematic illustration of the polysaccharide during shear and extensional deformations (dotted lines represent intermolecular hydrogen bonds) 159
Figure 8.2 – Schematic illustration of overview of effects of temperature, urea, cations and pH on the polysaccharide during shear 160
Figure 8.3 – Schematic illustration of purification and structural characterisation of the polysaccharide.....161

Figure 8.4 – Schematic illustration of possible hydrogen bond configurations between functional groups in the polysaccharide chain responsible for hydrogen bonding 162
Figure 8.5 – Schematic illustration on effects of mamaku polysaccharide on the food intake, body weight and gastric emptying in rats 163

List of Tables

Table 2.1 – Plant polysaccharides of industrial significance and their sources and applications 4
Table 2.2 – Proximate and mineral composition of freeze-dried extract from the mamaku fronds (Goh, et al., 2007) 8
Table 2.3 – Molecular characteristics of the water-soluble extract from mamaku 8
Table 2.4 – Structural levels of polysaccharides (Walter, 1998) 9
Table 3.1 – Comparison between elastic solids and viscous liquids based on the spring and dashpot mechanical models (adapted from Trinh & Trinh, 2009) 37
Table 3.2 - Specifications for Paar Physica rheometer MCR-301 39
Table 4.1 – Zero-shear viscosity (η_0), surface tension (σ), extensional relaxation time (λ_E) and shear relaxation time (λ_s) of 2.5, 5.0 and 7.0% w/w mamaku solutions 81
Table 4.2 – Trouton ratios of various polymers 85
Table 5.1 – Activation energy of viscous flow (kJ/mol) for various polymers 97
Table 5.2 –Mineral composition of native and dialysed mamaku extract (mg/g NSP†) 103
Table 5.3 – Ionic and hydrated ionic radius of various cations 112
Table 6.1 – Protein content of purified mamaku obtained with protein removal using protease or Sevag's reagent determined using the Leco total combustion method 129
Table 6.2 – Comparison of chemical composition of native and purified mamaku fractions 134
Table 6.3 – Constituent sugar composition of purified mamaku polysaccharide determined using HPAEC and GC-MS 137
Table 6.4 – Glycosyl linkage composition of carboxyl-reduced mamaku polysaccharide 139

List of Publications

Based on the thesis:

1. Wee, M. S. M., Matia-Merino, L., Carnachan, S. M., Sims, I. M., Goh, K. K. T. (2014). Structure of a shear-thickening polysaccharide extracted from the New Zealand black tree fern, *Cyathea medullaris*. *International journal of biological macromolecules*, 70(0), 86-91.

2. Wee, M. S. M., Matia-Merino, L., Goh, K. K. T (2015). Time and shear-history dependence of rheological properties of a water soluble extract from the fronds of the black tree fern, *Cyathea medullaris*. *Journal of Rheology*, *59*, 365.

3. Wee, M. S. M., Matia-Merino, L., Goh, K. K. T. (accepted in Carbohydrate Polymers). Effect of cation concentration and valency on shear-induced thickening of mamaku polysaccharide.

4. Jaishankar, A., Wee, M. S. M., Matia-Merino, L., Goh, K. K. T., McKinley, G. H. (2015). Probing hydrogen bond interactions in a shear-thickening polysaccharide using nonlinear shear and extensional rheology. *Carbohydrate Polymers*, *123*, 136-145.

5. Wee, M. S. M., Jaishankar, A., Matia-Merino, L., Goh, K. K. T., McKinley, G. H. (in preparation). Large amplitude oscillatory shear characterisation of a shear-thickening polysaccharide extracted from the New Zealand black tree fern, *Cyathea medullaris*.

Others

6. Wee, M. S. M., Nurhazwani, S., Tan, K. W. J., Goh, K. K. T., Sims, I. M., and Matia-Merino, L. (2014). Complex coacervation of an arabinogalactan-protein extracted from the *Meryta sinclarii* tree (puka gum) and whey protein isolate. *Food Hydrocolloids*, *42*, 130-138.

7. Goh, K. K. T., Wee, M. S. M., and Hemar, Y. (2013). Phase stability-induced complex rheological behaviour of galactomannan and maltodextrin mixtures. Food & Function 4, 627-634.

8. Wee, M. S. M., Goh, K. K. T., Sims, I. M., and Matia-Merino, L. (in preparation). Rheological and molecular characterisation of an arabinogalactan-protein extracted from the *Meryta sinclarii* tree (puka gum).

Chapter 1 Introduction

"All I ever really want is sugar." – Andy Warhol.

And all this thesis ever really has is millions of sugar, or what we scientifically call as polysaccharides. (Unfortunately, polysaccharides are not going to suit Warhol's taste buds very well.)

Polysaccharides are carbohydrate macromolecules of monosaccharide units which depending on the makeup of individual units, how the units are linked, and how flexible they move etc. can result in endless permutations of the final product. Every one of these factors will govern the behaviour of the polysaccharide, thereby equipping them with functionalities sought after by the food, cosmetic and pharmaceutical industries. Furthermore, polysaccharides are *au naturel*, biodegradable and sustainable, giving them an edge over synthetic polymers especially in food products. Polysaccharides typically come from plants and bacteria (exopolysaccharides), which means that the number of polysaccharides one could choose from should be limitless, given the number of species of plants and bacteria we have on Earth. This is however not the case. When it comes to polysaccharides, typical names which come to people's mind include xanthan gum, guar gum, pectin, alginate, carrageenan etc. Polysaccharides extracted from novel sources do show up in literature every now and then, but the relatively little known information about them deters them from being utilised. Therefore it is essential to drive research for polysaccharides with real potential and push for new applications.

There are currently over 2000 species of flora in New Zealand, but the percentage of these plants being scientifically researched on is disproportionately small. As most of these plants are endemic *i.e.* can only be found in New Zealand, studies are likely to be limited to local scientists. Thus there are still plenty of unchartered territories for research within the New Zealand plant kingdom. In this thesis, the polysaccharide (mucilage) extracted from the New Zealand black tree fern, *Cyathea medullaris* (or Mamaku in Māori) was characterised extensively. The mamaku tree fern is a native and endemic New Zealand plant, which can grow up to 20 metres in height. The Māori people have cooked the stem pith and consumed it for food, or applied the mucilage to burn wounds as a demulcent. The extracted mamaku mucilage is slimy, stringy, and ropy, which is reminiscent of okra, spinach or tuber root slime. The unusual properties of the mucilage have sparked interests in its characterisation, especially with rheological techniques.

Being presented with a polysaccharide with potentially interesting properties, it piques one's curiosity to delve further This thesis therefore aimed to characterise the polysaccharide in depth, and be able to answer the big research question of 'what is the mamaku polysaccharide', first by answering more specific questions (objectives) such as 'what are its rheological properties', 'what is the polysaccharide made of', and 'what can the polysaccharide be used for'. These questions were explored using a combination of rheological, structural and *in vivo* research techniques. The list of questions could go on, but for now, these four questions would put together a nice 'résumé' for the mamaku polysaccharide. An outline of the thesis is presented in the flow diagram below (Figure 1.1).

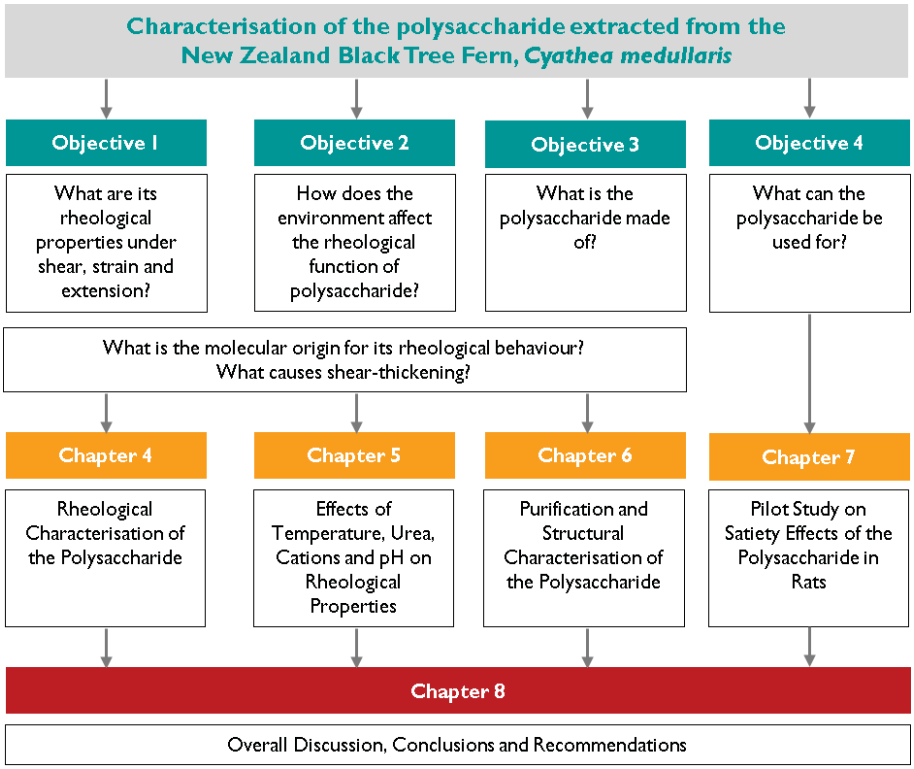

Figure 1.1 – Flow diagram of thesis overview

Chapter 2 Literature Review

2.1 Polysaccharides

Polysaccharides are a magnificent architectural creation of nature. Tens of thousands units of monosaccharides join together in a seemingly random and chaotic fashion yet their resulting macromolecular structures function with precise roles in the living organism where they are from. Land or marine plants often synthesise polysaccharide-type materials to assist its survival and/or reproduction, although some bacteria produce them as by-products during metabolism i.e. exopolysaccharides. Polysaccharides can be homopolysaccharides, i.e. consisting of only one monosaccharide type, or heteropolysaccharides. By varying the building monosaccharide blocks and linkage type, the permutation for the type of polysaccharide is infinite. Fortunately for scientists, most non-starch polysaccharides (NSP) from related sources have similar monosaccharide compositions and functionalities. They can be broadly classified mainly into cellulose, galactomannans (e.g. guar, locust bean, tara gum), carrageenans (kappa-, iota- lambda-carrageenan), glucomannans (konjac), pectins, alginates, xyloglucans (xanthan gum), or β-glucans (Alistair & Shirley, 2010). Galactomannans are usually found in seed cell walls, carrageenans and alginates in seaweeds, glucomannans in plant tubers, pectins and cellulose in plant cell walls, xyloglucans are from bacteria and β-glucans are from cereal grains.

Conventionally, polysaccharides are used in foods as texture modifiers, i.e. thickeners or gelling agents, or as stabilisers in emulsions and dispersions due to the thick consistency provided. Not only do polysaccharides improve the textural and organoleptic properties of the food, certain polysaccharides from plants e.g. guar gum also function as dietary fibre. Over the years, there has been an increasing demand for polysaccharides in food manufacture (Williams & Phillips, 2009) as well as in the cosmetics, biomedical and pharmaceutical industries. This is owing to the shift in consumer awareness, with more consumers demanding natural materials whether in their sauces, night creams or surgical implants. Researchers have also recognised the benefits of using natural polymers, such as its biocompatibility, biodegradability, and renewability. Novel applications of polysaccharides outside the food industry include mucoadhesion, controlled drug delivery (Avachat, Dash, & Shrotriya, 2011; Reddy, Mohan, Satla, & Gaikwad, 2011), tablet binder (Jani, Shah, Prajapatia, & Jain, 2009; Nep & Conway, 2010), wound healing (Athanasiadis et al., 2008) and textile printing (Vrblac & Sostar Turk, 2000).

Functionalities of polysaccharides originate from their molecular properties based on their composition and structure. The supramolecular polysaccharide assembly which dictates its functional properties is dependent on the molecular weight, conformation and chain rigidity of the individual polysaccharide chains, which in turn are dependent on what the monomer units are (i.e. monosaccharides), how many of them, and how they are linked (Walter, 1998). Furthermore, these monomers may be ionic (e.g. $–COO^-$, $-OSO_3^-$), polar, nonpolar or hydrophobic. Functional properties such as gelation require the formation of junction zones between polysaccharide chains and the subsequent aggregation, i.e. a supramolecular assembly. Other properties such as flow behaviour (rheology) depend largely on the secondary and tertiary structures such as degree of branching and presence of chain entanglements respectively. The environmental conditions i.e. pH,

temperature, ionic strength, solvent type and osmotic pressure can also largely affect the functionalities of the polysaccharides (Oakenfull, 1998).

Although many existing polysaccharides have been extracted and characterised for their functional properties, there is still great potential for discovering new sources of polysaccharides which may be more suitable for a particular food system or application, with similar functionalities and at a lower cost. Similarly there is room for polysaccharides with an entirely novel functionality which may not be represented by existing polysaccharides. This thesis focuses on characterising a polysaccharide extracted from the New Zealand Black Tree Fern (*Cyathea medullaris* or mamaku in Māori).

2.1.1 Plant Polysaccharides

Plants are a major source of carbohydrates in the human food chain. Carbohydrates are synthesised and stored in plant tissues mainly as energy reserves or structural materials e.g. plant cell wall; they are also secreted as gums upon injury such as bark removal or damage from weather or insects as a form of defence mechanism. These carbohydrates occur in the form of mono-, oligo- and polysaccharides. **Error! Reference source not found.** lists some plant polysaccharides of industrial importance and their applications.

Table 2.1 – Plant polysaccharides of industrial significance and their sources and applications

Polysaccharide	Plant Source	Country	Applications
Guar gum	Seeds of guar plant	India; Pakistan	Bakery, ice cream
Locust bean gum	Seeds of carob tree	Mediterranean region	Bakery, ice cream
Carrageenan	Red seaweed	Philippines; Chile	Puddings, meat
Gum arabic	Sap of acacia tree	Arabia	Confectionery, beverages
Gum tragacanth	Sap of astragulus tree	Iran	Sauces, confectionery
Alginates	Brown algae	California	Jellies, beverages
Pectin	Citrus peel; apple pomace	Multiple	Jams, confectionery
Inulin	Roots of rhizomes	Multiple	Dietary fibre

Polysaccharides may be extracted from the seed, roots, tuber, flower, fruit, stem, or bark of the plant in the form of gums, exudate, mucilage. There is no clear distinction between these terms, perhaps only differentiated by their texture and origin. Gums are thought to be stickier while mucilage is used when the material is slimy. Exudates are more often used to refer to secretions on tree surfaces and mucilages for substances that flow from the bark or soft stems of the plant.

A review by Mirhosseini and Amid (2012) summarises the chemical composition and molecular structure of polysaccharides recently extracted and characterised from various plant sources and parts. Seed mucilage has reportedly different functions from root or stem mucilage. Seed mucilage mainly facilitates seed hydration, adherence to soil and animals for dispersal and trigger germination in waterlogged soils (Western, 2012). Exudates are triggered by external stresses such as plant wounding, fungal attack or diseases and the exudate dries to a hard glass as a form of physical barrier to protect the plant (Alistair, Shirley, Peter, & Glyn, 2006;

Sims & Furneaux, 2003). Root or stem mucilages are thought to play a role in regulating ionic balance of plant cells, facilitate ion-transport (as cited in Clifford, Arndt, Popp, & Jones, 2002), provide salinity tolerance (Edmond-Ghanem et al., 2010), or protect the plant from aluminium toxicity (Geng et al., 2011; Kinraide, Parker, & Zobel, 2005; Watanabe, Misawa, Hiradate, & Osaki, 2008).

Note: The term 'polysaccharide' will be used interchangeably with 'hydrocolloid', 'gum', 'mucilage' or 'exudate' in this research. Colloids are generically particles dispersed within another system; therefore hydrocolloids are in the same sense polysaccharide particles dispersed in water. The term 'hydrocolloid' is more used in the context of the polysaccharide as a food ingredient, where the hydrated form of the polysaccharide is important for imparting properties such as viscosity and gelation. 'Gum', 'mucilage' and/or 'exudate' emphasises the botanical nature of the polysaccharide.

2.1.1.1 Extraction and Isolation

Polysaccharides are complicated materials with differing physical, chemical and molecular properties. They can be neutral or anionic, linear or branched, soluble or insoluble in water, and homogenous or heterogeneous amongst other classifications. It is therefore almost impossible to have a universal extraction scheme which will suit all polysaccharides. Specific extraction and purification methods and conditions have been developed and continuously refined for existing known polysaccharides, while a general approach can be taken for unknown polysaccharides.

The starting material of plant polysaccharides may be the seed, gum exudate, cell wall tissue or leaf of the plant. Extraction of polysaccharides from gum exudates is comparatively easier than from the structural matrix of plant cell walls. Most water-soluble polysaccharides such as neutral polysaccharides, β-glucans, arabinoxylans and arabinogalactans can be easily extracted with water (usually at elevated temperatures), coupled with mechanical action such as stirring or agitation. Charged or acidic polysaccharides such as pectin can be extracted with acids, while alkali (potassium hydroxide) is used for polysaccharides bound in plant cell walls (Izydorczyk, 2005). Therefore in general, the charge and structure of the polysaccharide mainly determine the reagents to be used for extraction. For polysaccharides with unknown structures, extraction with acid or alkali is avoided to prevent hydrolysis of the glycosidic linkages.

At this point, a crude polysaccharide extract is obtained. However, it will comprise of other materials such as proteins, starch, seed endosperm, lipids or insoluble fibres in addition to the polysaccharide. Lipids or lipid-soluble substances are first removed from the dried material using solvents such as chloroform-methanol mixture or hexane. Low molecular weight compounds, soluble sugars and ash are then extracted with hot 80% w/v ethanol which polysaccharides and proteins are insoluble in. Protein is subsequently removed via enzyme-catalysed hydrolysis e.g. using papain or precipitation with trichloroacetic acid. Any remaining solubilised polysaccharide is precipitated with ethanol and sodium chloride. If starch is present, it should be removed by adding glucoamylase or amyloglucosidase to break down the amylose and amylopectin fractions of starch. Insoluble fibres are removed with centrifugation (BeMiller, 2006; Izydorczyk, 2005; Steve & Yolanda, 2006).

The final objective is to obtain a high yield polysaccharide material without compromising the integrity of the polysaccharide structure and its chemical purity. However, increasing purity often comes at the expense of causing further changes to the structure with extra uses of chemical reagents. It is therefore up to the user to define the acceptable purity level of the polysaccharide with its intended functionalities.

2.1.1.2 Polysaccharide Extracted from the New Zealand Black Tree Fern (*Cyathea medullaris* or Mamaku)

The New Zealand black tree fern (*Cyathea medullaris*), also known as mamaku in Māori, is one of the most common endemic plants found throughout damp lowland forests in New Zealand (Figure 2.1). Growing up to 20 metres, it is one of the world's tallest fern. The centre of the trunk, i.e. pith (*Medullaris* means "pithy"), the bases of the frond stems, as well as the uncurled part of the new shoots are edible. Apart from being a food source for the Māori, the mamaku is also traditionally used for medicinal purposes, either by consumption or external application. The brownish-red gum exudate with a slimy consistency of the bruised and uncooked pith and fronds has been used to treat swellings, bruises and wounds (Crowe, 2004; Foster, 2008). Mamaku fern extracts have been used in cosmetic products as a bioactive ingredient, such as Sothys Paris®'s total cohesion cream and eye distressing masks, Ora®'s body scrubs, and Fresh®'s mamaku night serum. No scientific evidence was however found on the immunological or anti-inflammatory properties of the mamaku extract, although the Māori have claimed wound-healing properties.

Figure 2.1 – Picture of the New Zealand black tree fern plant (*Cyathea medullaris*)

The botanical parts of the black tree fern are illustrated in Figure 2.2. The black tree fern may appear similar to tree ferns of the same family e.g. silver tree fern (*Cyathea dealbata*), but there are distinctive features which

differentiate it from other tree ferns. The trunk is black with distinctive hexagonal patterns and the fronds are large and leafy, with thick black stipes (stem) (Crowe, 2009). The mucilage characterised in this thesis is extracted from the thick, fleshy stem pith of either the old or young fronds. The cross-sectional image of the stipe shows a white pulpy flesh within the stipe which consists of mainly starch (Crowe, 2004). Breaking a slice of the stem pith revealed strands of thin viscoelastic filaments (presumably the polysaccharide) resembling spider silk (Figure 2.2).

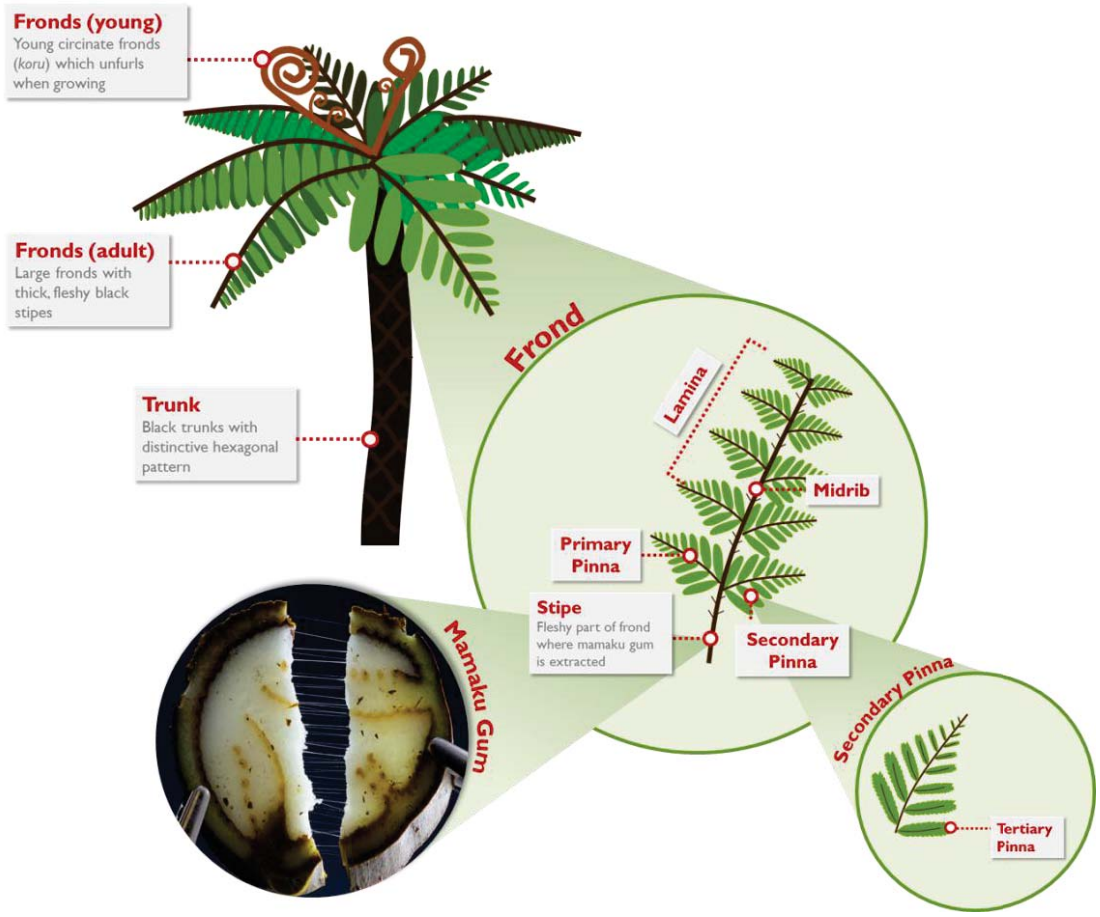

Figure 2.2 – Botanical parts of the New Zealand black tree fern plant (*Cyathea medullaris*)

A separate study on the effects of volume and viscosity of gastric contents on the antral and fundic activity of the (rat) stomach employed mamaku and guar gum as test materials (Lentle, Janssen, Goh, Chambers, & Hulls, 2010). With the mamaku extract infused in the stomach, the stomach wall activity was significantly different from that of guar gum. The viscoelasticity of the mamaku solution resulted in accumulation of residual stress as the stomach wall contracts, which alters subsequent antrocorporal contractions. With these findings, the authors suggested that the presence of mamaku or a mamaku-like material in the stomach may help to prevent transport of other undesirable digesta to the small intestine.

No studies have been made on the mamaku plant mucilage until recently. Goh, Matia-Merino, Moughan and Singh (2007) isolated the mamaku extract and explored some rheological properties, analysing for the first time its chemical composition (Table 2.2). The mamaku extract was found to contain mainly carbohydrates (~60% w/w) in the form of simple sugars, starch (~10.3% w/w; from current research), and non-starch

polysaccharides (~10% w/w). About 10% w/w of the extract remained unknown, which indicates that further purification of the material is required. Rheological characterisation of the material revealed complex viscoelastic properties, such as the rod-climbing (or Weissenberg) and self-siphoning effects. Subjected to various shear rates, and at a given concentration, the material may be shear-thickening, shear-thinning, thixotropic, antithixotropic, and/or Newtonian. Such complex rheological properties prompted further necessary studies on the mamaku extract.

A second study on the molecular characteristics of the mamaku frond extract was carried out by Goh, Matia-Merino, Pinder, Saavedra and Singh (2011). Table 2.3 summarises the physical molecular parameters obtained using techniques such as capillary viscometry, size exclusion chromatography coupled with multi-angle laser light scattering (SEC-MALLS) and dynamic light scattering. This work defined the fundamental molecular properties of mamaku from which its functional and rheological properties can be better predicted.

Table 2.2 – Proximate and mineral composition of freeze-dried extract from the mamaku fronds (Goh, et al., 2007)

Composition	% (w/w)
Moisture	9.25
Ash	16.07
Crude protein	2.02
Fat	0.17
Crude fibre	0.24
Tannins	0.09
Sugars	44.3
Non-starch polysaccharides	9.8
Unknown	18.06
Minerals	**mg/kg**
Potassium	51800
Sodium	30400
Calcium	1200
Magnesium	1000
Aluminium	710
Zinc	54
Manganese	26
Iron	7.7
Copper	7.4
Selenium	0.28
Lead	0.072
Mercury	<0.01

Table 2.3 – Molecular characteristics of the water-soluble extract from mamaku

Intrinsic viscosity, η	**2020 ± 23 ml/g (in milliQ water)**
Weight-average molar mass, M_w	3.20 ± 0.11 x 10^6 Da (in 0.1M NaCl)
Differential refractive index, dn/dc	0.178 ± 0.006 ml/g
Root-mean square radius, $(R^2_g)_z^{1/2}$	144 ± 1 nm (in 0.1M NaCl)
Z-average diameter	~ 75 nm
Polydispersity index	1.08 ± 0.05
Molecular conformation	Semi-flexible (extended) random coil (in 0.1M NaCl)

Further characterisation work was carried out in a third paper by Matia-Merino, Goh and Singh (2012) to elucidate the mechanism behind shear thickening property of mamaku. The nature of the intermolecular forces between the polysaccharide chains were probed by manipulating the temperature (5-80°C), ionic strength (0-1M NaCl) and pH (1-12) of the native extract. The rheological properties of the native extract in the concentrated regime was found to be rather resistant to salt and pH changes, but the shear thickening effect was highly sensitive to temperature. At temperatures above 50°C, the extract no longer shear thickened and exhibited only shear thinning flow. It was therefore concluded that electrostatic and hydrophobic attractive forces are not likely to be the source of interaction responsible for shear thickening in the material. Instead, evidence pointed towards hydrogen bonding as the cause of shear thickening. More references to these works will be made in the main body of the research thesis.

2.2 Structural Properties of Polysaccharides

Polysaccharides are macromolecules with molecular weights of up to 10^6 Daltons, or the approximate equivalent of 5500 glucose molecule units. The complexity of structural analysis increases with molecular size, heterogeneity of the composition, as well as irregularities in glycosidic linkages occurring along the chain. Even within the same polysaccharide solution, the structure may still vary from molecule to molecule. The polymolecular nature of polysaccharides makes detailed structural characterisation elusive, and one can at most obtain a representative structure based on the general compositional and linkage analyses.

For plant polysaccharides, the structure may also be influenced by the cultivar, climate and soil conditions. The constituents of plant polysaccharides often include high contents of carboxylic acids, especially D-glucuronic acid (D-GlcA) and D-galacturonic acid (D-GalA). Methyl ester groups are also prevalent, in particular methyls of L-rhamnose (L-Rha), L-Fucose (L-Fuc) and 4-O-methyl-D-GlcA (4-O-Me-D-GlcA). These methyl groups make up the hydrophobic regions in the polysaccharide chain (Alistair, et al., 2006).

Biomacromolecules like proteins and polysaccharides are able to arrange themselves into higher levels of structure, which plays an important role in their functional properties. The structure of polysaccharides can be broadly divided into four levels, i.e. the primary, secondary, tertiary and quaternary (or supramolecular) structures (Table 2.4).

Table 2.4 – Structural levels of polysaccharides (Walter, 1998)

Primary Structure	Monosaccharide composition and sequence; linkage position and configuration
Secondary Structure	Helices, ribbons, stiff rod, random coil, globular (branched polymers)
Tertiary Structure	Double/triple helices
Quaternary/ Supramolecular Structure	Aggregates, gels, films, crystals

2.2.1 Monosaccharides

The primary structure of a polysaccharide mainly constitutes the type and distribution of monosaccharide (monomer) units along the chain. Monosaccharides are chemically defined as polyhydroxy aldehydes (R-C=O-H) or polyhydroxy ketones (R-C=O-R') which often exist in cyclic hemiacetal forms. They can be classified according to the number of carbon atoms in the monosaccharide e.g. pentoses (C5) or hexoses (C6). The structures of a few monosaccharides commonly found in plant polysaccharides are shown in Figure 2.3.

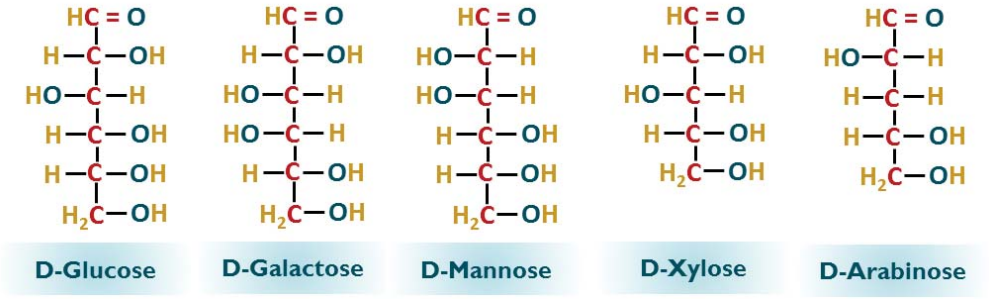

Figure 2.3 – Chemical structures of some monosaccharides commonly found in plant polysaccharides (adapted from Izydorczyk, 2005)

The carbon number is assigned from the aldehyde end. These monosaccharides can exist in either D- or L-form, depending on the position of the OH group attached to the highest numbered chiral carbon. The chiral carbon is the carbon attached to four different other groups i.e.-CHO, -OH, -H and –R. It belongs to the D-chiral family if the OH group is written to the right and the L-chiral family if written to the left (Figure 2.4). The ring form of D-glucose can further exist in two anomeric forms, α-D- and β-D-glucose (Figure 2.5). α-anomers have the hydroxyl group projected downwards (or opposite direction from the CH_2OH group at C6), and upwards for the β-anomers.

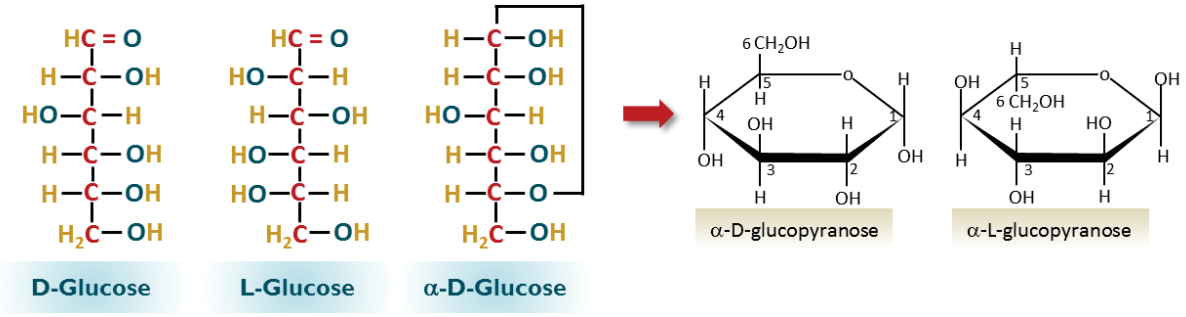

Figure 2.4 – Comparison of structures between L- and D-glucose (adapted from Oakenfull, 1998)

These monosaccharides can undergo further reduction, oxidation or derivatisation etc. reactions to yield similar compounds such as sugar alcohols (e.g. xylitol, maltitol), sugar (uronic) acids (e.g. glucuronic, galacturonic acid), amino sugars (-OH groups replaced by NH_2), deoxysugars (-OH groups replaced by H), or sulphosugars (-OH groups replaced by $–OSO_3$). Many of these alter-forms of monosaccharides may be naturally found in polysaccharides (Izydorczyk, 2005).

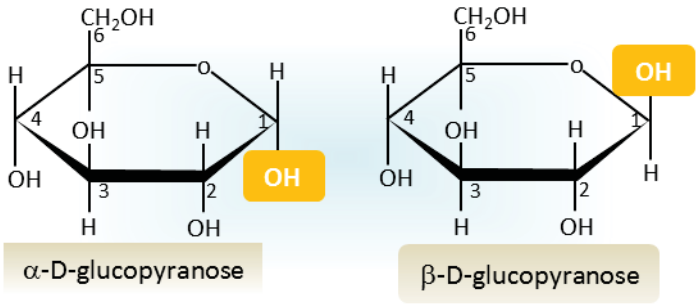

Figure 2.5 – Comparison of structures between α-D and β-D-glucose

2.2.2 Glycosidic Linkages

The individual monosaccharide units are joined together by glycosidic linkages. Glycosidic linkages are formed when the hydroxyl groups from a monosaccharide reacts with the hemiacetal group of another. A disaccharide is first created, and subsequent linking of more monosaccharides form tri-, oligo- and eventually polysaccharides. Theoretically, a glycosidic linkage can form between the first carbon (C1) of a monosaccharide e.g. D-glucose and C1, C2, C3, C4 or C6 of another. The linkage is defined by the anomeric configuration at C1 of the first monosaccharide and the carbon number of the second monosaccharide unit.

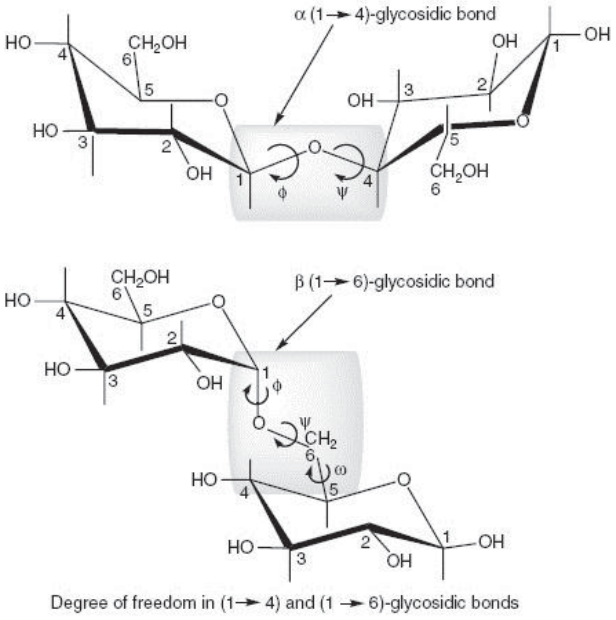

Figure 2.6 – Torsion angles of glycosidic bond (Izydorczyk, 2005)

The linkage determines the relative orientation of the monosaccharide units to each other, and can be characterised by the conformational (or torsion) angles ϕ, ψ and/or ω (if linked at C6) (Figure 2.6). In theory, the monosaccharides are free to rotate about glycosidic bonds and the units would adopt the angles which require the least conformation energy. However, in solution, hydrogen bonds may interfere with the conformation and prevent the monosaccharide conformation which has minimum conformational energy (Izydorczyk, 2005; Oakenfull, 1998). The structure and therefore functional properties of the molecule is in

fact largely dependent on the linkages. Conformation, flexibility of the polysaccharide chain, solubility etc. are all dictated by the glycosidic linkages and are further discussed in the next few sections.

2.2.3 Conformation

Conformation of a polysaccharide usually refers to the secondary structure of the polysaccharide, which can be classified into an ordered or disordered conformation. The conformation which the polysaccharide assumes is a result of the chain maintaining a geometrical shape of lowest possible entropy about the glycosidic bonds. The spatial arrangement of the monosaccharides determine whether a regular crystalline structure can be formed, or if the polymer will be irregularly branched (Steve & Qi, 2005a).

A very good example would be to compare cellulose and amylose, both of which are homopolymers of D-glucose yet differ largely in their physical properties especially solubility. Cellulose is $\beta(1\rightarrow4)$ linked while amylose is $\alpha(1\rightarrow4)$ linked. Referring to Figure 2.7, (a) represents cellulose and (f) amylose. The $\beta(1\rightarrow4)$ in cellulose leads to an overall zig-zag arrangement of the polysaccharide, which allows regular packing and alignment of more zig-zag chains via van der Waals forces and hydrogen bonds between the numerous hydroxyl groups. As a result, cellulose is insoluble in water or even alkali, as the tight packing prevents solvent penetration and hydration. Amylose on the other hand, forms alternating U-turn structures which adopts a helical structure and is soluble in water. Other figures illustrate the various linkage types and their geometry. The zig-zag types i.e. $\beta(1\rightarrow4)$ linked glucose (a) and $\alpha(1\rightarrow4)$ linked galactose (e) usually form a ribbon conformation while the U-turn types i.e. $\beta(1\rightarrow3)$ (b) and $\alpha(1\rightarrow4)$ (f) form a hollow helix conformation. In these ordered conformations (helices and ribbons), the torsion angles of glycosidic linkages (ϕ, ψ or ω) are fixed due to interactions between residues. Xanthan, carrageenan and gellan gum adopt a helical structure in solution while alginates are of the ribbon type conformation. The conformation is however highly subjected to concentration, solvent, temperature, pH or ionic strength conditions (Serge & Karim, 2004; Steve & Qi, 2005a).

The random coil is a typical disordered conformation of most linear polysaccharides in solutions, whereby the local conformation (between individual monosaccharide units) and overall chain conformation is constantly fluctuating as a result of a high degree of freedom and flexibility about the glycosidic linkages. The random coil therefore has no well-defined shape or size as it is continuously changing its shape. Most linear polysaccharides adopt the random coil conformation in solution, especially in dilute concentrations. Highly branched polysaccharides exist in the form of compact globular structures in solution instead (Pieter, 2003).

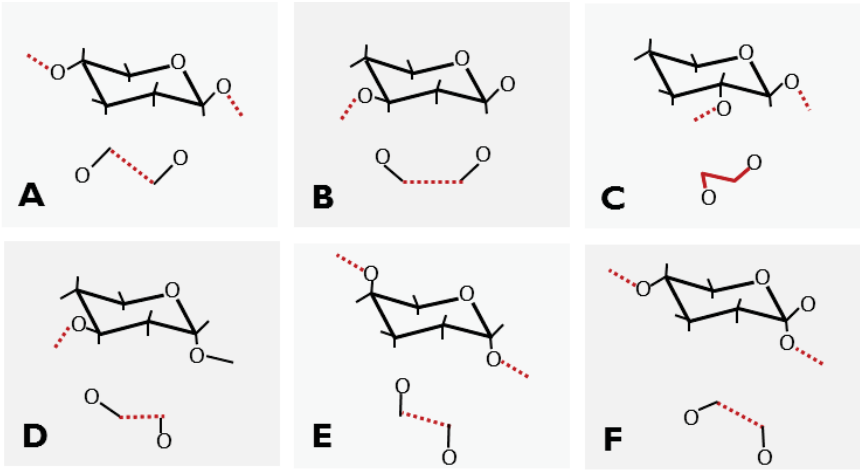

Figure 2.7 – Geometrical representation of various glycosidic linkage types in D-glucose; a) zig-zag β(1→4), b) U-turn β(1→3), c) twisted β(1→2), d) zig-zag α(1→3), e) zig-zag α(1→4)-D-galactose, f) U-turn α(1→4) (adapted from Oakenfull, 1998)

2.3 Physical and Molecular Properties of Polysaccharides

2.3.1 Molecular Weight and Distribution

Molecular weight is a fundamental property of polysaccharides which many other physical properties are dependent on. However, it cannot be expressed as an absolute figure for a particular polysaccharide as with smaller molecules. This is owing to the polydispersity of polysaccharides, i.e. not every polysaccharide chain has the same number of monomer units, which gives a distribution of molecular weight instead. Therefore molecular weights are expressed as *averages*, mainly the number average molecular weight (M_n) (Equation 2.1), weight average molecular weight (M_w) (Equation 2.2), z-average molecular weight (M_z) (Equation 2.3), and viscosity average molecular weight (M_v) (Equation 2.8), where n_i is the number of molecules and c_i is concentration of the molecules having molecular weight M_i.

The weight average molecular weight (M_w) is most commonly used for polysaccharides as it is most accurate for large polymer chains. It emphasises on the heavier molecules whereas M_n is more sensitive to smaller molecules present (if any). The polydispersity index is used to measure the extent of molecular weight distribution. It is the ratio of $M_w/M_{n,}$ with polysaccharides generally having a polydispersity index between 1.5 and 2.0 (Steve & Qi, 2005b). The molecular weight type measured depends on the technique used. Light scattering and sedimentation equilibrium measures M_w, membrane osmometry measures M_n and sedimentation equilibrium measures M_z. Figure 2.8 compares the different molecular weight values obtained for the same heterogeneous polysaccharide solution.

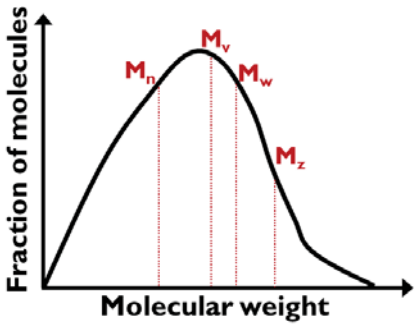

Figure 2.8 – Comparison between molecular weight measurement types (M_n, M_v, M_w, M_z) for a heterogeneous polysaccharide (adapted from Steve & Qi, 2005b)

$$M_n = \frac{\sum_{i=1}^{\infty} M_i n_i}{\sum_{i=1}^{\infty} n_i} = \frac{\sum_{i=1}^{\infty} c_i}{\sum_{i=1}^{\infty} c_i / M_i} \qquad \textbf{Equation 2.1}$$

$$\boldsymbol{M_w = \frac{\sum_{i=1}^{\infty} M_i^2 n_i}{\sum_{i=1}^{\infty} M_i n_i} = \frac{\sum_{i=1}^{\infty} M_i c_i}{\sum_{i=1}^{\infty} c_i}} \qquad \textbf{Equation 2.2}$$

$$M_z = \frac{\sum_{i=1}^{\infty} M_i^3 n_i}{\sum_{i=1}^{\infty} M_i^2 n_i} = \frac{\sum_{i=1}^{\infty} M_i^2 c_i}{\sum_{i=1}^{\infty} M_i c_i} \qquad \textbf{Equation 2.3}$$

2.3.2 Intrinsic Viscosity

Intrinsic viscosity is a property of dilute polysaccharide solutions used to characterise the hydrodynamic volume occupied by the individual polymer chains in a given solvent. It is not explicitly related to viscosity, since its units are expressed in [volume]/[mass] form i.e. ml/g. The molecular structure of the polysaccharide is the primary determinant of intrinsic viscosity. In general, the intrinsic viscosity increases in the following molecular structure order: branched < random coil < linear (Pieter, 2003).

Intrinsic viscosity is derived from two other properties of the dilute polysaccharide solution, relative viscosity and specific viscosity. Relative viscosity is simply the ratio of polysaccharide solution viscosity to solvent viscosity (Equation 2.4), where η_{rel} is the relative viscosity, η the viscosity of polysaccharide solution and η_s the viscosity of the solvent. Specific viscosity describes the fractional increase in viscosity of the solvent in the presence of the polysaccharide, which is therefore linked to relative viscosity as shown in Equation 2.5. Relative and specific viscosities usually increase with polymer concentrations; however, intrinsic viscosity is a property inherent to the polymer thus it does not depend on polymer concentration (Steve & Qi, 2005b).

$$\eta_{rel} = \frac{\eta}{\eta_s} \qquad \textbf{Equation 2.4}$$

$$\eta_{sp} = \frac{\eta - \eta_s}{\eta_s} = \eta_{rel} - 1 \qquad \textbf{Equation 2.5}$$

Equation 2.6a and Equation 2.7a are the Huggins (1942) and Kraemer (1938) equations respectively, where [η] is the intrinsic viscosity (ml/g), c is the concentration of the polymer (g/ml) and K' and K" are the Huggins and Kraemer coefficients. By extrapolating both equations Equation 2.6a and Equation 2.7a to zero (i.e. lim→0), the intrinsic viscosity can be obtained. To obtain linear plots of the relationship between η_{sp} and ln(η_{rel}) and c, the graph of η_{sp}/c and ln(η_{rel})/c vs. c is constructed and [η] is obtained as the average intercept of the two equations.

The Huggins coefficient, K' characterises the hydrodynamic interactions between polymer chains. Polysaccharides in good solvents usually have values between 0.3-0.4, and 0.5-0.8 in theta solvents (Morris, 1989). Also, for a random coil polymer, theoretical values of K'-K"=0.5 are obtained.

$$a)\ \eta_{sp} = [\eta]c + K'[\eta]^2c^2;\ b)\ [\eta] = \lim_{c\to 0}\left(\frac{\eta_{sp}}{c}\right) \quad \text{Equation 2.6}$$

$$\text{a)}\ \ln(\eta_{rel}) = [\eta]c + \left(K^{"} - 0.5\right)[\eta]^2c^2;\ b)\ [\eta] = \lim_{c\to 0}\left(\frac{ln\eta_{rel}}{c}\right) \quad \text{Equation 2.7}$$

$$[\eta] = kM_v{}^{\alpha} \quad \text{Equation 2.8}$$

The molecular weight of the polysaccharide can also be related to its intrinsic viscosity according to the Mark-Houwink relationship (Equation 2.8), where both k and α are constants which can be used to estimate the conformation of the polysaccharide. The exponent α usually has a value in the range of 0.5-0.8 for flexible polymers in a good solvent. Branched polymers e.g. gum arabic or amylopectin would have values below 0.5, and stiff linear polymers above 0.8 (Steve & Qi, 2005b).

2.3.3 Solubility

As mentioned previously in section 2.2.3, the solubility of polysaccharides depends highly on the regularity of its structure and conformation. Polysaccharide chains which are too closely packed in regular crystalline structures (e.g. cellulose) would not allow solvent penetration–dissolution, whereas molecules with irregularities along the chain would prevent close-packing and allow the solvent molecules to interact and hydrate the polysaccharide. Polysaccharides therefore exhibit a wide range of solubility; some like cellulose are insoluble in water, some which are only soluble in hot water e.g. locust bean gum, and most which are readily dissolved in cold water e.g. xanthan gum. The presence of ionic/hydrophilic groups also confers solubility to the polysaccharide. The charged groups e.g. carboxylic acid (COOH) or sulphonate groups (OSO_3) form stronger hydrogen bonds with the water molecules as they are more polar than the hydroxyl (OH) groups of neutral polysaccharides.

2.3.4 Concentration

The physical and therefore functional properties of polysaccharides are highly dependent on their concentration. Polysaccharide solutions can be dilute, semi-dilute, or concentrated (Morris, Cutler, Ross-Murphy, Rees, & Price, 1981); a specific concentration level distinguishes one regime from another for every individual polysaccharide. Figure 2.9 compares and illustrates the difference in volume occupied by the polymer chains in a dilute, semi-dilute or concentrated solution.

For a dilute solution, each polysaccharide molecule and its solvent occupy a discrete hydrodynamic space in solution and the whole molecule is free to assume any orientation with respect to neighbouring molecules. A dilute solution would not exhibit any functional properties such as thickening or gelation; however, fundamental molecular properties such as intrinsic viscosity, molecular weight, radius of gyration and conformation are studied in the dilute concentration regime. Above a critical concentration i.e. overlap concentration, c*, the individual molecular domains start to overlap with each other and form entangled networks. The solution is now in the semi-dilute regime. The rheology of polysaccharides in this concentration regime is of greatest interest in food applications as they start to display non-Newtonian behaviour. When c >> c*, the solution is in the concentrated regime (Pieter, 2003). For a large number of polysaccharides, plotting

the specific viscosity η_{sp} with coil-overlap parameter c[η] gives a slope of approximately 1.4 and 3.3 in the dilute and concentrated regime respectively (Figure 2.9) (Morris, et al., 1981).

Figure 2.9 – Concentration regimes of polysaccharide solutions. From left: dilute, semi-dilute and concentrated (adapted from Pieter, 2003)

2.4 Rheological Properties of Polysaccharides

The rheology of polysaccharides is often studied from three approaches – macrorheology, structural rheology and applied rheology (Miri, 2010). Macrorheology is concerned with the bulk rheology of the polysaccharide on a macroscopic level. The main objective is to obtain rheological parameters using equations which apply to the deformation response of the material, such as viscosity and normal stresses. The molecular nature of the polysaccharide is not of interest in macrorheology, but it is the domain for structural rheology. Structural rheology is concerned with the relationship between the bulk rheological properties and its microscopic structure. Molecular conformation, molecular weight and degree of branching of the polysaccharide is most commonly inferred from complementary intrinsic viscosity, zero-shear and shear-dependent viscosity data. Other molecular phenomena such as gelation, structural breakdown, phase separation, polymer association, electrostatic screening/repulsion, particle jamming and viscoelasticity can be elucidated from various rheological methods. Finally, applied rheology pertains to simulating conditions of processing e.g. extrusion, pipe-flow and mixing, handling and consuming food products where their rheology is governed by the polysaccharide.

2.4.1 Shear-dependent Viscosity

The shear-dependent viscosity (frequently referred to as rheology itself) is intricately related to the concentration regime of the polysaccharide i.e. whether dilute, semi-dilute or concentrated. In the dilute regime, polysaccharide solutions usually exhibit Newtonian flow behaviour and thus they do not display any functionality at dilute concentrations. For practical reasons, this concentration region is only used for studying molecular characteristics of the polysaccharide. At concentrations above the critical overlap concentration i.e. into the semi-dilute and concentrated regimes, non-Newtonian flow behaviour and viscoelasticity start to manifest. The flow behaviour can be shear-thinning or shear-thickening, although it is perhaps the former for nearly all natural unmodified polysaccharides characterised till date. The molecular origin of shear-thinning in polysaccharides is described here, and the shear-thickening behaviour will be discussed in the next section.

Figure 2.10 illustrates the typical viscosity curve of a shear-thinning polysaccharide. It is divided into three main regions – i) the Newtonian plateau at low shear rates, ii) the shear-thinning region at intermediate shear rates and iii) the Newtonian plateau at high shear rates. In reality, the Newtonian region at high shear rates is usually not observed as the shear rate range of laboratory-scale rheometers or viscometers is limited to about $3000s^{-1}$. The shear rate at which onset of shear-thinning occurs is termed the critical shear rate. Again, depending on the sensitivity of the instrument, the low shear Newtonian plateau may or may not be accurately recorded.

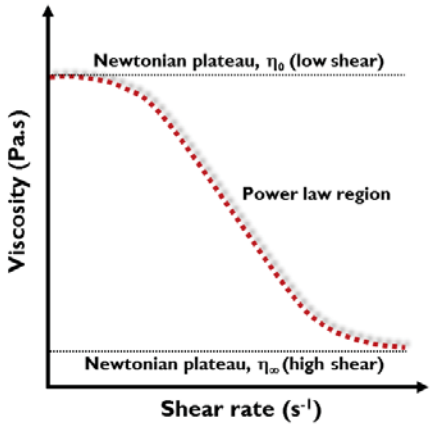

Figure 2.10 – Typical flow curve exhibited by a shear-thinning polysaccharide(Jacques & Jean-Louis, 2004)

In simple terms, the shear-thinning behaviour is the result of chain disentanglement with shear, and the subsequent alignment of the chains in the direction of the shear field. Since chain entanglement is the main cause of shear-thinning behaviour, this effect is therefore only observed when concentrations are in the semi-dilute or concentrated regime.

At rest, the polysaccharide chains would adopt a conformation of least energy, presumably a spherical coil which is entangled with the neighbouring chains. In the presence of a shear field, the chains are disentangled from one another, but Brownian motion restores the entanglements back to the state of least energy. The viscosity at any one shear rate is the net balance of entanglement density reduction by shear and the re-entanglement by Brownian motion. Porter & Johnson (1966) interpreted the Newtonian and shear-thinning regions based on a characteristic time of the polymer. The characteristic time, τ_e, of the polymer is the time associated with the movement of the polymer and the duration for which it stays in proximity of neighbouring chains in order for entanglements to take place. At higher shear rates, the molecules are separated by flow thus τ_e is short. In order for entanglements to form, relaxation time of the polymer λ must be greater than τ_e i.e. chain is re-entangled before the polymer completely relaxes and disentangles from other chains; Therefore at low shear rates, $\lambda>\tau_e$, and viscosity appears to remain constant i.e. Newtonian. An alternative characteristic time parameter apart from the τ_e interpreted by Porter & Johnson (1966) is τ_d, in the reptation theory by Doi and Edwards (1988). This is the time required for the chain to diffuse one chain length L along its own contour. Similarly, when $\lambda>\tau_d$, the chains are able to re-entangle and maintain viscosity. Above the critical shear rate, the chains disentangle at a faster rate than chain re-entanglement therefore shear-thinning occurs, i.e. $\lambda<\tau_{e/d}$.

The flow curves from the low shear Newtonian to power law region can be predicted using constitutive equations of the Cross (Equation 2.9) and Carreau (Equation 2.10) models where η is the viscosity at a shear rate, $\dot{\gamma}$, η_0 is the zero-shear viscosity, and λ is the structural relaxation time. For shear-thickening fluids, a modified Cross model (Equation 2.11) based on different regions of the curve can be used (Galindo-Rosales, Rubio-Hernández, & Sevilla, 2011; Galindo-Rosales, Rubio-Hernández, Sevilla, & Ewoldt, 2011) where λ_I, λ_{II}, λ_{III} are the characteristic relaxation times associated with regions I (prior to shear-thickening), II (during shear-thickening) and III (after shear-thickening) respectively, $\dot{\gamma}_c$ is the shear rate at onset of shear-thickening, $\dot{\gamma}_{max}$ is the shear rate at the peak of shear-thickening and η_{crit} and η_{max} are the critical and maximum viscosities at $\dot{\gamma}_c$ and $\dot{\gamma}_{max}$, respectively.

$$\eta(\dot{\gamma}) = \frac{\eta_0}{[1+(\lambda\dot{\gamma})^{1-n}]} \qquad \textbf{Equation 2.9}$$

$$\eta(\dot{\gamma}) = \frac{\eta_0}{[1+(\lambda\dot{\gamma})^2]^{(1-n)/2}} \qquad \textbf{Equation 2.10}$$

$$\eta(\dot{\gamma}) = \begin{cases} (a)\ \eta_I\ (\dot{\gamma}) = \eta_c + \dfrac{\eta_0 - \eta_c}{1+\left[\lambda_I\left(\dfrac{\dot{\gamma}^2}{\dot{\gamma}_c \cdot \dot{\gamma}}\right)\right]^{\eta_I}} & \text{for } \dot{\gamma} \le \dot{\gamma}_c \\ (b)\ \eta_{II}\ (\dot{\gamma}) = \eta_{max} + \dfrac{\eta_c - \eta_{max}}{1+\left[\lambda_{II}\left(\dfrac{\dot{\gamma} - \dot{\gamma}_c}{\dot{\gamma}_{max} - \dot{\gamma}}\right)\right]^{\eta_{II}}} & \text{for } \dot{\gamma}_c < \dot{\gamma} \le \dot{\gamma}_{max} \\ (c)\eta_{III}(\dot{\gamma}) = \dfrac{\eta_{max}}{1+[\lambda_{III}(\dot{\gamma} - \dot{\gamma}_{max})]^{\eta_{III}}} & \text{for } \dot{\gamma}_{max} < \dot{\gamma} \end{cases} \qquad \textbf{Equation 2.11}$$

2.4.2 Viscoelasticity

The thick, slimy consistencies of polysaccharides are usually indicators of viscoelasticity in the polysaccharide. In other words, the polysaccharide exhibits both elastic and viscous behaviour under deformation, which is characterised with dynamic oscillatory shear and quantified using parameters such as storage (G') and loss (G") moduli.

When an oscillatory flow is applied to a dilute polysaccharide solution (in the linear viscoelastic region), configurational motions are derived from rotations around the bonds in the chain backbone. G' is contributed by the polysaccharide solute alone, while G" measures energy dissipation from both the solute and solvent. At very low frequencies, all possible configurational rearrangements of the molecule can occur. The polymer coil deforms easily and spontaneously such that the force in phase with displacement is negligible and G'→0. At higher frequencies, neighbouring regions of the chain have time to change their relative positions within a period of cyclic deformation and deforms more easily. At very high frequencies, there will be no time for any internal rotation within a cycle, and response of the molecule will be limited to bending and stretching of chemical bonds (Lapasin & Pricl, 1999).

For concentrated polysaccharide solutions, the chains are entangled and form a physical network. The typical mechanical spectrum of an entangled polymer solution over a wide frequency range is shown on Figure 2.11. In the terminal region, polymer chains are able to regain their equilibrium configuration through Brownian motion within the time scale of the experiment, hence the solution appears to be a viscous liquid where G''>G'. On increasing frequency, it reaches a point where G'=G''; the inverse of the frequency at this point (crossover frequency) is the relaxation time, τ_d. To put it simply, the relaxation time is the time taken for the polymer to return to equilibrium state after being disturbed in some manner. The material reaches the viscoelastic plateau where G' dominates and the solution shows elastic behaviour. At still higher frequencies, the molecule transitions to the glassy zone where there is less dependence on frequency. The frequency is so high that no configurational rearrangements of the chain backbones have enough time to take place, and effects are similar to those seen for dilute solutions.

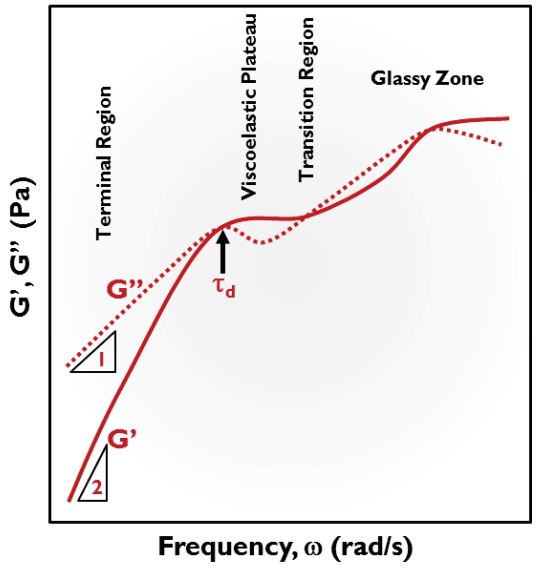

Figure 2.11 – Typical mechanical spectrum *i.e.* storage (G', —) and loss (G'', ---) moduli with angular frequency of an entangled polymer system; τ_d: relaxation time at crossover frequency (adapted from Jacques & Jean-Louis, 2004)

2.4.3 Extensional Viscosity

Apart from shear viscosity and viscoelasticity, extensional viscosity of polysaccharide solutions can also be measured and characterised. Extrusion, sheeting, coating, stretchability, pourability, stringiness, swallowing (Mackley et al., 2013), perception of taste (Koliandris, 2010) and mouthfeel are examples of some events which have a large extensional component which has to be taken into consideration (Padmanabhan, 2010). Not limited to food applications, extensional rheometry is also significant in turbulent drag-flow reduction, inkjet printing and oil recovery. However, considerably less information in the literature is available on the extensional viscosity of polysaccharide solutions compared to rotational shear viscosity data. Polysaccharide solutions are often too weakly viscoelastic to be measured in most standard extensional rheometers, where a steady-state extensional rate is difficult to achieve (Dogan & Kokini, 2006).

Under shear, the polymer molecules rotate and gradually align in the direction of flow whereas under extensional flow, they are orientated and stretched, possibly to full extension or alignment with flexible or rigid molecules respectively (Figure 2.12) (McKinley & Sridhar, 2002; Padmanabhan, 2010). Therefore further information on the molecular structure can be elucidated from extensional testing, complementing data from shear rheology. The ratio between extensional and shear viscosity is known as the Trouton (*Tr*) ratio. For Newtonian fluids, *Tr* is constant *i.e.* 3. The numbers are much higher for viscoelastic or highly elastic fluids, finding values up to 10^4 (Macosko, 1994).

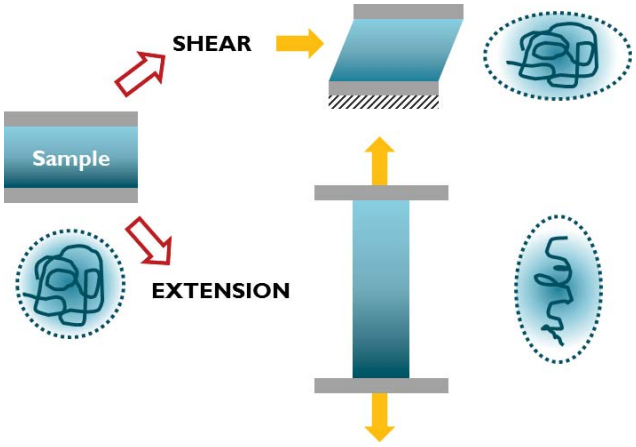

Figure 2.12 – Illustration of molecule under shear (weak) and extensional (strong) deformation (adapted from Padmanabhan, 2010)

The deformation of many biological materials is poorly represented by conventional rotational rheology alone. Many biological processes such as blood circulation (Lacombe & Essabbah, 1981) and the role of saliva during mastication (Haward, Odell, Berry, & Hall, 2011) include both shear and extensional components. In plants, extensional properties would be relevant to cell wall extension (Cleland, 1971).

There are several techniques available to measure extensional viscosity, depending on the viscosity and elasticity of the material. High viscosity polymer melts are typically measured using for example drum windup, bubble collapse, or converging die flow. Viscoelastic solutions such as polysaccharides, foodstuffs, suspensions and paints are commonly measured using filament stretching or capillary breakup rheometers. Even lower viscosity solutions which are not well-characterised with filament devices can be measured using opposed jet devices in stagnation or contraction flows (Macosko, 1994; Shaw, 2012).

Comparing extensional viscosity, relaxation time, elastic moduli and filament breakup time of various galactomannans helped to differentiate the strength of intermolecular associations of LBG, guar gum and galactomannans from unconventional seed sources (Bourbon et al., 2010). Presence of xanthan gum mixed with saliva improved the filament breakup time, indicating a slower flavour release from foods thickened with the gum (Choi, Mitchell, Gaddipati, Hill, & Wolf, 2014). Extensional rheology can also provide information on conformation of the polymer, where the magnitude of extensional viscosity is proportional to its degree of branching (Hwang & Kokini, 1991).

2.5 Shear-Thickening Rheology

Shear-thickening is principally defined as the increase in apparent viscosity of a fluid when shear rate increases. It is synonymous with the term 'dilatancy', although dilatancy implies attributing shear thickening to a volume increase. It is not common to come across shear-thickening in materials. The earliest shear thickening material reported dates back to 1954 on polyvinyl chloride suspended in plasticizers (as cited in Chaffey, 1977). Subsequently, with the advent of controlled shear rheometers, other shear-thickening materials surfaced, notably polyvinyl alcohol-borate complexes (Savins, 1968), polymethyl methacrylate (PMMA) (Jiang et al., 2010), (as cited in Chaffey, 1977) polyethylene oxides (PEO) (S. X. Ma & Cooper, 2001), partially hydrolysed polyacrylamide (HPAM) (Hu, Wang, & Jamieson, 1995), hydrophobically modified ethoxylated urethane (HEUR) (Tam, Jenkins, Winnik, & Bassett, 1998) and silica nanoparticle suspensions (Bender & Wagner, 1996). Researchers have continuously attempted to unravel the molecular origin of shear thickening, using methods such as rheological modelling of polymer dynamics, varying polymer molecular weight, concentration and solvent, and employing rheo-optical techniques. However till date, the true mechanism still remains unclear for most systems. Two materials exhibiting similar shear-thickening flow curves may be of a completely different molecular origin of shear-thickening.

When a material is said to be shear-thickening, it does not imply that the apparent viscosity only increases throughout the whole shear rate range measured. Instead, it may refer to a shear-thickening effect observed within certain shear rates. In fact, most materials referred to as 'shear-thickening' in this research exhibit a typical Newtonian, followed by shear-thickening and then shear-thinning behaviour. Figure 2.13 shows three common flow regimes for shear-thickening materials.

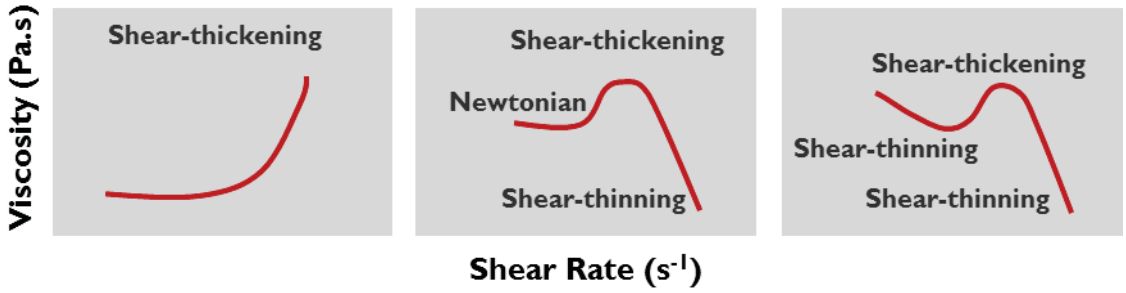

Figure 2.13 – Schematic viscosity curves of different shear-thickening behaviour in materials

A literature search on shear-thickening materials revealed that most of the shear-thickening materials are synthetic and/or non-organic polymers and molecules. Naturally occurring polymers – biopolymers - with shear-thickening properties are rarely encountered and most are chemically modified. Some examples of shear-thickening biopolymers include pectin (Kjøniksen, Hiorth, & Nyström, 2005; Kjøniksen, Hiorth, Roots, & Nyström, 2003), hydrophobically modified HM-alginate (Burckbuchler et al., 2006), waxy maize starch (S. Kim, Willett, Carriere, & Felker, 2002), 1-deoxylactit-1-yl chitosan (Yalpani, Hall, Tung, & Brooks, 1983), enzymatically-synthesised dextran (Sabatié, Choplin, Paul, & Monsan, 1986), dextran-honey (Bagley & Dintzis, 1999) and β-glucan-amylodextrin (Carriere & Inglett, 1998) systems.

Whether synthetic or natural, these shear-thickening materials can be broadly classified into three key classes i.e. suspensions, worm-like micelles and associating polymers. Materials within the same class are more likely to originate from the same cause of shear thickening, although there have certainly been exceptions. The last review made on shear-thickening materials (suspensions, associating polymers, worm-like micelles and poor polymer solutions) and the associated mechanisms was done by van Egmond (1998). In the case of polysaccharides, shear-thickening in associating polymers would be a more appropriate model to compare and reference against. This work therefore aims to build on the existing review by van Egmond on shear-thickening materials and the mechanisms by focusing on literature work published within the last decade (2000-2014), on associative polymers in particular.

2.5.1 Associative Polymers

Associative polymers are polymers which contain segments that tend to associate together in selective solvents. These groups may be grouped together in blocks or randomly distributed along the chain. In a recent review by Chassenieux, Nicolai and Benyahia (2011) on associative polymers, the authors have classified associative polymers into three major groups: i) polymers with a single associative block (Figure 2.14a), ii) polymers with two associative end blocks (Figure 2.14b), and iii) polymers with many associative groups (Figure 2.14c). These associative groups are usually hydrophobic or ionic groups, or groups capable of forming hydrogen or dipolar bonds with another group. Polyelectrolytes belong to the third group of associative polymer with ionic groups randomly distributed along the chain. The presence of associating groups in polymers gives rise to functional rheological properties, such as shear-thinning, gelation and shear-thickening. However, only the shear-thickening associative polymers are of interest in this work.

Figure 2.14 – a) polymers with a single associative block b) polymers with two associative end blocks c) polymers with many associative groups (red: associating blocks, blue: solvophilic blocks) (adapted from Chassenieux, et al., 2011)

The terms 'telechelic polymer' and 'ionomer' are frequently come across in associative polymers; the former refers to a polymer with associative groups at the ends (i.e. Figure 2.14b), while the latter refers to a polymer containing ionic groups, but no more than 15% of the polymer. Several works have also referred the associative groups as 'sticker' groups (Baljon-Haakman & Witten, 1992; Leibler, Rubinstein, & Colby, 1991).

2.5.2 Shear-Thickening Mechanisms

The interest on shear thickening materials and mechanisms was high from the late 1980s till early 2000s. During this period, many researchers have either come up with theoretical models predicting molecular associations and chain behaviour under shear, or made use of these models to explain shear thickening in the material studied. The most widely accepted (and also challenged) theories were the shear-induced cross-linking (Ballard, Buscall, & Waite, 1988; Witten Jr & Cohen, 1985), the transient network theory (Tanaka &

Edwards, 1992; S. Q. Wang, 1992) and the sticky reptation theory (Leibler, et al., 1991). Further theories and molecular simulations on shear-thickening were subsequently developed based on these earlier studies. The underlying concept of shear-thickening in associative polymers is that associations leading to structure formation should only take place *during* shear. If association already occurred in the quiescent state then a shear flow would only deform the network and produce free associative groups at high shear rates with no shear-thickening observed.

2.5.2.1 Shear-Induced Cross-Linking

Shear-thickening quintessentially means 'shear-induced' thickening, and 'thickening' would imply some sort of structural formation/change as a result of polymer associations. Then, based on the fundamental notion of 'shear-induced associations', pioneering researchers have come up with theoretical models with various cross-linking pathways induced by shear (Ballard, et al., 1988; Witten Jr & Cohen, 1985).

One of the earliest mechanisms was proposed by Witten and Cohen in cross-linking ionomers (Witten Jr & Cohen, 1985). They postulated that shear flow increases the probability of intermolecular associations at the expense of intramolecular ones, and have proven this hypothesis by mean-field approximation and statistical calculations. The occurrence of shear thickening is described as a positive-feedback cycle; elongation of chain leads to intermolecular associations, which results in an increase in viscosity, which increases relaxation time, and produces further elongation. A first-order gelation was predicted as a result of the intermolecular associations, where a fluid phase coexists with the gel phase. Subsequent shear-thinning of the polymer occurs when the shear becomes larger than the chain relaxation rate.

A similar mechanism was also put forward by Ballard, Buscall and Waite (Ballard, et al., 1988). They also suggested that shear-thickening was caused by a transfer from intra- to intermolecular associations, and agreed with Witten et al's theory that the elongation of the chain during shear increases the number of cross-links between polymer chains. At rest, the polymer adopts a coiled conformation which is linked intra-molecularly. Under shear, the chain extends and the intramolecular associations are broken. The extended conformations of the chains allow the formation of intermolecular bonds, which become a physical network of increased resistance to flow. Viscosity therefore increases, leading to what is observed as shear-thickening. This model however only accounts for finite viscosity increase with shear, and does not predict any shear-thinning which may occur after shear-thickening.

Figure 2.15 illustrates the generic shear-thickening mechanism of cross-linking polymers, as a result of increased intermolecular association during shear and chain extension.

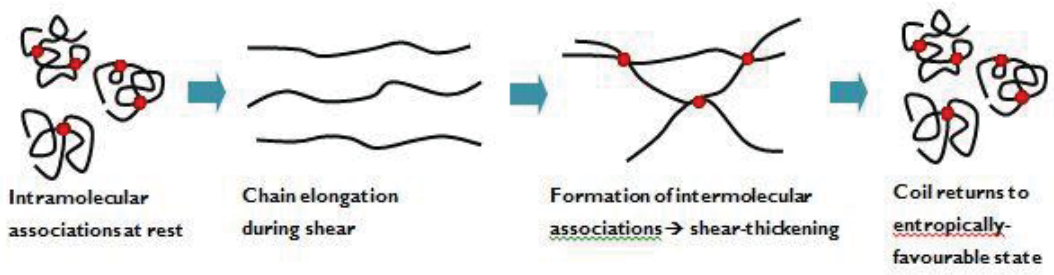

Figure 2.15 – Schematic mechanism of shear-thickening due to cross-linking during shear (adapted from Ballard, et al., 1988)

2.5.2.2 Transient Network Theory

A transient network is a network made up of elastic strands which are joined by temporary reversible junctions. The underlying principle of a transient network is the continuous creation and destruction of random junctions, which causes the strands to connect or disconnect from the network, giving rise to the 'transience' in transient networks. The material is therefore never at a quiescent state, even at equilibrium. Brownian motion is the cause of this phenomenon. The transient network theory was originally developed by Green and Tobolsky (1946) to describe the stress-relaxation behaviour of viscoelastic polymers. Under deformation, the disappearing network has already been strained by the deformation accumulated during its lifetime, while the forming network incorporates strands with less stress as it had additional time to relax before joining the network. The net overall effect leads to stress-relaxation in the polymer, and relaxation time is related to the junction lifetime. A key assumption/feature of a transient network is that the total concentration of junctions always remain constant, therefore elastic properties are constant as well. The transient network theory was later on refined by Tanaka and Edwards (1992), and subsequently extended to integrate shear-thickening in materials (Indei, Koga, & Tanaka, 2005; Koga & Tanaka, 2005; S. Q. Wang, 1992).

Wang (1992) distinguished chain types involved in cross-linking and network formation, namely stress-bearing effective chains, dangling chains with one end attached to the network, and individual chains free of interchain bonding (Figure 2.16). Shear-thickening arises when free chains are attached into the network by shear, producing effective chains which participate in network formation. The model predicts that at higher shear rates, rate of chain breakage increases and relaxation time of the network shortens, which result in shear-thinning. A limitation of transient network theory models is that only telechelic polymers (i.e. associative groups at chain ends) have been used in the model development. Polymers with associative groups distributed along the chain may not behave as described by the models.

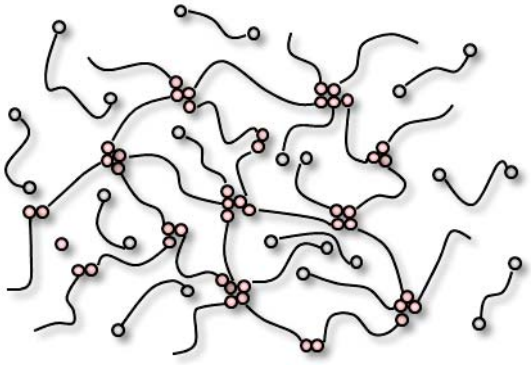

Figure 2.16 – Schematic illustration of effective (●--●), free (○--○) and dangling (●--○) chains in a transient network model (adapted fromS. Q. Wang, 1992)

2.5.2.3 Non-Gaussian Chain Stretching

Marrucci, Bhargava and Cooper (1993) proposed a theory which is distinctly different from previous shear-induced cross-linking or network formation models. It builds on the transient network theory but instead of attributing shear-thickening to associative actions, they suggested that shear-thickening is caused by the network chains stretching into the non-Gaussian regime. However, the magnitude of shear-thickening observed for non-Gaussian chain stretching is small, and may not be sufficient to explain the shear-thickening observed in various systems (S. X. Ma & Cooper, 2001).

A Gaussian chain is a mechanical model (also known as random walk model), describing a polymer constructed by (N+1) 'beads' connected by a harmonic spring of stored potential energy, U_0. In a Gaussian chain, the distribution of the vector $R_n - R_m$ between any two units n and m is Gaussian.

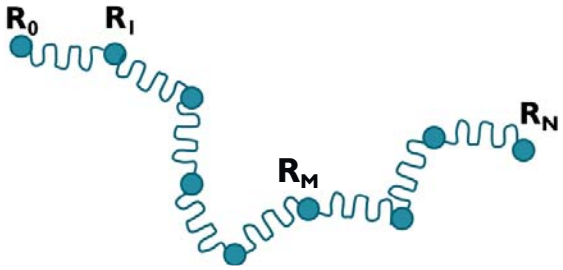

Figure 2.17 – Gaussian chain (adapted from Doi & Edwards, 1988)

When the chain end dissociates from a network junction, it can only partially relax its extended conformation since it is soon recaptured by the network again. As a consequence, the maximum viscosity occurs at a critical shear rate when the ratio of the detachment frequency to the shear rate (which decreases monotonically with increasing shear rate) has not dropped to its asymptotic lower bound, and yet the polymer chains are already stretched close to their maximum extension.

2.5.2.4 Structural Breakdown (TCMM Model)

Contrary to the usual school of thought that shear leads to association of molecules, structure formation and therefore the increase in viscosity. Edwards, Keefer & Reneau (2002) have found based on flow birefringence

and dichroism that shear-thickening was in fact caused by breakdown of structures formed at lower shear rates. Previously, Kishbaugh & McHugh (1993) observed that the critical shear rate (shear rate at onset of shear-thickening) was found to coincide with the shear rate at maximum dichroism. The linear birefringence also increased with shear rate. They explained that the growth in dichroism values prior to shear thickening was attributed to formation of optically isotropic particles (of micron size) consisting of associated polymer chains. The stretching and extension of the remaining non-associated polymer chains in solution was the cause for the increase in linear birefringence. Edwards *et. al.* (2002) then contested that the occurrence of shear thickening at the same shear rate as maximum linear dichroism was a coincidence, since dichroism should theoretically continue to rise as the structures continued to grow. They proposed the Two-coupled Maxwell Modes (TCMM) model, which states that the structures grow at low shear rates (way before critical shear rate), and cause the dichroism values to increase. At the critical shear rate, strong hydrodynamic forces cause the structures to decrease in size and also increase shear stress (therefore viscosity). Consequently the reduction in particle size results in the retraction of the dichroic signal. The TCMM model and previous rheo-optical studies by Kishbaugh and McHugh were based on dilute polymer solutions e.g. polypropylene, polystyrene.

2.6 Intermolecular Interactions in Polysaccharides

Biopolymers like polysaccharides and proteins are made up of numerous functional groups capable of intermolecular associations via electrostatic attraction ($-COO^-$, $-SO_3^-$), hydrogen-bonding (-OH, $-NH_2$, -C=O) and/or hydrophobic associations ($-CH_3$, $-COOCH_3$). Studies done on various classes of materials such as micelles (Vasudevan, Shen, Khomami, & Sureshkumar, 2008) (cetyl-trimethylammonium bromide/sodium salicylate solution), polysaccharides (pectin) (Kjøniksen, et al., 2003) and hydrophobic polymers (Feng, Grassl, Billon, Khoukh, & François, 2002; Tan, Tam, & Jenkins, 2001) have attributed intermolecular associations formed during shear to the shear-thickening phenomenon, similar to the mamaku polysaccharide.

2.6.1 Hydrogen Bonds

Hydrogen bonds are a special class of directional dipole-dipole interaction between a positively polarised (electron depleted) hydrogen atom and an electronegative atom as depicted by $–X^-\cdots H^+–$ (Israelachvili, 2011). The monosaccharides e.g. pentoses which make up the polysaccharide typically consist of three hydroxyl (OH) groups, the ring O atom, glycosidic bond O atom and C-H groups, all of which are capable of forming weak to moderately strong hydrogen bonds. For acidic polysaccharides, hydrogen bonds could also be formed between carboxyl (C=O) and/or hydroxyl groups of the neutral sugar and uronic acid groups (Oakenfull, 1998). Solvation of the polysaccharide is controlled by hydrogen bonding between water molecules and the polysaccharide chains, with also intramolecular hydrogen bonding stabilising intermolecular structures (Whistler, 1973). Intra- and intermolecular hydrogen bonding in galactomannans have given rise to higher viscosities as a result of ordered packing between the mannose backbone and galactose side chains (Morris, et al., 1981).

Hydrogen bonds are enthalpy-driven, and the bond length and strength is in the order of kT, where k is the Boltzmann constant and T is the absolute temperature. Increasing the temperature would promote thermal motion, and break the existing hydrogen bond if kT exceeds the interaction energy of the hydrogen bond. (Dougherty, 1998; Israelachvili, 2011). For polymers e.g. poly(vinyl alcohol) and poly(ethylene oxide) with rheological properties highly dependent on hydrogen bonding, a significant change in flow behaviour with temperature could be observed (Briscoe, Luckham, & Zhu, 2000; Rivero, Gouveia, Mueller, & Saez, 2012). Urea is a chaotropic agent (i.e. disrupts hydrogen bonds) which is commonly used to interfere with secondary and/or tertiary structures formed via hydrogen bonding, especially in the denaturation of proteins (Rossky, 2008). Other chaotropic agents include guanidine and guanidinium chloride. Urea has three polar groups, two NH_2 groups and one C=O group, all of which are capable of forming hydrogen bonds with other polar functional groups containing hydrogen such as amine (NH_2) or hydroxyl (OH) groups. Therefore it interferes with the existing hydrogen bonds by coming between hydrogen bond-forming groups and forming new hydrogen bonds with these groups. The use of urea in probing shear-induced association and/or gelation in polymers has been effective as many of these associations are based on hydrogen bonding (Cho, Heuzey, Begin, & Carreau, 2006; Kjøniksen, et al., 2005; Kjøniksen, et al., 2003).

2.6.2 Hydrophobic Interactions

Hydrophobic interaction is the strong attraction between hydrophobic (non-polar) molecules in water, which cannot be accounted for by mere van der Waals interaction energy alone. It is the result of rearrangement of H-bond configurations in the overlapping solvation zones as two hydrophobic entities come together. Hydrophobic interactions are enhanced with increasing temperature in the region of 5-55°C (Oakenfull & Fenwick, 1977; Oakenfull & Scott, 1984). Compared to hydrogen bonds, hydrophobic interactions are of a much longer range and of an entropic origin (Israelachvili, 2011). Hydrophobic interactions are less encountered amongst naturally-occurring polysaccharides. A familiar example would be high-methoxyl (HM) pectins, where hydrophobic interactions between the methylesters (-$COOCH_3$) groups along with hydrogen bonds contribute to its gelation (Oakenfull & Scott, 1984). Polysaccharides can however be hydrophobically modified to tailor to various physical properties and industrial applications (Nystrom, Kjoniksen, Beheshti, Zhu, & Knudsen, 2009). An example it is a hydrophobically modified alginate which was also found to exhibit shear-thickening properties (Burckbuchler, et al., 2006).

2.6.3 Electrostatic Attractions

A third mode of association, *i.e.* electrostatic interactions and/or cross-linking can occur for charged polysaccharides. For example, the binding of divalent counterions *e.g.* Ca^{2+} between guluronic groups in alginate results in gelation (Grant, Morris, Rees, Smith, & Thom, 1973; Rinaudo, 2009). Shear-induced cross-linking between the charged groups, like in ionomers, could also possibly lead to shear-thickening (Witten Jr & Cohen, 1985). Electrostatic attractions are a class of intermolecular interactions unique to charged polymers. Ionic polysaccharides generally exhibit more complex behaviours than neutral polysaccharides. The ability of charged groups to bind and interact with other charged species gives rise to functional properties such as gelation, complexation with cations (Rendleman, 1978a, 1978b), formation of protein-polysaccharide

complexes (de Kruif, Weinbreck, & de Vries, 2004) and biological activities (Vijayanathan, Thomas, & Thomas, 2002). Metal-polysaccharide interactions are governed by key parameters of both polysaccharides and cations: i) polysaccharide concentration, ii) linear charge density of the polysaccharide backbone, iii) distribution of ionic sites along the chain, iv) ionic charge, v) cation-specificity and vi) ionic radius. Polysaccharides have complicated structures thus, it is challenging to identify and control the factors above. This is especially true for polysaccharides with less well-known structures.

The sensitivity of charged polysaccharides to salts is manifested in its rheology. The concentration of salts can alter the chain conformation and their interactions. In the absence of salts, electrostatic repulsion between similarly charged groups along the backbone expands the chain and results in an extended conformation contributing to a higher intrinsic viscosity. When salts are present in solution, the counterions screen the electrostatic repulsion between charged groups therefore shrinking the conformation of the chain and lowering its viscosity (Jacques & Jean-Louis, 2004). In some acidic polysaccharides such as pectin and alginate, the intermolecular network formed with cations could lead to gelation. Apart from the well-known viscosity reduction of polyelectrolytes in the dilute and semi-dilute concentration regime, charged polysaccharides like xanthan, carrageenan and welan exhibit an increase in viscosity with cations in the electrostatic blob overlapping concentration (C_D) (Dobrynin, Colby, & Rubinstein, 1995; Wyatt, Gunther, & Liberatore, 2011; Wyatt & Liberatore, 2010). This phenomenon is attributed to the formation of hydrogen bonds when the electrostatic repulsions are screened (Wyatt & Liberatore, 2010).

2.7 Applications of Polysaccharides

The functional properties of the polysaccharide govern the applications which it can be used for. Often, the same polysaccharide has multiple functionalities and can be used for more than one purpose, and vice versa, different polysaccharides could be used for a specific application. Figure 2.18 gives an overview of current uses of polysaccharides based on their functional properties. The functional properties can be further classified as rheological, structural or physiological. In this thesis, one of the aims was to test the effects of the mamaku gum on satiety in rats. Therefore a more detailed review on satiety effects of polysaccharides is given.

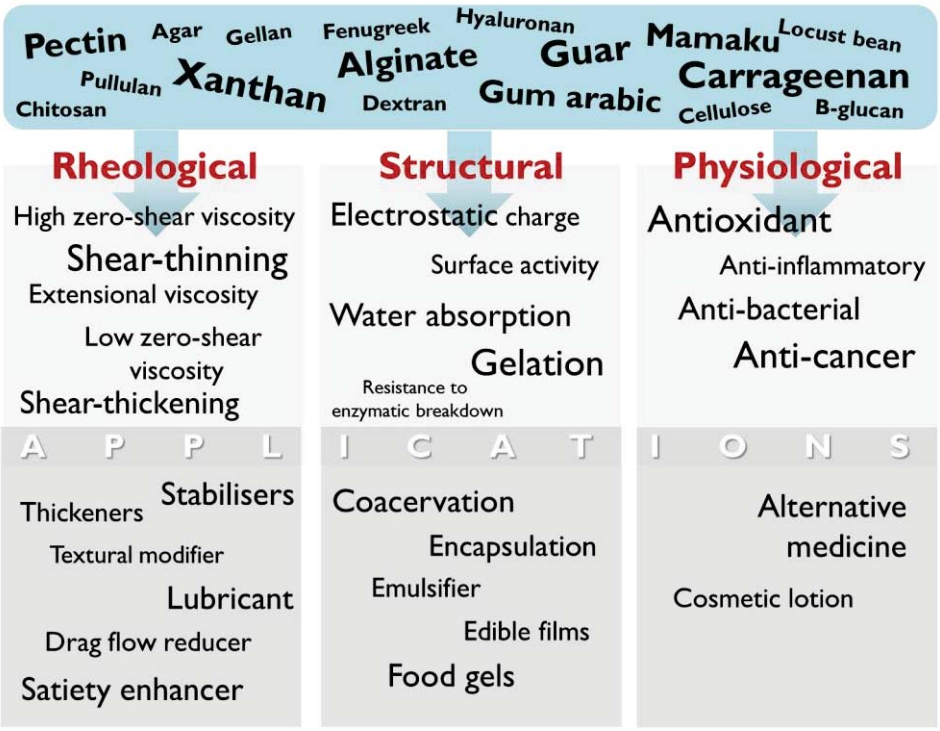

Figure 2.18 – Functional properties and applications of polysaccharides based on their rheological, structural and physiological properties

2.7.1 Satiety Effects of Polysaccharides

The alarm for a worldwide epidemic obesity has been set off. With an increase in economic statuses and spending power, consumers are now able to purchase and eat more, having easy access to food, in many occasions energy-dense foods (Stern & Kazaks, 2009). It may be in the consumers' willpower to limit and watch what they eat, but ingrained societal and psychological influences force another approach to this problem. Food manufacturers have stepped up to the responsibility of developing healthier foods. Taking one step further, foods are now specially formulated to target obesity, by incorporating functional ingredients with physiological effects to actively cause satiety.

Satiety is defined as the suppression of further food intake and appetite, given the feeling of fullness in the postprandial (post-consumption) state. It determines the time interval between two meals and the amount of food consumed in the next eating event (Bellisle & Blundell, 2013). The assessment of satiety usually involves: i) psychological feedback (in humans), such as the feeling of fullness after a meal, and the desire to consume additional food or snacks, ii) biomarkers such as levels of satiety-related hormones e.g. cholecystokinin (CCK) in the blood post-prandial (de Graaf, Blom, Smeets, Stafleu, & Hendriks, 2004) and iii) magnetic resonance imaging (MRI) scanning of gastric activity (Marciani et al., 2001). Long-term studies also include measurements of weight gain, average daily energy intake, and gastric emptying kinetics (in rats post-mortem).

Polysaccharide gums, referred to as soluble fibres, have played a major role in inducing satiety alongside with proteins. The main functional properties of the polysaccharide gums responsible for conferring satiety have been identified as viscosity, gelation, and fermentability (Fiszman & Varela, 2013).

Viscosity

Meal viscosity is a significant factor in governing satiety levels (Marciani, et al., 2001; Mattes & Rothacker, 2001). Polysaccharides are excellent viscosity modifiers, requiring only a low concentration to impart high viscosities, and not contributing to additional caloric content of the food being a soluble fibre. This makes polysaccharide gums the choice over protein, to be used as functional ingredients in foods for imparting satiety.

There are many proposed physiological mechanisms by which viscosity confers satiety (Fiszman & Varela, 2013). These effects may be additive or synergistic. A high viscosity meal delays gastric emptying, which prolongs the satiety signals from the stomach and the physical feeling of fullness (Marciani, et al., 2001). Additionally, the transit time of the meal through the small intestine may be extended, thus increasing the period of contact between the nutrients and the small intestine epithelium (J. Slavin & Green, 2007). Polysaccharide gums are hydrocolloids which absorb large quantities of liquid in the stomach *i.e.* gastric antrum distension, contributing to the feeling of 'bloatedness'. Moreover, the efficacy of digestive enzymes is reduced in high viscosity environments, thus delaying the breakdown of other food components for absorption (Fiszman & Varela, 2013).

Viscosity of the polysaccharide is not a static physical property. Most polysaccharides are pseudoplastic (shear-thinning), and therefore the viscosity is highly dependent on the shear rate. Digestion is a dynamic process involving local contractions and peristalsis motions, which have a shear rate of approximately $20s^{-1}$ (Kozu et al., 2010). Ideally, the polysaccharide should be able to perform at its optimum viscosity under the conditions of the digestive system: acidic pH (pH 2), in the presence of digestive enzymes, cations (minerals) and other components (such as lipids), under the physiological shear rate in the stomach and with certain amount of water available

Guar gum is commonly used in satiety studies, although its effects on satiety are still ambiguous. It appeared to have positive effects when added to high-fat soup, suggesting an interaction between the gum and fat (French & Read, 1994). Milkshakes thickened with microcrystalline cellulose (MCC) contributed to postprandial satiety (Mattes & Rothacker, 2001) with all other nutrient content remaining the same in the control milkshake. Agar, an algal polysaccharide (Clegg & Shafat, 2014), pectin (Tiwary, Ward, & Jackson, 1997), psyllium (Rigaud, Paycha, Meulemans, Merrouche, & Mignon, 1998) and alginate (Solah et al., 2010) were found to delay gastric emptying due to their high viscosities.

Apart from viscosity, it is possible that flow behaviour or other rheological properties of the polysaccharide may also delay gastric emptying, therefore conferring satiety. In one study, the effects of guar and mamaku gums on the antral and fundic activities in the rat stomach maintained *ex vivo* were compared (Lentle, et al., 2010). The mamaku gum (which is shear-thickening and exhibits normal stresses) was found to increase frequency and velocity of antrocorporal contractions and therefore causing inconsistent direction of propagations. The unusual rheological properties generated patterns of wall tension during peristaltic compression that would not occur with normal digesta. Guar gum, which has a high viscosity but is shear-thinning, did not have these effects. Gastric emptying can thus be prolonged by modifying the mechanics of antral contractions.

Gelation

Gelling polysaccharides such as alginate and pectin are able to impart satiety via spontaneous gelation in the stomach which delays gastric emptying (Fiszman & Varela, 2013). The gel formed in the stomach would occupy a larger gastric volume as well as exhibit greater mechanical strength as it is not broken down during mastication. Under acidic conditions of the stomach (<pK_a of polysaccharide), alginates are able to form acidic gels due to complete screening of the uronic acid groups with protons. Alternatively, calcium ions released from milk micelles during acidification can also mediate gelation. MRI images revealed gel lumps in the stomach, which had a significant effect on the sense of fullness although gastric emptying was similar to the control (Hoad et al., 2004).

Fermentability

Gut fermentation of the polysaccharide also affects satiety. Short-chain fatty acids such as butyrate, acetate and propionate produced by colonic fermentation may influence the response and actions of the gut hormones *i.e.* gastric inhibitory peptide, glucagon-like peptide-1, and CCK (Fiszman & Varela, 2013). These hormones are responsible for regulating meal intake and hunger by sending signals to the brain. The rate of fermentation differs between polysaccharides, where a slower fermentation is more conducive due to less flatulence (J. L. Slavin, Savarino, Paredes-Diaz, & Fotopoulos, 2009).

Chapter 3 Experimental Techniques

3.1 Mamaku Gum Extraction

The mamaku fronds (~12 kg) were harvested from the grounds of Massey University, Palmerston North in June 2011. The leaves on the fronds were first removed, and the fronds were chopped into smaller logs (~50cm; Figure 3.1a). The fronds were washed and cut into slices of approximately 6mm thick using a slicer (Figure 3.1b). Warm water (~50°C) was added to the sliced fronds (material/water = 1/2 w/w) (Figure 3.1c). The mixture of sliced fronds was blended in a wet disintegrator for 2 minutes (Figure 3.1d). This step removed the mucus-like material from the fronds into the continuous phase of the mixture. The crude water-soluble extract was separated from the disintegrated fronds using muslin (cheese) cloth (Figure 3.1e). The crude extract solution was then centrifuged at 13600g for 30 minutes at 20°C to remove any insoluble materials. The supernatant was filtered through a sieve of (aperture size 345μm) (Figure 3.1f) and then freeze-dried. This extraction method yields approximately 1% w/w of freeze-dried material per unit frond weight.

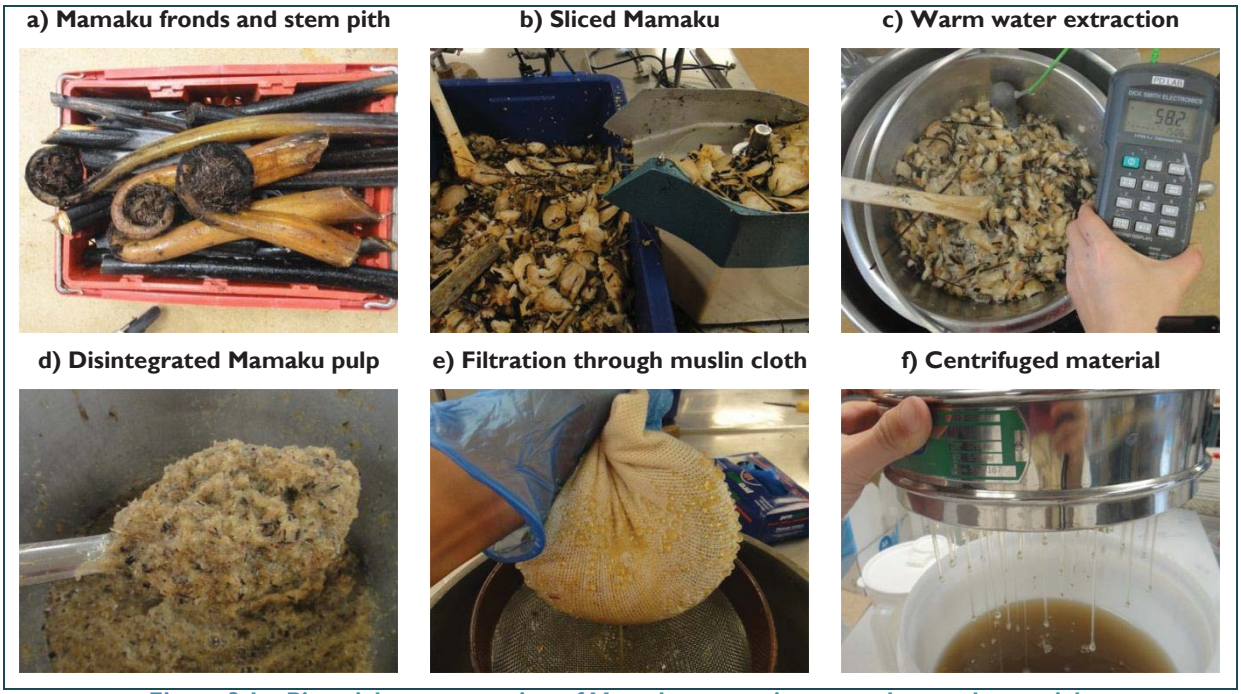

Figure 3.1 – Pictorial representation of Mamaku extraction procedure and materials

3.2 Rheological Characterisation

Rheology is the study of deformation and flow of materials under an external stress or force. From rheology many properties of the material can be revealed, such as viscosity, viscoelasticity, flow behaviour and relaxation time. These properties allow one to probe the molecular structure of the material as it is primarily manifested in the rheological properties. The material can be ideally viscous, ideally elastic like solids, or with viscoelastic behaviour by being somewhere between an ideal solid and liquid. Most food systems and ingredients have complicated flow behaviour and characterisation of their rheology is essential for predicting the state of the material during processing, transporting, and ingesting. The rheology of non-Newtonian and viscoelastic liquids/solutions is of main interest in this research thesis.

3.2.1 Rotational Shear Rheology

3.2.1.1 Viscosity

Viscosity is a physical property derived from the constant coefficient of shear stress and shear rate. It is a very important property of liquids, which gives an indication of its consistency and how easily it would flow under an applied force. The application of shear stress and shear rate to a fluid is often explained with the two-plates model (Figure 3.2). In the two-plates model, the fluid is sheared between a moving top plate with of area A and a stationery bottom plate with a resulting velocity V. The distance between the two plates is defined by the length h. Two assumptions are used in this model (or any other measuring system used) - the sample covers the entire shear surface area i.e. complete wall adhesion without wall-slip effects, and the flow of the sample is laminar (i.e. Re < 3000).

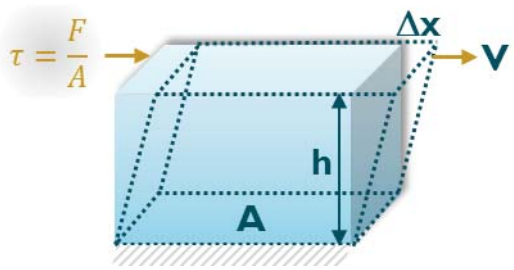

Figure 3.2 – Two-step model demonstrating relationship between shear stress and shear rate

$$\tau = \frac{F}{A} \qquad \textbf{Equation 3.1}$$

$$\dot{\gamma} = \frac{v}{h} = \frac{dv}{dh} \qquad \textbf{Equation 3.2}$$

$$\eta = \tau/\dot{\gamma} \qquad \textbf{Equation 3.3}$$

Shear stress is mathematically defined as force (F) over area (A) with the units of Newton (N), or kg/m.s^2 (Equation 3.1). Shear rate is the resulting velocity (V) of the applied force over the distance of the material (h) (Equation 3.2) with the units of s^{-1} or 1/s. Viscosity η is the ratio of the shear stress τ to the corresponding shear rate $\dot{\gamma}$ (Equation 3.3) with the units Pa.s or kg/s.m.

The viscosity of Newtonian (or ideal viscous) fluids is independent of shear stress, shear rate and/or the duration of shear. The viscosity of non-Newtonian fluids however, is shear rate dependent. The viscosity can

increase or decrease with shear i.e. shear-thinning or shear-thickening. For these non-Newtonian fluids, the shear rate has to be specified for each viscosity value reported. This viscosity is known as the *apparent viscosity* (η_{app}), which becomes a function of shear rate.

Non-Newtonian Shear-Dependent Viscosity

The origin of shear-thinning, shear-thickening or Newtonian behaviour is in the molecular structure of the material. Random coil polymers including many polysaccharides with a large molecular weight are generally shear-thinning. Under shear, the entangled macromolecules are disentangled and stretched out to align with the shear flow. The resistance to flow is reduced and therefore viscosity drops. Other materials such as dispersions may show shear-thinning when the shear force breaks up particle agglomerates. Shear-thickening materials on the other hand are more rarely seen in materials, but they occur most frequently in concentrated suspensions, pastes and in some polymers. The increase in viscosity with shear does not necessarily have to span across the entire shear rate range measured as demonstrated in

Figure 3.3. In fact, in most non-Newtonian materials characterised over the last decade, the shear-thickening effect is only seen within a certain shear rate range and accompanied by Newtonian or shear-thinning in other shear rate regions. The molecular arrangement during shear-thinning or shear-thickening is further discussed in the main literature review body.

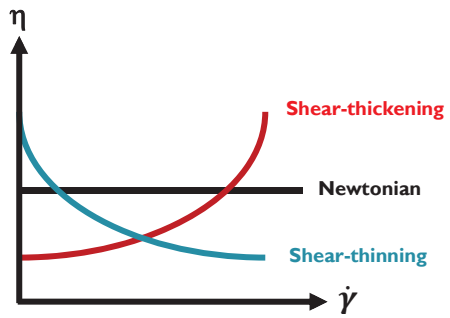

Figure 3.3 – Typical viscosity curves for a Newtonian, shear-thickening and shear-thinning fluid

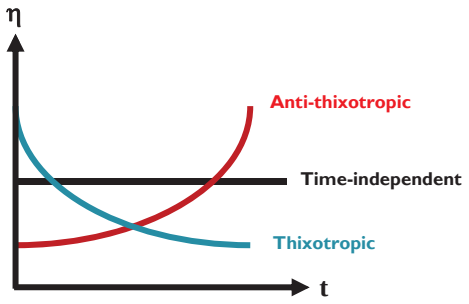

Figure 3.4 – Typical viscosity curves for a thixotropic, anti-thixotropic and time-independent fluid at a constant shear rate

Non-Newtonian Time-Dependent Viscosity

The viscosity of the material may also be time-dependent, where viscosity increases or decreases with time at a fixed shear rate due to structural agglomeration or breakdown over time (Figure 3.4). The material is known to be thixotropic if viscosity decreases with time and anti-thixotropic if viscosity increases with time.

3.2.1.2 Normal Stresses

Viscoelastic materials exhibit other behaviour than just simple flow like in Newtonian fluids. A viscoelastic material can deform in three dimensions. If the material was cube-shaped, the directions of deformation would be in the plane of the x, y and z-axes (Figure 3.5). The x-direction is the direction of shear deformation, the y-

direction is the direction of the shear gradient and the z-direction is the neutral direction. The directional-dependent stress responses are known as stress tensors. Viscous liquids deforms single-dimensionally in the same direction as the direction of shear because only the σ_{yx} (i.e. = σ_{xy}) component dominates and the other stress tensors become negligible. The stresses σ_{xx}, σ_{yy} and σ_{zz} are the normal stresses, and σ_{xx} dominates for viscoelastic materials (the symbols τ and σ can be used interchangeably to represent shear stresses).

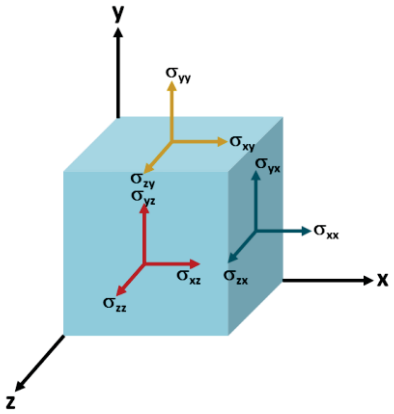

Figure 3.5 – Three-dimensional deformation of viscoelastic material in the x, y and z-direction

$$N_1 = \tau_{xx} - \tau_{yy} \qquad \textbf{Equation 3.4}$$

$$N_2 = \tau_{yy} - \tau_{zz} \qquad \textbf{Equation 3.5}$$

$$\psi_1 = N_1/\dot{\gamma}^2 \qquad \textbf{Equation 3.6}$$

$$\psi_2 = N_2/\dot{\gamma}^2 \qquad \textbf{Equation 3.7}$$

Normal stresses (N_1 and N_2) occur when the stress components in different directions are not equal. The anisotropy of stresses rises from the anisotropic microstructure of the molecules under shear. At rest, the molecules are in a state of lowest entropy which takes on a spherical shape. It deforms to an ellipsoidal shape under shear which, in order to return to the spherical conformation of lowest energy, forces opposite the shear direction reacts, giving rise to the anisotropy of shear stresses (Barnes, Hutton, & Walters, 1989). These restoring forces against the shear stress result in the first and second normal stress differences as shown in equations Equation 3.4 and Equation 3.5.

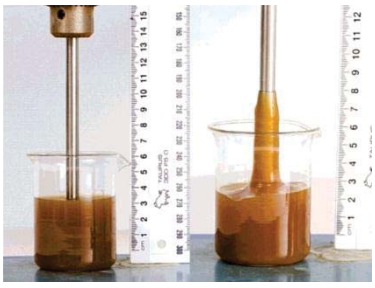

Figure 3.6 – Weissenberg (or rod-climbing) effect of 7% w/w mamaku solution with rod rotating at ~120 rev/min (Goh, et al., 2007)

The presence of normal stresses in viscoelastic materials is indicative that a phenomenon known as the Weissenberg (also known as rod-climbing) effect would be observed in the fluid (Figure 3.6). The normal stress σ_{xx} loops around the rod when rotated. In a measurement geometry system such as the cone and plate or parallel plate setup, the first normal stress difference exerts a force between the bottom plate and the perpendicular geometry, therefore measurements of normal force F_N can be made.

3.2.1.3 Stress Relaxation

Viscoelastic materials exhibit properties combined that of viscous liquids and elastic solids. Their response to stress and/or strain lies between a solid and a liquid, and can be characterised by the fraction of viscous and elastic component in them. The simplest mechanical model to describe viscoelastic materials is the Maxwell model, which combines in series the spring model of ideally elastic solids with the dashpot model of ideally viscous liquids.

Table 3.1 – Comparison between elastic solids and viscous liquids based on the spring and dashpot mechanical models (adapted from Trinh & Trinh, 2009)

	Elastic solid	**Viscous liquid**	**Viscoelastic Material**
Mechanical model	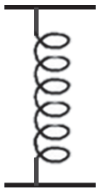 Spring	 Dashpot	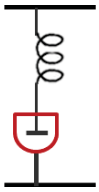 Maxwell
Strain response to stress	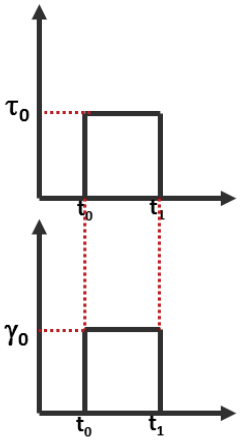 For an ideally elastic solid, the strain γ_0 occurs instantaneously with stress τ_0 when applied and removed	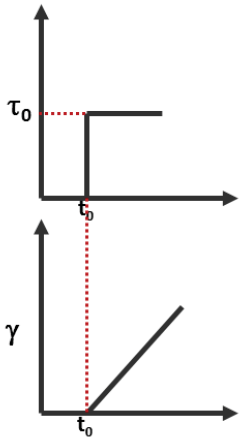 For an ideally viscous liquid, the liquid is deformed at a constant rate of strain and strain increases linearly at constant stress (for Newtonian liquids)	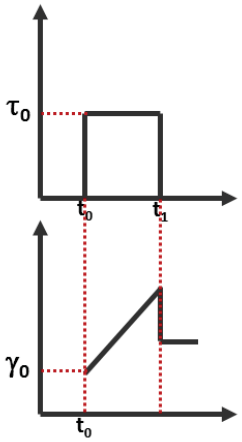 There is an instantaneous strain response γ_0 to stress τ_0 at t_0 (elastic portion) but it does not go back to original position when stress is removed
Shear stress	$\tau = G\gamma$ Shear stress τ is proportional to strain γ and the proportionality constant is G, i.e. modulus of rigidity.	$\tau = \mu_a\dot{\gamma}$ Shear stress τ is proportional to strain rate $\dot{\gamma}$ and the proportionality constant is μ_a, i.e. apparent viscosity.	$\tau = \lambda\frac{d\tau}{dt} + \tau$ Shear stress is the sum of stress contribution by the elastic and viscous components.

The Maxwell model combines the contribution of both the elastic and viscous fractions to strain and rate of strain and behaviour of viscoelastic material can be analysed based on the constitutive equation (Equation 3.8). λ is the relaxation time of the Maxwell viscoelastic fluid, i.e. the ratio of μ/G. The first term λ(dτ/dt) represents the stress arising from the elastic component while the second term represents the stress arising from the viscous component. From this equation, one can derive that when the stress is applied very quickly i.e. dt→0 and dτ/dt→∞, the first term λ(dτ/dt) becomes very large in comparison to τ.

Total strain under stress τ: $\gamma = \gamma_s + \gamma_d$

Total rate of strain: $\dot{\gamma} = \dot{\gamma}_s + \dot{\gamma}_d = \frac{d\gamma}{dt}$

Elastic component (Spring) Viscous component (Dashpot)

$$\gamma_s = \tau/G \qquad \dot{\gamma}_d = \tau/\mu$$

$$\frac{d\gamma_s}{dt} = \dot{\gamma}_s = \frac{1}{G}\frac{d\tau}{dt}$$

$$\therefore \dot{\gamma} = \dot{\gamma}_s + \dot{\gamma}_d = \frac{1}{G}\frac{d\tau}{dt} + \frac{\tau}{\mu}$$

Equation 3.8

$$\mu\dot{\gamma} = \frac{\mu}{G}\frac{d\tau}{dt} + \tau = \lambda\frac{d\tau}{dt} + \tau$$

Under a constant strain, the instantaneous stress response gradually decays for a viscoelastic fluid. We have seen that for elastic solids the stress response is in phase with strain, while the stress immediately drops to zero for a viscous liquid. For viscoelastic (or Maxwell) fluids, the decay in stress over time under a constant strain is known as the stress relaxation property of the material (Figure 3.7).

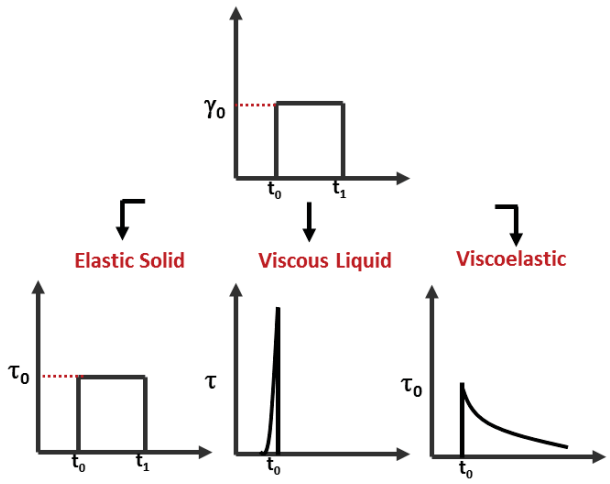

Figure 3.7 – Comparison between stress responses of an elastic solid, viscous liquid and viscoelastic fluid under constant strain (adapted from Trinh & Trinh, 2009)

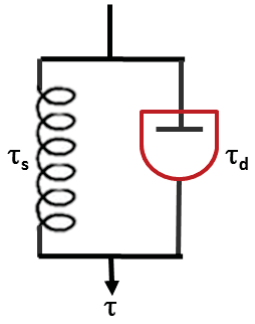

Figure 3.8 – Kelvin/Voigt mechanical spring and dashpot mechanical model for viscoelastic fluid

The Maxwell model is used to describe in the most simplistic manner the behaviour of viscoelastic fluids. Most real polymeric liquids however behave in a much more complicated manner. In terms of spring and dashpot responses, it may be multiple spring/dashpot units arranged in parallel and/or series (somewhat analogous to the setup of an electrical circuit with various resistor arrangements). The Kelvin model (Figure 3.7) has the spring and dashpot setup in parallel arrangement and shear stress is the summation of stress contributions by the spring and dashpot (in contrast to Maxwell's model where total strain is the sum of strain in the spring and dashpot respectively).

3.2.1.4 Flow Instabilities

The specifications of the Paar Physical MCR-301 rheometer are shown in Table 3.2. The torque values were checked for data measured at low frequencies and shear rates to ensure minimum torque was achieved. One major concern was the reliability of the rheological data captured by the rheometer. The unusual viscoelastic nature of the material proved to be a challenge for accurate and reliable measurements. Centrifugal expulsion of the material was observed with the cone-and-plate geometry (Figure 3.9) while rod climbing effects were seen for the cup-and-bob geometry at high shear rates. These observed effects indirectly affect the surface area and/or volume of sample in contact with the geometry, which compromised the accuracy of the captured data.

Table 3.2 - Specifications for Paar Physica rheometer MCR-301

Parameter	Units	Value
Shear rate (CSR)		
Minimum	min^{-1}	10^{-6}
Maximum	min^{-1}	3000
Shear rate (CSS)		
Minimum	min^{-1}	10^{-7}
Maximum	min^{-1}	3000
Torque		
Minimum (rotational)	μNm	0.1
Minimum (oscillation)	nNm	2
Maximum	mNm	200
Frequency		
Minimum	Hz	10^{-4}
Maximum	Hz	100
Normal force	N	0.005-50
Temperature	°C	-150-1000

Figure 3.9 - Centrifugal expulsion of 5% w/w mamaku sample during viscosity measurements at approximately 50s^{-1}

This issue was addressed by showing that flow behaviour is similar even using different measurement geometries (Figure 3.10). Nevertheless, there was still the possibility of flow instabilities such as wall-slip or shear-banding across all geometries. To test for wall-slip, the parallel plate geometry was used with and without sandpaper, and one with a serrated plate texture (Figure 3.11). There did not appear to be a difference with using the sandpaper, therefore wall-slip effects were probably not significantly present. The viscosity obtained using the serrated plate was lower, presumably due to a difference in actual gap height between the plates.

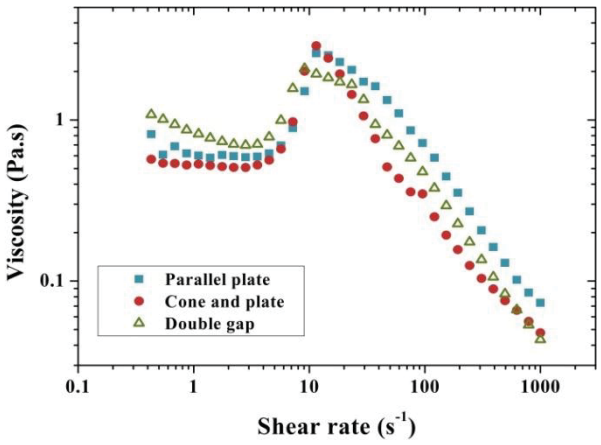

Figure 3.10 - Viscosity curves of 5% w/w mamaku obtained using the parallel plate, cone and plate and double gap geometries

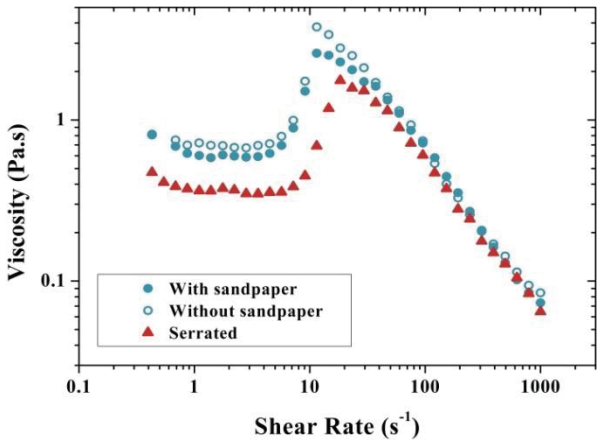

Figure 3.11 - Viscosity curves of 5% w/w mamaku obtained using the parallel plate with sandpaper, without sandpaper, and with serrated plates

3.2.2 Small Amplitude Oscillatory Shear Rheology

Viscoelastic materials are commonly characterised using oscillatory shear in addition to stress relaxation and creep tests using rotational shear. The objective is usually to determine viscoelastic material parameters (G' and G") over a wide range of frequency, temperature and time etc. In food applications, oscillatory shear measurements are useful in characterising gelation processes (gel-point determination), aging, viscoelasticity of hydrocolloids, glass transition temperature, sensory perception and texture (Gunasekaran & Ak, 2000).

In oscillatory shear, both stress (τ) and strain (γ) vary cyclically with time, usually following a sinusoidal waveform (Figure 3.12a). The raw stress and strain data can also be represented using Lissajous plots (Figure 3.12b), where an elastic solid would be a straight line, a Newtonian fluid a perfect circle, and an ellipsoid for viscoelastic materials.

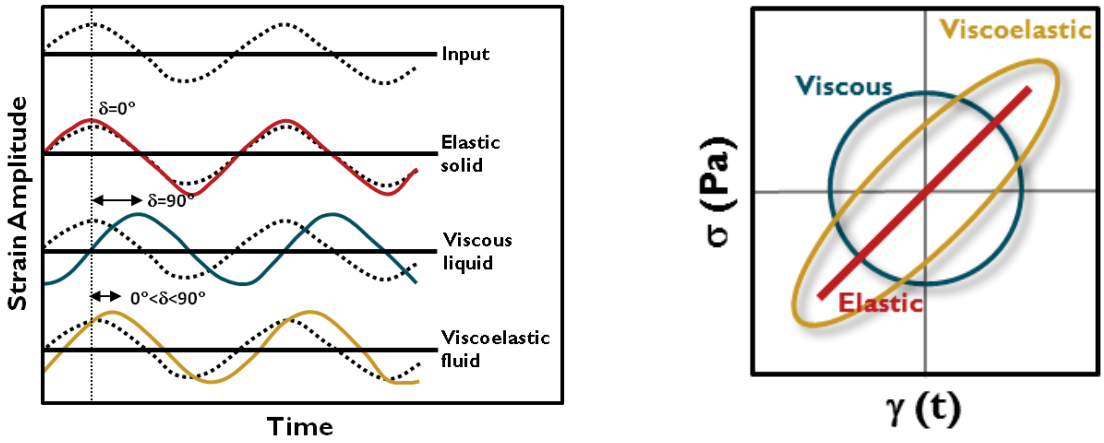

Figure 3.12 – Stress vs. strain response (left) and Lissajous plots (right) of elastic solid, Newtonian fluid and viscoelastic fluids under small oscillatory shear

The deformation of the material in the linear region is commonly referred to as small amplitude oscillatory shear, where the stress response of the material is linearly proportional to the strain input. Under the linear viscoelastic region (as indicated by a constant G' and G" with strain), material deformation is reversible and no permanent structural changes are imposed on the material. However, beyond the linear region, the material undergoes structural or configurational changes which loses G' and G" their constant values (Mezger, 2011). This region of non-linearity is referred to as large amplitude oscillatory shear (LAOS) which is further described in the next section.

$$\gamma = \gamma_0 \sin \omega t \qquad \textbf{Equation 3.9}$$

$$\dot{\gamma} = \gamma_0 \cos \omega t \qquad \textbf{Equation 3.10}$$

$$\sigma = \sigma_0 \sin(\omega t + \delta) \qquad \textbf{Equation 3.11}$$

The sinusoidal strain and strain rate applied to the material at a frequency of ω for time t are represented by Equation 3.9 and Equation 3.10 respectively. The corresponding stress is then represented in Equation 3.11

where δ is the shift angle (or phase lag). Storage and loss moduli are defined as the ratios of stress and strain amplitudes (Equation 3.12 & Equation 3.13).

$$G' = \frac{\tau_0}{\gamma_0}\cos\delta \qquad \textbf{Equation 3.12}$$

$$G'' = \frac{\tau_0}{\gamma_0}\sin\delta \qquad \textbf{Equation 3.13}$$

$$\sigma = G'\sin\omega t + G''\cos\omega t \qquad \textbf{Equation 3.14}$$

Based on these mechanical parameters, the stress response can be rewritten in the form of Equation 3.14. The storage modulus is related to the elastic component or the amount of energy stored in a material during deformation. For a perfectly elastic solid, all the energy is stored and the stress response is in phase with strain input, therefore δ=0°. The loss modulus is related to the viscous character of the material or energy dissipated with deformation. For a Newtonian fluid, all the energy is dissipated as heat represented by a phase lag of δ=90°. A viscoelastic material lies between that of an elastic solid and a Newtonian liquid, which results in 0°<δ<90°. The ratio of the two moduli G"/G' is defined as the loss tangent (Equation 3.15) which is a useful property for determining whether the material is predominantly elastic or viscous, and the crossover frequency where tanδ=1. The complex modulus (G*) can also be used to represent contributions from both the storage and loss modulus (Equation 3.16). For viscoelastic fluids like polymer solutions, the dynamic viscosity (η') (Equation 3.17) and complex viscosity (η*) functions derived from oscillatory shear can also be used.

$$tan\delta = \frac{G''}{G'} \qquad \textbf{Equation 3.15}$$

$$G^* = \sqrt{(G')^2 + (G'')^2} \qquad \textbf{Equation 3.16}$$

$$\eta' = \frac{G''}{\omega} \qquad \textbf{Equation 3.17}$$

$$\eta^* = \sqrt{\left(\frac{G'}{\omega}\right)^2 + \left(\frac{G''}{\omega}\right)^2} \qquad \textbf{Equation 3.18}$$

Rotational shear and small amplitude oscillatory shear properties can be related via the Cox-Merz rule (1958). The Cox-Merz rule predicts that the magnitude of complex viscosity η* is equal to the steady state shear viscosity η at corresponding values of angular frequency and shear rate (Equation 3.19). This rule has been found to apply for many random coil polysaccharide solutions (Kaur, Singh, & Singh, 2009; X. Xu, Liu, & Zhang, 2006), where rotational and oscillatory shear data were superimposable across the shear rate range.

$$\eta^*(\omega) = \eta(\dot{\gamma})|_{\dot{\gamma}=\omega} \qquad \textbf{Equation 3.19}$$

3.2.3 Large Amplitude Oscillatory Shear Rheology

Moduli parameters G' and G" as described in the previous section have been defined under conditions of linear viscoelasticity. An amplitude sweep is usually carried out prior to further tests to determine the limiting strain γ_L (Figure 3.13) *i.e.* the maximum strain at which G' and/or G" remains constant with strain, where strain values γ_0 used in Equation 3.9 to Equation 3.13 therefore have to be within the LVE ($\gamma_0<\gamma_L$). In the nonlinear region, G' and G" becomes a function dependent on strain amplitude (at a fixed frequency), and the resulting stress waveforms are distorted from sinusoidal waves (Figure 3.13). The raw data signal (Lissajous plots) *i.e.* parametric plots of stress vs. strain) of viscoelastic materials loses their ellipsoidality beyond the linear viscoelastic region (Figure 3.15). Therefore the interpretation of nonlinear parameters becomes difficult and mathematically inaccurate to define. Higher harmonics come into the picture and the stress response is not simply a sinusoid of the same applied frequency and phase shifted, as would be the case in linear regime. In other words, the data no longer follow sine or cosine functions (Equation 3.9 to Equation 3.13). Fourier transformation (FT) has to be applied in order to quantify the stress response, as represented by a Fourier series of odd harmonics. As each oscillation period is represented by two mirror images of the sinusoidal function, only the odd harmonics are used in the Fourier series (Equation 3.20).

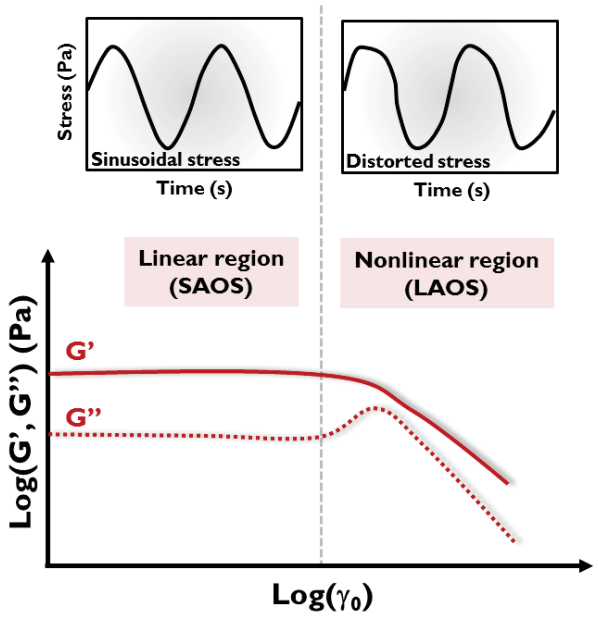

Figure 3.13 – Comparison of stress waveforms in the linear and nonlinear viscoelastic regions as represented on an amplitude sweep

$$\sigma(t) = \gamma_0 \sum_{n\,odd} \{G'_n(\omega,\gamma_0)\sin n(\omega t) + G''_n(\omega,\gamma_0)\cos n(\omega t)\} \qquad \text{Equation 3.20}$$

Nevertheless, the large amplitude oscillatory shear sweep of most materials falls into one of the four types as classified by Hyun, Kim, Ahn & Lee (2002) (Figure 3.14). Type I strain-thinning materials are most commonly observed in shear-thinning polymer and polysaccharide solutions (Razavi, Taheri, & Sanchez, 2013). The microstructural origin of strain-softening is likely to be analogous to shear-thinning, where increasing strain disentangles the polymer chains and aligns them with the flow field. Type II strain-hardening materials is the opposite of type I materials, where G' and G" increases with strain amplitude. This phenomenon is attributed

to the formation of complex and stable microstructures with strain e.g. cross-linking between PVA and borate ions (Hyun, et al., 2002). Type III weak strain overshoot materials refer to an overshoot/peak in G". The overshoot observed results from resistance to structural breakdown of the material formed by weaker associations e.g. hydrogen bonding. At large enough strain deformations, the polymer chains align to the flow field resulting in decrease of G". Xanthan gum is an example of a type III material (Song, Kuk, & Chang, 2006). Type IV strong strain overshoot materials refer to overshoot in both G' and G". The interaction energy for type IV materials is likely to be weaker than type II but stronger than type III materials, commonly observed in associative polymers (Tirtaatmadja, Tam, & Jenkins, 1997).

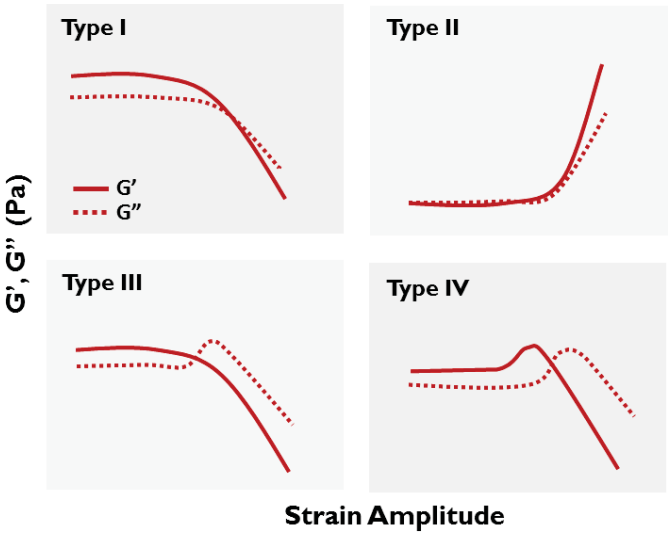

Figure 3.14 – Classification of materials into type I) strain-thinning, II) strain-hardening, III) weak strain overshoot and IV) strong strain overshoot

A new ontology has been developed by Ewoldt and coworkers (2008b) for additional quantitative characterisation of nonlinear properties using only the Lissajous plots. The parameters are defined as i) minimum-strain modulus, G'_M, or the tangent at zero strain (Equation 3.21), ii) large-strain modulus, G'_L, or the secant at maximum strain (Equation 3.22) on an elastic Lissajous plot (stress vs. strain), iii) minimum-strain rate dynamic viscosity, η'_L (Equation 3.23) and iv) maximum-strain rate dynamic viscosity η'_M on the viscous Lissajous plot (stress vs. strain rate) (Equation 3.24). Figure 3.15a shows an example of determining G'_M and G'_L from a viscoelastic material in the linear region and Figure 3.15b in the non-linear region. In the linear region for an ellipsoid, $G'_M = G'_L = G'_1$, where G'_1 is the storage modulus of the first harmonic, or simply, the familiarly known G'. The same is applied to viscous Lissajous plots (stress vs. strain rate) to obtain η'_M (Equation 3.23) and η'_L (Equation 3.24), and $\eta'_M = \eta'_L = \eta'_1$ (G") in the linear region.

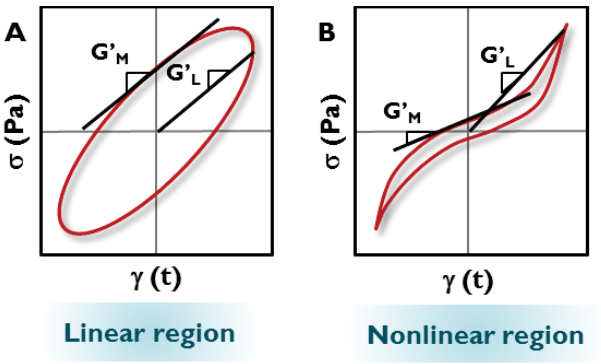

Figure 3.15 – Quantification of G'M and G'L from Lissajous plots in a) linear and b) nonlinear viscoelastic regions

$$G'_M(\gamma_0) = \frac{d\sigma}{d\gamma}|_{\gamma=0} \quad \textbf{Equation 3.21}$$

$$G'_L(\gamma_0) = \frac{\sigma}{\gamma}|_{\gamma=\gamma_0} \quad \textbf{Equation 3.22}$$

$$\eta'_M(\gamma_0) = \frac{d\sigma}{d\dot{\gamma}}|_{\dot{\gamma}=0} \quad \textbf{Equation 3.23}$$

$$\eta'_L(\gamma_0) = \frac{\sigma}{\dot{\gamma}}|_{\dot{\gamma}=\dot{\gamma}_0} \quad \textbf{Equation 3.24}$$

Using these parameters, *intra*-cycle nonlinearities can be further quantified. The strain-stiffening ratio, S, is defined in Equation 3.25. A value of S > 0 indicates intra-cycle strain-stiffening and S < 0 corresponds to intra-cycle strain-softening. Similarly, shear-thickening ratio, T, is defined in Equation 3.26. T > 0 represents intra-cycle shear-thickening T < 0 indicates intra-cycle shear-thinning. In the linear region, both S and T are equal to zero.

$$S = \frac{G'_L - G'_M}{G'_L} \quad \textbf{Equation 3.25}$$

$$T = \frac{\eta'_L - \eta'_M}{\eta'_L} \quad \textbf{Equation 3.26}$$

A more general representation of the stress response that also accounts for nonlinear behaviour with higher harmonics can be written as a sum of Chebyshev modes given in Equation 3.27 and Equation 3.28. The total stress $\sigma = \sigma' + \sigma''$, and $T_n(x)$ are the *n*th-order Chebyshev polynomials of the first kind, where e_n and v_n are the elastic and viscous Chebyshev coefficients at the n^{th} harmonic respectively. Briefly, $e_1 \rightarrow G'$ and $v_1 \rightarrow \eta' = G''/\omega$ in the linear region, and $e_n > 0$ corresponds to *intra*-cycle strain-stiffening and $v_n > 0$ to *intra*-cycle shear-thickening in the nonlinear region at higher harmonics. The elastic and viscous stress contribution to the total stress is represented by the dashed lines in elastic (Figure 3.16a) and viscous (Figure 3.16b) Lissajous plots respectively. The maximum stress σ_{max} is indicated above each curve.

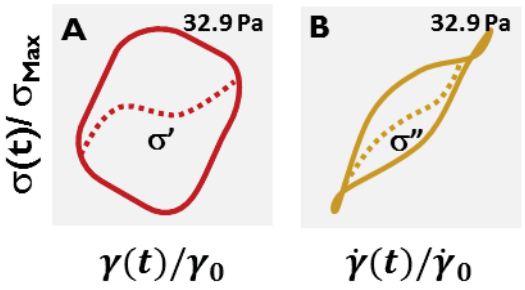

Figure 3.16 – a) Elastic and b) viscous Lissajous curves (solid lines) with contributions from elastic and viscous stress components (dotted lines)

$$\sigma'(x) = \gamma_0 \sum_{n\ odd} e_n(\omega, \gamma_0) T_n(x) \qquad \text{Equation 3.27}$$

$$\sigma''(x) = \dot{\gamma}_0 \sum_{n\ odd} v_n(\omega, \gamma_0) T_n(y) \qquad \text{Equation 3.28}$$

$$Chebyshev\ polynomials\ of\ first\ kind \begin{cases} T_0(x) = 1 \\ T_1(x) = x \\ T_{n+1}(x) = 2xT_n(x) - T_{n-1}(x) \end{cases} \qquad \text{Equation 3.29}$$

MITlaos Program

The viscoelastic parameters and Chebyshev coefficients G'_M, G'_L, η'_M, η'_L, S, T, e_n, v_n, σ' and σ'' can be obtained from using the MITlaos program (Ewoldt, Hosoi, & McKinley, 2009; contact mitlaos@mit.edu) run in Matlab®. The raw stress, strain and time data output *i.e.* $\gamma(t)$, $\sigma(t)$ from the rheometer is processed by MITlaos via filtering and application of Fourier transform to construct Lissajous plots and calculate the parameters. An example of the output graphs is shown in Figure 3.17, with the data exportable to .txt formats. More details on the operating instructions of MITlaos is available by Ewoldt *et al.* (2009).

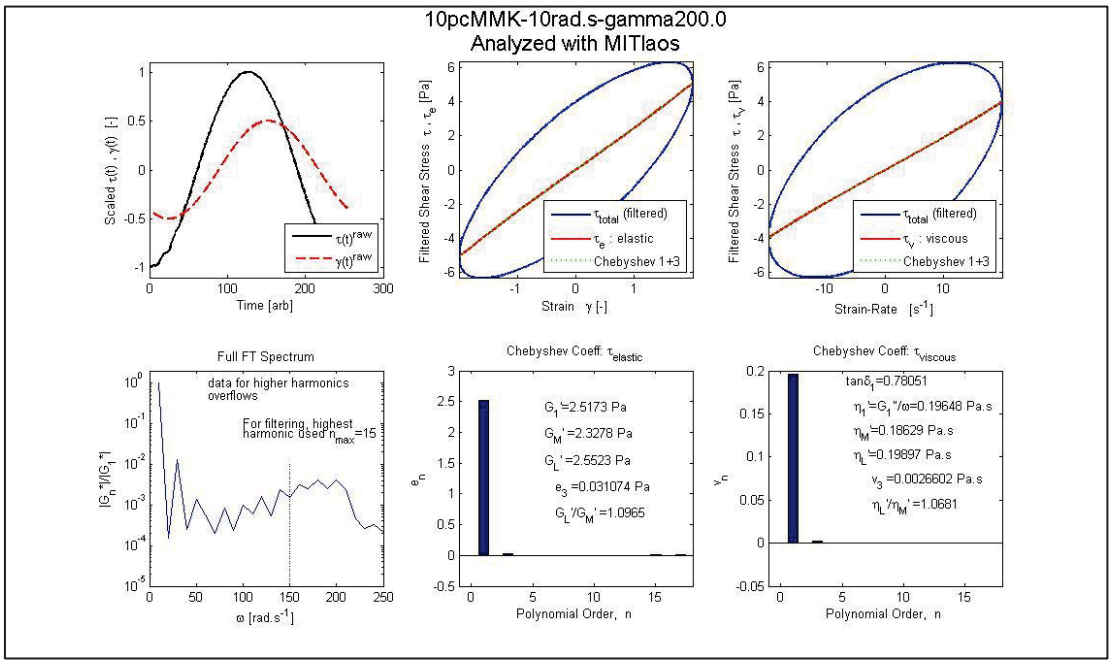

Figure 3.17 – Example of LAOS data analysed using MITlaos

3.2.4 Extensional Rheology

Polysaccharides have complex structural components which its extensional flow kinematics may differ dramatically from its shear rheology (Padmanabhan, 2010). Rheological properties obtained from shear flow paints only a portion of the picture. A rubber-band can be either sheared or stretched, but clearly the latter deformation would provide more useful information on the material properties. A simple 'thumb and forefinger' test on the mamaku solution showed significant extensibility and 'stringiness', which forms the motivation behind characterising the polysaccharide using extensional flow.

For steady extensional flows under uniaxial deformation (Figure 3.18), the length (l) at time (t) is an exponential functional of time, where the extension rate $\dot{\varepsilon}_0$ is constant and l_0 is the initial separation of the material (Equation 3.30). The strain imposed on the material is represented by the Hencky strain (Equation 3.31) or Cauchy/engineering strain (Equation 3.32) at infinitesimally small strains (Padmanabhan, 2010).

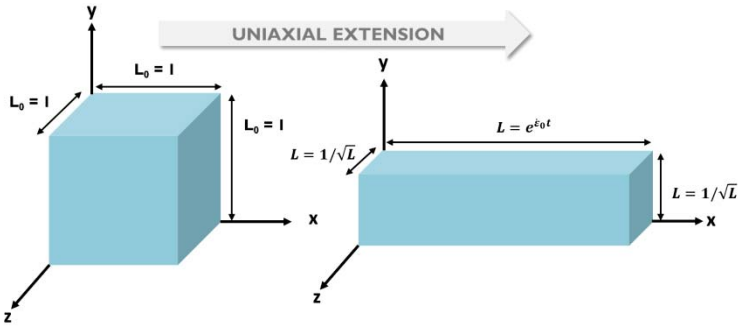

Figure 3.18 – Uniaxial deformation of material

$$L = L_0 e^{\dot{\varepsilon}_0 \Delta t} \qquad \text{Equation 3.30}$$

$$\varepsilon_h = \dot{\varepsilon}_h \Delta t = \ln \frac{l}{l_0} \qquad \text{Equation 3.31}$$

$$e = \frac{l - l_0}{l_0} \qquad \text{Equation 3.32}$$

Analogous to shear deformation where apparent shear viscosity (η_S) is the coefficient between shear stress and shear rate, steady state extensional viscosity η_E is the ratio between extensional stress σ_E and strain rate (Equation 3.33a). However, in most cases where a steady strain rate cannot be achieved (sample fails or fractures before reaching steady-state), the transient extensional viscosity as indicated by a '+' sign is described instead (Equation 3.33b).

At low strain rates, the normalised uniaxial extensional viscosity is the same as shear viscosity (curve 1 of Figure 3.19). For Newtonian fluids or measurements made in the linear viscoelastic region, the Trouton ratio (ratio of extensional to zero-shear viscosity; Equation 3.34) is three. When extensional viscosity increases with time at higher strain rates, the material is known as strain-hardening or extensional thickening (curve 2). Many polymer melts such as low density polyethylene (LDPE) exhibit strain-hardening, and degree of branching influences their extensional behaviour (Macosko, 1994).

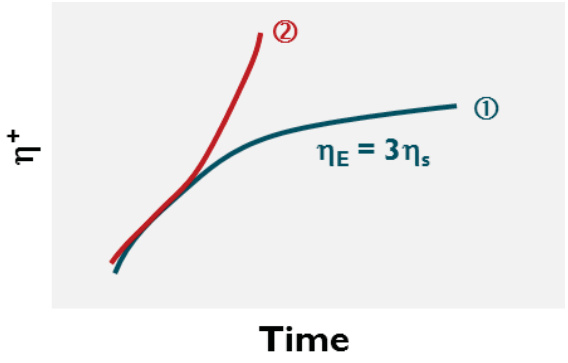

Figure 3.19 – Typical transient extensional and shear viscosity of polymer solutions with time

a) $\eta_E = \frac{\sigma_E}{\dot{\varepsilon}}$

b) $\eta_E^+(t) = \frac{\sigma_E^+(t)}{\dot{\varepsilon}(t)}$

Equation 3.33

$$Tr = \frac{\eta_E}{\eta_S}$$

Equation 3.34

Capillary breakup extensional rheometer (CaBER)

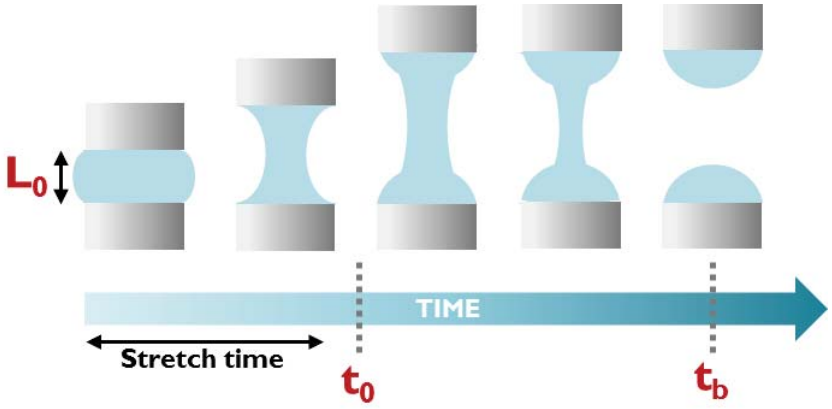

Figure 3.20 – Schematic illustration of capillary breakup extensional rheometer

The measurement of extensional viscosity and extensional relaxation times of the mamaku polysaccharide solution in this thesis was carried out using a capillary breakup extensional rheometer (CaBER). More information on the experimental setup and procedure is described in the methodology section of Chapter 4. The measurement was based on filament stretching, where evolution of filament diameter with time was quantified. The CaBER is suitable for polysaccharide solutions which are of low to moderate viscoelasticities (Anna & McKinley, 2001; Rodd, Scott, Cooper-White, & McKinley, 2005).

The CaBER consists of a fluid sample between two plates, which forms a fluid filament when the end plates are stretched. The fluid is stretched from an initial length of L_0 to final length of L_f with an exponential stretch profile (Equation 3.30), from time t_0 to breakup time t_b. A combination of inertial, viscous, elastic and capillary forces causes drainage of the fluid filament and subsequent breakup of the filament. Changes in the filament midpoint diameter with time, $D_{mid}(t)$ are monitored using a laser micrometer (Figure 3.20).

Inertial and viscous forces are dominant at the start of the experiment where $t/t_b << 1$. Elastic and capillary forces become dominant during fluid drainage and this region is known as the elasto-capillary regime. The onset of this region is located by image analysis taken with a high-speed camera at 60 frames per second (fps). In the elasto-capillary region, the mid-plane diameter D(t) of the liquid bridge evolves according to Equation

3.35, where D_0 is the initial diameter of the liquid bridge, G is the relaxation modulus associated with the longest relaxation mode, σ is the surface tension of the fluid, *t* is the time elapsed since the start of experiment and λ is the longest relaxation time of the fluid (Anna & McKinley, 2001). Viscous forces dominate towards the end of the experiment where $t/t_b \approx 1$. The elasto-capillary and long-time behaviour of the fluid diameter can be fitted with an equation in the form of Equation 3.36a, where *A*, *B*, *C* and *D* are fitting parameters and relaxation time can be calculated from *B* (Equation 3.37).

$$D(t) = D_0\left(\frac{GD_0}{4\sigma}\right)^{1/3}\exp[-\frac{t}{3\lambda}] \quad \textbf{Equation 3.35}$$

$$\text{a) } D(t) = Ae^{-Bt} - Ct + D$$

$$\text{b) } \frac{dD(t)}{dt} = -ABe^{-Bt} - C \quad \textbf{Equation 3.36}$$

$$B = \frac{1}{3\lambda} \Rightarrow \lambda = \frac{1}{3B} \quad \textbf{Equation 3.37}$$

The transient extensional viscosity of the fluid can also be determined from CaBER experiments. The instantaneous strain rate $\dot{\varepsilon}(t)$ can be calculated based on the rate of change in instantaneous diameter D(*t*) at time *t* (Equation 3.38). The Hencky strain at time *t* is the integral of instantaneous strain rate (Equation 3.39). The ratio between extensional stress difference $\Delta\tau(t)$ (Anna & McKinley, 2001) (Equation 3.40) and instantaneous strain rate (Equation 3.38) gives the transient extensional viscosity as shown in Equation 3.41. The term dD(*t*)/d*t* can be found by differentiating Equation 3.36a to Equation 3.36b.

$$\dot{\varepsilon}(t) = -\frac{2}{D(t)}\frac{dD(t)}{dt} \quad \textbf{Equation 3.38}$$

$$\varepsilon_H(t) = \int_0^t \dot{\varepsilon}(t)dt = 2\ln\left(\frac{D_0}{D(t)}\right) \quad \textbf{Equation 3.39}$$

$$\Delta\tau(t) = 3\eta_s\dot{\varepsilon}(t) + (\tau_{zz} - \tau_{rr}) = \frac{2\sigma}{D(t)} \quad \textbf{Equation 3.40}$$

$$\eta_E = -\frac{\sigma}{dD(t)/dt} \quad \textbf{Equation 3.41}$$

Relaxation times obtained from filament thinning measurements is often several times longer than the relaxation time obtained from shear rheology (Clasen et al., 2006; Liang & Mackley, 1994), since the material is deformed to a larger extent under extension. Therefore it is essential to characterise the fluid and its relaxation parameters from both shear and extensional rheology.

3.3 Structural Characterisation

In order to elucidate the structure of a polysaccharide, the structural analysis can be approached from three main aspects: 1) constituents, 2) linkage, and 3) sequence. For the mamaku polysaccharide, the constituents and linkage were analysed and the sequence was deduced based on linkages identified and similar polysaccharides.

3.3.1 Monosaccharide Composition

Monosaccharide composition is usually determined by hydrolysing the polysaccharide to its constituent monosaccharides i.e. depolymerisation. Hydrolysis is done using acid or enzymes. High performance liquid chromatography (HPLC) or gas chromatography (GC) is then subsequently used to quantitatively and qualitatively detect the monosaccharide fractions.

3.3.1.1 Acid Hydrolysis

The glycosidic bonds between monosaccharides of a neutral polysaccharide are heat and acid labile. In the presence of a strong acid and heat, these bonds are cleaved and the monosaccharide units are released from the polysaccharide. Concentrated sulphuric acid, hydrochloric acid, and trifluoracetic acid (TFA) can be used for the hydrolysis reaction. TFA is usually used due to its volatility which makes it easy to remove via rotary evaporation after hydrolysis. Generally for an unknown polysaccharide, the material is heated in 1M TFA at 121°C for an hour (Cui, 2005). However, once the monosaccharides are released, it will be subjected to degradation by the hot concentrated acid. Therefore the reaction time, temperature, and acid concentration must be adjusted accordingly such that the reaction conditions are sufficient for complete glycosidic linkage hydrolysis and yet not cause sample degradation. Polysaccharides containing uronic acids i.e. acidic form of the monosaccharide are more difficult to hydrolyse. The linkage between uronic acid residues are more resistant to acid hydrolysis (Cui, 2005), therefore incomplete depolymerisation of the polysaccharide is more likely to occur.

3.3.1.2 Derivatisation (Acetylation)

The monosaccharides obtained after acid hydrolysis are not volatile – therefore in order to analyse the monosaccharide composition using gas chromatography, the monosaccharide fractions have to be made volatile through a process called derivatisation (Cui, 2005). Derivatisation involves converting the neutral monosaccharide into alditol acetates and the acidic monosaccharides into trimethylsilyl (TMS) derivatives as shown in Figure 3.21. The conversion of a neutral monosaccharide into its alditol acetate involves two steps. It is first reacted (reduced) with sodium borohydride in ammonium hydroxide to form an alditol. Excess sodium borohydride is removed by adding acetic acid (which neutralises the sample as well) and methanol, and continuously dried with nitrogen. The alditols are then acetylated by reacting with acetic anhydride at 121°C for a few hours. The resulting dry alditol acetates are dissolved in the solvent methylene chloride prior to GC analysis. Acidic monosaccharides on the other hand are converted to trimethylsilyl (TMS) ethers. The first reaction step is the same as with neutral monosaccharides, i.e. addition of sodium borohydride and subsequent

removal with acetic acid. It is then treated with a mixture of reagents containing pyridine, hexamethyldisilazne and trifluoracetic acid in order to facilitate acetylation (Cui, 2005).

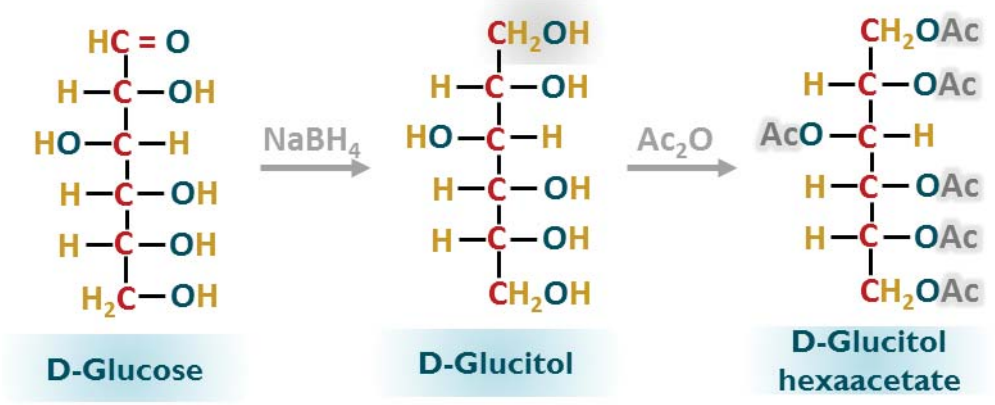

Figure 3.21 – Derivatisation of neutral monosaccharides into alditol acetates and TMS derivatives (adapted from Cui, 2005)

3.3.2 Linkage Analysis

Apart from knowing the types of monosaccharides which make up the polysaccharide, it is also essential to obtain information on how these monosaccharides are linked together throughout the polymer chain. Polysaccharides with the same monosaccharide composition but differently linked will have markedly different properties. The flexibility of the polymer chain depends on the freedom of the glycosidic bonds to rotate and therefore its ability to form ordered/regular or disordered structures. Glycosidic bonds can also be either α- or β-linked, depending on the configuration of the monosaccharide at the anomeric carbon atom (C1) of the residue involved. Again, two monosaccharide units linked at the same positions but having different anomeric configuration (i.e. α- or β-) will result in different properties of the polysaccharide as well.

Methylation is the most widely used method to determine glycosidic linkage positions present in polysaccharides. A typical methylation test would give information on the molar percentage of the various linkage types present within the polysaccharide. However, results would not show the sequence of monosaccharides or the anomeric configuration of the glycosidic bonds. Methylation involves four main steps: 1) conversion of all free hydroxyl groups into methoxyls, 2) acid hydrolysis of inter-glycosidic linkages, 3) reduction and acetylation to give volatile partially methylated alditol acetates (PMAA) and lastly, 4) analysis with gas chromatography coupled with a mass spectroscopic detector (GC-MS) (Cui, 2005). The conversion of hydroxyl groups into methoxyls can be done using dry powdered sodium hydroxide (NaOH) and methyl iodide (CH_3I) (Cui, 2005). Trifluoracetic acid (TFA) is used to hydrolyse the methylated polysaccharide into monosaccharides, which are then deuterised with sodium borodeuteride into partially methylated alditols. A deuterium atom is introduced at C1 of the monosaccharide, which distinguishes C1 from C6 carbon. The final step is acetylation of the alditols into partially methylated alditol acetates (PMAA), for which the oxygen atoms involved in the glycosidic linkage are acetylated. The PMAAs are then qualitatively and quantitatively analysed using GC-MS.

3.3.3 Nuclear Magnetic Resonance (NMR)

Nuclear magnetic resonance is one of the most common and useful techniques for determining structures of polysaccharides. It is often used as a complementary technique in addition to the previously described chemical methods to identify and quantify monosaccharide constituents, sequence distribution, detect functional groups and intermolecular interactions etc. Nuclear magnetic resonance is based on the principle of nuclear spin. When placed in a strong magnetic field, the positively charged atom protons align either in the same direction or opposite direction to the field. The action of alignment is known as the intrinsic angular momentum of the atom *i.e.* nuclear spin. The difference in alignment directions results in two states separated by an energy difference ΔE. The ΔE and therefore resonance frequency also depends on the chemical environment of the nucleus in a molecule, an effect known as the chemical shift. The intensity of the frequency/chemical shift (in ppm) can be calculated based on the strength of the magnetic field. Different protons within the molecule will emit different energies at specific frequencies, depending on its environment e.g. shielding by electrons which gives an NMR spectrum unique to the molecule (Balci, 2005).

For polysaccharides, hydrogen and carbon are the most abundant elements in the molecule with NMR active isotopes ^{1}H and ^{13}C respectively, with ^{1}H abundance close to 100% but relatively lesser for ^{13}C of 1.1%. Internal chemical shift references are used to 'calibrate' frequencies e.g. 1,4-dioxane in D_2O for ^{13}C NMR where the chemical shift is 67.40 ppm. The number of monosaccharide units in the repeating unit can be known by counting the resonances in the anomeric region (4.4-5.5 ppm). Common hexoses e.g. glucose show up here as well as in chemical region of 95-110 ppm of ^{13}C NMR spectra (Jonsson, 2010). Other resonances may reveal $-CH_3$ groups (1 ppm) or presence of N-acetyl (2.0 ppm) and/or O-acetyl groups (2.1 ppm) (Zaccheus, 2012). Monosaccharides have complicated NMR spectra, and therefore even more so for polysaccharides. The macromolecular structure of high molecular weight polysaccharides tumble slowly in solutions (on top of high viscosity effects), which causes the excited spins to relax more rapidly, translating to broad resonances which are difficult to singularise (Cheng & Neiss, 2012). The interpretation of NMR spectra is often based on reference spectra (assignments based on literature review), since the NMR shifts show general trends for carbon atoms or protons at a particular ring position (Table 3.3).

Table 3.3 – Key ^{1}H and ^{13}C chemical shifts for nuclei of polysaccharides (adapted from Perlin & Casu, 1982)

^{1}H	Shift (ppm)	^{13}C	Shift (ppm)
CH_3C	~1.5	CH_3C	~15
CH_3CON	1.8-2.1	CH_3COH)	20-23
CH_3CO_2	2.0-2.2	CH_3CO_2)	
CH(NH)	3.0-3.2	CH_2C	38
CH_3C	3.3-3.5	CH_3O	55-61
H-2 to H-6'	3.5-4.5	CH(NH)	58-61
H-5	4.5-4.6	CH_2OH	60-65
H-1 (ax)	4.5-4.8	C-2 to C-5	65-78
$H\text{-}C(OH)_2$	5.2	C-1 (ax-O, red)	90-95
HO	5.0-5.4	C-1 (eq-O, red)	95-98
H-1 (eq)	5.3-5.7	C-1 (ax-O, glyc)	98-103
$H\text{-}CO_2$	5.9	C-1 (eq-O, glyc)	103-106
		C-1 (fur)	106-109
		COOH	174-174
		COOR	175-180

Ax: axial; eq: equatorial; red: reducing; glyc: glycosidic; fur: furanosyl

3.4 Animal Studies

3.4.1 Rats

Animals such as mice, rats, guinea pigs, or pigs are animals typically used for feeding research studies. Rats were chosen in this study for a few reasons: i) the gastrointestinal tract of rats are relatively similar to humans as compared to other small species e.g. mice (DeSesso & Jacobson, 2001) ii) limited quantities of mamaku gum which require use of a smaller animal species, and iii) the previous study by Lentle et. al. (2010) on effects of the mamaku gum on stomach motility was carried out in rat stomachs maintained *ex vivo*. Pigs, which have a digestive physiology similar to humans, would be ideal as second choice for this study (Paeschke & Aimutis, 2011). The Sprague Dawley, Wistar and Long-Evans rats are most commonly used rat species for general purpose and dietary/nutritional studies.

3.4.1.1 Stomach

There are a few disparities between the rat and human stomach which should be noted. Although both humans and rats have a single-chambered stomach, the rat stomach is comprised of two different regions – the forestomach and the glandular stomach, separated by a limiting ridge which prevents vomiting in rats by closing the orifice to the oesophagus (Figure 3.22). The forestomach is connected to the oesophagus and lined by a stratified epithelium. Bacterial digestion of the food takes place in this region. The glandular stomach is responsible for acidic and proenzymes secretion, therefore having a secretory epithelium similar to the entire human stomach. The absolute surface area of the rat stomach is $0.00062m^2$ as compared to $0.053m^2$ for the human stomach. The relative surface area (ratio of absolute surface area to body surface area) is 0.016 and 0.029 for the rat and human stomachs respectively (DeSesso & Jacobson, 2001).

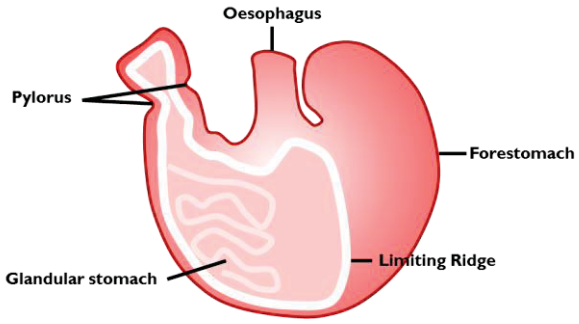

Figure 3.22 – Illustration of a rat stomach (adapted from DeSesso & Jacobson, 2001)

The relationship between stomach capacity and body weight of young Sprague Dawley rats could be estimated using Equation 3.42:

$$Y = 0.038x - 0.770 \quad \textbf{Equation 3.42}$$

where Y is the stomach capacity (ml) and X is the body weight (g) (Bull & Pitts, 1971). This gives an approximate stomach volume of 7ml for Sprague Dawley rats weighing 200g.

3.4.2 Oral Gavage

Oral (or orogastric) gavage is the intragastric administration technique used to deliver substances into the stomach accurately (Turner, Vaughn, Sunohara-Neilson, Ovari, & Leri, 2012). A curved or straight blunt-ended needle is used to administer the substance. The size (length and width) of the needle depends on the size and weight of the rats. During gavage, the rat is held firmly by the skin on the neck and back such that the head is kept immobile and in line with the back. The needle, attached to the syringe, is inserted into the mouth, passing the oesophagus and into the stomach (Figure 3.23) (Waynforth & Flecknell, 1992). Oral gavaging of rats in this study was performed by a highly skilled technician to prevent administration of substance into the lungs. Gavage volume used in various studies ranged from 2 to 40ml/kg body weight of the rat (Okva et al., 2006), although most studies prefer to use smaller volumes such as 5 ml/kg (Turner, et al., 2012). Large dosage volumes (≥20ml/kg) could have adverse effects on the rat such as increased stress levels (Brown, Dinger, & Levine, 2000), as well as unintentional delivery of the substance to the small intestine. Oral gavaging is generally not well received by the rats, with research showing increased diastolic and systolic blood pressure and heart rate after gavage (Okva, et al., 2006) especially if stainless steel gavage needles were used as compared to the flexible Teflon needles. However, Teflon or other softer needles can be bitten by the rat and pose a hazard to the rat. Ultimately, the experience of the technician plays a great role in determining the level of stress induced during gavage (McIntyre, 2001).

Figure 3.23 – Oral gavaging rats with mamaku gum

3.4.3 Statistical Analysis

Data were statistically analysed using one-way analysis of variance (ANOVA), including repeated measures ANOVA with software programs Minitab (Minitab Inc., PA, USA) and Mystat (Systat Software Inc., CA, USA). One-way ANOVA was used to test for any significant differences between the treatment groups (mamaku and water). Repeated measures ANOVA is also considered a one-way ANOVA, but it is used in situations where the groups are related. The independent variable, *i.e.* gavage number, has different levels or related groups, which in this case is the first, second, third and fourth gavages. In short, the repeated measures ANOVA was used to test differences in dependent variables e.g. body weight or food consumption between the mamaku and control groups over four time points (gavages) combined. Differences were considered to be significant when $p \leq 0.05$. Group means, standard deviation and standard error were calculated using Equation 3.43Equation 3.44 and Equation 3.45 respectively.

$$\bar{X} = \frac{1}{n}\sum_{i=1}^{n} X_i \qquad \textbf{Equation 3.43}$$

$$\sigma = \sqrt{\frac{\sum_{i=1}^{n}(X_i - \bar{X})^2}{n-1}} \qquad \textbf{Equation 3.44}$$

$$SE = \frac{\sigma}{\sqrt{n}} \qquad \textbf{Equation 3.45}$$

Chapter 4 Rheological Characterisation of Mamaku Polysaccharide

4.1 Introduction

Rheology, or the deformation and flow of the material, is an important functional property of polysaccharides for use in thickening and processing etc. (Lapasin & Pricl, 1999). There are two main methods of deformation which can be applied to the material *i.e.* by shear or extension. Within each deformation mode there are various experimental set-ups and conditions which can be used to probe molecular behaviour of the polymer. Figure 4.1 illustrates the various shear and extensional rheological techniques used to characterise the mamaku polysaccharide. This chapter covers rotational shear rheology *i.e.* shear- time- and shear history-dependent rheology, small (linear) and large (non-linear) oscillatory shear rheology and finally extensional rheology using the capillary breakup extensional rheometer (CaBER). Further studies on the extensional properties of the mamaku using the filament breakup extensional rheometer (FiSER) and optimised shape cross-slot extensional rheometer (OSCER) were carried out in collaboration with the Hatsopoulos Microfluidics Laboratory of Massachusetts Institute of Technology and are not included in this thesis. The various rheological techniques complement each other on the linear and nonlinear responses of the polysaccharide, based on a spectrum of deformation modes possible during applications.

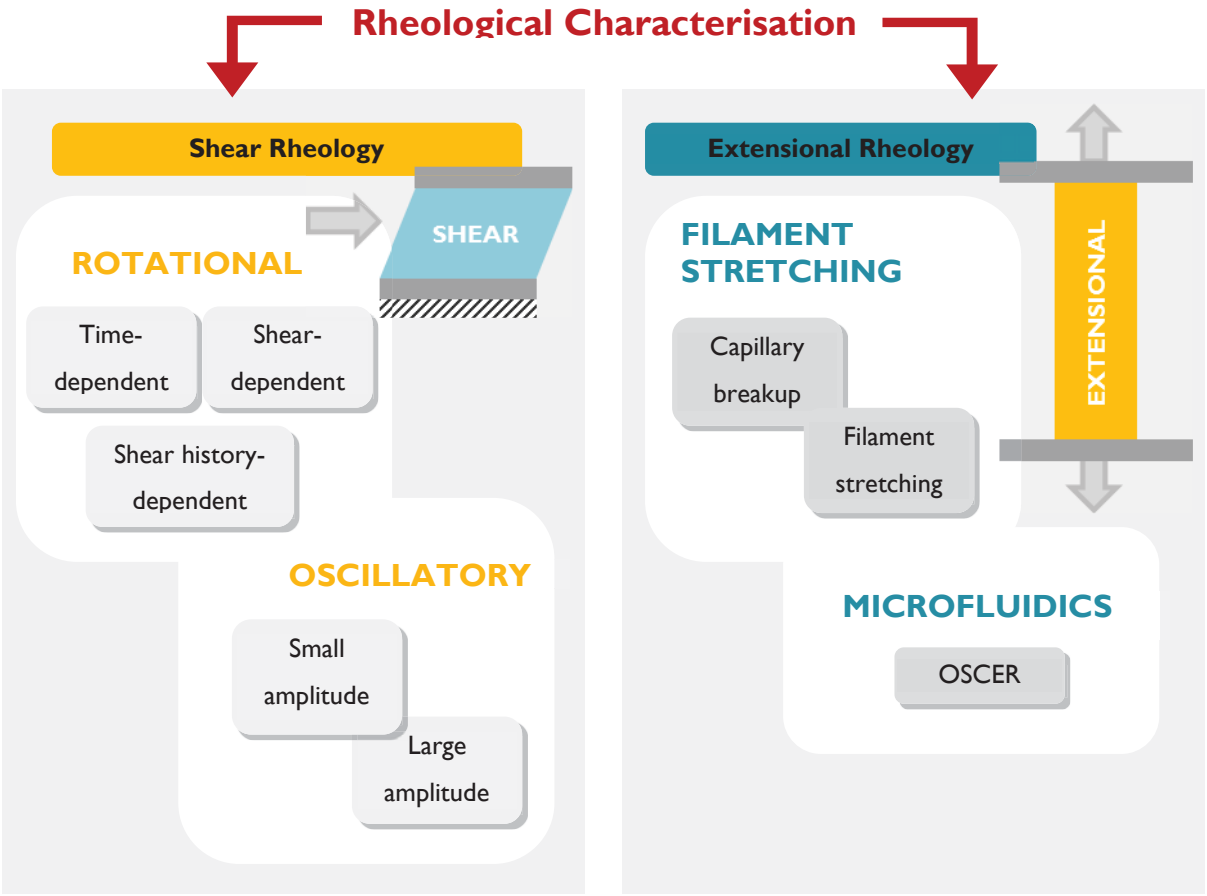

Figure 4.1 – Flow diagram of rheological techniques (shear and extensional) used to characterise the mamaku polysaccharide

4.2 Materials and Methods

4.2.1 Rotational Shear Rheology

All rotational and oscillatory shear rheological measurements were made using a Paar Physica MCR 301 rheometer (Anton-Paar, Graz, Austria) in controlled shear rate (CSR) mode at 20°C (unless otherwise stated). The specifications and instrument limitations are shown in section 3.2.1.4 (Table 3.2). Flow instabilities such as wall-slip were also discussed and investigated using various measurements geometries and surfaces (Figure 3.10 andFigure 3.11).

4.2.1.1 Shear-Dependent Rheology

Shear-dependent rheology was measured using either the double gap (DG 26-7 and C-PTD 200) or cone-and-plate (CP 40-4 and P-PTD200/56, gap = 0.049 μm) geometry. Data points were collected using a log-ramp time setting of 30 to 2s (initial to final). The temperature of the rheological measurement was controlled using a Peltier system to an accuracy of 20 ± 0.1°C.

4.2.1.2 Time-Dependent rheology

Constant-shear and normal stress measurements were made with the cone-and-plate (CP 40-4 and P-PTD200/56, gap = 0.049 μm) geometry. Data points were collected at 10 second intervals. The temperature was controlled using a Peltier system to an accuracy of 20 ± 0.1°C. The samples were allowed to rest for 10 minutes after loading into the geometry prior to starting the test. This was done to reduce any effects of shear history and for temperature equilibration. A new sample was loaded into the geometry for each data series.

4.2.2 Oscillatory Shear Rheology

4.2.2.1 Small Amplitude Oscillatory Shear

Amplitude sweeps (0.1 to 100% strain) were carried out prior to frequency sweeps to determine the linear viscoelastic region. Frequency sweeps were made in the range of 0.01 to 100Hz using a strain value of 5%. Data points were collected using the 'no time setting' option *i.e.* data recorded after equilibration.

4.2.2.2 Large Amplitude Oscillatory Shear

Large amplitude oscillatory shear (LAOS) measurements were made in the direct strain oscillation (DSO) mode which allows for real time position control for setting an ideal sinusoidal strain waveform required in LAOS tests. Amplitude sweeps were conducted in the range of 0.1 to 10,000% strain (γ_0) at an angular frequency (ω) of 10 rad/s. The 'no time setting' option on the rheometer was used to record data points. The samples were allowed to rest for 10 minutes prior to starting the test for temperature equilibration as well as to reduce any effects of shear history. Geometry inertia may affect torque readings at high frequencies and strain amplitudes. The waveforms (and raw phase angle) were constantly monitored to ensure that raw phase

angle did not exceed 170°. Above 170°, the contributions from inertia dominate and the data becomes unreliable. However, the Paar Physica rheometer directly controls sample torque in the DSO mode which could eliminate interference from sample inertia. Hence, at low frequencies the inertia effects were not likely to be present.

Raw stress, strain and strain rate values were exported from the Paar Physica Rheometer software and processed using MITlaos version 2.1 beta, a freeware LAOS data analysis program run on MATLAB® kindly provided by Ewoldt, Hosoi and McKinley (2009). The MITlaos software was used to determine the moduli parameters large-strain modulus (G'_L) (Equation 3.22), minimum-strain modulus (G'_M) (Equation 3.21) , large-rate viscosity, (η'_L) (Equation 3.24), minimum-rate viscosity (η'_M) (Equation 3.23), strain-stiffening ratio (S) (Equation 3.25) and shear-thickening ratio (T) (Equation 3.26).

$$G'_L(\gamma_0) = \frac{\sigma}{\gamma}|_{\gamma=\gamma_0} \quad \textbf{Equation 4.1}$$

$$G'_M(\gamma_0) = \frac{d\sigma}{d\gamma}|_{\gamma=0} \quad \textbf{Equation 4.2}$$

$$\eta'_L(\gamma_0) = \frac{\sigma}{\dot{\gamma}}|_{\dot{\gamma}=\dot{\gamma}_0} \quad \textbf{Equation 4.3}$$

$$\eta'_M(\gamma_0) = \frac{d\sigma}{d\dot{\gamma}}|_{\dot{\gamma}=0} \quad \textbf{Equation 4.4}$$

$$S = \frac{G'_L - G'_M}{G'_L} \quad \textbf{Equation 4.5}$$

$$T = \frac{\eta'_L - \eta'_M}{\eta'_L} \quad \textbf{Equation 4.6}$$

4.2.3 Extensional Rheology (CaBER)

Extensional properties were characterised using a capillary breakup extensional rheometer (CaBER) device. The principles of its operation are as described in the experimental techniques section (Chapter 3). The native mamaku solution (5% w/w, 25°C) was initially loaded between the plates (plate diameter or initial fluid filament diameter, D_0 = 6mm), with the initial length L_0 = 1.6mm (initial aspect ratio $\Lambda_0 = L_0/D_0$ = 0.27), and stretched to a final length L_f = 7.4mm (final aspect ratio $\Lambda_f = L_f/D_0$ = 1.23). The initial length was chosen such that $L_0 < L_C$, where L_C is the capillary length of $L_C = \sqrt{\sigma/\rho g} \approx 2mm$, and σ is the surface tension of the solution, ρ the density and g the acceleration due to gravity. The mid-plane diameter of the fluid filament was monitored using a laser micrometer with time. High-speed video at 60 frames per second using a Canon EOS 7D camera was taken to locate and confirm the onset of the elasto-capillary regime by monitoring the shape of the fluid filament between plates. Each sample was repeated at least five times and the data was averaged. Surface tension of the polysaccharide solution was measured separately using a Krüss digital K10ST digital tensiometer which the procedures are not be described in this study.

4.3 Results and Discussion

4.3.1 Shear-Dependent Rotational Shear Rheology

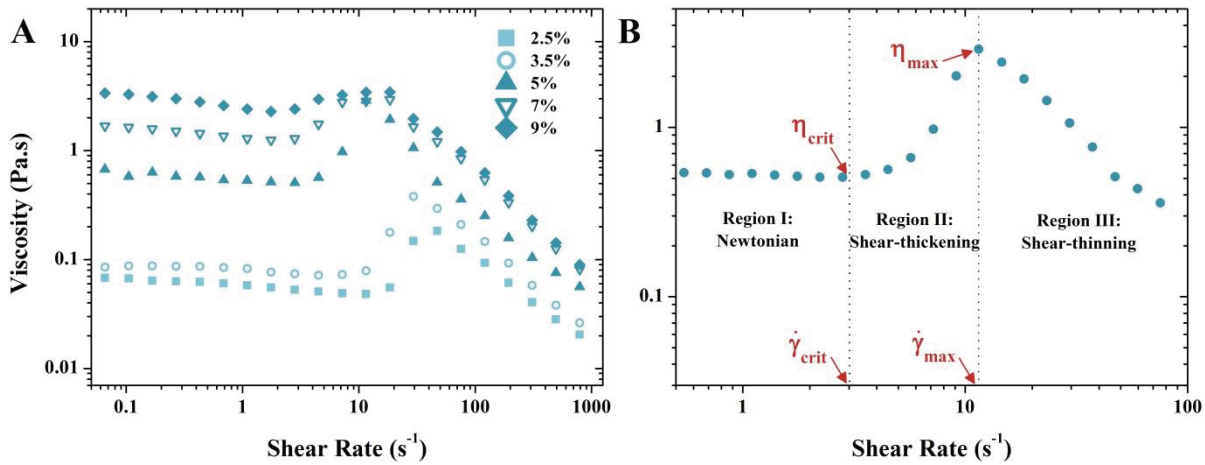

Figure 4.2 – a) Viscosity curves of 2.5 (■), 3.5 (○), 5 (▲), 7 (▽) and 9% (◆) w/w native mamaku polysaccharide; b) representation of Newtonian, shear-thickening and shear-thinning regions on a viscosity curve

The viscosity curves (viscosity with shear rate) of the mamaku solution at various concentrations are shown in

Figure 4.2a. Three distinct regions for the viscosity curves were observed (

Figure 4.2b) – the first region (low shear rates) was Newtonian, with increasingly shear-thinning tendencies at higher concentrations. The second region (intermediate shear rates) was the shear-thickening region, where onset of shear-thickening took place at $\dot{\gamma}_{crit}$ and η_{crit} After reaching a local maximum in viscosity η_{max} at $\dot{\gamma}_{max}$, the viscosity started to decrease in the third region (high shear rates) *i.e.* shear-thinning. A modified Cross' equation for shear-thickening fluids (Galindo-Rosales, Rubio-Hernández, Sevilla, et al., 2011) was also fitted to the viscosity curve of the mamaku polysaccharide (Appendix A, Figure A1 & Table A1). With increasing concentration, the onset of shear-thickening was shifted to lower shear rates, the extent of shear-thickening (η_{max}/η_{crit}) diminished, and shear-thickening took place over a wider shear rate range. The critical stress at which the network ruptures increased with concentration as well (Appendix A, Figure A2).

This behaviour of shear-thickening followed by shear-thinning is typical of shear-thickening fluids or associative polymers (Galindo-Rosales, Rubio-Hernández, & Sevilla, 2011; Van Egmond, 1998). A simple hypothesis for shear-thickening of the mamaku polysaccharide is as follows: at low shear rates (region I), the polysaccharide molecule remains in equilibrium as the time scale of deformation is longer than its disentanglement time. Intra- and intermolecular associations are recovered faster than its rate of deformation, thus resulting in a Newtonian behaviour. At higher concentrations, entanglements start to dominate and shear-thinning becomes more distinct even at the lower shear rates. Moving to intermediate shear rates, the molecules start to unravel and align with the flow direction. For most polymers, this disentanglement continues with increasing shear and manifests as a typical shear-thinning behaviour. However, for shear-thickening polymers, shearing exposes

certain groups within the molecule which can associate with other molecules, resulting in an increase in viscosity (Ballard, et al., 1988). Finally, at high shear rates (region III) above a critical stress limit, these transient associations are broken up resulting in shear-thinning behaviour. This hypothesis was tested using various rheological techniques in this chapter. In the next chapter, the rheological properties were further explored under the influence of various environmental factors such as temperature, urea, ionic strength and pH.

4.3.2 Time-Dependent Rotational Shear Rheology

4.3.2.1 Viscosity

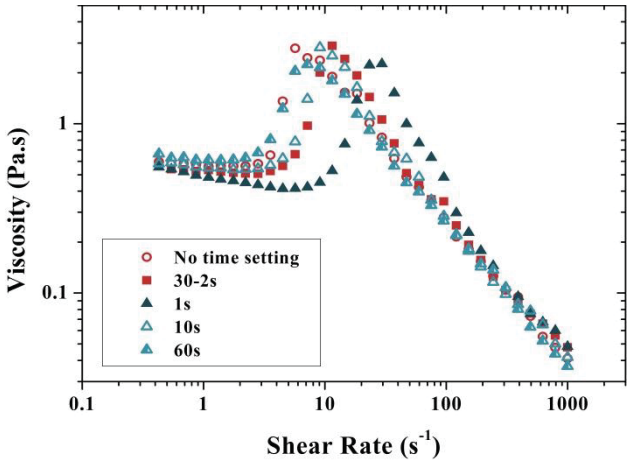

Figure 4.3 – Viscosity curves of 5% w/w mamaku obtained with various data collection time settings at 20°C

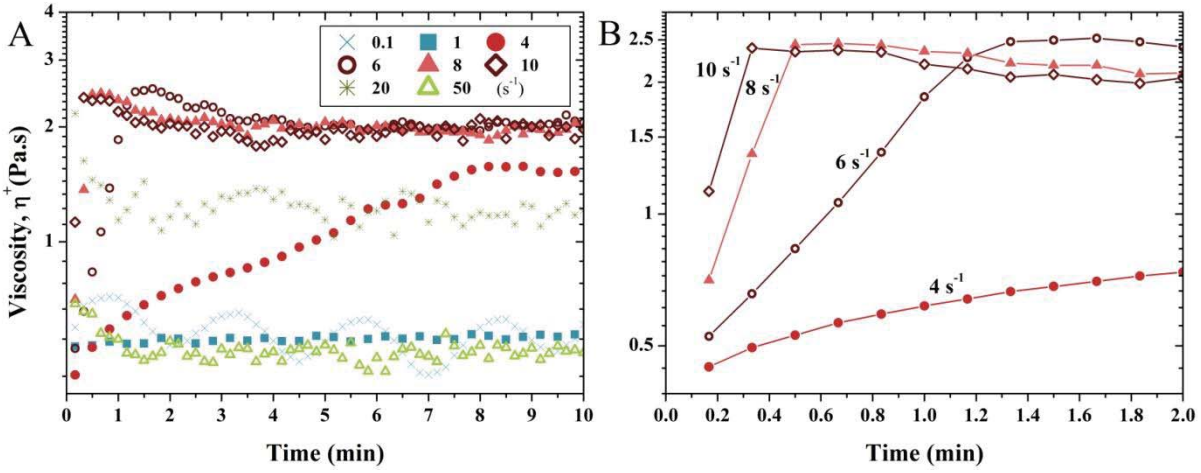

Figure 4.4– a) Viscosity of 5% w/w mamaku as a function of time at various shear rates at 20°C; b) magnified at 4 (●), 6 (○), 8 (▲) and 10s-1 (◇) during the first two minutes of the measurement

A reliable measurement of viscosity requires that the material reaches steady state at each shear rate. The rheometer software offers various standard time settings for data collection. Viscosity measurements can be taken at fixed time intervals, they can vary with shear rate, or a steady-state option can be selected ("no time setting"). Figure 4.3 shows the viscosity curves obtained for 5% w/w mamaku solution using different measurement time settings. The difference in viscosity curves obtained indicate that time effects were present along with shear effects. The shear rate at which the onset of shear-thickening and maximum viscosity occurs

is sensitive to the time setting, but the maximum viscosity reached appeared to be independent of it. The steady-state viscosity was not reached when short measurement time intervals were used (1, 10, or log ramp 30-2s). A log ramp time setting of 30-2s refers to a measurement time of 30s at the lowest shear rate ($0.1s^{-1}$), and logarithmically decreasing to 2s at the highest shear rate ($1000s^{-1}$).

Time-dependent viscosity of the mamaku was further investigated at various shear rates, especially at shear rates at which shear-thickening was observed (Figure 4.4a-b). The viscosity did not show time-dependency at $1s^{-1}$ or below. However, at a higher shear rates e.g. $4s^{-1}$, the viscosity increased slowly and steadily and finally plateauing after approximately eight minutes. For shear rates 6, 8 and $10s^{-1}$, the viscosity increased rapidly and plateaued at 2 Pa.s within two minutes. The viscosity at $10s^{-1}$ reached steady-state in a shorter time as compared to 8 and $6s^{-1}$ (Figure 4.4b). In other words, the polysaccharide exhibited anti-thixotropic behaviour at shear rates from 4 to $10s^{-1}$. At $20s^{-1}$, the viscosity decreased initially and continued to fluctuate around an average of 1.2Pa.s. This viscosity value at $20s^{-1}$ was lower than at 6-$10s^{-1}$, with the lowest value of 0.55 Pa.s at $50s^{-1}$, indicating shear-thinning behaviour after shear-thickening of the material. Shear-thickening observed in a viscosity curve may sometimes be due to elastic instability (Neelamegam, Shankar, & Das, 2013). By obtaining increasing steady state viscosity values at shear rates 4 to $10s^{-1}$ for the mamaku gum, it was ascertained that shear-thickening is a real rheological property of the polysaccharide. Since it was established that the measurement time settings have a substantial effect on the viscosity curves obtained, care was taken to ensure that samples were measured using the same settings for a fair comparison even if an absolute steady-state was not reached.

The gradual increase in viscosity of the material under certain shear rates with time is an indication of intermolecular associations taking place within the polymer chain. Furthermore, these increments do not resemble start-up transient stress overshoots sometimes observed when initiating a test. The association is a relatively slow process, which could only be captured at specific shear rates. The hypothesis for shear-thickening and anti-thixotropic behaviour is that shear flow stretches and aligns the polysaccharide chains which expose certain sites available for forming intermolecular junctions. Hydrogen bonds are often responsible for such anti-thixotropic associations in polymers such as pectin (Kjøniksen, et al., 2003), hyaluronan (Maleki, Kjoniksen, & Nystrom, 2007), semidilute poly(2-hydroxyethyl methacrylamide) in glycerine solutions (Kosvintsev, Riande, Velarde, & Guzman, 2001), chitosan-grafted polyacrylamide solutions (Jin et al., 2013) and polystyrene solutions (Laufer, Jalink, & Staverma.Aj, 1973). This is due to their relatively strong interaction energies, as well as their dependencies on bond orientation and distance (Israelachvili, 2011), which are easily influenced by shearing.

The mechanism of this process could be qualitatively explained by the energetically crosslinked transient network (ECTN) model (Lele & Mashelkar, 1998), where the associations are thermodynamically driven transient crosslinks. The ECTN model describes that there needs to be cooperative mobility and orientation of the polysaccharide chains, leading to cooperative zipping of the stretched chain through intermolecular associations and forming ladder-like structures. The dynamics of this process are inherently slow, which could explain the time required for the viscosity of the mamaku solution to increase at e.g. $4s^{-1}$ (~8 minutes to reach steady state). As the shear rate increased from 6 to $10s^{-1}$, the chains are stretched more quickly which

promotes interactions at a faster rate. Hence, the viscosity increase is more rapid. These shear rates are able to sufficiently stretch the chain and increase interactions without destruction of the crosslinks, therefore an overall net increase in viscosity is observed. However, at higher shear rates like $20s^{-1}$, the shear rate contribution to crosslink dissociation becomes more dominant and competition between association and dissociation led to fluctuations in viscosity with time. Likewise, a constant viscosity was observed at $1s^{-1}$ probably because the shear flow is too weak to stretch the polymer chain and form associations.

4.3.2.2 Normal Stresses

Normal stresses in polymers arise from their elastic nature. The deformation of the polymer under shear causes the polymer to store energy. Under sufficiently high shear rates, this energy is released and the polysaccharide returns to an entropically favourable conformation (Shaw, 2012). The energy is usually released at a direction perpendicular to the shearing direction, which results in a force to the normal direction *i.e.* normal force. Earlier studies have shown that the mamaku solution displayed rod-climbing (or Weissenberg) effects (Goh, et al., 2007). The first normal stress difference N_1 *i.e.* stress difference between direction of shear and the direction perpendicular to the shearing plates, is responsible for various viscoelastic phenomena such as rod-climbing, die-swell and the open-siphon effect (Macosko, 1994).

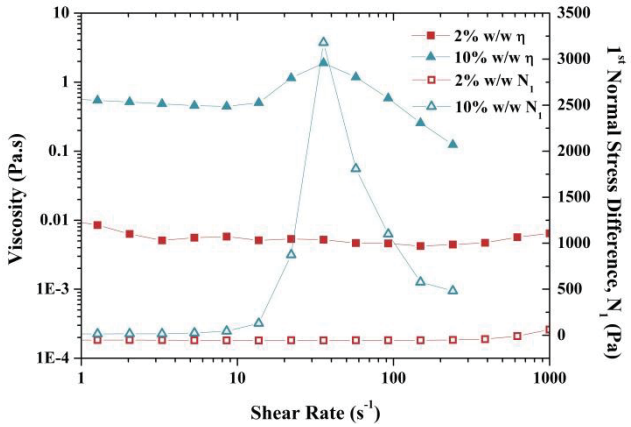

Figure 4.5 – Viscosity and first normal stress difference vs. shear rate for 2 and 10% w/w mamaku solutions at 20°C

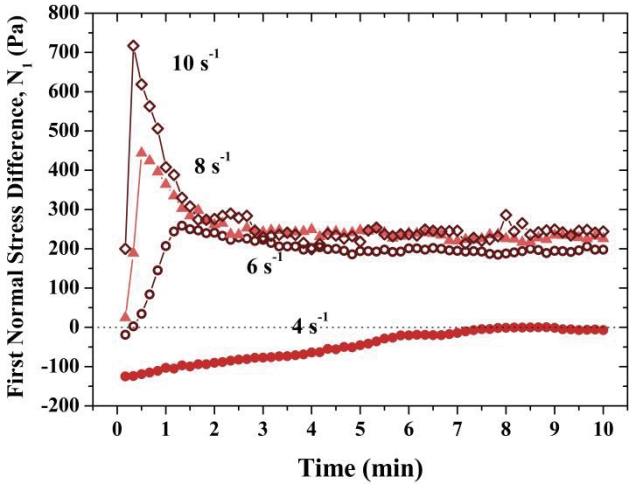

Figure 4.6 – First normal stress difference (N_1) of 5% w/w mamaku with time at constant shear rates 4, 6, 8 and 10s-1 at 20°C

Figure 4.5 shows the change in N_1 with shear rate for 2% w/w mamaku (non-shear thickening) and for 10% w/w mamaku (shear-thickening). For 2% w/w mamaku, there was no shear-thickening nor changes in N_1 observed ($N_1 \leq 0$ Pa). For 10% w/w mamaku at low shear rates prior to critical shear rate (shear rate at onset of shear-thickening, $\dot{\gamma}_c$), the normal stresses were not considered large. However, there was a rapid increase in N_1 which coincides with the onset of shear-thickening, reaching a maximum N_1 (~3000 Pa) at a similar shear rate as the maximum viscosity. Furthermore, the increase in viscosity under a constant shear rate also corresponded to an increase in N_1 (Figure 4.4 and Figure 4.6). The normal stress difference recorded at $4s^{-1}$ was markedly lower than at $6\text{-}10s^{-1}$, with negative values ($N_1 \leq 0$) throughout the measurement period as it approached 0 Pa after 7 minutes. Strong normal stress difference overshoots were observed for 8 and $10s^{-1}$ initially, which all plateaued to similar values of ~200 Pa with time including the profile at $6s^{-1}$. The appearance of normal stresses (or 1st normal stress differences) coincides with shear-thickening and anti-thixotropy as seen from Figure 4.4. Therefore, it seems reasonable to assume that the same molecular interactions causing shear-thickening and anti-thixotropy are most likely also responsible for the normal stresses. It appears that the time-scale at $4s^{-1}$ is optimum for observing molecular rearrangement within the experimental time of ten minutes. The slow increase in viscosity or normal stresses suggests successive unravelling of the polysaccharide chain and its progressive formation of associations. When the shear rate was increased e.g. to $6s^{-1}$, the chain was stretched at a faster rate and increased number of associations could be formed simultaneously. Also, the final plateau viscosity (and normal stress) at $4s^{-1}$ is still lower than at $6\text{-}10s^{-1}$, indicating that the molecule was not fully stretched under this shear rate and therefore the number of associations was correspondingly lower.

A strong positive first normal stress difference is often observed with shear-thickening in polymers (Aitkadi, Carreau, & Chauveteau, 1987; Munoz & Santamaria, 2003). Shear-induced intermolecular hydrogen bonds in these polymers have been attributed to the enhancement of solution elasticity and subsequently normal stresses and viscosity. The molecular origin of shear-thickening in associating telechelic polymers in transient networks have also been shown to be the same for the increment in the corresponding first normal stress coefficient Ψ_1 (Koga & Tanaka, 2010). Nevertheless, there have been instances in hydrophobically modified ethoxylated urethane (HEUR) solutions where an increase in first normal stress differences is not accompanied

by shear-thickening (Pellens, Corrales, & Mewis, 2004; Suzuki, Uneyama, & Watanabe, 2013). The intermolecular associations formed on stretching and cooperative alignment of the mamaku chains in our case, are very likely to have contributed to the elasticity of the material.

4.3.2.3 Shear History

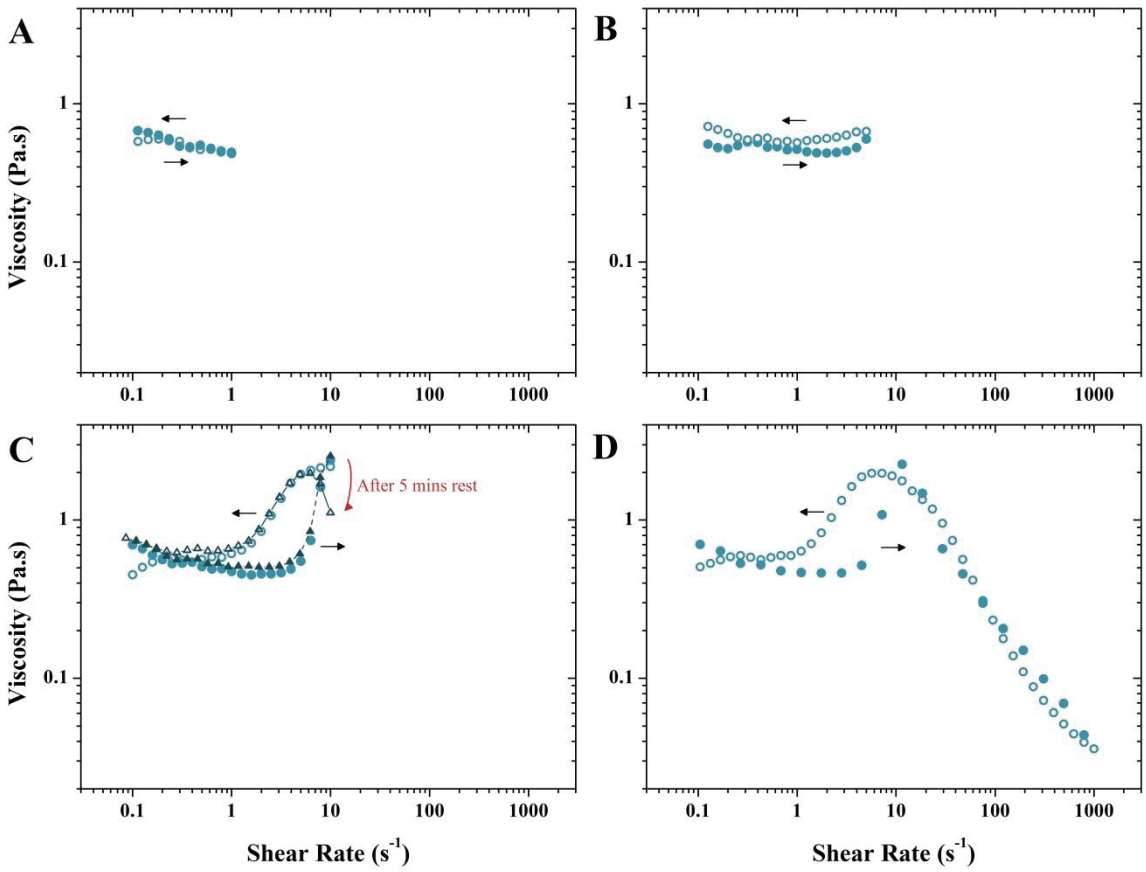

Figure 4.7 – Viscosity curves of 5% w/w mamaku on increasing (filled symbols) and decreasing (unfilled symbols) shear rates at 20°C; a) 0.1 to 1s^{-1}; b) 0.1 to 5s^{-1}; c) 0.1 to 10s^{-1} (additional ▲/△ symbols indicate viscosity with 5 minutes rest after the up-curve); d) 0.1 to 1000s^{-1}

The shear-history dependence of the mamaku polysaccharide was tested by increasing and subsequently decreasing the shear rate to observe any hysteresis (Figure 4.7a-d). The up-curve coincided with the down-curve when the polysaccharide was sheared to 1s^{-1} *i.e.* no hysteresis observed (Figure 4.7a). However, the down-curve exhibited slightly higher viscosities when sheared to 5s^{-1} (Figure 4.7b). Hysteresis was most distinct when the polysaccharide was sheared to 10s^{-1} (Figure 4.7c), with viscosities being higher in the down-curve for almost the entire shear rate range. When sheared all the way to 1000s^{-1}, no hysteresis effects were observed between 10 and 1000s^{-1}, but again higher viscosities were measured on the down-curve at shear rates ≤ 10s^{-1} (Figure 4.7d). Similar viscosities for the down-curve were obtained when the material was sheared from 0.1 to 10s^{-1}, rested for five minutes and then sheared from 10 to 0.1s^{-1} (Figure 4.7c; ▲ and △ symbols). One would expect a higher viscosity on the down-curve in the case of structural recovery after five minutes of rest. However, the viscosity was found to be lower. Therefore these hysteresis effects were not likely due to structural regeneration (rheopexy) with time (or at least within the time-scale of the experiment).

Furthermore, a lower viscosity at $10s^{-1}$ (see red arrow in Figure 4.7c) was measured after resting, indicating that the associations had relaxed upon cessation of shear, but quickly reformed after reinstating shear.

As discussed earlier in Figure 4.4, the onset of the increase in viscosity over time occurred at $4s^{-1}$, which means associations were formed at shear rates between $4\text{-}10s^{-1}$ and broken down at higher shear rates ($>10s^{-1}$). By shearing the polymer at $10s^{-1}$, associations or crosslinks were formed which were not as easily disrupted at the lower shear rates, therefore higher viscosities were observed on the down-curves (Figure 4.7c-d).

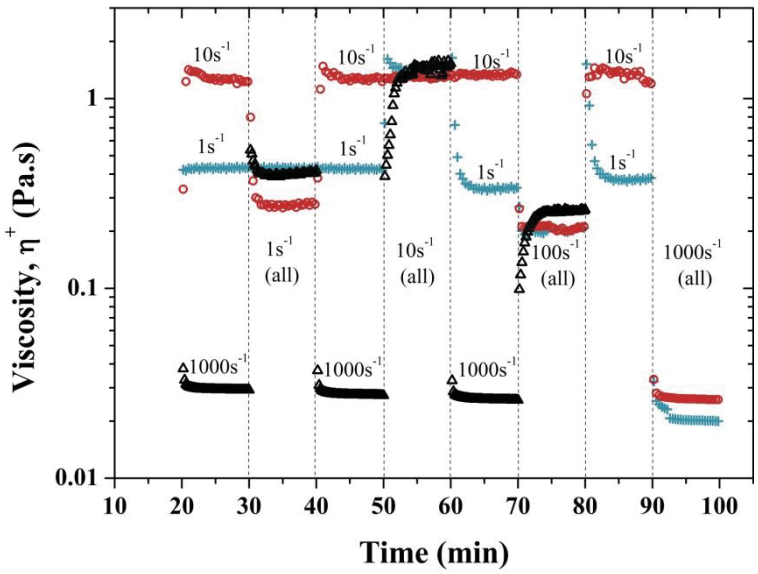

Figure 4.8 – Viscosity changes with time as a function of shear history of 1 (+), 10 (○) or $1000s^{-1}$ (△) of 5% w/w mamaku at 20°C; each symbol represents one data series sheared for a total of 80 minutes. For example, to test the effects of shear history at $1000s^{-1}$ (△/black symbols), the sample was sheared at $1000s^{-1}$, followed by $1s^{-1}$, and subsequently back to $1000s^{-1}$, and then followed by $10s^{-1}$, and again back to $1000s^{-1}$ then followed by $100s^{-1}$.

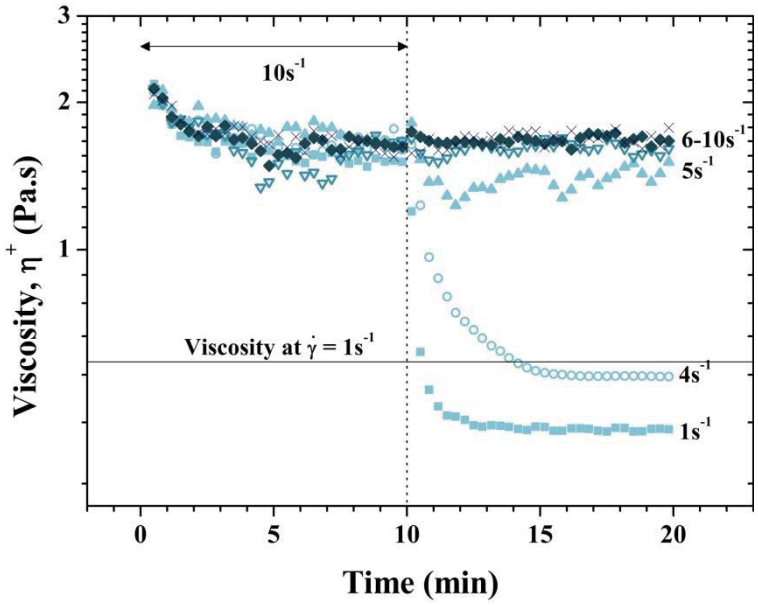

Figure 4.9 – Viscosity changes with time as a function of pre-shear at $10s^{-1}$ for 5% w/w mamaku at 20°C; solid line represents viscosity of 5% w/w mamaku at $1s^{-1}$ from rest

Figure 4.8 shows the viscosity profile when the mamaku solution was first subjected to pre-shearing rates of 1, 10 or 1000s^{-1} followed by either 1, 10, 100 or 1000s^{-1}. Overall, the material showed interesting dependence on shear history, which further revealed the possible intermolecular associations between polymer chains responsible for shear-thickening. A main observation was that a high pre-shear rate (1000s^{-1}) led to slow viscosity recovery at subsequent shearing of 10 or 100s^{-1} (△ symbols between 50-60 and 70-80 minutes). This suggests a slow restructuring of the transient network after the chain has been stretched considerably at 1000s^{-1}. Also, the final viscosity obtained at 100s^{-1} after pre-shearing at 1000s^{-1} was slightly higher than pre-shearing at 1 or 10s^{-1} (△ symbols between 70-80 minutes), suggesting that more 'zipping' sites have become available for intermolecular associations. A stretched conformation encourages more intermolecular associations between aligned chains (Kjoniksen, Hiorth, & Nystrom, 2005; Kjøniksen, et al., 2003; Maleki, et al., 2007). This agrees with the ECTN model whereby the associations are formed via cooperative zipping.

It has been established earlier that 10s^{-1} is the shear rate at which the rate of association is greater than the rate of dissociation which leads to higher viscosities. An initial decrease in viscosity at 1s^{-1} after being pre-sheared at 10s^{-1} supports that association structures are being broken down (○ symbols between 30-40 minutes). However, the viscosity at 10s^{-1} was lower, as compared to pre-shearing at 1 or 1000s^{-1}. It was expected that the viscosity should be higher than pre-shearing at 1 or 1000s^{-1} due to the formed transient structure. It could be possible that the stretched and aligned zipped structures are able to slide past each other, as compared to the molecule returning to a random coil state from 1000 to 1s^{-1}. Adding to the complexity of the system, the viscosity obtained with the same shear-history of 10 to 1s^{-1} was not the same as the other data set shown in the figure (+ symbols from 50-70 minutes). Therefore shear-history effects may not be easily erased even with ten minutes of shearing at any particular shear rate.

The material also exhibited thixotropic behaviour at 1s^{-1} after it was sheared at the higher shear rates *i.e.* 10, 100 or 1000s^{-1} (+ symbols at 60-70 and 80-90 minutes; △ symbols at 30-40 minutes). The shear rate of 1s^{-1} is too small to sustain the stretched conformation of the chain i.e. the structures formed during chain stretching at higher shear rates cannot be maintained at 1s^{-1}. The slow decrease in viscosity may indicate the chains returning to an entropically favourable random coil state with possibly a reassembled structure similar to (but not quite the same as) the original sample.

Pre-shearing at 1s^{-1} did not have significant effect as deformation at this shear rate may be too small to stretch and expose association sites nor maintain any existing 'zipped' structures. However, the viscosity at 1000s^{-1} after pre-shearing at 1s^{-1} is lower than pre-shearing at 10s^{-1} (+ symbols between 90-100 minutes) or without pre-shearing. This may be the effect of cumulative shear-histories or rearrangement with different network structures.

The effect of shear-history at 10s^{-1} *i.e.* shear rate in the shear-thickening region was further explored in Figure 4.9. As previously discussed, pre-shearing at 10s^{-1} followed by shearing at 1s^{-1} caused the viscosity to be lower as compared to a non-pre-sheared sample. On the other hand, the viscosity growth at 4s^{-1} as observed previously was lost. It is possible that by pre-shearing at 10s^{-1}, association structures are formed and the polysaccharide chains have not relaxed back to the conformation which allows growth of intermolecular interactions.

There was a large contrast between shearing at 4 and $5s^{-1}$, as shearing at $5s^{-1}$ did not decrease and stabilise the viscosity with time as in the case of 1 and $4s^{-1}$. A shear rate between 4 and $5s^{-1}$ may be the critical shear rate for onset of anti-thixotropy in the mamaku polysaccharide at 5% w/w concentration. Changing the concentration would result in a different critical shear rate. No effects were observed when pre-shearing at $10s^{-1}$ followed by shearing at 6, 8 or $10s^{-1}$. Based on the results, it is evident that a specific shear rate is required to trigger intermolecular associations

The ECTN model was first put forward in an attempt to explain various rheological phenomena in semi-dilute and concentrated solutions of hydrophilic polymers such as polyacrylamide (PAM), poly(acrylic acid) (PAA), poly(vinyl alcohol) (PVA) and poly(ethylene oxide) (PEO). The peculiar rheological observations made with these polymers include shear stress and normal stress overshoots with shearing and centrifugal expulsion of sample from geometry gap (Lele & Mashelkar, 1998); shear-thickening of high molecular weight PEO (Rivero, et al., 2012); and Weissenberg and open-siphon effects (Boger & Walters, 1993). Interestingly, the mamaku solution bears some rheological similarities to these polymers (PEO in particular). Both the mamaku polysaccharide and PEO exhibit the tubeless siphon effect and slimy and gel-like consistency when poured (Boger & Walters, 1993; Goh, et al., 2007).

The ECTN model predicts that for hydrogen bonded energetic crosslinks: i) there needs to be H-bonding groups on the chain, ii) hydrogen bond energy is of the order of kT where k is the Boltzmann constant and T is the absolute temperature, iii) specific site orientation is necessary for cooperative zipping and unzipping of ladder-like structures and iv) solvent quality affects the hydrogen bonds. As mentioned in the introduction, a previous study has demonstrated the loss of shear-thickening at elevated temperatures (~50°C), which strongly indicates the involvement of hydrogen bonds in intermolecular associations (Matia-Merino, et al., 2012). However, the ECTN model does not account for shear-thickening, with transient stress growths occurring within a relatively short time frame (< 3s) for synthetic polymers as compared to the mamaku polysaccharide (~60s). Overall, the model still has its inadequacies in explaining the shear-thickening of the polysaccharide, although there may be factors such as molecular weight and hydrogen bonding to water molecules which have not been accounted for (Rivero, et al., 2012).

4.3.3 Small Amplitude Oscillatory Shear Rheology

4.3.3.1 Frequency Sweeps

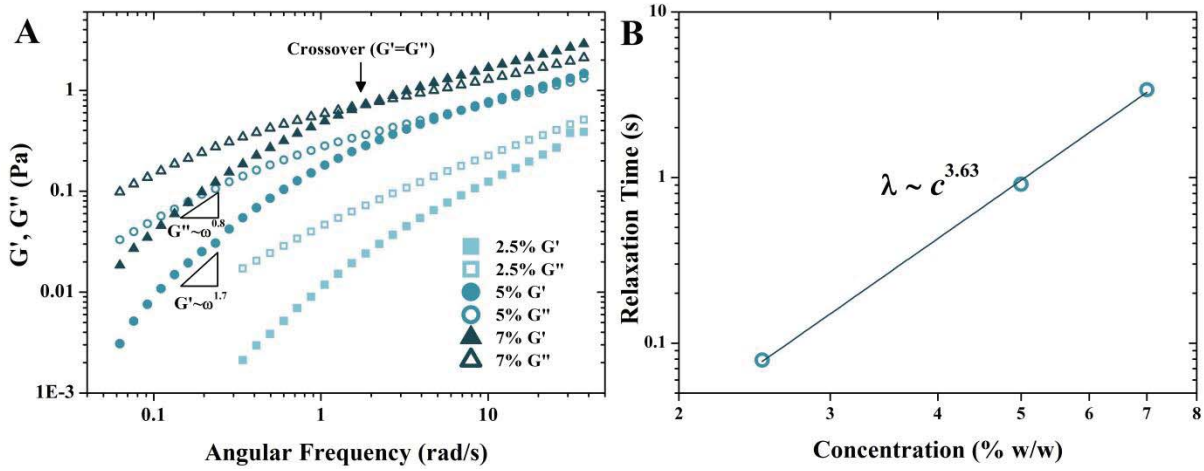

Figure 4.10 – a) Frequency sweep (γ_0 = 5%) and b) concentration dependence of relaxation time for 2.5, 5 and 7% w/w mamaku polysaccharide

The frequency sweeps of the mamaku solution were typical of entangled viscoelastic polymers (Figure 4.10a). At low frequencies, G"'>G' *i.e.* the material exhibited viscous flow. The polysaccharide chains were able to relax to the original equilibrium configuration through Brownian motion within these time scales (Lapasin & Pricl, 1999). On increasing frequency, a point was reached where G'=G". This is known as the crossover point, where above this frequency the elastic modulus predominates. The inverse of the frequency at crossover point is the terminal (or longest) relaxation time, λ, which showed a power-law dependence on concentration of $\lambda \sim c^{3.6}$ (Figure 4.10b). The exponent of 3.6 was relatively high as compared to other polysaccharide e.g. 2.0 for hyaluronan (Oelschlaeger, Coelho, & Willenbacher, 2013) and 3.1 for guar gum solutions (Jacques & Jean-Louis, 2004). As polymer concentration increased, the chain network density increases and intramolecular motion of chain segments became more restricted, thus prolonging the relaxation times. The higher exponent value of mamaku suggests additional intra- or intermolecular interactions per unit mass of polysaccharide material which retarded the relaxation process.

The relaxation spectrum of the material did not follow the Maxwell model where the slopes of G' and G" are 2 and 1 respectively. For a 5% w/w mamaku solution, G' $\propto\omega^{1.7}$ and G" $\propto\omega^{0.8}$, indicating that there was more than one mode of relaxation within the material. The relaxation behaviour may be better represented using fractional Maxwell models, where a broad spectrum of discrete relaxation times of the material is taken into account (Jaishankar & McKinley, 2013). The multiple relaxation times may have arisen from relaxation of intermolecular associations between discrete chain segments.

4.3.3.2 Complex Viscosity

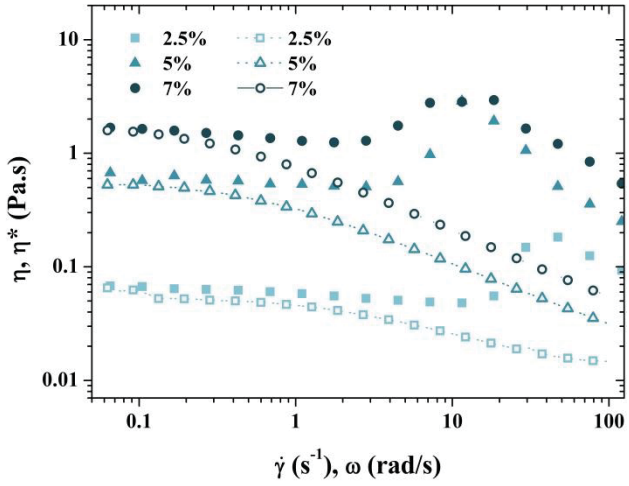

Figure 4.11 – Superposition of apparent viscosity (η, filled symbols) obtained by steady-shear measurements and complex viscosity (η*, unfilled symbols) obtained by oscillatory measurements for 2.5 (■), 5 (▲) and 7% (●) w/w mamaku solutions

Figure 4.11 shows the viscosity curves (viscosity vs. shear rate) and complex viscosity curves (complex viscosity vs. angular frequency) of 2.5, 5 and 7% w/w mamaku superimposed on the same graph. A shear-thinning profile without shear-thickening was detected with complex viscosity under oscillatory shear (up to 100 rad/s). Complex viscosity vs. angular frequency of the mamaku solution did not superimpose on its shear viscosity at angular frequency or shear rate above ~0.5 rad/s or s^{-1} (Figure 4.11). The values however did coincide at low values of angular frequency or shear rate below 0.5 rad/s or s^{-1}. In other words, the material disobeys the empirical Cox-Merz rule whereby a superposition should be observed. The Cox-Merz rule has been verified for many polymer melts, homogenous solutions and even shear-thickening suspensions (Cox & Merz, 1958; Raghavan & Khan, 1997; X. Xu, et al., 2006). However, deviation from the Cox-Merz rule is not uncommon especially for materials with shear-sensitive supramolecular structures, typically associative polymers, with the complex viscosity often being lower than shear viscosity (Alhadithi, Barnes, & Walters, 1992; Tanaka & Edwards, 1992). Disentanglement of the polymer is a nonlinear rheological function which occurs under large deformation, while complex viscosity is obtained as a linear viscoelastic property under small deformations. The fact that the mamaku solution disobeys the Cox-Merz rule supports the hypothesis of shear-thickening due to shear-induced associations, whereby associative groups within the polysaccharide were exposed only upon disentanglement.

4.3.4 Large Amplitude Oscillatory Shear Rheology

4.3.4.1 Amplitude Sweep

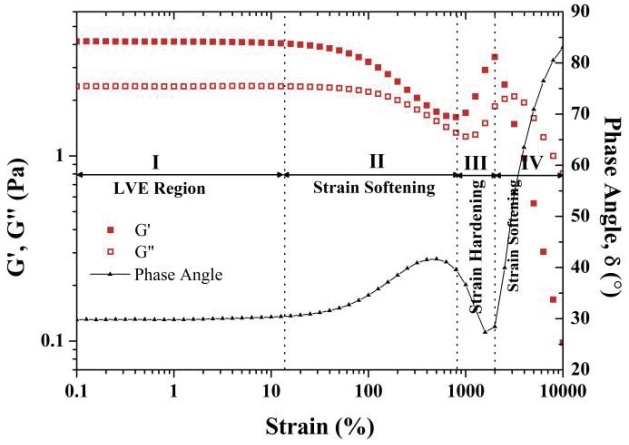

Figure 4.12 – Amplitude sweep (G' (■), G" (□) and δ (▲) as a function of % strain) of 10% w/w mamaku at ω = 10rad/s, 20°C.

The overall viscoelastic response of the 10% w/w mamaku gum is illustrated in an amplitude (strain) sweep test at ω=10 rad/s performed from 0.1 to 10,000% strain (Figure 4.12). The moduli (G' and G") response of the mamaku gum with strain can be divided into four regions as indicated in Figure 4.12: i) a large linear viscoelastic region (0.1 to ~20%) *i.e.* constant G' and G" independent of strain followed by ii) a decrease in moduli (strain-softening; 20-800%), iii) a strong increase in moduli (strain-hardening; 800-2000%) and v) a sharp drop in moduli (strain-softening; 2000-10,000%). The change in phase angle δ with strain is also shown (Figure 4.12). The phase angle (δ) represents the ratio between G' and G" ($\delta = \tan^{-1}(G''/G')$), which indicates whether the material is predominantly elastic (δ<45°) or viscous (δ>45°) at a given frequency.

The mamaku polysaccharide exhibited strong viscoelastic characteristics at 10% w/w concentration and a frequency of 10 rad/s, with G'>G" (*i.e.* δ<45°; Figure 4.12) within the LVER (0.1-20% strain). The material showed a relatively large LVER, with G' and G" independent of strain amplitudes up to 20%. A large LVER is often observed with entangled polymer solutions and melts of high molecular weight and long chain lengths, which requires much larger strains for disentanglement (Mezger, 2011).

The subsequent strain-softening for both G' and G" could be attributed to similar mechanisms involved in shear thinning (Hyun, et al., 2002). Beyond the LVER, the larger strain caused the entanglement points to break up and the polymer molecules to align with the oscillatory shear direction. This resulted in the decrease of moduli until a critical strain γ_{crit} (800%). The phase angle is ~30° in the LVER, which increases to ~40° (sample became less resistant to flow) as the material strain-softened and changed its molecular conformation during flow.

Above the critical strain, the moduli started to increase, entering into the region of strain hardening. The strain amplitude at the onset of strain-hardening and the strain-hardening peak are defined as critical strain γ_{crit} and maximum strain γ_{max} respectively. With the onset of strain-hardening, the phase angle dropped to 27° at G'_{max}

which was slightly smaller than the phase angle in the LVER of 30°. This indicates an increase in the proportion of stored energy to dissipated energy during strain-hardening, which could be due to the formation of elastically active chains (D. Xu & Craig, 2011) in an associative network. Beyond G'_{max}, the material strain-softened again and the phase angle rapidly increased to >45°. At this point, a crossover between G' and G" at ~3000% strain was also observed, indicating viscous flow.

According to the classification by Hyun *et. al.* (2002), the mamaku gum exhibited a strong strain overshoot (type IV) behaviour where both G' and G" reach a maximum peak *i.e.* an increase followed by a decrease. Strong strain overshoot is commonly observed in associative polymers (Tirtaatmadja, et al., 1997), which is believed to be the case of mamaku polysaccharide. As such, a network model based on creation (a) and loss (b) rates of associative junctions can be used to explain the different behaviour types (Sim, Ahn, & Lee, 2003). For strain-softening (type I) materials, creation rate is negative but loss rate is positive (*i.e.* $a < 0$, $b > 0$). For strain-hardening (type II) materials, the creation rate is positive and greater than two times the magnitude of loss rate (*i.e.* $a > 0$, $a > 2b$). For materials which show weak strain overshoot (type III), associative junctions are both created and lost, with the creation rate is smaller than the loss rate parameter (*i.e.* $a > 0$, $b > 0$, $a < b$). Type IV materials (strong strain overshoot) like the mamaku polysaccharide are similar to type III, where both the creation and loss rates are positive. However, the creation rate is greater than loss rate but smaller than two times the magnitude of loss rate (*i.e.* $a > 0$, $b > 0$, $b < a < 2b$).

Strain-stiffening appears to be characteristic to some biological materials such as collagen networks (Kurniawan, Wong, & Rajagopalan, 2012), keratin (L. L. Ma, Xu, Coulombe, & Wirtz, 1999) and F-actin (Semmrich, Larsen, & Bausch, 2008). The strain-stiffening behaviour of these anatomical biopolymers (e.g. collagen, myofibrils) serve to resist large deformations in order to reduce tissue damage (Storm, Pastore, MacKintosh, Lubensky, & Janmey, 2005). In the case of mamaku polysaccharide, it could be possible that the strain-hardening property has a protective function in the fronds and cell walls of the tree fern, for instance, i) to prevent the tree trunk from snapping under the common strong westerly winds in the Pacific and ii) to provide additional support to the unfurling and lengthening of the fronds during growth (Niklas & Spatz, 2012).

These observations fit the previous hypothesis that under strain deformation, the mamaku polysaccharide is stretched and disentangled, which then exposes its associative groups within the chain. These groups associate via intermolecular interactions causing strain-hardening at a certain applied strain or an increased resistance to strain deformation. On reaching a critical strain (or stress), the rate of disruption of intermolecular interactions becomes larger than its association, resulting in subsequent strain-softening after strain-hardening. This is likely due to destruction of the temporary molecular interactions with large polysaccharide chains.

4.3.4.2 Lissajous Plots

The individual stress vs. strain or strain-rate profiles at various fixed strain amplitudes along the amplitude sweep (Figure 4.12) was further examined using Lissajous-Bowditch plots (Figure 4.13). Lissajous-Bowditch (or Lissajous) curves are parametric plots of stress vs. strain (*elastic* Lissajous curve) or stress vs. strain rate ($\dot{\gamma} = \gamma_0 \omega$) (*viscous* Lissajous curve). Each curve represents an oscillatory shear cycle at a fixed frequency and amplitude with a sinusoidal strain input (Ewoldt, Clasen, Hosoi, & McKinley, 2007). It should be noted that an

amplitude sweep measures the viscoelastic response of the material under *steady-state* oscillatory shear across varying strain amplitude cycles γ_0, *i.e. intercycle*, whereas the Lissajous plots capture the *instantaneous* response of the material to the oscillatory shear at varying time-resolved strain, $\gamma(t)$, *i.e. intracycle*. A Hookean elastic solid is represented by a straight line (area=∅) and a Newtonian fluid represented by a circle (Deshpande, 2010) in an elastic Lissajous plot. The area of a stress-strain Lissajous curve is equal to the energy dissipated per unit volume per cycle, and therefore directly related to the loss modulus G''_1. Therefore a material with linear viscoelastic response would produce an ellipsoidal Lissajous curve, due to a first-order stress response to strain input. The onset of non-linearity can be easily detected from Lissajous curves, with the ellipsoids appearing stretched or deformed. Observation of the shape of Lissajous plots is therefore a qualitative and convenient tool to monitor nonlinearities in the material.

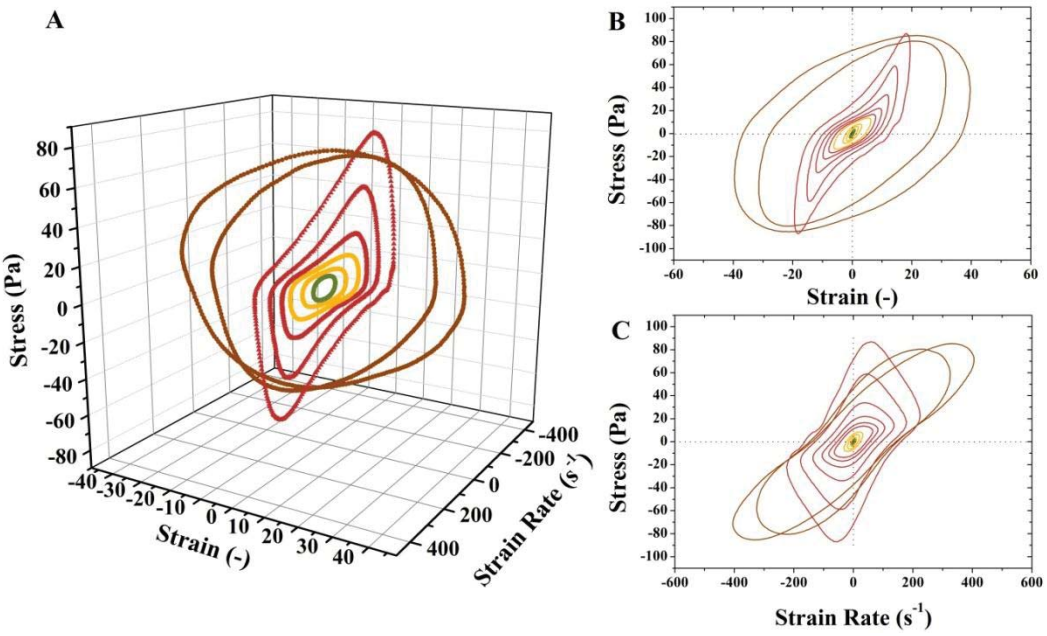

Figure 4.13 – a) Three-dimensional and b) two-dimensional Lissajous-Bowditch plots of stress vs. strain and c) stress vs. strain rate of 10% w/w mamaku at ω=10 rad/s from 0.1 to 3,000% strain, 20°C; The linear viscoelastic, strain-softening, strain-hardening and strain-softening regions are coloured green, yellow, red and brown respectively.

The Lissajous plots of 10% w/w mamaku are presented as a three-dimensional (3D) plot (Figure 4.13a), showing the evolution of stress vs. strain and strain rate from 0.1 to 3000% strain amplitude at a constant frequency of 10 rad/s. The 3D plot helps to visualise the stress output of the material when taking both strain and strain rate into account, thereby generating a unique rheological fingerprint of the material. In the case of mamaku polysaccharide, the plot revealed an interesting 'chair conformation' in the strain-hardening region. Such extent of nonlinearities were not observed in the 3D Lissajous plots of pseudoplastic materials such as xanthan gum (Ewoldt, Winter, Maxey, & McKinley, 2010), which are rectangular with strongly rounded corners (Appendix A Figure A6). The 3D plots were further decomposed into their respective 2D stress-strain (Figure 4.13b) and stress-strain rate (Figure 4.13c) Lissajous plots for a clearer representation.

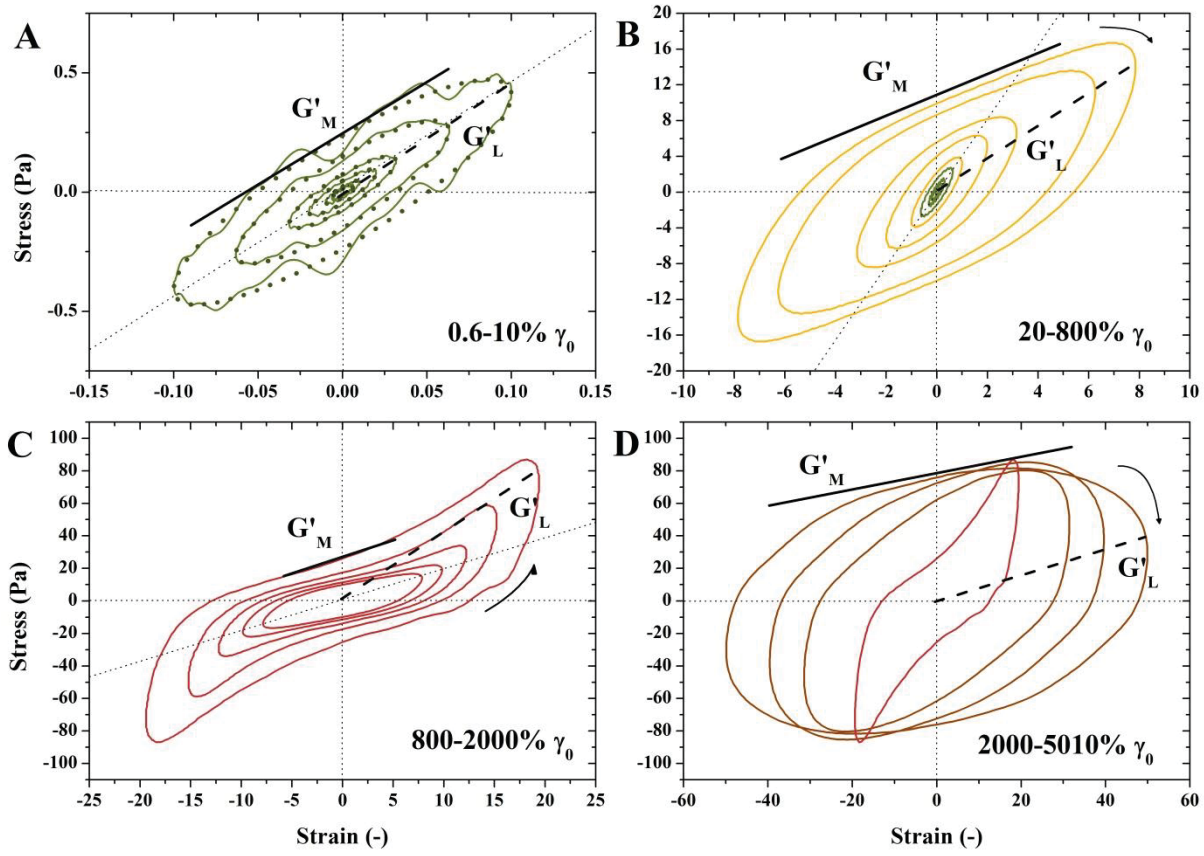

Figure 4.14 – Elastic (stress vs. strain) Lissajous-Bowditch plots of 10% mamaku at ω=10 rad/s for a) LVER (region I, 0.6-10% γ_0, green, dotted lines outline the overall ellipsoidal shape of the Lissajous plots); b) strain softening (region II, 20-800% γ_0, yellow, clockwise arrow indicate inter-cycle strain-softening) ; c) strain-hardening (region III, 800-2000% γ_0, red, anti-clockwise arrow indicates inter-cycle strain-hardening) and d) strain-softening (region IV, 2000-5010% γ_0, brown); Examples of determining G'_M (minimum strain modulus, gradient of tangent at γ_0=0, solid line) and G'_L (maximum strain modulus, gradient of secant at γ_{max}, dashed line) are shown for each region.

To observe the elastic Lissajous plots at smaller strain amplitudes in their appropriate scale, we divided the Lissajous plots according to their strain region *i.e.* linear viscoelastic (Figure 4.14a), strain-softening (Figure 4.14b), strain-hardening (Figure 4.14c) and the second strain-softening (Figure 4.14d) based on the amplitude sweep (Figure 4.12). In the LVER, the Lissajous curves overall remained ellipsoidal in shape (Figure 4.14a) which were consistent with the linear viscoelastic response up to 20% strain amplitude. However, the rippled or 'amoeba-like' appearance of the Lissajous plots in the LVER (e.g. at 10% strain) could be due to sensitivity of the material elasticity at small values of γ_0. Microstructural breakup of weak intermolecular bonds within the material which recovered at a timescale shorter than the timescale of instantaneous deformation could result in the rippling effect. Caution was taken in interpreting this phenomenon, and it will be further explored at various frequencies in the next section. On increasing strain amplitude (20-800%), the ellipsoids appeared to be stretched 'clockwise' (Figure 4.14b), indicating a decreasing elastic contribution to total stress with strain. The curves became increasingly rectangular with rounded corners, reminiscent of strain-softening in xanthan gum (Ewoldt, et al., 2010). In this region, the mamaku polysaccharide exhibited both intra- and intercycle strain-softening. The third region, the strain-hardening region (800-2000%) is the region of interest for the mamaku gum. The Lissajous curve deviated from the ellipsoidal shapes seen so far, with the ends curved upwards (Figure 4.14c). This indicates a sharp increase in stress at large strain, which can be interpreted as

intracycle strain-stiffening (Ewoldt, et al., 2007). Beyond 2000% strain, the material flowed like a viscous material (G''>G') and the shape of the Lissajous plot transformed abruptly from sigmoidal shape (strain-stiffening) to an almost circular plot with high energy dissipation (large area) (Figure 4.14d).

Similar sigmoidal intracycle strain-stiffening shapes were observed in collagen (Kurniawan, et al., 2012), drilling fluid (Ewoldt, et al., 2010), gastropod pedal slug mucus (Ewoldt, et al., 2007) and F-actin (Semmrich, et al., 2008). For these materials, intracycle strain-stiffening accompanies intercycle strain-hardening like the mamaku gum. In other words, the response of these materials seems to resist deformation in order to maintain structural integrity when either instantaneous or steady-state strain exceeds a critical limit. There are also materials which show intercycle strain-hardening but not intracycle strain-stiffening (ellipsoidal plots) e.g. poly(4-vinylpryridine) (PVP) in dimethyl sulfoxide cross-linked with bis-Pd(II) (D. Xu & Craig, 2011). In this case, increasing strain amplitude does not alter the molecular structure of PVP but it is proportional to the number of bis-Pd(II) cross-linkers binding to PVP. Therefore the network strengthens at larger strain amplitudes but the instantaneous response remains linear.

4.3.4.3 Pipkin Diagram

To visualise the effect of frequency on the Lissajous plots, LAOS tests at four different frequencies *i.e.* 1, 2.5, 5 and 10 rad/s were conducted. The normalised (σ/σ_{max} vs. γ/γ_{max}) elastic Lissajous plots at 10%, 631%, 1580% and 2510% strain were selected to represent the LVE (green), strain-softening (yellow), strain-hardening (red) and the second strain-softening (brown) regions respectively. The overview of Lissajous plots of 10% w/w mamaku at various strain amplitudes and frequencies are summarised in a Pipkin diagram (Figure 4.15).

Increasing the strain beyond the LVE (moving up the rows) would cause the distortion of the ellipsoidal shape of the Lissajous plots as shown in earlier (Figure 4.13). Increasing the frequency (across the column from 1 to 10 rad/s) also had an effect on the shape and area of Lissajous plots. The plots occupied a smaller normalised area as well as having sharper corners with higher frequencies at the same strain. A higher frequency would restrict the time allowed for structural relaxation and therefore energy dissipation, hence the smaller area and sharper corners. At 10% strain, increasing the frequency appeared to de-stabilise the stress response and resulted in the ripple plots. However, it was not likely a result of instrumental error or noise since noise to signal ratio would be more pronounced at higher strains at the same frequency (Ewoldt, et al., 2010). The real cause of this phenomenon is unclear, although it could be associated with the elastic effects of the material. The onset of nonlinearity was observed at smaller strains with higher frequencies (631%, 10 rad/s) where the Lissajous plot began to lose its ellipsoidal shape more visibly. Intracycle strain-hardening was also more distinctive at higher frequencies, where the sigmoidal feature was stronger for 10 rad/s than 1 rad/s at 1580% strain. At 2510%, strain-hardening persisted at 1 rad/s while undergoing strain-softening at all other frequencies. It is likely that the required stress to rupture the elastic network of the material was not sufficient at 2510% for 1 rad/s.

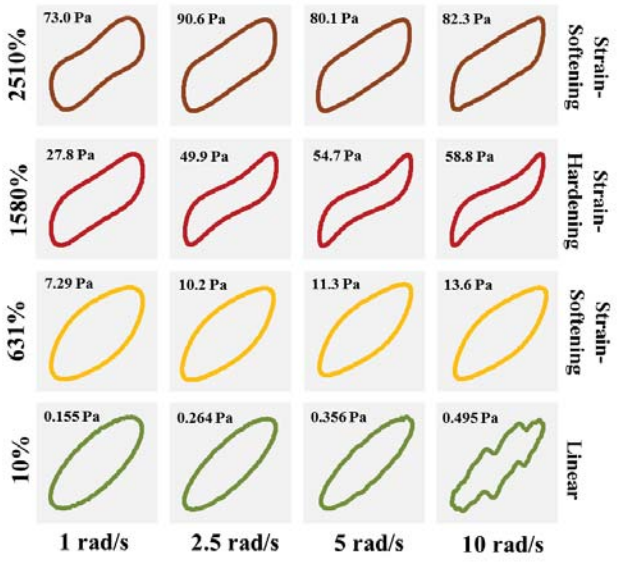

Figure 4.15 – Normalised elastic Lissajous curves (stress vs. strain) for 10% w/w mamaku solution arranged in a Pipkin space at ω = 1, 2.5, 5, 10rad/s and γ_0 = 10, 631, 1580 and 2510%. Maximum stress values are indicated at the top left corner of each Lissajous plot. The linear viscoelastic, strain-softening, strain-hardening and strain-softening regions are coloured green, yellow, red and brown respectively.

4.3.4.4 Quantifying LAOS Properties (G'_L, G'_M, η'_L, η'_M, S and T)

Now that nonlinearities have been visually identified from the Lissajous plots, these nonlinearities can be quantified using new parameters *i.e.* large-strain modulus G'_L (Equation 3.22), minimum-strain modulus G'_M (Equation 3.21), large-rate viscosity η'_L (Equation 3.24) and minimum-rate viscosity η'_M (Equation 3.23) introduced by Ewoldt and coworkers (Ewoldt, Hosoi, & McKinley, 2008a; Ewoldt, et al., 2009) using the MITlaos program (Ewoldt, et al., 2009). These are new measures of material elasticity and viscous dissipation which are valid in both linear and nonlinear regions. Examples of determining G'_L and G'_M from the Lissajous curve are shown in Figure 3.15. These parameters were re-plotted as a function of strain (Figure 4.16a) for 10% w/w mamaku at 10 rad/s.

Briefly, the minimum-strain modulus G'_M is the tangent modulus at γ=0, where the strain rate $\dot{\gamma}$ (and the viscous contribution to stress) is at a local maximum, $d\dot{\gamma}/dt$=0, therefore changes in stress are related to only elasticity. The maximum-strain modulus G'_L is the secant modulus at $\gamma=\gamma_0$ where $\dot{\gamma}$=0 and the residual stress in the material results only from the elasticity of the material. In the linear viscoelastic region, the minimum- and large-strain moduli (G'_M & G'_L) converges to G'_1 *i.e.* $G'_L=G'_M=G'_1$ due to the ellipsoidal shape of the Lissajous curve. The minimum- and large-rate dynamic viscosities η'_M and η'_L are the instantaneous viscosities (or coefficient of viscous dissipation) at the smallest and largest shear rates respectively, whereas the first-harmonic loss modulus G''_1 is the average dissipation coefficient over the cycle. Similar to G'_M and G'_L, η'_M is the tangent modulus at $\dot{\gamma}$=0 and η'_L the secant modulus at $\dot{\gamma}=\dot{\gamma}_0$.

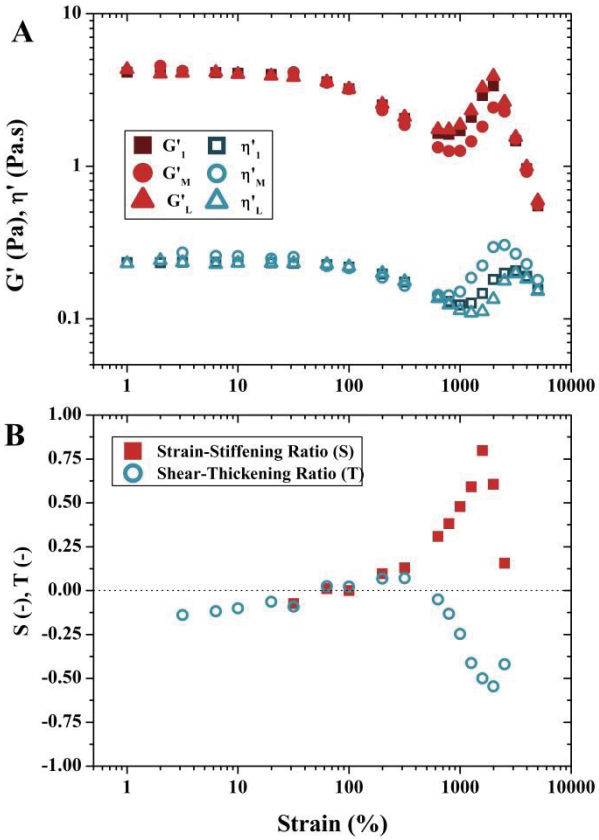

Figure 4.16 – a) Comparison of new LAOS parameters with original first-harmonic moduli; b) strain-stiffening and shear-thickening ratio of 10% w/w mamaku at 1-6000% strain amplitude

Figure 4.16a shows that the large and minimum strain moduli were close to the first-harmonic moduli, *i.e.* $G'_L \approx G'_M \approx G'_I$ and $\eta'_L \approx \eta'_M \approx \eta'_I$, whereby the LVE, strain-softening, strain-hardening, and second strain-softening regions of G'_I and G''_I (Figure 4.12) were preserved. The entire Lissajous plot appear to have rotated along the major axis with increasing γ_0, thus resulting in fairly equal changes to both G'_M and G'_L. Therefore the discussions made previously in the amplitude sweep (Figure 4.12) *i.e.* disentanglement of chains during strain-softening followed by intermolecular associations during strain-hardening region should therefore apply to Figure 4.16a as well.

The deviation of these viscoelastic parameters from linearity (ellipsoidality) at each strain cycle was further quantified using the strain-stiffening ratio, $S \equiv (G'_L - G'_M)/G'_L$) (Equation 3.25), and shear-thickening ratio, $T \equiv (\eta'_L - \eta'_M)/\eta'_L$) (Equation 3.26) (Figure 4.16b). It is easy to visualise that the less ellipsoidal the Lissajous plot, the greater the difference between G'_L and G'_M (or η'_L and η'_M). Therefore when $G'_L > G'_M \rightarrow S > 0$, it indicates an intracycle strain-stiffening response. Conversely, when $G'_L < G'_M \rightarrow S < 0$, it indicates an intracycle strain-softening response. The same applies to the shear-thickening ratio, *i.e.* when $\eta'_L > \eta'_M \rightarrow T > 0$, it indicates an intracycle shear-thickening response, and $\eta'_L < \eta'_M \rightarrow T < 0$ indicates an intracycle shear-thinning response. For a linear viscoelastic response, S=0 and T=0.

The strain-stiffening and shear-thickening ratios of the mamaku gum were close to zero ($S \approx 0$, $T \approx 0$) in the linear viscoelastic region (1-20%). Likewise, no major intracycle nonlinearities were detected in the strain-

softening region (20-300%). Interestingly, S began to increase at 300% strain which was still within the strain-softening region, and continued to rise in the strain-hardening region (800-2000%). At the same time, the shear-thickening ratio appeared to mirror the strain-stiffening ratio along the horizontal axis at strains >300%. As S increases, T decreases and vice versa.

Focusing solely on interpreting the strain-hardening region which is the region of interest, it can be observed that intracycle strain-stiffening and shear-thinning occurred concurrently with intercycle strain-hardening. This could be related to formation of intermolecular associations while promoting viscous flow, resulting in *intracycle* instantaneous strain-stiffening and shear-thinning at the same time. The overall steady-state *intercycle* viscoelastic response is a net result between formation of associations with chain stretching, and its destruction with viscous flow. In the strain-hardening region, intermolecular associations dominated over viscous flow, thus resulting in an overall net increase of both elastic and viscous moduli.

4.3.4.5 Relationship between Strain-Hardening and Shear-Thickening

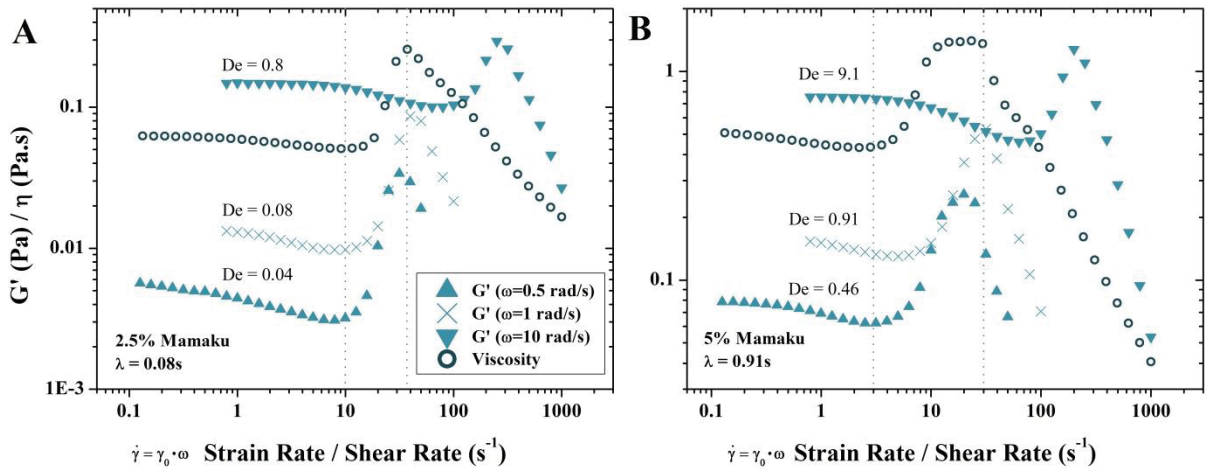

Figure 4.17 – Superposition of oscillatory measurements (G' vs. strain rate) on rotational measurements (η vs. shear rate) for a) 2.5% and b) 5% w/w mamaku

The mechanism behind shear-thickening (section 4.3.1) may be analogous to strain-hardening observed in LAOS. To compare shear-thickening with strain-hardening, the shear rate imposed during the amplitude sweep can be calculated using the formula $\dot{\gamma} = \gamma_0 \cdot \omega$, where γ_0 is the strain amplitude and ω is the angular frequency of the strain oscillation in rad.s^{-1}. The onset of shear-thickening for 2.5% w/w mamaku occurred at a shear rate of ~9.1s^{-1} (Figure 4.17a), while the onset of strain-hardening occurred at various strain rates, depending on the frequency used. The higher the frequency used, the larger the critical strain value. For 5% w/w mamaku, shear-thickening occurred at a shear rate of ~3.0s^{-1} (Figure 4.17b). Two concentrations were compared as they had different terminal relaxation times (0.08 and 0.91s for the 2.5% and 5% w/w mamaku respectively, obtained from frequency sweep measurements at γ_0=5% in the LVER).

It was unknown if the mechanism behind shear-thickening and strain-hardening were analogous or different. To further explore, the Deborah number ($De = \omega \cdot \lambda$), where ω is the angular frequency and λ is the relaxation time at crossover point of a frequency sweep, was considered. It was noted that critical strain rate and shear rate values were closer when De<<1. For 2.5% w/w mamaku, the critical values coincided at De=0.08 (1 rad/s) and were fairly close at De=0.04 (0.5 rad/s). Likewise for 5% w/w, the superposition was closest at De=0.46 (0.5 rad/s). Similar dependencies of γ_{crit} and γ_{max} on Deborah number and frequency have been observed in other systems (Erk, Henderson, & Shull, 2010; Tung & Raghavan, 2008; D. Xu & Craig, 2011), where γ_{crit} and γ_{max} decrease when De<1 and remain constant when De>1. At De<1 (therefore G'<G"), the material is predominantly viscous, which is the state of the material during rotational shear measurements (D. Xu & Craig, 2011). Therefore the comparison between nonlinear steady shear flow was made at similar time-scales.

4.3.5 Extensional Rheology

4.3.5.1 Extensional Relaxation Times

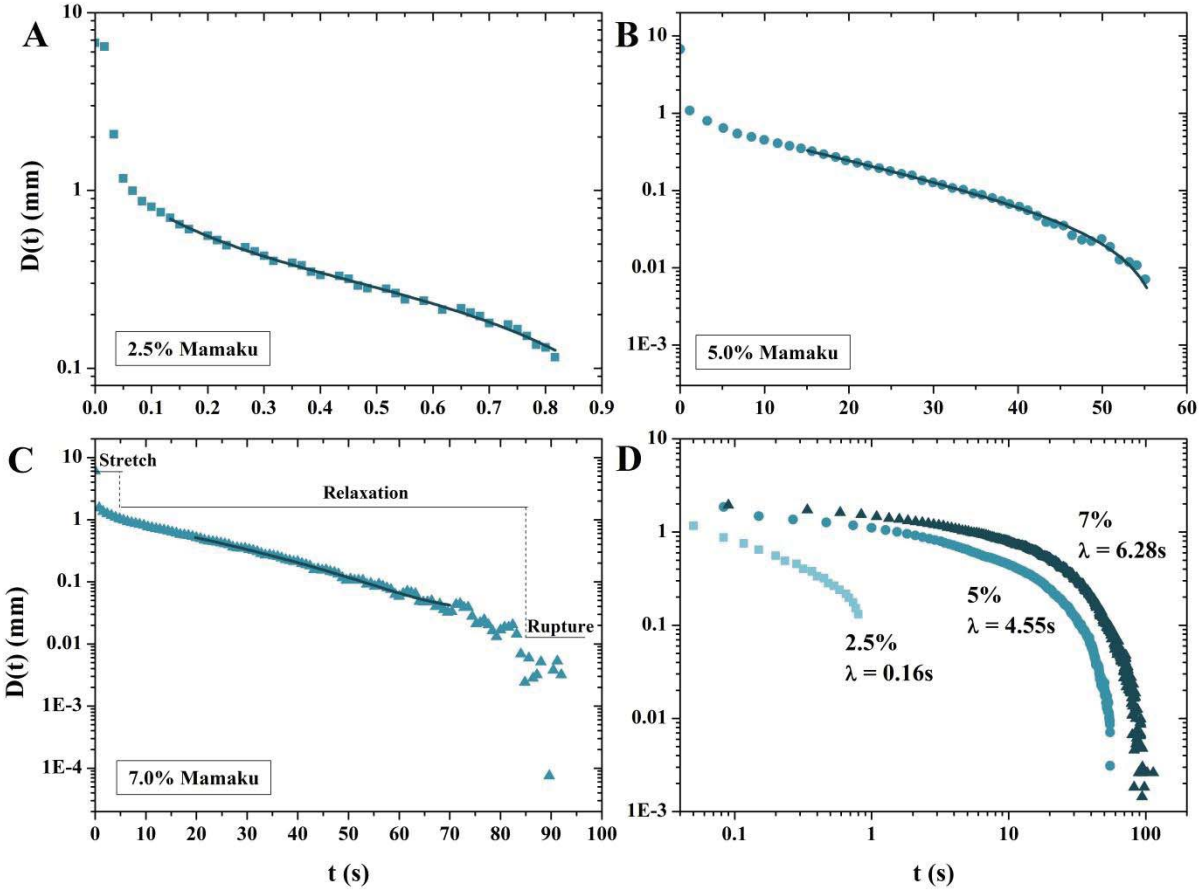

Figure 4.18 – Evolution of fluid filament diameter with time for a) 2.5, b) 5.0 and c) 7.0% w/w using CaBER; initial aspect ratio $\Lambda_0 = L_0/D_0 = 1.6/6 = 0.27$ and final aspect ratio $\Lambda = 7.4/6 = 1.23$; solid lines represent fitted data in the elasto-capillary regime using Equation 4.8; d) comparison between 2.5, 5.0 and 7.0% w/w on a log-scale with their respective relaxation times at 25°C

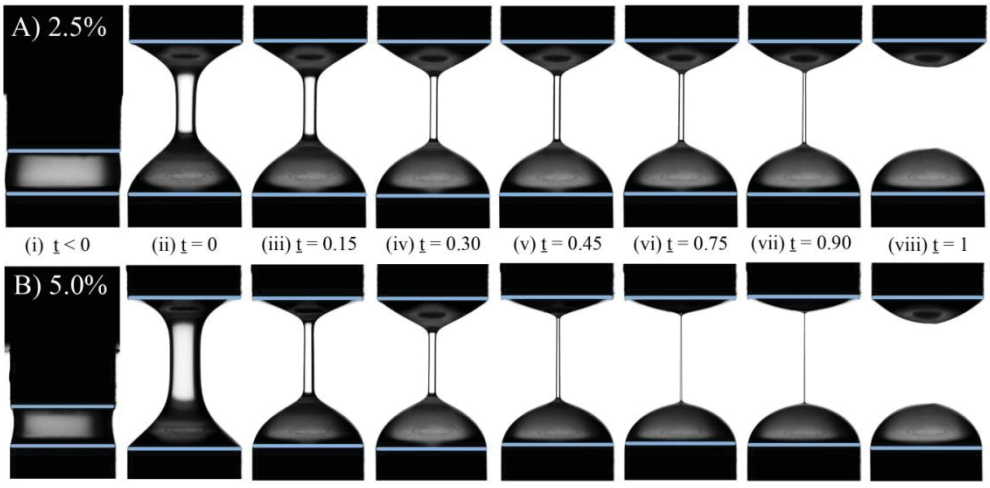

Figure 4.19 – Still frames of fluid filament during CaBER experiment at 25°C for a) 2.5% w/w (breakup time, t_b=0.80s) and b) 5.0% w/w (t_b=55.3s) at various times normalised by breakup time, $\underline{t}$, where $\underline{t}=t/t_b$

During a CaBER experiment, the mamaku filament undergoes an initial stretch phase characterised by a sharp reduction in diameter, followed by a relaxation phase where the diameter reduces exponentially and finally the filament breaks up (Figure 4.18a-c for 2.5, 5 and 7% w/w mamaku respectively). Viscous and inertial forces dominate during the start of extension, and are replaced by elastic and capillary forces in the second phase. Therefore the second stretch phase is termed the elasto-capillary regime (Anna & McKinley, 2001). Increasing the concentration of the mamaku solution has pronounced effects on its extensional behaviour, notably the time required for the filament to reach breaking point, t_b. For 2.5% mamaku, t_b = 0.80s and this increases to 55.3s for the 5.0% and approximately 120s for the 7.0% w/w solution. At higher concentrations e.g. 5.0%, a more gradual thinning of fluid filament towards filament breakup was observed, demonstrating viscous-like behaviour rather than elastic-thinning.

The changes in diameter with time (relative to breakup time) are illustrated on Figure 4.19 as captured using a high speed camera. The images confirm the presence of a stable axially uniform cylindrical fluid filament which thins with time, and can also provide information of the time at which onset of elasto-capillary region occurs. At higher concentrations (5%), the mamaku solution were able to sustain a thinner fluid filament without breaking (compare Figure 4.19a(iv-viii) and Figure 4.19b(iv-viii)). This was due to greater elastic stress at higher concentrations, which sustained the fluid filament for longer time periods.

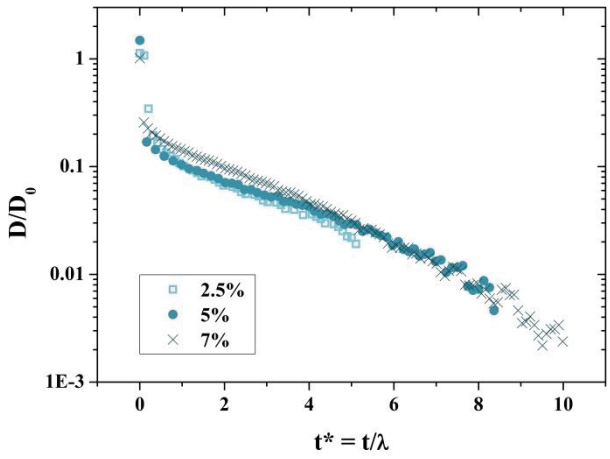

Figure 4.20 – Normalised diameter D(t)/D_0 plotted against non-dimensional time t* = t/λ where λ is the corresponding relaxation time of the three mamaku gum solutions

Table 4.1 – Zero-shear viscosity (η_0), surface tension (σ), extensional relaxation time (λ_E) and shear relaxation time (λ_S) of 2.5, 5.0 and 7.0% w/w mamaku solutions

Concentration (%w/w)	η_0 (Pa.s)	σ (mN/m)	λ_E (s)	λ_S (s)
2.5	0.0670	44.6	0.16	0.079
5.0	0.780	33.7	4.55	0.910
7.0	1.640	33.5	6.28	3.393

In the elasto-capillary thinning region, the fluid filament should be axially uniformly cylindrical, connecting two hemispherical fluid reservoirs (convex shape) at both endplates (Anna & McKinley, 2001). Based on elasto-capillary force balance, the exponential decay of the mid-plane diameter in the elasto-capillary regime (as confirmed using the still frame images in Figure 4.19) can be predicted using Equation 4.7 (Rodd, et al., 2005), where D_0 is the initial diameter of the liquid bridge, G is the relaxation modulus associated with the longest relaxation mode, σ is the surface tension of the fluid, t is the elapsed experimental time and λ is the longest relaxation time of the fluid. Anna and Mckinley (2001) fitted a generalised form of Equation 4.7 (Equation 4.8) to data which includes both the elasto-capillary regime and the long-time viscous-like behaviour. *A*, *B*, *C* and *D* of Equation 4.8 are fitting parameters. The extensional relaxation time, λ of the polysaccharide can be obtained where $B = 1/3\lambda$.

$$D(t) = D_0\left(\frac{GD_0}{4\sigma}\right)^{1/3}\exp[-\frac{t}{3\lambda}] \quad \textbf{Equation 4.7}$$

$$D(t) = Ae^{-Bt} - Ct + D \quad \textbf{Equation 4.8}$$

Good fits for all three concentrations were obtained (solid lines on Figure 4.18a-c) using data after onset of elasto-capillary region *i.e.* t > 0.15. The calculated relaxation times of 2.5, 5.0 and 7.0% w/w mamaku were 0.16, 4.69 and 6.28 seconds respectively (Table 4.1), which gives a concentration dependence exponent of 3.76 (*i.e.* $\lambda_E \sim c^{3.76}$). Above coil overlap concentration *i.e.* in the semi-dilute/concentration regime, the relaxation time of the polymer becomes strongly dependent on the concentration (Duxenneuner, Fischer, Windhab, & Cooper-White, 2008; Stelter, Brenn, Yarin, Singh, & Durst, 2002; Tirtaatmadja, McKinley, & Cooper-White, 2006). The concentrations 2.5, 5.0 and 7.0% w/w were above the coil overlap concentration, c^* of 2.2% w/w as determined from a previous study (Goh, et al., 2007). In some studies, the coil overlap concentration for extensional flow is defined $c^* = 0.77/[\eta] = 0.77/2020 = 0.038\%$ w/w (Clasen, et al., 2006; Duxenneuner, et al., 2008; Goh, et al., 2011; Graessley, 1980). Polymer chains become much more extended and exposed under extensional flow resulting in more interactions between chains. Therefore it is expected that the extensional coil overlap concentration would be lower than the conventional c^* in a shear flow. However, 1% w/w mamaku solutions were too viscoelastically weak to run CaBER experiments on, reaching filament breakup before stretch completion. In this case, the coil overlap concentration of the mamaku polysaccharide under extensional flow may be the same as for shear flow *i.e.* ~2.2% w/w and not 0.038% w/w.

The scaling exponent (3.76) for concentration dependence of extensional relaxation time of mamaku solutions is significantly higher than other polysaccharides or polymers found in literature. A universal scaling exponent of 1.63 was found for dilute random coil polysaccharides including guar gum, locust bean gum, konjac glucomannan, dextran, pullulan and methylcellulose (Koliandris, 2010). Although the scaling exponent is expected to be higher for semi-dilute or concentrated solutions, reported exponent values of semi-dilute scleroglucan (Japper-Jaafar, Escudier, & Poole, 2009), hydroxypropyl ether guar gum (Duxenneuner, et al., 2008) and schizophyllan (De Dier, Mathues, & Clasen, 2013) were 1.33, 1.5 and 1.52 respectively, similar to other polysaccharides.

The concentration dependence of relaxation time indicates the interaction strength and degree of physical entanglement between the polymer chains. Although there are currently no theoretical predictions for scaling of λ_E with concentration for semi-flexible polymers, the smaller exponent values in other polysaccharides suggest weaker interactions between chains e.g. intermolecular hydrogen bonds and the absence of significant entanglement effects (Bourbon, et al., 2010; Duxenneuner, et al., 2008). Conversely, the large exponent value for the mamaku solution signifies strong intermolecular interactions and dense physical entanglements. Further investigation on apparent extensional viscosity and concentration are discussed in the next section. By scaling the diameter-time profile of the various mamaku concentrations with relaxation time (Figure 4.20), a good overlap between the curves *i.e.* master curve is obtained. This implies that the mechanism of extension and relaxation is likely to be the same across all three concentrations in the elasto-capillary regime.

Comparing Extensional Relaxation with Shear Relaxation

Relaxation times obtained using oscillatory measurements (reciprocal at cross-over frequency *i.e.* G'=G") under shear flow, λ_s were compared to the extensional relaxation times, λ_E (Table 4.1). Overall, λ_E is > λ_s for all three concentrations. The concentration dependence of λ_E is similar to λ_S, with exponents of 3.8 and 3.6 respectively. The mode of shear relaxation differs from extensional relaxation. Under extension, the relaxation time is also the longest relaxation time, referring to a relaxation-controlled disentanglement of the entire polymer chain (Clasen, et al., 2006). Shear relaxation time on the other hand is the time a disentangled polymer requires to re-entangle with other polymer molecules (Oakley, Giacomin, & Yosick, 1998). For $c>c^*$, relaxation times are also dependent on the intermolecular interactions when the polymers are in an entangled state (as confirmed by using frequency sweeps in oscillatory shear). It has been shown in some studies that for dilute solutions ($c<c^*$), λ_E is larger than λ_S whereas for semi-dilute to concentrated solutions ($c>c^*$), λ_E is shorter than λ_S (Clasen, et al., 2006; Tirtaatmadja, et al., 2006). However, this does not appear to be the case for the mamaku solution between concentrations of 2.5 to 7% w/w. The extensional relaxation time λ_E is longer than the shear relaxation time λ_S. The scaling exponents were however similar for extensional (3.8) and for shear flow (3.6). Earlier on in this chapter, it was hypothesised that shearing exposes the associative group needed for intermolecular interactions, thus form an associated structure or network. In this case, by fully stretching the polysaccharide under extension, there would be more associations formed than under shear. Consequently, the relaxation time would be longer, comprising of a time-scale associated with destruction of intermolecular bonds and the elongation of the polysaccharide molecule (Bourbon, et al., 2010; Kheirandish, Guybaidullin, Wohlleben, & Willenbacher, 2008; Tan, Tam, Tirtaatmadja, Jenkins, & Bassett, 2000). Shear relaxation times λ_S obtained in the linear viscoelastic region are thus shorter since shear-induced associations only occur under nonlinear deformation. The comparable exponent values of λ_E and λ_S suggests that the effect of changing concentration affects physical entanglements and intermolecular interactions under extension to a similar extent, and the interaction sites under extension and shear are likely to be the same.

4.3.5.2 Apparent Extensional Viscosity

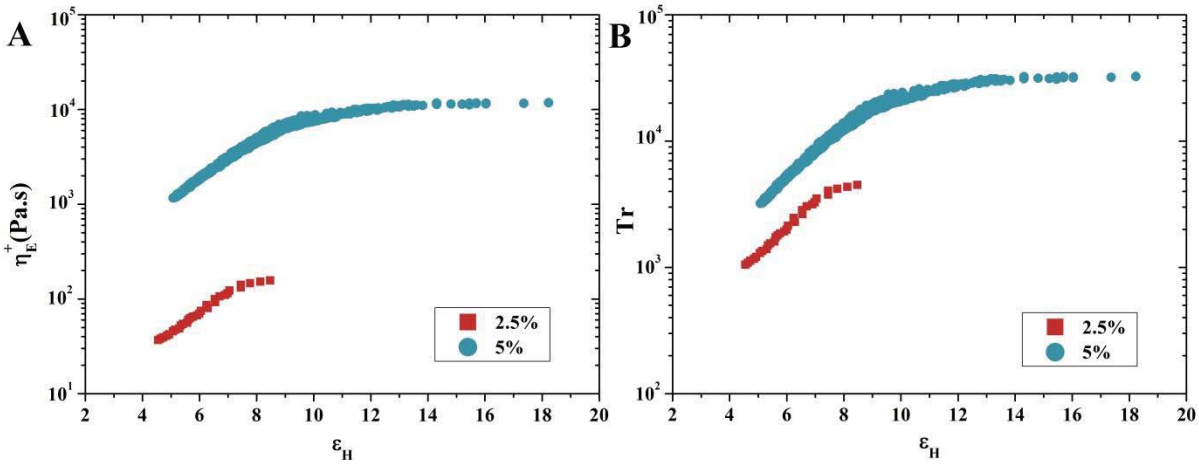

Figure 4.21 – a) Extensional viscosity and b) Trouton ratio of 2.5 (■) and 5% (●) w/w mamaku as a function of accumulated Hencky strain at 25°C

The transient elongation viscosity (or apparent steady-state extensional viscosity) η_E^+ can also be determined from CaBER experiments (Anna & McKinley, 2001). Like shear viscosity, extensional viscosity is the ratio of stress vs. strain rate (Equation 4.9). However, because steady-state extensional rates are not obtained in CaBER experiments, the transient extensional viscosity was determined instead (Equation 4.10) using changes in extensional stress difference with time (Equation 4.11) and the instantaneous strain rate (Equation 4.12). By substituting equations (Equation 4.11) and (Equation 4.12) into (Equation 4.10), the transient extensional viscosity is simplified to a ratio of surface tension σ to change in filament diameter with time (obtained by differentiating Equation 4.13). The Hencky strain is obtained by integrating the instantaneous strain rate (Equation 4.14).

$$\eta_E = \frac{\tau}{\dot{\varepsilon}} \ (steady\ state) \qquad \textbf{Equation 4.9}$$

$$\eta_E = \frac{\Delta\tau(t)}{\dot{\varepsilon}(t)} \ (transient) \qquad \textbf{Equation 4.10}$$

$$\Delta\tau(t) = 3\eta_s\dot{\varepsilon}(t) + (\tau_{zz} - \tau_{rr}) = \frac{2\sigma}{D(t)} \qquad \textbf{Equation 4.11}$$

$$\dot{\varepsilon}(t) = -\frac{2}{D(t)}\frac{dD(t)}{dt} \qquad \textbf{Equation 4.12}$$

$$\eta_E = -\frac{\sigma}{dD(t)/dt} \qquad \textbf{Equation 4.13}$$

$$\varepsilon_H(t) = \int_0^t \dot{\varepsilon}(t)dt = 2ln\left(\frac{D_0}{D(t)}\right) \qquad \textbf{Equation 4.14}$$

Figure 4.21a shows the extensional viscosity of the mamaku solution with Hencky strain ε_H. An increase in ε_H was accompanied by the increase in η_E^+ for all concentrations of mamaku (strain-hardening) due to the stretching of the polymer chains. Extensional viscosity eventually plateaus at higher ε_H as the molecules reaches full extensibility *i.e.* at large Hencky strain plateau. The mamaku solution would be considered as highly viscous

in terms of extensional viscosity, with η_E^+ ~200 Pa.s (2.5% w/w or $c/c^*\approx1$) considering other polysaccharides e.g. xanthan or locust bean gum with η_E < 10 Pa.s for ($c/c^*=2$) (Koliandris, 2010).

The Trouton ratio, ($Tr = \eta_E/\eta_0$) was calculated (values of η_0 in Table 4.1) and plotted with ε_H in Figure 4.21b. Extremely large values of plateau Tr ratio ranging from 10^3 to 10^5 were recorded, indicating that the rheological response of the mamaku solution under extension is much more dramatic than under shear. High Tr ratios are commonly found in dilute polymeric solutions due to their low zero-shear viscosities.

Table 4.2 – Trouton ratios of various polymers

Material	Tr	Concentration	Reference
Cellulose in ionic liquid	~18	8% w/w	(Haward, Sharma, Butts, McKinley, & Rahatekar, 2012)
Human saliva	120	-	(Haward, et al., 2011)
Hydroxypropyl ether guar gum	440	0.2% w/w	(Duxenneuner, et al., 2008)
Casein	11.9	20% w/w	(Chan et al., 2007)
Waxy maize starch	4.9	35% w/w	
Wormlike micelles (CTAB/NaSal†)	1000	10/10 mM	(Bhardwaj, Miller, & Rothstein, 2007)
HASE‡	50	1% w/w	(Tan, et al., 2000)

†: Cetyl trimethylammonium bromide in sodium salicylate;

‡: Hydrophobically modified alkali soluble associative polymers

Table 4.2 compares the Tr ratio of various biological and synthetic polymers which exhibit extensional behaviour. These Tr values are the highest recorded from the reference at the stated concentration. Clearly, the mamaku solution has the most significant Tr up to magnitudes of 10^4 in its fully extended state. This strong extensional behaviour is uncommon in other polysaccharides or synthetic polymers, reminiscent of its shear-thickening property. The molecular associations giving rise to shear-thickening is expected to be manifested and magnified in extensional flow, since the polysaccharide is stretched out even further. Elongation of the molecule under stretch deformation is governed by molecular structure, polymer concentration, concentration regime (dilute or concentrated), molecular weight and conformation (De Dier, et al., 2013).

The glycosidic linkages and therefore torsion angle between the monosaccharide groups in the mamaku polysaccharide may also partly contribute to its extensional properties. Flexible linkage configurations e.g. (1→6) would allow the monosaccharide groups to rotate freely about the glycosidic linkage and align with the stretch direction (Pendrill, Sawen, & Widmalm, 2013; Steve & Qi, 2005a). James and Sridhar (1995) predicted that the arrangement of carbon atoms (in the case of polyisobutylene) would determine the total length of the chain when stretched. A longer chain length can be obtained if the carbon atoms are positioned in a sawtooth fashion. Analogous to a spring or a slinky™ being stretched, a longer extension can be achieved at the same molecular weight if the initial or equilibrium conformation of the molecule is one that favours elongation

(Smith & Chu, 1998). Studies on the molecular structure and linkages of the mamaku polysaccharide will be made in Chapter 6 to complement the extensional data.

4.4 Conclusion

A wide spectrum of material response has been elicited from various rheological deformation modes. The key rheological features identified of the mamaku polysaccharide were: shear-thickening, anti-thixotropy (time-dependency), growth of normal stresses, and shear history dependency during rotational shear. From small amplitude oscillatory shear, the material was found to have a high concentration dependency of (terminal) relaxation time based on frequency sweeps ($\lambda_S \propto c^{3,6}$). The disobeying of Cox-Merz rule implied shear-thickening as a nonlinear property requiring molecular disentanglement (large deformation). Under large amplitude oscillatory shear, intra- and intercycle nonlinearities *i.e.* strain-stiffening were observed which was likely to be of same molecular origin as shear-thickening. With CaBER, the extensional properties of the polysaccharide were measured. Large extensional viscosities, Trouton ratios and long extensional relaxation times comparable to synthetic polymers and far exceeding natural biopolymers were found.

The findings suggest that the polysaccharide is a long-chain molecule which forms relatively strong intermolecular associations under specific deformation rates. Deformation at intermediate shear rates (~1 to $10s^{-1}$) exposes associative groups within the molecule, which form intermolecular bonds in a slow and cooperative zip-like manner. At higher shear rates the bonds are dissociated at a rate faster than association, which prevents shear-thickening or anti-thixotropy. The ordered and therefore stronger intermolecular association of the polysaccharide resulted in longer relaxation times in both shear and extension.

The rheological methods covered in this chapter would be relevant for relating the behaviour of the polysaccharide under processing or physiological etc. applications. In the next chapter, effect of environmental conditions *i.e.* temperature, urea, ionic strength and pH were tested to elucidate the mode of intermolecular association - hydrogen bonding, hydrophobic interactions or electrostatic attraction.

Chapter 5 Effects of Temperature, Urea, Ionic Strength and pH

5.1 Introduction

Polysaccharides are often part of complex food systems and therefore they co-exist with other components such as lipids, proteins, acids and salts etc. The presence of these components may alter the overall conditions of the system, introducing variables such as ionic strength, pH or dielectric constant of the solvent. Processing conditions such as pasteurisation and sterilisation, as well as consumer end-uses also involve that polysaccharides undergo heat treatment. Polysaccharides with charged groups e.g. carboxylic groups are exceptionally sensitive to ionic strength and pH. Small changes to the ionic strength and/or temperature could induce a large change in the physical properties and secondary structure of some polysaccharides, and therefore their functionalities. For example, the addition of small quantities of salt to xanthan gum would cause a conformational change from an ordered helix to a disordered coil, and thus disrupting its weak gel structure (Rochefort & Middleman, 1987). Therefore the functionalities of polysaccharides are dynamic and susceptible to changes with varying environmental conditions. A stable polysaccharide may be considered as one which retains its functionality when subjected to changes in one or more of these external factors. Instability would be caused by disruption to polymer-polymer or polymer-solvent interactions, which are mainly hydrogen bonds, hydrophobic interactions or electrostatic attractions, thus losing its functionalities (Gerald O. Aspinall, 1982).

The effect of environmental conditions *i.e.* temperature, solvent (urea), ionic strength, and pH on the rheological properties of mamaku polysaccharide were tested in this chapter. A previous study (Matia-Merino, et al., 2012) had characterised the effect of salt (mono- and divalent ions) and pH on the native extract. However, the total salt concentration within the extract was probably too high for any additional cationic effects to be appreciable. In this chapter, the effects were tested on the dialysed mamaku extract instead (>90% w/w endogenous salt removed) where salt concentration and valency (mono-, di- and trivalent) were expected to induce a stronger rheological response. These factors would contribute to elucidating the type of intermolecular interaction responsible for its unusual rheological behaviour. A summary is illustrated in Figure 5.1.

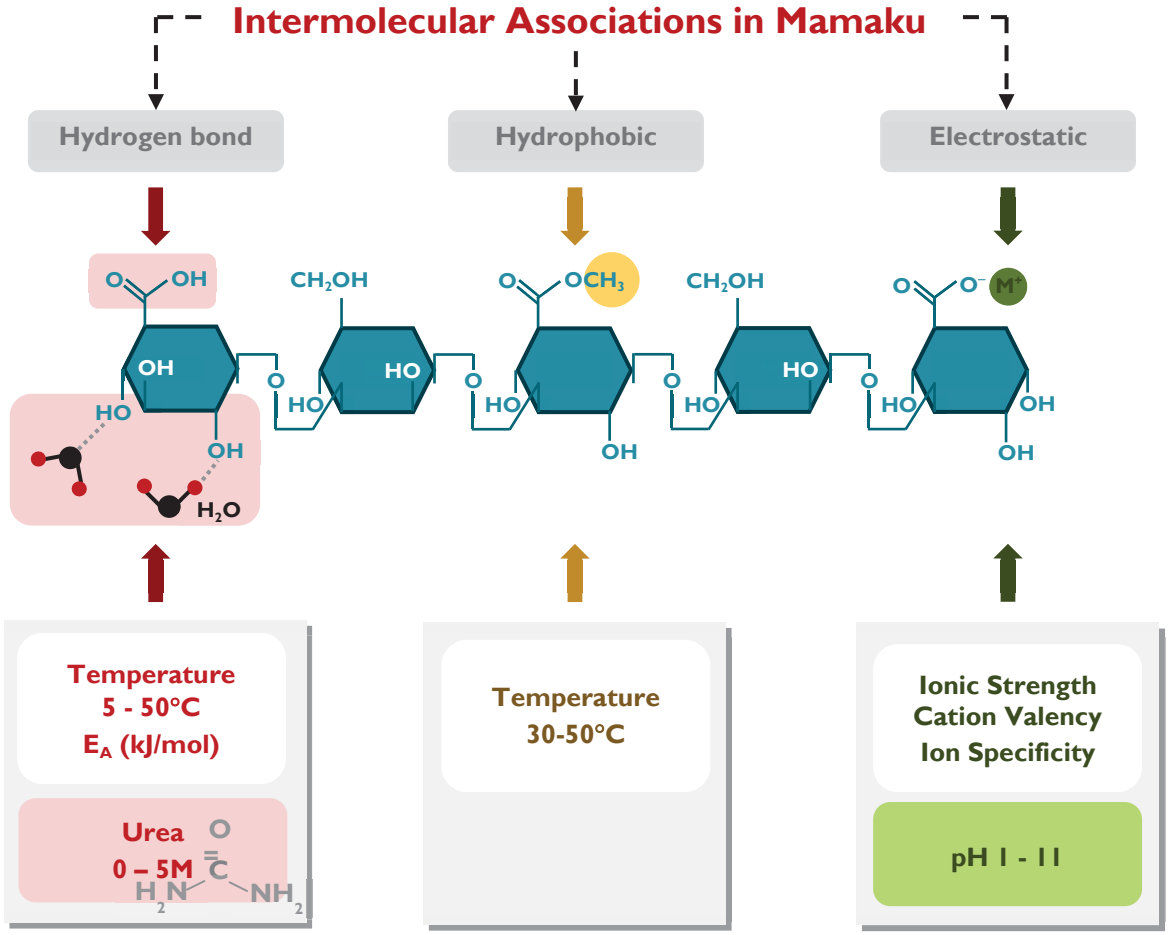

Figure 5.1 – Flow diagram for probing stability and intermolecular associations in mamaku polysaccharide

5.2 Materials and Methods

5.2.1 Sample Preparation

The freeze-dried native mamaku extract was dispersed and hydrated in milli-Q water overnight under continuous stirring at the required concentration. Urea (LabServ) was first dissolved in milli-Q water first prior to hydrating the polysaccharide, in samples where the effect of urea was tested.

5.2.1.1 Membrane Dialysis

The freeze-dried extract (6.5% w/w) (50g) was first dispersed and hydrated in water overnight under continuous stirring (native extract). The hydrated native extract with a starch content of 3.7% w/w was subjected to starch hydrolysis with thermostable α-amylase (100 U/ml in 100mM sodium acetate buffer, pH 5.0; 1ml) at 100°C for 6 minutes and then with amyloglucosidase (330 U/ml; 0.1ml) at 50°C for 30 minutes (Megazyme). Rheological properties of the extract did not change after starch hydrolysis. The starch-hydrolysed native extract was dialysed stepwise in reducing concentrations of sodium chloride (NaCl) solutions. The native extract has a high salt concentration (~20% w/w), therefore it was dialysed against 0.01M NaCl solution, followed by 0.001M NaCl and lastly against milli-Q water. This was to prevent 'bloating' of the dialysis tubing, whereby water molecules diffuse into the membrane instead, as a result of large osmotic pressure difference across the membrane hence diluting the material. Glucose released from starch hydrolysis would also be removed in this step. Five litres of buffer were used (1:100 volume ratio of sample to buffer) and replaced once every 8 hours (minimum) for a total of 3 times. The molecular weight cut-off (MWCO) of the dialysis tubing is 12,000 – 14,000 (SpectraPor). The weight of the sample was measured before and after dialysis to account for dilution. The sample was diluted to about 5.5% w/w mamaku solution after dialysis.

5.2.1.2 Addition of Salt to Dialysed Samples

Aliquots of stock salt solution *i.e.* sodium chloride (NaCl; Analar BDH), potassium chloride (KCl; LabServ), tetramethylammonium chloride ($N(CH_3)_4Cl$; Sigma Aldrich), calcium chloride dihydrate ($CaCl_2 \cdot 2H_2O$; Analar BDH), magnesium chloride hexahydrate ($MgCl_2 \cdot 6H_2O$; LabServ), aluminium chloride hexahydrate ($AlCl_3 \cdot 6H_2O$; Biolab) or lanthanum chloride heptahydrate ($LaCl_3 \cdot 7H_2O$; Sigma Aldrich) in either 0.1, 1.0 or 5.0M concentration prepared using the final dialysate, were added to the dialysed mamaku solution (6.3g). Dialysate was further added to top up to the total required weight (7g) to give the final required salt concentration and extract concentration of approximately 5% w/w. For the tests using urea, urea (LabServ) was dissolved in the solvent first before hydrating the polysaccharide (5% w/w). No preservatives were used *i.e.* sodium azide as the polysaccharide properties are affected by the presence of the sodium ion. Samples were prepared immediately after dialysis of the extract and rheological measurements taken 15 minutes after adding the salt solutions. Addition of trivalent cations resulted in precipitation of the polysaccharide after some time therefore rheological measurements had to be carried out immediately. Ionic strength was calculated using the following equation:

$$I = \frac{1}{2}\sum_{i=1}^{n} c_i z_i^2 \quad \text{Equation 5.1}$$

where I is the ionic strength, c_i the molar concentration of the ion and z_i is the charge valency of the ion. For monovalent ions, ionic strength will be equal to its concentration.

5.2.1.3 pH Adjustment

The mamaku sample (6.5% w/w) was first dialysed as above and the pH was adjusted using 0.1 or 1.0M hydrochloric acid (HCl) or sodium hydroxide (NaOH) under continuous stirring. The pH was measured using a pH meter (±0.1 units; Jenway 3510 pH meter). The final concentration of the dialysed mamaku was adjusted to 5% w/w. The pKa of 5% w/w dialysed mamaku was determined using acid-base titration.

5.2.2 Rheological Measurements

Rotational rheological measurements were made using a Paar Physica rheometer MCR 301 (Anton-Paar, Graz, Austria) in controlled shear rate (CSR) mode at 20°C with the double gap geometry (DG 26-7) and C-PTD 200 peltier unit. Data points were recorded using a log-ramp profile at time intervals of 30 seconds (initial) to 2 seconds (final). The temperature of the rheological measurement was controlled using a Peltier system to an accuracy of ±0.1°C. Oscillatory measurements (frequency sweeps) in the range of 0.01 to 100Hz were made using a strain value of 1% (within the linear viscoelastic region). The samples were allowed to rest for 10 minutes after loading into the geometry prior to starting the test. This was done to reduce any effects of shear history and at the same time for temperature equilibration. Zero-shear viscosity was estimated using the following modified Cross' equation (Equation 5.2) from the shear-thinning region *i.e.* region I (prior to onset of shear-thickening) for shear-thickening fluids (Galindo-Rosales, Rubio-Hernández, Sevilla, et al., 2011), where η_I is the predicted viscosity, η_{crit} the viscosity at critical shear rate (shear rate at the onset of shear-thickening), η_0 the zero-shear viscosity, λ_I the relaxation time constant, $\dot{\gamma}_c$ the critical shear rate and n_I the viscosity constant.

$$\eta_I(\dot{\gamma}) = \eta_c + \frac{\eta_0 - \eta_c}{1 + \left[\lambda_I\left(\frac{\dot{\gamma}}{\dot{\gamma}_c - \dot{\gamma}}\right)\right]^{n_I}} \quad \text{Equation 5.2}$$

5.2.2.1 Time-Temperature/Urea Superposition

Time-temperature superposition is a rheological technique typically used to measure the relaxation spectra at frequencies which are experimentally inaccessible. In order to probe the material at high frequencies, the temperature can be reduced and vice versa. This method however, is only applicable to thermorheologically simple materials e.g. polyethylene oxide, or materials which do not undergo microstructural changes or phase transitions upon a change in temperature therefore having only a single relaxation mode at different temperatures (Mezger, 2011). This principle was extended to urea concentration, and time-urea concentration superpositions were also carried in this study.

For rotational measurements, the viscosity curves at various temperatures were shifted along both the x- and y-axis using shift factors, a_T and b_T respectively (the subscript 'c' is used instead for urea concentration) with respect to the viscosity curve at 20°C (T_{ref}= 20°C). The shear rate (x-axis) values were multiplied by a_T, giving a reduced shear rate ($\dot{\gamma}_r$) (Equation 5.3), while the viscosity (y-axis) values were multiplied by b_T, giving a reduced viscosity (η_r) (Equation 5.4). For oscillatory frequency sweeps, the angular frequencies were shifted along the x-axis by multiplying with shift factor a_T at T_{ref}=20°C, giving a reduced angular frequency (ω_r) (Equation 5.5) and subsequently reduced storage modulus (G'_r) on the y-axis.

$$\dot{\gamma}_r = a_T \cdot \dot{\gamma} \quad \textbf{Equation 5.3}$$

$$\eta_r = b_T \cdot \eta \quad \textbf{Equation 5.4}$$

$$\omega_r = a_T \cdot \omega \quad \textbf{Equation 5.5}$$

5.2.3 Relative Viscosity

Relative viscosities (η_{rel}) of dilute mamaku solutions (1% w/w) in the presence of salts were measured using a Cannon-Ubbelohde dilution capillary viscometer (Viscometer Size 100, 9722-M59, Cannon Instrument Co., PA, USA). The relative viscosity is calculated as the ratio of efflux time of the sample to the efflux time of the solvent, which is the dialysate obtained after dialysis of the extract. The samples were prepared similarly as described in section 5.2.1, except that the dialysed mamaku extract was further diluted to 1% w/w concentration with the stock salt solutions made up using the dialysate.

5.2.4 Zeta-Potential

Zeta-potential was measured using a Zetasizer Nano ZS (Malvern Instruments Ltd, Worcestershire, UK) based on electrophoresis and laser Doppler velocimetry techniques. The samples were measured in universal folded capillary cells (DTS1060C; Malvern Instruments Ltd, Worcestershire, UK) at 20 ± 0.02°C.

5.2.5 Mineral Analysis

Mineral compositions of the native and dialysed mamaku extract were determined by an accredited chemical laboratory (Nutritional Laboratory, Institute of Food, Nutrition & Human Health, Massey University) using inductively coupled plasma-optical emission spectrometer.

5.3 Results and Discussion

5.3.1 Effect of Temperature

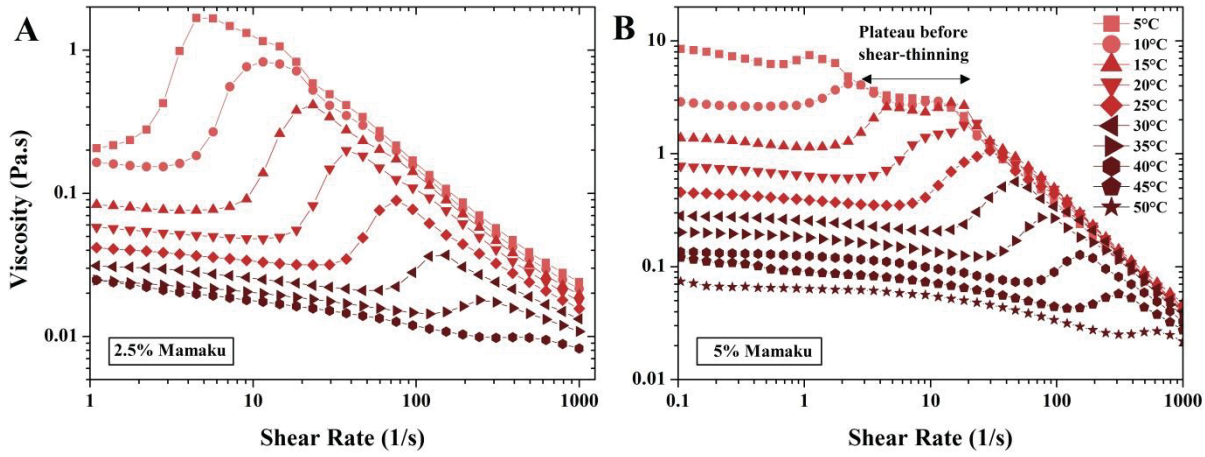

Figure 5.2 – Viscosity curves of a) 2.5% and b) 5 %w/w mamaku polysaccharide at 5 (■), 10 (●), 15 (▲), 20 (▼), 25 (◆), 30 (◀), 35 (▶), 40 (⬢), 45 (⬟) & 50°C (★)

Temperature is one of the major external parameters which affect the physical properties of the polysaccharide. Changes in temperature would occur during processing etc., and therefore it is important to characterise the material under various temperatures. Furthermore, subjecting the material to elevated temperatures may elucidate the type and strength of associative bonds present in the polysaccharide responsible for its rheological properties. Various time-temperature treatments of the material at higher temperatures and their effect on the rheological properties can be found in Appendix B (Figure B1).

The effect of temperature in the range of 5 to 50°C on the viscosity of the polysaccharide solution is shown in Figure 5.2. This chapter focuses on this temperature region since distinctive rheological changes were observed within this range. Overall, a systematic shift of the viscosity curves along the x-axis (to the right) and y-axis (downwards) was observed, with loss of shear-thickening at 40°C for 2.5% and 50°C for 5.0% w/w solutions. The reduction in (zero-shear) viscosity with increasing temperature is a common phenomenon in many polymer solutions, and they show an Arrhenius-like temperature-dependency on its zero-shear viscosity. For shear-thickening materials, the effect of temperature can also be manifested in the changes to critical shear rate (shear rate at onset of shear-thickening), peak viscosity at shear-thickening and extent of shear-thickening (η_{max}/η_{crit}).

The reduction in viscosity of the mamaku polysaccharide could be attributed to additional thermal energy which enhanced chain mobility and reduced flow resistance (Kulicke & Clasen, 2004). The rise in temperature is also known to increase the free volume of the system, leading to larger intermolecular distances and lower viscosities (Briscoe, Luckham, & Zhu, 1996; Rivero, et al., 2012). This means that higher shear rates would be required to induce shear-thickening. Similar effects of temperature in shear-thickening high molecular weight poly(ethylene oxide) (PEO) solutions have been previously observed (Rivero, et al., 2012). The effect of temperature on the shear-thickening behaviour was further quantified and explored by analysing the

characteristic timescale of association $(1/\dot{\gamma}_{max})$, time-temperature superposition and the Arrhenius's activation energy of flow.

The peak viscosity (η_{max}) and the inverse of the shear rate at peak viscosity $(1/\dot{\gamma}_{max})$, showed similar exponential dependencies on temperature *i.e.* ~$e^{-0.1T}$ (Figure 5.3a). This suggests that the onset of shear-thinning occurred at an approximately constant value of stress (Equation 5.6; Appendix B Figure B2), σ_0, which is a function of the number and strength of these associations contributing to the total network strength at rupture (Tan, et al., 2001). The inverse of the shear rate at peak viscosity $(1/\dot{\gamma}_{max})$ can be interpreted as the mean relaxation time of the associations *i.e.* the association lifetime. At shear rates smaller than $\dot{\gamma}_{max}$, the experimental timescale was longer than the lifetime of the associations, therefore allowing shear-thickening to occur (Kosvintsev, et al., 2001). Shear rates above $\dot{\gamma}_{max}$ disrupted the intermolecular association faster than its formation or association lifetime, resulting in shear-thinning. A master curve could be obtained by normalising $1/\dot{\gamma}_{max}$ with concentration which has the same exponential dependency of ~$e^{-0.1T}$ (Figure 5.3b). Therefore these observations suggest that increasing the temperature (between 5-50°C) did not change the average number of association junctions per chain, but only modified the average lifetimes of the association.

$$\sigma = \eta \cdot \dot{\gamma} = c_1(e^{-0.1}) \cdot c_2(1/e^{-0.1}) = \sigma_0\ (constant) \qquad \textbf{Equation 5.6}$$

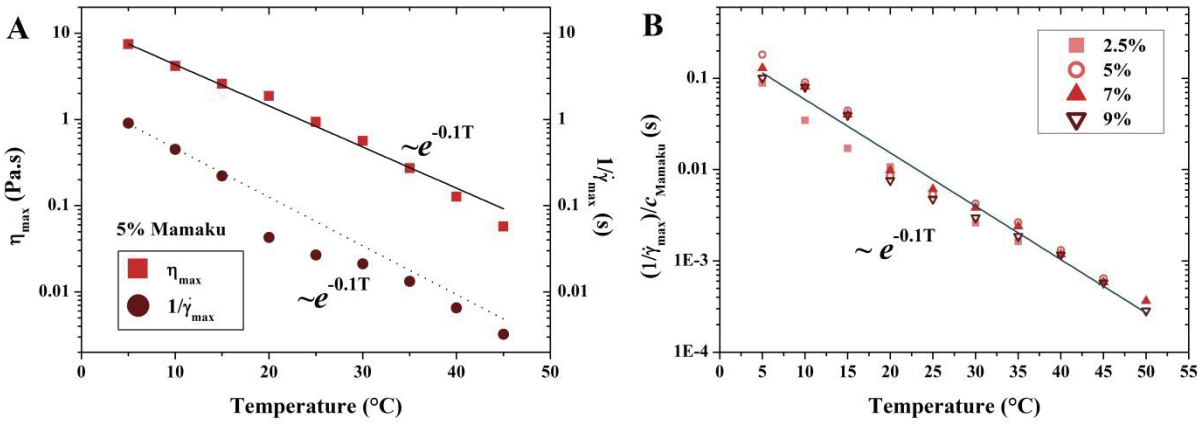

Figure 5.3 – a) Dependence of peak viscosity, η_{max} (■) and characteristic time scale, $1/\dot{\gamma}_{max}$ (●)on temperature for 5% w/w mamaku; b) characteristic time scale normalised by concentration (2.5 (■), 5 (○), 7 (▲) & 9% w/w (▽)) with temperature

5.3.1.1 Time-Temperature Superposition

Time-temperature superposition of 5% w/w mamaku was carried out with the viscosity curves (Figure 5.4) and the frequency sweeps (Figure 5.5). As described in the introduction, thermorheologically simple materials have curves which are superimposable, whereby all relaxation mechanisms of the material have the same temperature dependence. As such, these thermorheologically simple materials do not undergo microstructural changes or phase transitions upon a change in temperature (Malkin & Isayev, 2012).

Viscosity is controlled by both shear stress and time parameters, therefore the viscosity curves for the mamaku solution were shifted along the x-axis for time by a horizontal shift factor, a_T, and along the y-axis for stress by a vertical shift factor, b_T (Figure 5.4). The flow behaviour curves prior to the onset of shear-

thickening were superimposable, but not for the shear-thickening region. The shift factors a_T and b_T had exponential dependencies of -0.14 and 0.1 on temperature respectively, with a_T similar to the value obtained with the association lifetime (-0.1) (Figure 5.3). The non-superimposable shear-thickening region indicates the presence of additional intermolecular associations in the nonlinear viscoelastic region, which had a different relaxation mode from simple chain relaxation. In contrast, the frequency sweeps obtained under linear viscoelastic behaviour could be superimposed (Figure 5.5). Therefore it can be concluded that temperature does not alter the structure or phase properties of the mamaku polysaccharide, and it behaves as a thermorheologically simple material in the linear region. The smaller exponential value of -0.08 for the horizontal shift factor in the frequency sweeps also suggests that there were a lower number of associations (approximately half) involved in intermolecular interactions as compared to the nonlinear region at higher shear rates.

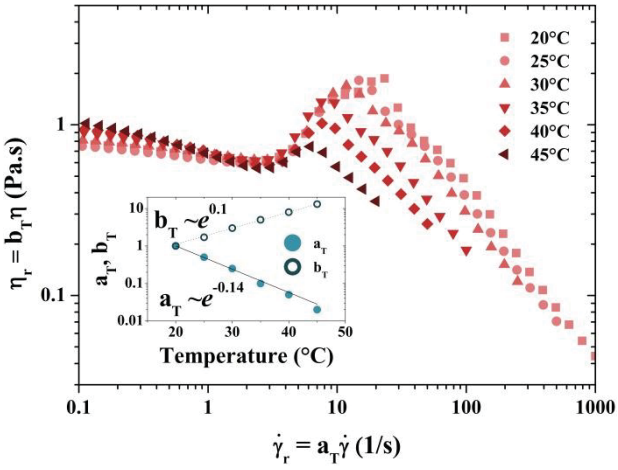

Figure 5.4 – Reduced viscosity (η_r=b_T·η) vs. reduced shear rate ($\dot{\gamma}_r$=a_T·$\dot{\gamma}$) of 5% w/w mamaku at various temperatures; inset: horizontal (a_T) and vertical (b_T) shift factors with temperature, T_{ref}=20°C

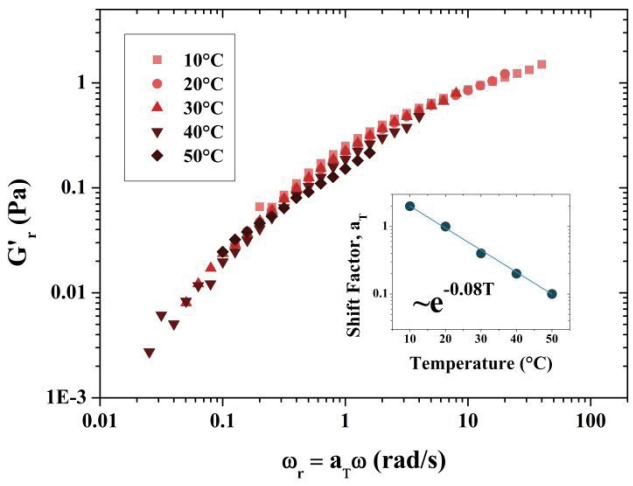

Figure 5.5 – Time-temperature superposition of reduced storage modulus (G'_r) vs. reduced angular frequency (ω_r=a_T·ω) of 5% w/w mamaku at various temperatures (γ_0=5%); inset: horizontal shift factor (a_T) with temperature, T_{ref}=20°C

5.3.1.2 Activation Energy of Flow, E_a

The original Arrhenius equation was used to calculate the temperature dependence of a chemical reaction. The activation energy can be defined as the energy barrier required to be overcome before a reaction can take place. The Arrhenius theory was subsequently extended to the flow behaviour, and activation energy in the context of zero-shear viscosity was interpreted as the energy required for viscous flow *i.e.* overcoming frictional forces of neighbouring molecules (Equation 5.7) where η is the viscosity at temperature T, A is the Arrhenius constant, E_a is the activation energy and R is the gas constant (8.314 J/mol·K). The activation energy concept can still be used to characterise the polymer even in situations where time-temperature data do not superimpose (Dealy & Plazek, 2009). Similarly, the activation energy could also be used as an indicator of the sensitivity of the molecules to temperature (Lewandowska, 2007). The larger the activation energy, the more sensitive the polymer is to temperature *i.e.* the changes in properties with temperature would be more distinct.

$$\eta(T) = A \cdot \exp\left[\frac{E_a}{R}\left(\frac{1}{T}\right)\right] \quad \textbf{Equation 5.7}$$

In chemical reactions, reactants have to overcome an energy barrier *i.e.* activation energy, in order for the reaction to take place. Analogically, there is a potential energy barrier which the mamaku chains have to overcome by disengaging from each other, disrupting associations and leading to the shear-thickening phenomenon. This energy barrier can be lowered by altering the environment of the polymer solution, such as increasing the temperature, adding urea or lowering the dielectric constant of the solvent. The type of association present within the mamaku polysaccharide was postulated to be hydrogen bonding for the following reasons: the energy of hydrogen bonding is in the order of *kT*, where *k* is the Boltzmann constant and *T* is the absolute temperature (Lele & Mashelkar, 1998). The Boltzmann constant is closely related to the gas constant, R, which is expressed as the energy per temperature increment per particle (instead of per mole of gas) (Israelachvili, 2011). In other words, the dependence of shear-thickening on temperature should follow the conventional Arrhenius law (Equation 5.7), as the strength of hydrogen bond associations and subsequently shear-thickening weakens with increasing temperature. Figure 5.6 demonstrates a linear Arrhenius plot between the critical and maximum viscosities and their respective shear rates with temperature for the 2.5% w/w mamaku solution. This further ascertained the involvement of hydrogen bonding in the mamaku polysaccharide solution.

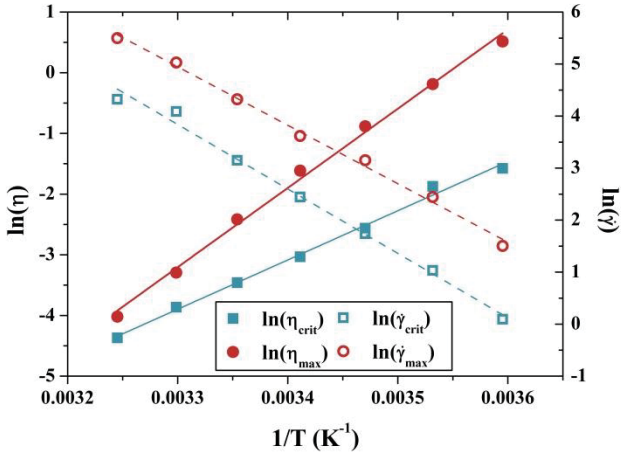

Figure 5.6 – Arrhenius plots of critical (squares) and maximum (circles) viscosities (filled) and shear rates (unfilled) of 2.5% w/w mamaku

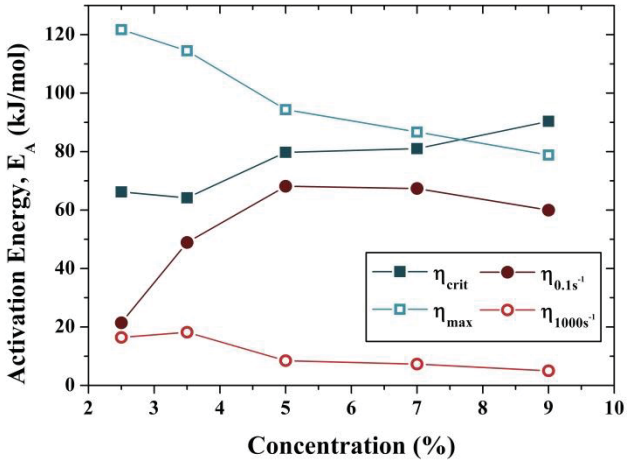

Figure 5.7 – Activation energies based on viscosity at critical (■), maximum (□), 0.1s^{-1} (●) and 1000s^{-1} (○) shear rates at different mamaku concentations (% w/w)

Using Equation 5.7, the activation energies for viscosities at various shear rates *i.e.* critical, maximum, 0.1s^{-1} and 1000s^{-1} were calculated and shown in Figure 5.7. In general for all mamaku concentrations, the highest activation energies corresponded to peak viscosity, followed by viscosity at critical shear rate, viscosity at low shear rate (0.1s^{-1}) and lastly viscosity at high shear rate (1000s^{-1}). The activation energy at peak viscosity ranged from 122 to 79 kJ/mol for mamaku concentration between 2.5 and 9% w/w, which were considerably large values as compared to other polymer solutions (Table 5.1). The values obtained were also in good agreement with that obtained by Matia-Merino et. al. (2012) for a 7% w/w native mamaku solution for viscosity at critical shear rate (82 kJ/mol).

Since intermolecular associations were strongest at η_{max}, the activation energy calculated at this viscosity would be the activation energy of association, or the energy barrier required to overcome the associations and resume to free-flowing state (Tan, et al., 2001). The large activation energy values at η_{max} could be attributed to the zipping effect (Lele & Mashelkar, 1998), where the chains were associated in cooperative alignment. Unlike shear-induced association in other polymers, the separation of mamaku chains with thermal mobility would therefore require successive dissociation *i.e.* unzipping. The activation energy at η_{max} decreased with

increasing concentration, presumably due to the presence of more entanglements at higher concentrations which interferes with cooperative alignment and association between the polymer chains.

Comparatively, the activation energies at η_{crit} and $\eta_{0.1}$ were lower than at η_{max}. At critical and $0.1s^{-1}$ shear rates, thermal energy is likely to be used towards increasing mobility of the polymer chains instead of dissociating intermolecular hydrogen bond associations. In addition, both increase with concentration unlike activation energy at η_{max} which decreases with concentration. At higher concentrations, the polymers chains are more entangled. As mentioned previously, the activation energy is the energy required for viscous flow or for overcoming frictional forces of neighbouring molecules. Therefore, at low shear rates in the absence of shear-thickening associations, activation energy would increase with concentration since it is harder for the polymer chains to disentangle and align at higher concentrations (Briscoe, Luckham, & Zhu, 1998; Rivero, et al., 2012). Finally, at high shear rates *i.e.* $1000s^{-1}$, the polysaccharide chains are most likely fully stretched and free-flowing, therefore not requiring additional energy to induce flow. Hence, activation energies at $1000s^{-1}$ were the lowest and plateau at ≥5% w/w concentrations.

Table 5.1 – Activation energy of viscous flow (kJ/mol) for various polymers

Polymer	Activation Energy of Flow (kJ/mol)	Reference Shear Rate (s^{-1})	Reference
HASE (in 0.6M NaCl) †	54 (at γ_{max})	$\gamma_{\eta peak}$	(Tan, et al., 2001)
HEUR†	71	-	(Annable, Buscall, Ettelaie, & Whittlestone, 1993)
PEO† (500ppm; $8x10^6$ Da)	21	10	(Rivero, et al., 2012)
PEO (1% w/w; $1x10^6$ Da)	29	10	(Briscoe, et al., 1998)
HPAM (80)	30.2	250	(Lewandowska, 2007)
Chitosan blend with PEO (1:1)	33	100	(Mucha, 1998)
Galactomannan from Leucaena leucocephala seed	26.4	0	(Nwokocha & Williams, 2012)
Lepidium sativum seed extract (2% w/w)	15.59	50	(Karazhiyan et al., 2009)
Palmate-tuber Salep	36.36	Consistency index, n	(Farhoosh & Riazi, 2007)

†*Shear-thickening systems;*

Abbreviations: Hydrophobically modified alkali soluble emulsion (HASE); Hydrophobically modified ethoxylated urethane (HEUR); Poly(ethylene oxide) (PEO); Partially hydrolysed polyacrylamide (HPAM)

These observations collectively suggest that hydrogen bonds were most likely to be the intermolecular interaction responsible for viscosity and shear-thickening. The minimum bonding distance for hydrogen bonds is 2-5 Å (Lele & Mashelkar, 1998), therefore hydrogen bonds causing shear-thickening would not take place if the polymer chains are unable to come in close proximity with one another at high temperatures due to

thermal mobility. Apart from hydrogen bonds, it is also possible that hydrophobic interactions may take place between the methyl (-CH_3) groups of the methylesterified glucuronic acid residues (27.9 mol%; Chapter 6) which give rise to shear-thickening in some polymers such as hydrophobically modified ethoxylate-urethane (HEUR) (Aubry & Moan, 1994; Tripathi, Tam, & McKinley, 2006). Hydrophobic interactions are enhanced when temperature is increased within the temperature range of 5-55°C as result of reduced solvent interaction (Oakenfull & Fenwick, 1977; Oakenfull & Scott, 1984). For example, shear-thickening is augmented in hydrophobically-modified alginates (in the presence of cyclodextrin compounds) at 35-45°C as compared to lower temperatures e.g. 15°C (Burckbuchler, et al., 2006). In the case of the mamaku polysaccharide, increasing the temperature from 5-50°C (Figure 5.2) did not enhance shear-thickening. Furthermore, η_{max} obeyed the Arrhenius Law with temperature, which strongly suggests that there were no other interactions simultaneously involved in contributing to shear-thickening.

5.3.2 Effect of Urea

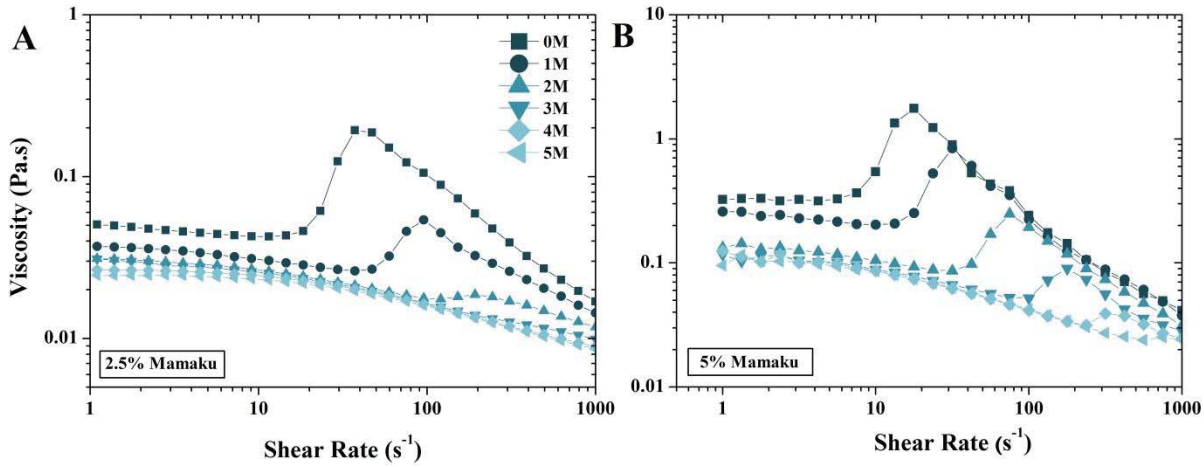

Figure 5.8 – Viscosity curves of a) 2.5 and b) 5% w/w mamaku polysaccharide with 0 (■), 1 (●), 2 (▲), 3 (▼), 4 (◆) & 5M (◀) urea at 20°C

The effects of increasing urea concentration in 2.5 and 5% w/w mamaku solutions are shown in Figure 5.8. For 2.5% w/w mamaku (Figure 5.8a), a large reduction in zero-shear viscosity was initially observed when the polysaccharide was dissolved in 1 and 2M urea concentration. However, the effects on zero-shear viscosity reduction plateaued above the concentration of 2M urea. Shear-thickening was completely lost at ≥3M urea. Similar effects were observed for 5% w/w mamaku (Figure 5.8b), but with the shear-thickening being lost at ≥5M urea. Therefore the concentration of urea required to suppress shear-thickening was proportional to polysaccharide concentration.

Urea is a chaotropic agent which disrupts hydrogen bonds by competing for binding sites. These observations strongly suggest that again, hydrogen bonds were most likely responsible for the viscosity of the polymer solution before and during shear-thickening, although affecting the latter more significantly. The reduction of zero-shear viscosity with urea indicates that hydrogen bonds were also present in the quiescent state, either due to breakup of aggregates (Jin, et al., 2013) or intra- and intermolecular bonds. No further reduction in zero-shear viscosity was achieved with increasing urea concentration ≥2M (5% w/w mamaku), although shear-

thickening further diminished. Hence there is strong evidence to indicate that the hydrogen bonds responsible for shear-thickening were formed only under shear. This agrees with the hypothesis that under shear, the polysaccharide could stretch out and exposes associative groups, changing from intra- to intermolecular bonds which would cause shear-thickening. In mamaku it is postulated therefore, that urea binds to associative groups along the polysaccharide, preventing the 'zipping' effect between mamaku chains during shear as it has been shown in literature with other polymers (Kjøniksen, et al., 2005; Kjøniksen, et al., 2003; Lele & Mashelkar, 1998). It is also possible that urea could disrupt the hydrogen-bonded polymer-solvent structure (Hammes & Swann, 1967), which contributes to rheological properties of synthetic polymers such as polyethylene oxide (Dormidontova, 2002) and polyvinyl alcohol (Gao, Yang, He, & Yang, 2010). This would affect the entire network structure of the mamaku in solution as well as the shear-induced intermolecular associations.

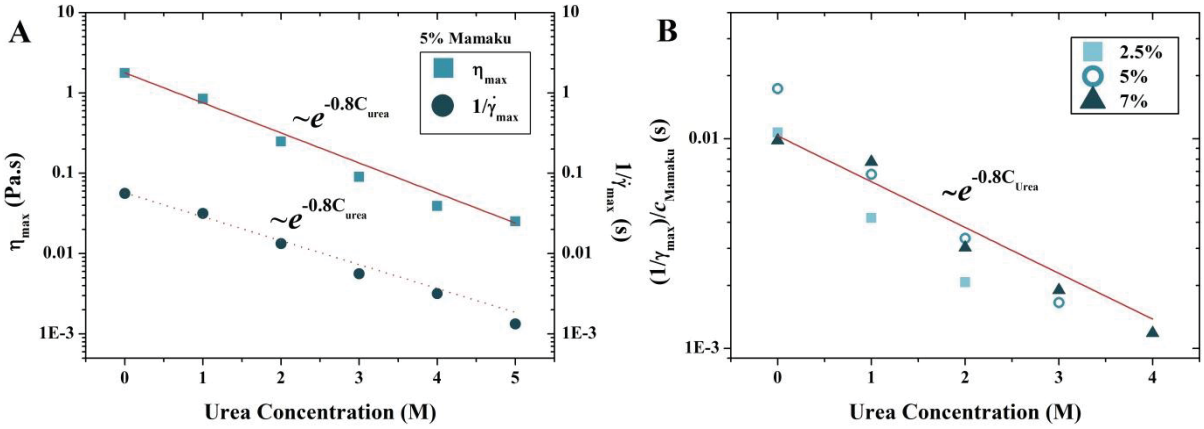

Figure 5.9 – a) Dependence of peak viscosity (η_{max}) (■) and characteristic time scale ($1/\dot{\gamma}_{max}$) (●) on urea concentration for 5% w/w mamaku; b) inverse of maximum shear rate normalised by mamaku concentration (2.5 (■), 5 (○), 7% w/w (▲)) at 20°C

Similar to temperature, the peak viscosity during shear-thickening and the characteristic time or association lifetime (inverse of shear rate at peak viscosity) exhibited an exponential dependency on urea concentration ($\sim e^{0.8Curea}$) (Figure 5.9a). Likewise, a master curve could be obtained by normalising $1/\dot{\gamma}_{max}$ with mamaku concentration which has the same exponential dependency of $\sim e^{-0.8Curea}$ (Figure 5.3b). Therefore similar conclusions could be drawn with urea as with temperature, addition of urea did not change the average number of association groups per chain but only modified the average lifetimes of the association, and therefore the onset of shear-thinning (network rupture) occurred at an approximately constant value of stress (Appendix B; Figure B3).

Large amplitude oscillatory shear and extensional viscosity experiments were also carried out on the mamaku gum in the presence of urea (Appendix B; Figure B4 & B5). Similar rheological responses were measured, with loss of strain hardening in LAOS and decrease in extensional relaxation time with increasing urea concentrations.

5.3.2.1 Time-Urea Concentration Superposition

Analogous to time-temperature superposition, the viscosity curves in the nonlinear region (Figure 5.10) and the frequency sweeps in the linear viscoelastic region (Figure 5.11) of 5% w/w mamaku with various urea concentrations were superimposed using shift factors. The same principle should apply, whereby superimposable curves indicate that all relaxation mechanisms of the material have the same urea concentration dependence, and it does not undergo microstructural changes or phase transitions upon addition of urea.

The shear-thinning prior to onset of shear-thickening was superimposable up to 3M urea, but began to deviate at 4 and 5M urea concentrations. The shear-thickening regions were not superimposable as the extent of shear-thickening (η_{max}/η_{crit}) clearly diminished with increasing urea concentration. The shift factors a_C and b_C had exponential dependencies of -0.9 and 0.4 on urea concentration, respectively. The larger exponent value of -0.9 for a_C as compared to -0.1 for a_T showed that urea had a more pronounced effect on shear-thickening (or hydrogen bonds) per unit concentration than per unit temperature does. Again, this confirmed the presence of additional intermolecular associations during shear-thickening, which had a different relaxation mode from simple chain relaxation.

Similar to time-temperature superposition, the linear viscoelastic behaviour based on frequency sweeps was superimposable (Figure 5.11). Therefore the presence of urea was not likely to have altered the structure or phase properties of the mamaku polysaccharide, and it behaves like a thermorheologically simple material in the linear region. Again, the exponential value of -0.4 for the horizontal shift factor in the linear region is approximately half of the value in the nonlinear region (-0.9), suggesting that twice as many associations would occur during shear-thickening as compared to the quiescent state. This supports the theory of shear-induced intra- to intermolecular association since every two associative groups involved in one intramolecular bond would then convert to two intermolecular bonds under shear *i.e.* pairwise association (Higgs & Ball, 1989).

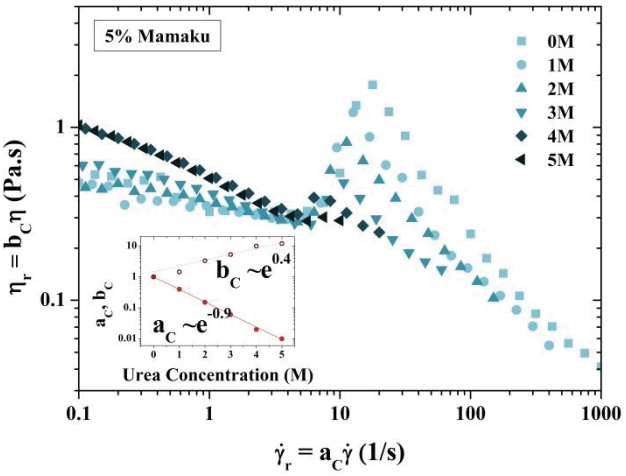

Figure 5.10 – Reduced viscosity (η_r=b_C·η) vs. reduced shear rate ($\dot{\gamma}_r$=a_C·$\dot{\gamma}$) of 5% w/w mamaku with 0 (■), 1 (●), 2 (▲), 3 (▼), 4 (◆) and 5M (◀) urea; inset: horizontal (a_C; ●) and vertical (b_C; ○) shift factors with urea concentration, C_{ref}=0M and 20°C

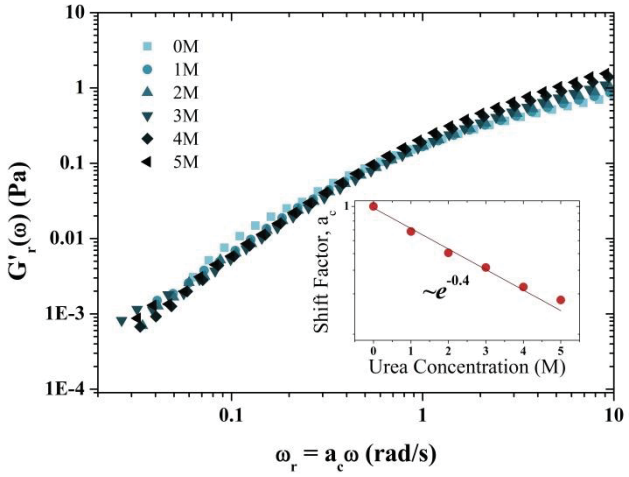

Figure 5.11 – Time-urea concentration superposition of frequency sweeps of 5% w/w mamaku with 0 (■), 1 (●), 2 (▲), 3 (▼), 4 (◆) and 5M (◀) urea by shifting along x-axis with shift factor, a_c; inset: shift factor values with urea concentration, C_{ref}=0M at 20°C

5.3.3 Effect of Ionic Strength

5.3.3.1 Effect of Salt Removal

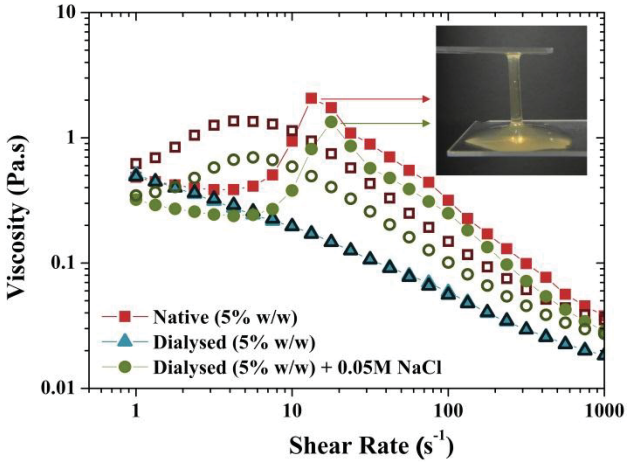

Figure 5.12 – Viscosity curves of 5% w/w native mamaku extract before (■) and after (▲) dialysis (MWCO 12-14,000 Da), and addition of 0.05M NaCl (●) for increasing (filled) and decreasing shear rates (unfilled symbols) at 20°C

Figure 5.12 shows the viscosity profiles of 5% w/w native mamaku extract before and after dialysis, and adding 0.05M NaCl to the dialysed sample. The native extract exhibited a shear-thickening behaviour at intermediate shear rates of around 5-20s^{-1}. This shear-thickening effect is often co-observed with a stringy or ropy consistency of the extract (Figure 5.12 inset). After dialysis (MWCO 12-14,000 Da), the shear-thickening along with the distinctive stringy and ropy consistency were lost and reverted to a shear-thinning behaviour typical of many food polysaccharides. Minerals (1.8 → 0.17 g/g NSP w/w), low molecular weight sugars (4.9 → 0.09 g/g NSP) and glucose from starch hydrolysis were the main components removed on dialysis. The viscosity curves generated by increasing and decreasing shear rates of the native and 'added NaCl after dialysis' extracts did not coincide. The hysteresis observed was related to its shear history and relaxation effects of its viscoelastic nature as reported earlier (Goh, et al., 2007). However, the dialysed extract did not exhibit hysteresis, which indicated the absence of an intermolecular network normally responsible for long relaxation times. As dilution effects of the extract during dialysis were accounted for, the loss of shear-thickening was not likely to be caused by a reduction in concentration as previous studies have shown to occur at mamaku concentrations ≤ c* (~2.5% w/w) (Goh, et al., 2007). The shear-thickening behaviour was qualitatively recovered on addition of NaCl (0.05M) back into the dialysed extract (Figure 5.12), which strongly indicated the involvement of cations in the shear-thickening behaviour of the polysaccharide. Zeta-potential values of 5% w/w native mamaku polysaccharide decreased from approximately -20mV to -60mV after dialysis, which highlighted the strong negative charge of the polysaccharide.

With the aim to further understand the nature of interaction between cations and the anionic polysaccharide, mono-, di- and trivalent cations at concentrations from 0.001 to 1.0M were tested, using two different metallic chlorides for each valency *i.e.* NaCl & KCl (+1), $CaCl_2$ & $MgCl_2$ (+2), and $AlCl_3$ & $LaCl_3$ (+3). It is important to

note that sodium, potassium, calcium, magnesium and aluminium were also originally present in the extract accounting for a large proportion of the minerals present (Table 5.2).

Table 5.2 – Mineral composition of native and dialysed mamaku extract (mg/g NSP†)

	Native (mg/g NSP†)	Dialysed (mg/g NSP†)
Potassium	612.2	21.3
Sodium	106.1	5.6
Calcium	18.6	8.0
Magnesium	10.7	3.2
Aluminium	11.6	4.6
Iron	0.1	0.3
Copper	0.1	0.03
Zinc	0.0054	0.01
Lead	0.0	0.02
Manganese	0.2	0.06
Mercury	0.0	0.0
Selenium	0.0	0.0

†*NSP: Non-starch polysaccharide*

5.3.3.2 Effect of Monovalent Cation Concentration

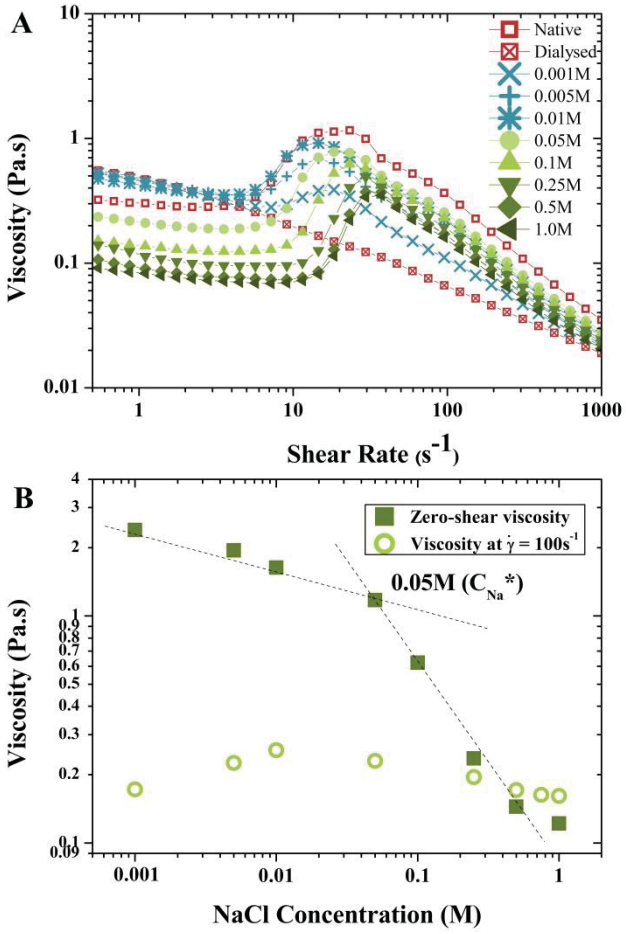

Figure 5.13 – a) Effect of NaCl concentration (0.001 (×), 0.005 (+), 0.01 (✳), 0.05 (●), 0.1 (▲), 0.25 (▼), 0.5 (◆) & 1.0M (◀) on shear-thickening of 5% w/w dialysed mamaku at 20°C; b) Zero-shear viscosity (■) estimated using a modified Cross' equation for shear-thickening fluids and viscosity at 100s-1 (○) at various NaCl concentrations

The effect of the monovalent cation Na^+ concentration on dialysed mamaku can be divided into two concentration regions of either above or below 0.05M (C_{Na}*). Flow curves of dialysed mamaku in 0.001 (×), 0.005 (+), and 0.01M (✳) NaCl are represented differently (highlighted in blue) (Figure 5.13a) because the rheological properties at these salt concentrations were noticeably different. At these salt concentrations (0.001 to 0.01M), the viscosity at low shear rates (< $3s^{-1}$) did not decrease much from the original dialysed extract. However, shear-thickening seemed to still be 'developing' towards the full extent observed in the native extract with increasing salt concentration (0.001 to 0.01M). The following general trends (for shear-thickening systems only excluding the dialysed sample without added salt) were observed with further increase in salt concentration from 0.001 to 0.1M: i) decrease in viscosity (*i.e.* progressive shift of entire viscosity profile), including zero-shear viscosity (Figure 5.13b), ii) an increase in critical shear rate (shear rate at the onset of shear thickening), and iii) increasing degree of shear thickening. The extent of shear-thickening is defined here as the ratio of peak viscosity during shear-thickening to the viscosity at onset of shear-thickening *i.e.* $\eta_{max}/\eta_{\dot{\gamma}_{crit}}$.

Zero-shear Viscosity The zero-shear viscosity was estimated using a modified Cross' equation for shear-thickening fluids (Galindo-Rosales, Rubio-Hernández, Sevilla, et al., 2011) (Figure 5.13b). More than a ten-fold reduction in zero-shear viscosity was seen with increasing salt concentration from 0.001M to 1.0M. The decrease in zero-shear viscosity of polyelectrolytes was expected in the presence of salts. The cations screen the negatively charged carboxylic acid groups on the polysaccharide backbone and the conformation becomes less extended, thus lowering the viscosity. A previous study on the mamaku extract has also shown the reduction of intrinsic viscosity of the polysaccharide (dilute regime) with increasing salt concentration (Goh, et al., 2011). In the present study however, there was no significant reduction of viscosity (of dialysed mamaku) at very low salt concentrations *i.e.* 0.001-0.01M. A substantial reduction was only observed between 0.01 and 0.5M, and plateaued at ≥0.5M NaCl concentration for the concentration range tested. The viscosity over a range of shear rates did not decrease even with further addition of salt. At very low salt concentrations the amount of cations present was probably insufficient to confer any significant conformational changes to the anionic polysaccharide. Above the plateau concentration (0.5M), the number of negatively charged groups on the polysaccharide available for counter-ion binding was probably less than/-or equal to the number of cations present. Further addition of salt therefore had no effect on its conformation and viscosity.

Viscosity at $\dot{\gamma} > \dot{\gamma}_{peak}$ The effect of salt was not as pronounced on the viscosity at higher shear rates, e.g. at shear rate of 100s^{-1} (Figure 5.13b). The viscosity increased slightly up to 0.01M NaCl, then decreased to a similar level at 1M (0.15 Pa.s) as compared to the viscosity at low salt content (~0.17 Pa.s at 0.001M). This observed viscosity at $\dot{\gamma} > \dot{\gamma}_{peak}$ is in contrast to that of zero-shear viscosity. At sufficiently high shear rates, majority of the polymer chains disentangled and aligned in the direction of shear, therefore arriving at similar conformation and resulting in very similar viscosities as observed here.

Critical Shear Rate The reduction in viscosity was also accompanied by a shift to a higher critical shear rate. As the viscosity curves plateaus ≥0.5M NaCl, the critical shear rate remained constant as well. This suggests that the critical shear rate may also be dependent on the conformation of the polysaccharide.

Extent of Shear-Thickening Shear-thickening was induced even at very low salt concentrations. The extent of shear-thickening would be the observed 'hump' in the shear-thickening region. At very low salt concentrations from 0.001 to 0.01M (<C_{Na}*), shear-thickening was seen to be 'developing' from the dialysed extract. Above C_{Na}* (0.05M), the extent of shear thickening remained fairly consistent even at higher salt concentration.

Frequency Sweep The effect of salt concentration on the dynamic rheological properties of the mamaku polysaccharide was also tested by changing the frequency of the application of the strain (Figure 5.14a). The shear-thickening (or shear-induced thickening) characteristics obtained by viscosity measurements were observed under large deformation beyond the linear viscoelastic regime. Therefore probing the response of the material in the linear region may provide further insight into the microstructure of the material in the quiescent state which would otherwise be obscured during rotational shear.

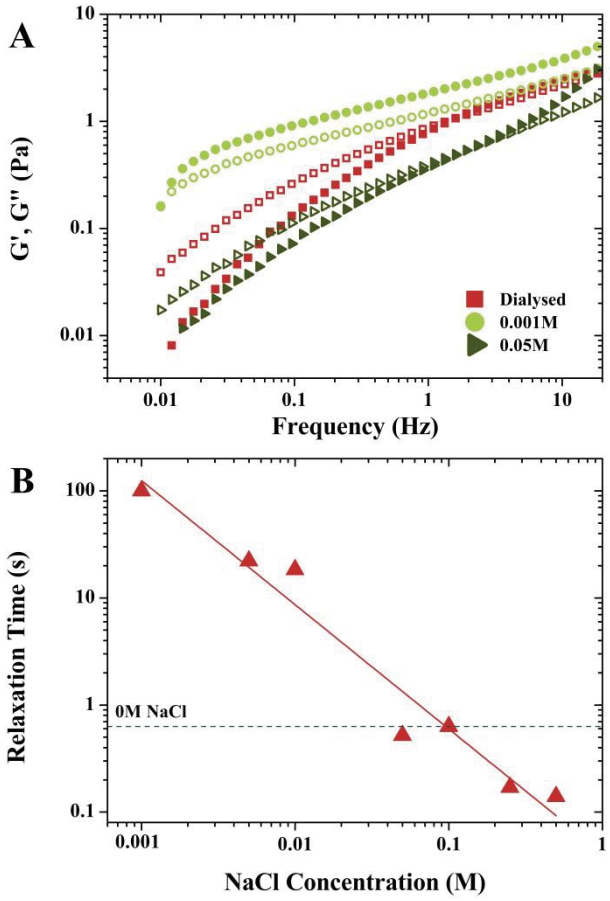

Figure 5.14 – a) Frequency sweeps G' (filled) and G" (unfilled) of 5% w/w dialysed mamaku at 0 (■), 0.001 (●) & 0.05M (▶) NaCl at 1% strain and 20°C; b) relaxation time of dialysed mamaku with NaCl concentration (0.001-0.5M)

Figure 5.14a shows the frequency sweep of the dialysed samples without and with 0.001 and 0.05M NaCl (γ=1%; LVE region). The dialysed sample (no added NaCl) behaved like an entangled polymer solution with a crossover of G' and G" at higher frequencies. Upon adding 0.001M NaCl, the material showed weak gel characteristics instead *i.e.* G'>G". However, the material lost its gel characteristic on further increasing the salt concentration e.g. 0.05M NaCl (and 0.1, 0.25, 0.5M NaCl, results not shown) with a crossover in G' and G" at frequencies between 1-10 Hz. This frequency sweep profile at 0.05M NaCl was also similar to the native extract. The relaxation time of the polysaccharide (calculated as the reciprocal of frequency at the crossover between G' and G" values or the lowest frequency value when tanδ=1) increased from 0.63s at 0M salt to >100s at 0.001M salt and then decreased with increasing salt concentrations.

Based on the results, the presence of cations could either promote or deter the assembling of network structure within the system, depending on its concentration. The elastic modulus (G') is interpreted as the network strength, which is reflected by the number of intermolecular mechanically active junctions (Green & Tobolsky, 1946; Tan, et al., 2001). The overall effect of salt on structural strength could be the result of two opposing phenomena - 1) G' increases due to intermolecular associations and 2) G' reduces due to a smaller chain conformation (*i.e.* intramolecular associations at the expense of intermolecular ones). This is shown by the reduction in G' with increasing salt concentration (at f=1Hz). This corresponds to the reduction in zero-shear viscosity as both parameters characterise the structure under small deformation. Above C_{Na}* most

chains in solution would have adopted the coil conformation as a result of electrostatic screening and hence effectively reducing the distribution of chain size in solution. The relaxation time was taken as the disentanglement time of the polymer. The large distribution of relaxation times over the salt concentrations demonstrated a strong dependency of the network entanglements with ionic strength of the solution.

Overall, the dialysed (0M salt) mamaku probably had the least number of intramolecular associations as well as intermolecular junctions due to electrostatic repulsion along and between polymer chains. This could prevent close proximity of the polymer chains and therefore the relaxation time for disentanglement would be relatively short. At extremely low salt concentrations (0.001-0.01M NaCl), the extract behaved like a weak gel (G'>G") for the entire frequency range (Figure 3a) due the presence of a more rigid network where intermolecular associations dominated over intramolecular ones. This stiff network prevented the chains from sliding past one another, which led to long relaxation times. Above 0.01M NaCl, the backbone charges were probably sufficiently screened and the polysaccharide chains could adopt more compact configurations. Hence, intramolecular associations were formed at the expense of intermolecular ones, reducing the number of active junctions which could contribute to an elastic network in the small deformation test range. Relaxation time therefore also decreased as the intermolecular associations which prevent disentanglement were compromised.

5.3.3.3 Effect of Divalent Cation Concentration

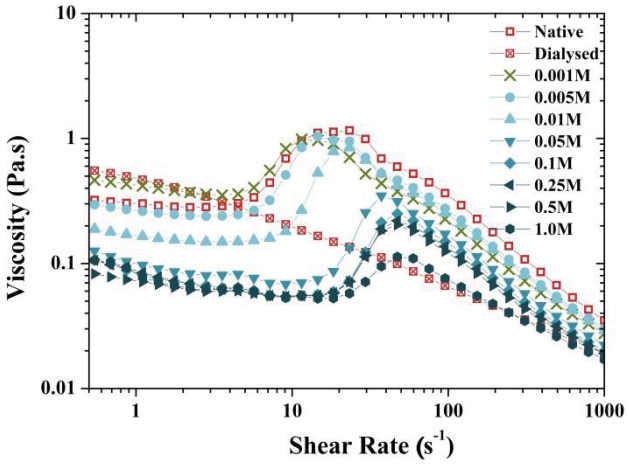

Figure 5.15 – Effect of CaCl2 concentration (0.001 (×), 0.005 (●), 0.01 (▲), 0.05 (▼), 0.1 (◆), 0.25 (◀), 0.5 (▶) & 1.0M (●)) on shear-thickening of 5% w/w dialysed mamaku at 20°C

The effect of the divalent cation Ca^{2+}on the dialysed mamaku extract was qualitatively similar to the monovalent cation, with similar trends in general (for shear-thickening systems): i) decrease in viscosity (progressive shift of the viscosity profile to lower values), ii) increase in critical shear rate, and iii) increase in the degree of shear thickening with increasing salt concentration (within 0.001-0.01M) (Figure 5.15). Below the critical concentration of $CaCl_2$ (C_{Ca}*; 0.001M), there was no significant reduction in viscosity ($\leq\dot{\gamma}_{crit}$). Also, one notable different feature of the divalent cations was that the shear-thickening 'hump' progressively diminished as salt concentration increased above 0.05M. The concentration of the divalent salt required to reach plateauing of the viscosity (i.e. no further reduction in viscosity) was also lower than monovalent salts *i.e.*

0.1M $CaCl_2$ versus 0.5M NaCl. No gelling or precipitation of the system was observed at any $CaCl_2$ concentration tested. Clearly, the total ionic strength of the divalent cations (due to more positive charges) had a greater influence on the rheological properties of the material than monovalent cations. In addition, the influence on mamaku viscosity was not cation-specific for both mono- or divalent cations. From the data, it was noted that several concentration regions could be identified where the cation had a different effect on the shear-thickening behaviour. Further discussion of these observations is given in the overall discussion (section 5.3.5).

5.3.3.4 Effect of Trivalent Cation Concentration

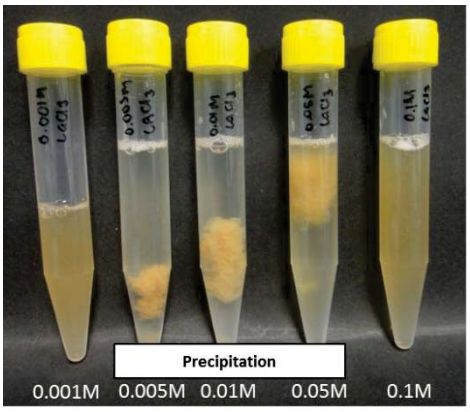

Figure 5.16 – Dialysed mamaku extract in (from left to right) 0.001-0.1M $LaCl_3 \bullet 7H_2O$

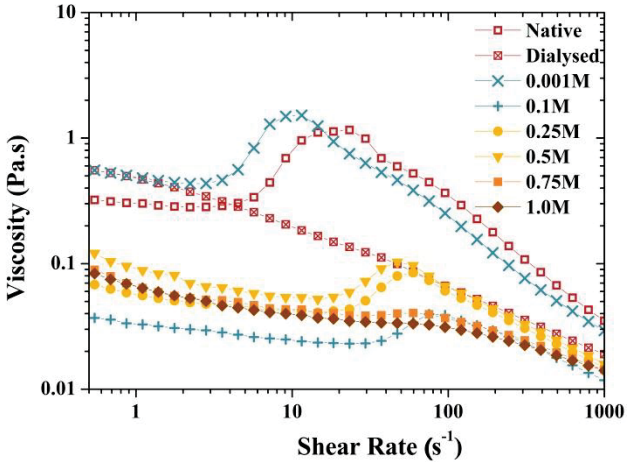

Figure 5.17 – Effect of $LaCl_3 \bullet 7H_2O$ concentration (0.001 (×), 0.1 (+), 0.25 (●), 0.5 (▼), 0.75 (■) & 1.0M (◆)) on shear-thickening of 5% w/w dialysed mamaku; sample precipitation occurs with 0.005, 0.01, 0.05M $LaCl_3 \bullet 7H_2O$ at 20°C

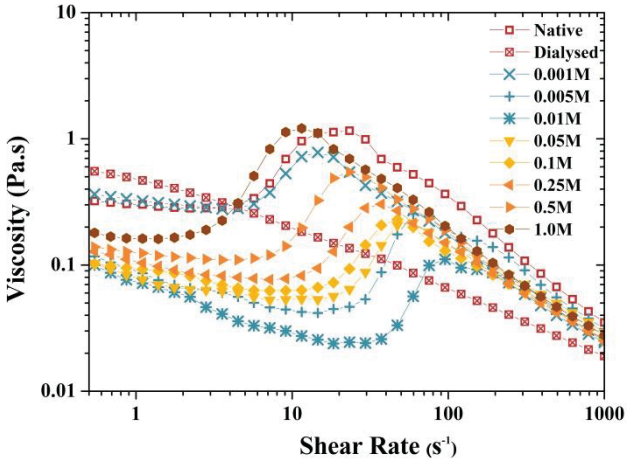

Figure 5.18 – Effect of $AlCl_3 \bullet 6H_2O$ concentration (0.001 (×), 0.005 (+), 0.01 (✱), 0.05 (▼), 0.1 (◆), 0.25 (◀), 0.5 (▶) & 1.0M (●)) on shear-thickening of 5% w/w dialysed mamaku at 20°C

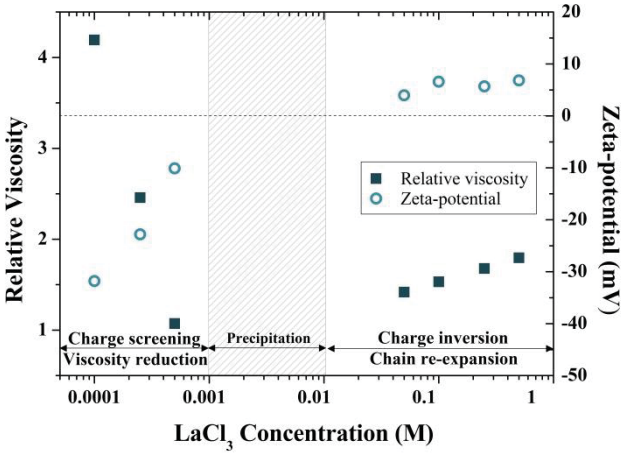

Figure 5.19 – Effect of $LaCl_3 \bullet 7H_2O$ concentration on relative viscosity (■) of 1% w/w dialysed mamaku and zeta-potential (○) of 5% w/w dialysed mamaku at 20°C

The effect of trivalent cations *i.e.* La^{3+} and Al^{3+} on the dialysed mamaku was markedly different from the mono- and divalent cations. For La^{3+} the shear-thickening was regained at a very low concentration of 0.001M, but within the concentration range of 0.005-0.05M $LaCl_3$, the polysaccharide aggregated and precipitated out of solution (Figure 5.16). Aggregation was strongest at 0.01M $LaCl_3$ where there is a distinct separation of the polysaccharide from the solvent. Above 0.1M concentrations, the precipitates redissolved and the shear thickening behaviour was regained. The shear-thickening was eventually lost at ≥0.75M (Figure 5.17). The same phenomenon was observed when anhydrous $AlCl_3$ was used (results not shown). The hydrated form of $AlCl_3$ *i.e.* $AlCl_3 \cdot 6H_2O$ however did not cause precipitation at the concentrations tested (Figure 5.18). Unlike the mono- and divalent cations, further increasing the concentration of $AlCl_3$ (>0.01M) did not lead to a decrease in viscosity. Instead, the viscosity increased and the critical shear rate shifted to lower shear rates.

The phenomenon of precipitation and redissolution of the polysaccharide with trivalent cations (La^{3+}) is also observed with highly charged polyelectrolyte chains (HCPC) such as polystyrene sulphonate (Jan & Breedveld, 2008; Olvera De La Cruz et al., 1995) and DNA (Nguyen, Rouzina, & Shklovskii, 2000). This effect is referred to as *re-entrant (ion) condensation* (Nguyen, et al., 2000). The authors explained that precipitation is the result of

chain collapse caused by short-range electrostatic intra- and/or intermolecular ion-bridging of the chains. In the case of mamaku polysaccharide, this occurred at salt concentration above the first critical concentration in the low ionic strength region. Redissolution of the precipitated polymer occurred at a second critical concentration value. The charge contribution by trivalent cations likely exceeded that required to neutralise the bare surface charge of polysaccharide, resulting in overcharging as described by Grosberg, Nguyen & Shklovskii (2002) and Hsiao (2008). Coulombic repulsion between monomers leads to chain reexpansion resulting in dissolution of the precipitates (Olvera De La Cruz, et al., 1995). However, the mechanism for chain redissolution is still under debate (Hsiao, 2008; Nguyen, et al., 2000; Olvera De La Cruz, et al., 1995). The increase in radius of gyration with chain expansion therefore can result in a viscosity increase (Hsiao & Luijten, 2006).

This condensation theory appeared to be applicable to the mamaku polysaccharide as evidenced by the reduction in the relative viscosity (at 0.0001-0.005M), followed by precipitation (0.001-0.01M) and then increment (>0.05M) of relative viscosity of the dilute mamaku polymer (1% w/w, <C*) with $LaCl_3$ concentration (Figure 5.19). Furthermore, it shows that the same effects could be observed whether the polymer was in the dilute (1% w/w) or semi-dilute (5% w/w) concentration regime. Moreover, the salt concentration at which precipitation occurred (~0.001M) was lower for the dilute as compared to the semi-dilute mamaku solutions (~0.005M), which agrees with reported literature findings where the concentration at collapse is proportional to polymer concentration (Hsiao, 2006; Hsiao & Luijten, 2006; Jan & Breedveld, 2008). Zeta-potential values also showed charge inversion (from negative to positive charge) at concentrations where re-dissolution occurred (Figure 5.19). Although precipitation and redissolution was not observed with Al^{3+}($\cdot 6H_2O$), the chain expansion theory still applies as viscosity increased at higher salt concentrations (≥0.05M). In this case, this effect without observed precipitation is known as chain collapse and reexpansion as reported by Hsiao and Luijten (2006).

It is unclear why La^{3+} (heptahydrate) would behave differently from Al^{3+} (hexahydrate). However, since similar precipitation effects were seen for anhydrous Al^{3+}, the cation form (whether hydrated or anhydrous) and/or size may be a determining factor. In solution, a fraction of the hydrated Al^{3+} or $[Al(OH_2)_6]^{3+}$ cation further hydrolyses to $[Al(OH)(OH_2)_5]^{2+}$ which reduces its effective trivalent charge to a divalent one (Whitten, Davis, Stanley, & Peck, 2006). The charge density therefore may not be as strong as that of anhydrous Al^{3+} or La^{3+}, which could be the reason why precipitation of the polysaccharide did not occur. Another plausible explanation is based on the re-entrant condensation theory in that precipitation and re-dissolution is highly dependent on ion size. It occurs only when the ion size is comparable to the monomer ($-COO^-$) size (Hsiao, 2008). The hydrated Al^{3+} is relatively bulkier than the anhydrous ion as the ion is surrounded by six water molecules in a hexahedral configuration. Selective precipitation with trivalent cations has also been observed in sodium poly(styrenesulfonate) solutions where indium chloride ($InCl_3$) does not cause precipitation while precipitation is seen for gallium ($GaCl_3$) and aluminium chloride hexahydrate ($AlCl_3 \cdot 6H_2O$) (Jan & Breedveld, 2008). Therefore trivalent cations which have an additional effect causing re-entrant condensation exhibit more variability for cation-specificity as compared to the mono- and divalent cations.

5.3.3.5 Effect of Cation Concentration and Cation Valency

The effects of different cation valencies (mono-, di- and trivalent) were compared (Figure 5.20) at a similar concentration (0.1M). The monovalent cations have the least reduction in viscosity, earliest onset of shear-thickening but similar extent of shear-thickening as compared to the multivalent cations. By increasing cation valency, the viscosity is lowered and the critical shear rate is extended to higher shear rates. Similar observations were made with increasing cation concentration. The viscosity curves obtained were qualitatively and quantitatively similar for cations of the same valency (monovalent and divalent) (Figure 5.20). The concentration of 0.01M $AlCl_3$ was also included as it was shown that at 0.1M (Figure 5.18) chain re-expansion is likely to have occurred and therefore the high viscosity would not be representative of the viscosity-reduction effect that the cations have as a result of charge screening.

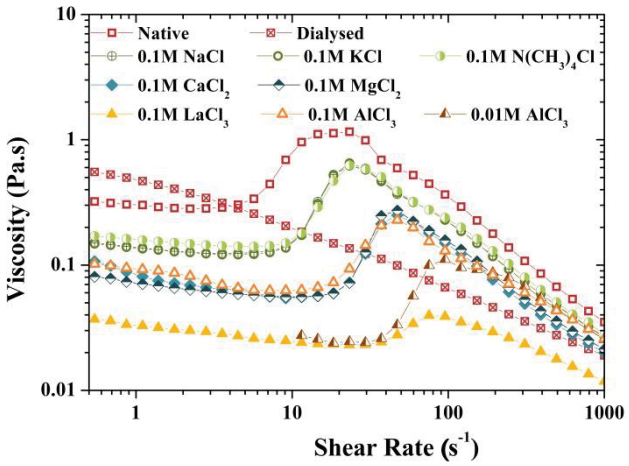

Figure 5.20 – Viscosity curves of native (☐) and dialysed (☒) mamaku extract with salts of different cation valencies i.e. monovalent (NaCl (⊕), KCl (○), TMAC (◑)), divalent (CaCl2 (◆), MgCl2 (◩)) and trivalent (AlCl3 (△) (also at 0.01M (▲)), LaCl3 (▲)) at 0.1M concentration and 20°C

The shear-thickening mechanism is therefore unlikely to be cation-specific but rather a function of ionic strength (cation valency and concentration). The addition of an organic monovalent cation in the form of tetramethylammonium chloride (TMAC; $N(CH_3)_4Cl$) also resulted in the regaining of shear-thickening and the effects were almost identical to those of NaCl and KCl (Figure 5.20). Apart from the organic nature of the cation, the size (ionic radius) of the cation was also much larger than its metallic counterparts due to the bulky alkyl ($-CH_3$) groups. The crystalline and hydrated ionic radii of the cations tested are compared in Table 5.3 for reference. The valency of the cation appeared to be directly linked to shear-thickening rather than its size.

The parameters critical shear rate, viscosity at critical shear rate and extent of shear thickening cannot be scaled linearly with cation valency. Figure 5.21 compares the various rheological parameters obtained with each salt plotted as a function of the total ionic strength which leads to a clearer correlation.

Table 5.3 – Ionic and hydrated ionic radius of various cations

Ion	Charge	Ionic Radius (Nightingale, 1959) (Å)	Radius in aqueous solution (Marcus, 1988) (Å)
Na^+	+1	0.95	0.96
K^+	+1	1.33	1.41
$N(CH_3)_4^+$	+1	3.47	-
Ca^{2+}	+2	0.99	1.03
Mg^{2+}	+2	0.65	0.70
Al^{3+}	+3	0.50	0.50
La^{3+}	+3	1.15	1.14

Regardless of the cation type, both the mono- and divalent cations in general showed fairly similar trends for the viscosity at critical shear rate, critical shear rate, and extent of shear-thickening at equivalent ionic strengths. The divalent cations were however more effective at shrinking the polysaccharide (Hsiao & Luijten, 2006; Liu, Ghosh, & Muthukumar, 2003) as shown by the lower viscosity (Figure 5.21a) and higher critical shear rate (Figure 5.21b) at the same ionic strength, compared to the monovalent cations. This difference cannot be attributed to charge concentration alone. Intramolecular chain-bridging by the divalent (or even trivalent) cations was likely to be responsible for the enhanced viscosity reduction in the polymer chain (Liu, et al., 2003). Trivalent cations were however markedly different from the mono- and divalent cations. For example, Al^{3+} clearly exhibited a minimum in the viscosity at the critical shear rate (Figure 5.21a) and a maximum for the critical shear rate (Figure 5.21b) and the extent of shear-thickening (Figure 5.21c). Furthermore, similar effects were not seen between trivalent cations. La^{3+} was able to cause precipitation, redissolution and eventually loss of shear-thickening but this was not the case for $Al^{3+}(\cdot 6H_2O)$. Although ionic strength accounts for cation valency and concentration, it appeared that Coulombic repulsion in multivalent ions has an equal, if not greater effect on the shear-thickening properties.

A distinct maximum in the extent of shear-thickening with ionic strength was observed for the di- and trivalent cations. It is possible that intermolecular associations between the polymer chains during shear enhanced the extent of shear-thickening while Coulombic repulsion between cations on the polymer interferes with it. It seems that at low ionic strengths, the contribution to viscosity by intermolecular associations was much greater than the opposing effects of Coulombic repulsion. Further increase in ionic strength shifted the system towards Coulombic repulsion and less intermolecular association, and hence, the extent of shear-thickening weakened. The bridging effect of divalent cations may also hinder intermolecular associations during shear. The increased intramolecular bridging decreased the probability of a transition from intra- to intermolecular associations during shear, thus the extent of shear-thickening was reduced. The positive charge of monovalent cations was neutralised with the negatively charged carboxylic acid groups so Coulombic repulsions would be insignificant and the extent of shear-thickening would not exhibit a maximum peak as with the multivalent cations. In the case of La^{3+}, the repulsion may be too excessive and strong to allow any intermolecular association leading to shear-thickening.

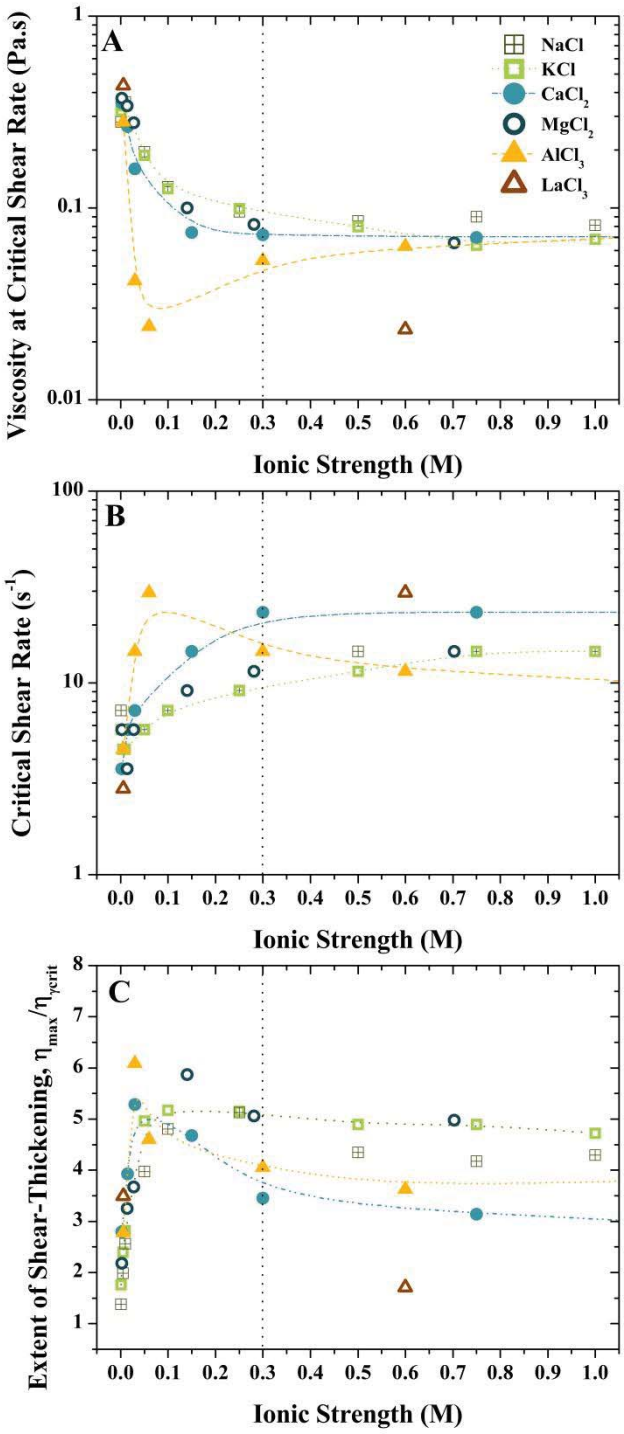

Figure 5.21 – Comparison of a) viscosity at critical shear rate, b) critical shear rate & c) extent of shear-thickening with various mono- (NaCl (⊞), KCl (□) , di- (CaCl2 (●), MgCl2 (○)) and trivalent (AlCl3 (▲), LaCl3 (△)) cations at equivalent ionic strengths (lines serve as visual guides)

Overall, a plateau was reached for viscosity at critical shear rate, critical shear rate, and extent of shear-thickening above 0.3M ionic strength. At this point, it was likely that the negative charges on the polysaccharide had been neutralised and reached the saturation point for cation binding. Activation energies using η_{crit} and η_{max} of the system with various concentrations of NaCl and $CaCl_2$ were also obtained (Appendix B; Figure B6). The activation energies decreased with increasing cation concentration, suggesting fewer

intermolecular associations during shear-thickening as a result of a more compact configuration in the quiescent state.

5.3.4 Effect of pH

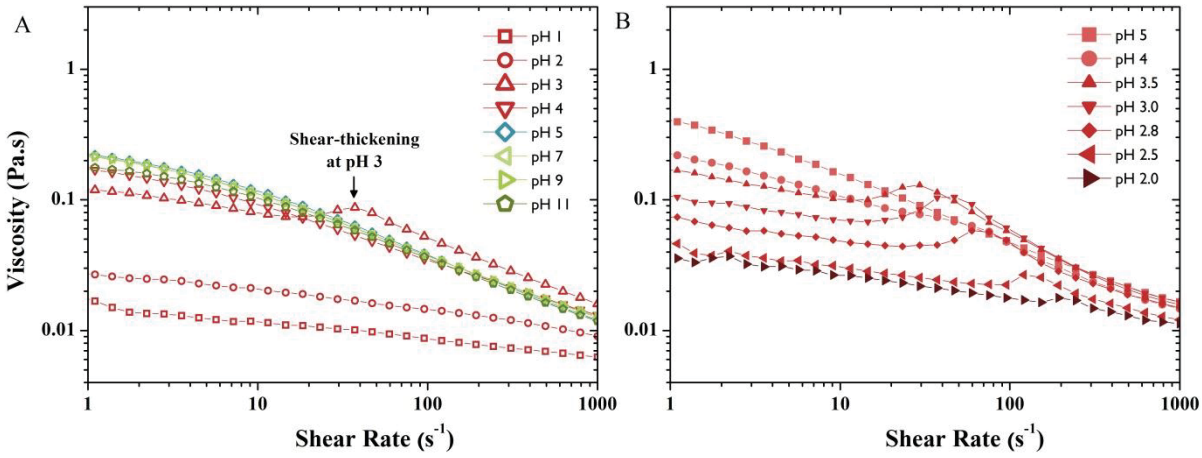

Figure 5.22 – a) Viscosity curves of 5% w/w dialysed mamaku under various pH conditions (pH 1-11) and b) magnified in pH region from 2.0-5.0

The effect of pH was further tested on the dialysed extract. Figure 5.22a shows the viscosity of the salt-free dialysed extract (original pH ~5) with pH adjusted from 1 to 11, and at smaller intervals between pH 2 and 4 (Figure 5.22b). The viscosity curves were considerably lowered at acidic pH *i.e.* 1 & 2 and remained fairly similar to the native (pH 5) sample at high pH values (Figure 5.22a). Shear-thickening occurred under the acidic pH range of 2 to 3.5 (Figure 5.22b) even in the absence of salt. No shear-thickening was detected at pH near and/or above native pH (*i.e.* pH 4-11), and the flow behaviours were fairly similar to each other. The viscosity curves at high pH revealed shear-thinning behaviour with a Newtonian region of high viscosity at low shear rates (~0.1-1s^{-1}) whereas a less strongly shear-thinning behaviour was seen for low pH (1 & 2).

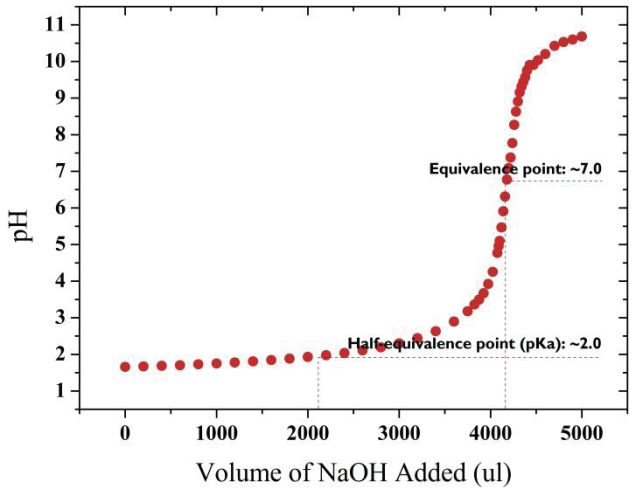

Figure 5.23 – pKa titration curve of dialysed mamaku solution (5% w/w)

The detection of shear-thickening even in the absence of salt indicates that the shear-thickening behaviour of the polysaccharide was not exclusively contributed by the cations. At pH below the half-equivalence point (*i.e.*

pKa 2.0; Figure 5.23) of the polysaccharide, all carboxylic groups are in the protonated form (COOH) while at high pH above pKa the carboxylic groups lose their protons and partially exist in the acidic form (COO^-). This supports the previous discussion that shear-thickening is caused by shear-induced formation of hydrogen bonds between polysaccharide chains as a result of the screening effect on the negative charges of the carboxylic groups. The absence of shear-thickening at the highly acidic pH (1 & 2) was not likely to be due to hydrolysis of the polysaccharide as viscosity could be recovered upon readjusting the pH from low to higher values. Therefore at very low pH, it is very likely that the shrinkage of the polymer conformation due to charge-screening was so strong that it would require much higher shear rates for the transition from intra- to intermolecular bonds.

5.3.5 Overall Discussion

It is possible that cations act as cross-linkers via electrostatic interactions between polysaccharide chains which give rise to shear-thickening, as observed in some synthetic polymer systems (Broze, Jerome, Teyssie, & Marco, 1983; Dong, Li, Xu, & Guo, 2011). However, this ion-bridging effect is applicable only to multivalent cations (Olvera De La Cruz, et al., 1995; Pu, Ng, Mok, & Chen, 2004). Clearly, the recovery of shear-thickening with monovalent salts was not a result of ionic-bridging between chains. Alternatively, cations may screen electrostatic repulsions and allow formation of intermolecular associations which result in shear-thickening or rheological changes. The latter mechanism is more frequently the case in shear-thickening or polysaccharide materials (Smolka & Belmonte, 2006; Tan, et al., 2001; Tepale et al., 2011; Vasudevan, et al., 2008). Additionally, shear-thickening was also reinstated in the dialysed mamaku at pH 3 where the charges were screened by H^+ ions (Figure 5.22). The intermolecular association can be either hydrophobic in nature (Burckbuchler, et al., 2006; Nystrom, et al., 2009) or via hydrogen bonding (Kjøniksen, et al., 2003; Munoz & Santamaria, 2003). The loss of shear-thickening with increasing temperature and urea concentration supports the latter type of bonding. Furthermore, previous studies on the effect of temperature on the native mamaku extract have shown the loss of shear-thickening at temperatures ≥50°C (Matia-Merino, et al., 2012). Hydrophobic associations are strengthened (Burckbuchler, et al., 2006) and hydrogen bonds weakened or disrupted (Briscoe, et al., 2000) at temperatures ≥50°C. It is therefore indicative that the shear-thickening is very likely of a hydrogen-bond origin. Based on the evidence gathered, the shear-thickening behaviour is hypothesised to be a result of a shear-induced transition from intra- to intermolecular hydrogen bond formation promoted by the screening effect of cations.

The formation of hydrogen bonds is only possible if i) the polysaccharide chains are within close proximity to each other and ii) the sites involved in hydrogen bonding are available. The role of cations seems to fulfil the first criteria by screening the negatively charged groups on the polysaccharide group allowing the chains to come closer. Shearing then could stretch out the chain and expose more sites within the large polysaccharide molecule for intermolecular hydrogen bonding. Hydrogen bonds are distance- and orientation-dependent (Israelachvili, 2011), therefore electrostatic repulsion between the unscreened groups on the polysaccharide chain would prevent the chains from coming in close proximity sufficient for formation of intermolecular hydrogen bonds during shear.

5.4 Conclusion

The rheological properties of the mamaku polysaccharide, specifically its shear-thickening behaviour are highly sensitive to temperature, urea, ionic strength (cations) and pH. Shear-thickening was suppressed at high temperatures (≥50°C) as a result of thermal mobility and breaking up of hydrogen bonds. The maximum viscosity during shear-thickening was inversely proportional to temperature in the order of kT (Arrhenius' Law), which was highly indicative of the involvement of hydrogen bonds. A large activation energy of viscous flow based on maximum viscosity (~90kJ/mol for 5% w/w mamaku) suggested strong associations formed during shear. Likewise, shear-thickening was diminished in the presence of urea (≥5M for 5% w/w mamaku), a hydrogen-bond breaker, which further points the origin of intermolecular association towards hydrogen bonding. Increasing the temperature and urea concentration did not change the fraction of hydrogen bonds associated or the strength of the associations, but it reduced the lifetime of the associations through thermal mobility and competitive hydrogen bond binding. Finally, the removal of salts from the native mamaku polysaccharide solution revealed a strong correlation between shear-thickening and ionic strength. The absence of salt results in intermolecular electrostatic repulsion which prevents formation of short-range hydrogen bonds. With added salt/cations, the shear-thickening is reinstated. Electrostatic screening with cations of the same valency has similar effects *i.e.* not cation-specific. Re-entrant condensation (precipitation followed by re-dissolution) was observed with trivalent cations. Electrostatic screening was also achieved at acidic pH (pH 2-3.5; >pKa) although the effect was not as significant as cations.

It is likely that shear-induced association, whereby the mode of association is hydrogen bonding, resulted in shear-thickening. The endogenous mineral content in the polysaccharide solution provides electrostatic screening, which allows the formation of short-range intermolecular hydrogen bonds. Hydrophobic interactions and electrostatic cross-linking did not appear to be involved in the shear-thickening behaviour. The structure of the polysaccharide is characterised in the next chapter, which can provide more information on the groups responsible for association and the mechanism behind shear-thickening.

Chapter 6 Purification and Structural Characterisation of Mamaku Polysaccharide

6.1 Introduction

Characterisation of polysaccharides often requires the material to be of high purity. This is a complex task for plant polysaccharides because the material usually contains other plant contaminants such as starch, lignin, insoluble fibres and sugars, etc. In the case of mamaku extract, although the crude aqueous extract of the mucilage (referred to as the 'native' fraction in this thesis) is capable of demonstrating behaviour governed by the polysaccharide, it will not be sufficiently pure for structural and molecular characterisation. Measurements using techniques such as nuclear magnetic resonance (NMR) and light scattering require the material to be non-aggregated and free from extraneous compounds in order to obtain high quality data. Based on earlier studies, the native material consists of ~10% w/w non-starch polysaccharide, which is rich in uronic acid (72.5% of NSP) and neutral sugars *i.e.* galactose (14.3%), xylose (7.1%) and arabinose (3.1%). Other constituents present in the mucilage are mainly low molecular weight simple sugars (~44% w/w), minerals (~16% w/w) and protein (~2% w/w) (Goh, et al., 2007). In an ideal state, these constituents should be removed from the mucilage before carrying out structural characterization studies. However, complete purification is not an easy task due to the diversity of physico-chemical interactions involved in a multi-components system. Hence, very often, a polysaccharide is considered 'pure' if the isolated material still possesses the same chemical and physical properties after employing various purification treatments (Walter, 1997). There is no universal method for extraction, isolation and purification of the polysaccharides. Methods vary widely depending on the laboratories carrying out the purification and the chemical and physical nature of the polysaccharides. However, a typical isolation and purification procedure usually involves starch and protein removal, de-salting, and precipitation of the polysaccharide. In this chapter, a purification method was developed for the mamaku polysaccharide. Various purification procedures were employed to remove protein, starch, and the small molecular weight components.

The fingerprint of a polysaccharide lies in its structure – the unique arrangements of molecules that make up the macromolecule. Eventually how these macromolecules are subsequently interacting with each other determine the properties of the polysaccharide system. Polysaccharides with common structural features are often grouped together into classes such as pectin-type galacturonans, arabinogalactans, xyloglucans, galactomannans, glucuronomannans, rhamnogalacturonans etc. Plant polysaccharides extracted from the seed, fruit and trunk are usually galactomannans (Michael & Reid, 2006), pectins (Rao & Silva, 2006) and arabinogalactans (Sims & Furneaux, 2003), respectively. Quite often, polysaccharides of similar structures yield similar functionalities and properties. Elucidating the structure of the mamaku polysaccharide gives it an identity and forms the basis for structural classification. Furthermore, knowledge of the primary structure may provide a better understanding of the physico-chemical properties of the polymer system in different environmental conditions such as pH, ionic conditions, temperature, etc. This chapter presents the purification

of mamaku polysaccharide and the subsequent characterization of its chemical structure, namely its neutral sugar (monosaccharide) composition and linkage analysis using NMR and GC-MS.

The objectives of this chapter were to:

1. Purify the native mamaku mucilage with the following criteria:
    a. Purified material consisted of ⩾75% w/w non-starch polysaccharide (NSP)
    b. Isolated polysaccharide fraction retained its shear-thickening behaviour
    c. Loss of polysaccharide material during purification was kept minimum so that the yield from native extract should be close to 10% w/w based on the reported NSP fraction reported (Goh, et al., 2007))
    d. Chemicals used should not cause polysaccharide degradation or structural modification
2. Determine the weight-average molecular weight using multi-angle laser light scattering (MALLS) technique
3. Characterise the rheological behaviour of the purified polysaccharide using a controlled shear stress rheometer to ascertain that the shear-thickening behaviour was retained
4. Determine the monosaccharide composition and linkages of the polysaccharide structure

6.2 Materials and Methods

6.2.1 Purification

6.2.1.1 Ultracentrifugation

The hydrated native solution was ultracentrifuged (when required) at 250,000*g* for 1 hour at 20°C (Sorvall Combi ultracentrifuge, T-865 motor, Dupont Instrument, DE, USA) to remove large aggregates.

6.2.1.2 Starch Hydrolysis

Starch was detected in the native extract using 0.5% iodine solution and the dialysed extract was found to consist of 3.4% w/w starch. Therefore starch removal by enzymatic hydrolysis was required to obtain the non-starch polysaccharide (NSP) fraction. The native extract was first subjected to hydrolysis by incubating thermostable α-amylase from *Bacillus licheniformis* (EC 3.2.1.1, Megazyme, Bray, Ireland, 100 U/ml in 100mM sodium acetate buffer, pH 5.0; 350μl/g sample) at native pH (~5.0) and 100°C for 6 minutes, with stirring at every 2 minutes interval. This was followed by hydrolysis with amyloglucosidase from *Aspergillus niger* (EC 3.2.1.3, Megazyme, Bray, Ireland, 330 units) at 50°C for 30 minutes. The hydrolysis conditions were selected based on the starch hydrolysis step described in the Megazyme total starch assay procedure (AOAC method 996.11). Completion of starch hydrolysis was verified visually using 0.5% iodine solution, ensuring the iodine solution did not turn dark blue. The rheological properties of the mamaku solution were unaltered after starch hydrolysis.

6.2.1.3 Protein Depolymerisation

Enzymatic

The protein content of the native mamaku extract was found to be 2% w/w from previous proximate analysis (Goh, et al., 2007). Therefore removal of protein from the native extract would be necessary for further purification work. After starch hydrolysis, the pH of the solution was adjusted to ~7.5 with 0.1M NaOH. The solution was then incubated with 100μl/g sample of protease (Megazyme; 50mg/ml or ~350 tyrosine units/ml) at 60°C for 30 minutes. The conditions selected were based on the protein depolymerisation step described in the Megazyme total dietary fibre assay procedure (AOAC method 991.43).

Sevag Reagent

An alternative method to remove proteins apart from the use of enzymes was carried out by adding Sevag reagent, a mixture of 1-butanol and chloroform in the proportion of 1:4 (Staub, 1971). Chloroform (6.4ml or 20% v/v of volume of aqueous phase) was added to the starch-hydrolysed mamaku solution (3% w/w, 32ml) followed by 1-butanol (1.6ml or 25% of volume of chloroform) and stirred for 30 minutes. The mixture was centrifuged at 900*g* (Heraeus Multifuge 15-R centrifuge Thermo Scientific) for 10 minutes at 20°C to separate

the aqueous from the chloroform phase. The denatured proteins formed a gel at the water-chloroform interface which was discarded with the chloroform phase.

6.2.1.4 Ethanol Precipitation

The solution was subjected to ethanol precipitation after starch hydrolysis and protein depolymerisation. To obtain a final ethanol concentration of 60, 70 and 80% v/v, the volume ratios of 95% v/v ethanol : sample were 1.7, 2.8 and 5.3 : 1 respectively. The mamaku solution was carefully poured into 95% v/v ethanol (LabServ, analytical reagent grade) while stirring the ethanol with a glass rod. The white thread-like precipitate (Figure 6.8) coiled around the glass rod and was left to stand for 60 minutes at room temperature (20°C). Large polymers *i.e.* polysaccharide, starch and protein are insoluble in high concentrations of ethanol (>~80% v/v) (Englyst, Quigley, Hudson, & Cummings, 1992), therefore resulting in precipitation. The ethanol precipitation step separated the soluble low molecular weight impurities e.g. simple sugars (monosaccharides), oligosaccharides, peptides, organic acids from the polysaccharide fraction. It was noted that factors such as final ethanol concentration, number of precipitation steps, time of precipitation and temperature would affect the final purity and composition of the sample (Goh, 2004). The precipitation time and temperature were fixed while the ethanol concentration and number of precipitation steps were varied to study their effects on sample yield. After allowing the polysaccharide fraction to precipitate, the precipitate was recovered by filtration (Whatman No. 1) under vacuum. The residue was successively washed with 15ml portions of 78% ethanol, 95% ethanol and acetone each, redissolved in ~60ml of milli-Q water and transferred to a round bottom flask for subsequent freeze-drying. For multiple precipitation steps, the precipitate obtained was redissolved in milli-Q water and re-precipitated in ethanol as described earlier. Residual ethanol or acetone was removed using a rotary evaporator (Buchi Rotavapor R-215, Flawil, Switzerland) at 75 mbars and 35°C for 15 minutes.

6.2.1.5 Freeze-drying

After removal of the organic solvents, the solution was frozen at -80°C and then freeze-dried for 48 hours under a vacuum of <1mbar overnight. The purified material obtained after freeze-drying was weighed immediately.

The overall purification steps are presented in the flow diagram as shown in Figure 6.1. The procedures in dashed boxes were further studied using various parameters or methods.

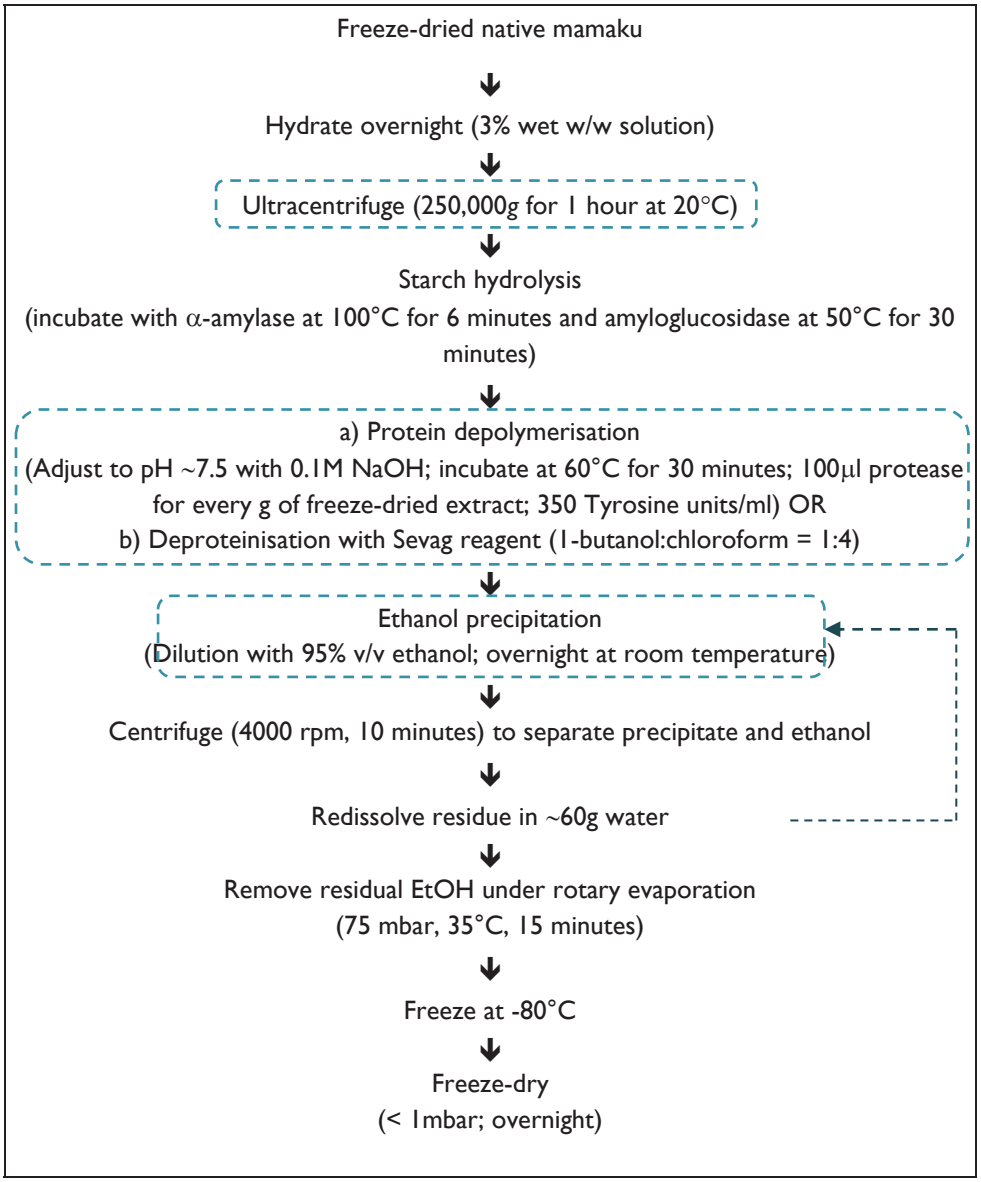

Figure 6.1 – Flow diagram of overall purification scheme of mamaku extract

6.2.2 Chemical Analysis

6.2.2.1 Total Carbohydrate

Total carbohydrate present in the freeze-dried material was estimated using the phenol-sulphuric acid method (Dubois, Gilles, Hamilton, Rebers, & Smith, 1956). The sample (0.01% w/w; 1ml), standard or blank (milli-Q water) was added to a test tube. Phenol (5% w/v; 1ml) was then added to the test tube, followed by 5ml of concentrated sulphuric acid, H_2SO_4. The mixture was mixed thoroughly using a vortex mixer (state model), after 10 minutes and 30 minutes for colour development (yellow-orange). The absorbance of the blank was first measured at 485nm with a UV-VIS spectrophotometer (ThermoFischer, MA, USA) and zeroed for subsequent sample or standard solutions. Standard curves were constructed with glucose (D-glucose; Sigma) at concentrations of 20, 40, 60, 80 and 100 mg/l. The standards and blanks were carried out in duplicates while the analysis of the samples was carried out in triplicates.

The total carbohydrate content determined includes the free sugars (especially native extract which was not subjected to ethanol precipitation) as well as sugars from the polysaccharide present in the extract. The carbohydrate content obtained is reported as glucose equivalents based on the calibration curve. The presence of uronic acids do not give absorbance readings as strongly as the neutral monosaccharides (Steve & Yolanda, 2006). Therefore the mamaku polysaccharide which has an uronic acid content of approximately 72.5% w/w (Goh, et al., 2007) would probably result in a lower total carbohydrate estimated.

6.2.2.2 Total Uronic Acid

The total uronic acid content of the material was determined using a colorimetric assay (*m*-hydroxydiphenyl; Sigma) method (Blumenkrantz & Asboe Hansen, 1973). The absorbance of the sample was compared to a standard absorbance curve prepared using different galacturonic and glucuronic acid standards at concentrations of 0, 25, 50, 75, 100 and 125 ppm. A stock 200ppm standard galacturonic acid in 0.4% ammonium oxalate was diluted to get 0.5ml of sample (0.01%), standard or blank (milli-Q water) was added to four test tubes each. Sodium tetraborate (BDH; AnalaR; 3ml) in concentrated sulphuric acid (0.0125M) was then added to the test tube and cooled for 10 minutes. The mixture was agitated using a vortex mixer and incubated in a boiling water bath at 100°C for 5 minutes and then cooled to room temperature using an ice bath. Fresh *m*-hydroxydiphenyl solution (0.15% in 0.5% NaOH; 50µl) was added to two of the four tubes for each sample or standard. 50µl of 0.5% NaOH were then added to the remaining two tubes as blanks. The mixture was agitated using a vortex mixer and left to stand for 5 minutes for colour development (pink). The absorbance of the blanks was first measured at 525nm with a UV-VIS spectrophotometer (ThermoFischer, MA, USA. The colour formed is unstable therefore absorbance was quickly read after addition of *m*-hydroxydiphenyl (Blumenkrantz & Asboe Hansen, 1973).

6.2.2.3 Ash Content Analysis

Ash is the inorganic residue remaining in the material after removal of organic matter at very high temperatures. The empty crucible was first prepared by heating at 525°C for 60 minutes and cooled for another 60 minutes and then weighed. The sample (~0.5g) was then weighed into the crucible and incinerated in a muffle furnace for 5 hours at 525°C, cooled in a desiccator for 60 minutes and then weighed again. The ash content is the weight of the material remaining in the crucible after all organic material has been burnt off.

6.2.2.4 Moisture Content Analysis

The moisture content of the mamaku fractions was measured by determining the weight difference after drying in an air oven. Aluminium moisture dishes with lids were dried in the air oven at 108°C overnight and stored in a desiccator at room temperature prior to use. The dishes were accurately weighed (±0.01g) with their lids and reweighed after placing the samples (~1g) on the dishes. The samples were dried in the air oven (Contherm Oven 240V, New Zealand) at 108°C for 4 hours, cooled in desiccator for 60 minutes and then weighed again. The procedure was repeated until a constant weight was achieved. The native mamaku samples

are particularly hygroscopic, therefore the moisture content must be known to accurately account for the yield of the NSP fraction obtained after purification.

6.2.2.5 Starch Content Analysis

Starch content was determined by an accredited chemical laboratory (Nutritional Laboratory, Institute of Food, Nutrition & Human Health, Massey University) based on the α-amylase method AOAC 996.11.

6.2.3 Structural Analysis

6.2.3.1 Constituent Sugar Analysis

The principle of constituent sugar analysis is to determine the monosaccharide composition of the polysaccharide by i) hydrolysing (breaking down) the polysaccharide, ii) converting the monosaccharides into forms appropriate for analysis (reduction and acetylation), and then iii) identifying the constituent monosaccharides qualitatively and quantitatively. More details on the theory of these individual reactions can be found in the experimental techniques section (Chapter 3).

The constituent monosaccharide composition of the purified mamaku polysaccharide was determined by three complementary methods either with different hydrolysis methods or analytical techniques:

Method 1: Samples (1 mg, in duplicate) were hydrolysed with aqueous trifluroacetic acid (TFA) (2 M, 500 µL, containing 0.406 mg/ml *myo*-inositol, 120°C, 1 h), filtered (0.2 µm, hydrophilic PTFE) hydrolysates, dried and neutralised by addition of 2 M NH_4OH (200 µL). The neutralised hydrolysates were then reduced, acetylated and analysed by GC-MS as described below. Weight calibration constants were determined from a seven sugar standard mix (rhamnose, fucose, arabinose, xylose, mannose, galactose & glucose; derivatised at the same time as the samples) following the TAPPI standard method T 249 cm-85 (1985) for quantification of monosaccharides in the sample by comparing peak areas and retention times of standards to sample. The TAPPI standard method T 249 is the standard for determining carbohydrate composition of extractive-free wood and wood pulp by gas-liquid chromatography. *Myo*-inositol of a known quantity was used as an internal standard in mass spectrometry to minimise inaccuracies in sample quantification. Monosaccharide yields were based on the mean values of duplicate samples and were expressed as weight percent anhydro-sugar because this is the form of sugar present in a polysaccharide.

Method 2: Samples (1 mg) were hydrolysed with methanolic acid (3 N, 500 µL, 80°C overnight) and aqueous TFA (2 M, 500 µL, containing 0.86 mg/ml D-allose as an internal standard, 120°C, 1 h). The hydrolysates were reduced and acetylated to form alditol acetates and analysed by GC-MS as described below

Method 3: The monosaccharides resulting from hydrolysis with methanolic acid and aqueous TFA from method 2 were analysed by high-performance anion-exchange chromatography (HPAEC). Samples (20 µL) dissolved in distilled water (0.5 mg/ml) were separated at 30 °C on a CarboPac PA-1 (4 x 250 mm) column equilibrated in 25 mM NaOH. Samples were eluted with simultaneous gradients of NaOH (25–10 mM from 0–

10 min, then 10–100 mM from 10–30 min and held to 55 min) and sodium acetate (0–500 mM NaOH from 30–55 min) at a flow rate of 1 ml/min and monitored by pulsed amperometric detection, using the Dionex standard carbohydrate waveform.

Reduction Sodium borodeuteride ($NaBH_4$, 2M) in 2M NH_4OH (200µl) was added to reduce (*i.e.* convert the acetal to corresponding alcohol groups) the hydrolysed samples overnight at 25°C. Glacial acetic acid (3 x 50µl) was added to stop the reaction. Acetic acid (5% v/v) in methanol (2x500µl) was added to remove borate as volatile trimethylborate and the samples were evaporated to dryness under 40°C air. Methanol was added and the samples were again dried under 40°C air (repeated twice). A dry white crystalline residue was obtained.

Acetylation Glacial acetic acid (40µl), ethyl acetate (200µl), acetic anhydride (600µl) and 60% v/v perchloric acid (23µl) were added to the sample and mixed gently. The tubes were left to stand at room temperature for 15 minutes. Distilled water (2ml) and 1-methlyimidazole (40µl) were added to decompose the acetic anhydride. Dichloromethane (DCM, 2ml) was added to the tubes, shaken and centrifuged at 1120*g* for 5 minutes to extract the alditol acetates from the aqueous phase. The top layer was removed using a Pasteur pipette and discarded. The DCM phase was washed, successively, with 0.5M sodium bicarbonate (Na_2CO_3, 2ml) and 2 x water (2ml) and centrifuged at 1120*g* for 5 minutes to wash the DCM phase. The washed DCM phase containing the alditol acetates was evaporated to dryness under 40°C air. Acetonitrile (500µl) was added to remove any residual water and then evaporated to dryness. Residues were re-suspended in an appropriate volume of acetone and run on GC-MS.

GC-MS The alditol acetate derivatives were separated by GC on an Agilent HP-5MS fused silica capillary column (30m x 0.25mm i.d., 0.25µm film thickness; Agilent, Santa Clara, CA) with the GC oven programmed from 50°C (held for 1 minute) to 130°C at a rate of 25°C/min, then to 230°C at a rate of 3°C/min and detected by MS using a Hewlett Packard 5973 MSD. Identifications were based on peak retention times and by comparison of electron impact mass spectra with standard spectra.

6.2.3.2 Glycosyl Linkage Analysis

Prior to glycosyl linkage analysis, uronic acid and methylesterified uronic acid residues were reduced using a two-step carboxyl reduction method as described by Sims and Bacic (1995) (procedures below; illustrated in Figure 6.2). Carboxyl-reduced samples (1 mg, in duplicate) were methylated (*i.e.* conversion of –OH to $–OCH_3$ groups with methyl iodide) with the method of Ciucanu and Kerek (1984) except that samples were dispersed in DMSO (200 µl). After extraction into chloroform, the methylated samples were hydrolysed with 2.5 M TFA, reduced and acetylated before analysis by GC-MS as described above (Figure 6.3).

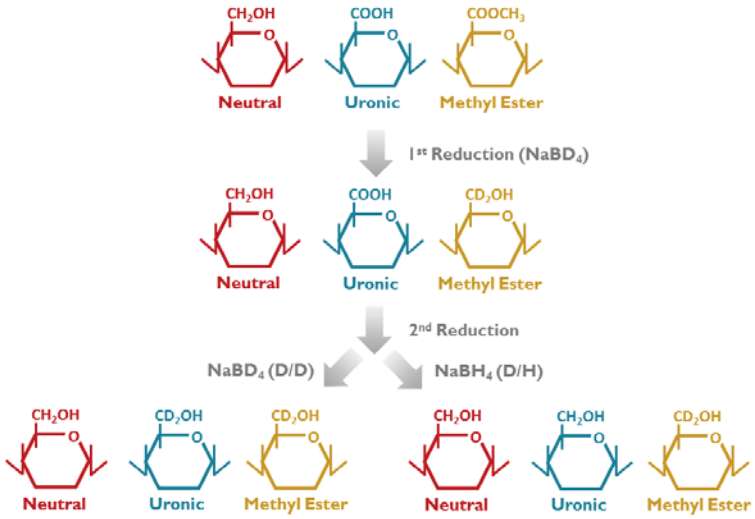

Figure 6.2 – Carboxyl reduction of methylesterified and non-methylesterified uronic acids (adapted from Pettolino, Walsh, Fincher, & Bacic, 2012)

Carboxyl Reduction of Uronic Acids

1st reduction Freeze-dried purified mamaku (10mg) was suspended in imidazole-HCl buffer (500mM, 10ml, pH 8.0) and cooled with ice to 4°C. Aliquots (3 x 1ml) of freshly prepared sodium borodeuteride ($NaBD_4$) in imidazole-HCl buffer was added to the solution at 10 minute intervals and then left to stand on ice for an hour. The samples were then brought to room temperature and left to stand for another hour. Excess $NaBD_4$ was destroyed by dropwise addition of glacial acetic acid (300µl) until the fizzing stopped. The samples were dialysed against distilled water in a 2000 MWCO membrane for 24 hours with 2 dialysate changes. The samples were freeze-dried.

2nd reduction Samples subjected to the first reduction were then prepared for a second reduction step. The freeze-dried samples were suspended in distilled water (1ml) and MES-KOH (0.2M, 200µl, pH 4.75) was added. Carbodiimide reagent (1-cyclo-hexyl-3-(2-morpholinoethyl)-carbodiimide-metho-p-toluenesulphonate, 400µl, 500mg/ml) was added and then the samples were sonicated in ice water for 30 minutes to aid dispersal. The samples were heated for 3 hours at 30°C. Tris-HCl (2M, 1ml, pH 8.0) was added and the samples were cooled to 4°C. Sodium borodeuteride ($NaBD_4$; 70mg/ml) was added to two sample tubes while sodium borohydride ($NaBH_4$; 70mg/ml) was added to another two sample tubes to further reduce the sample for 18 hours at 4°C. Excess reductant was destroyed by dropwise addition of glacial acetic acid (150µl) until the fizzing stopped. The samples were dialysed against distilled water in a 2000 MWCO membrane for 24 hours at 4°C with two dialysate changes. The samples were freeze-dried and weighed.

The overall glycosyl linkage analysis procedure is summarised in Figure 6.3.

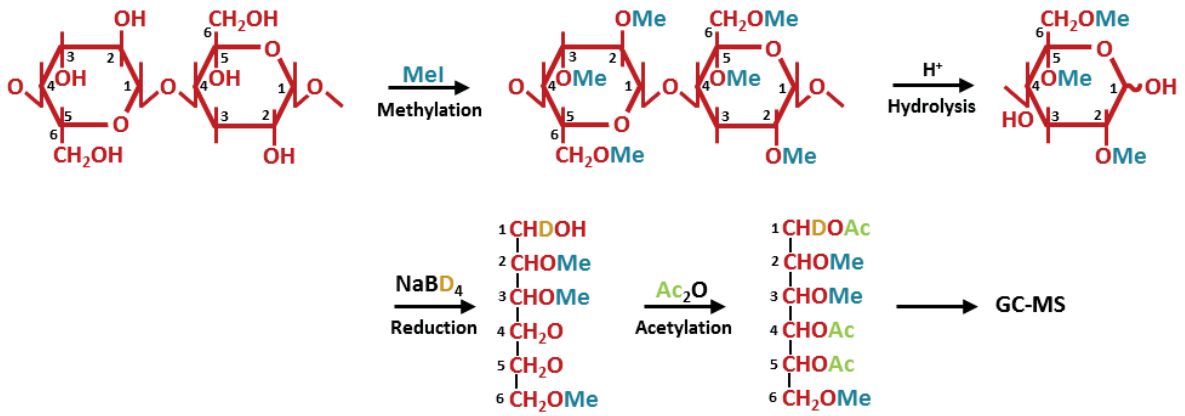

Figure 6.3 – Summary of glycosyl linkage analysis based on methylation, hydrolysis, reduction and acetylation reactions (adapted from Pettolino, et al., 2012)

6.2.3.3 NMR spectroscopy

Purified mamaku polysaccharide was exchanged with deuterium by freeze-drying with D_2O (99.9 atom%) three times. Samples were dissolved in D_2O and ^1H and ^{13}C (both ^1H coupled and decoupled) spectra were recorded on a Bruker Avance DPX-500 spectrometer at 90°C. The ^1H and ^{13}C chemical shifts were measured relative to an internal standard of Me_2SO (^1H, 2.70 ppm; ^{13}C, 39.5 ppm) (Sims & Furneaux, 2003). Assignments were made from double quantum filtered (DQF) correlation spectroscopy (COSY), heteronuclear multiple quantum coherence (HMQC) COSY, HMQC total correlated spectroscopy (TOCSY) and DEPT-135 (distortionless enhancement by polarization transfer with pulse (φ_3) flip angle of 135°) experiments and by comparing the spectra with published data (Appendix C Table C1 and C2).

6.2.4 Size-Exclusion Chromatography-Multi-Angle Laser Light Scattering (SEC-MALLS)

The molecular weight of the purified mamaku polysaccharide was determined using size-exclusion chromatography coupled with multi-angle laser light scattering (SEC-MALLS). Samples (5 mg/ml in 0.1 M $NaNO_3$) were centrifuged (14,000*g*, 10 min) before injecting the sample (100 µL) into the size exclusion columns TSK-Gel $G5000_{PWXL}$ and $G4000_{PWXL}$, 300 x 7.8 mm, Tosoh Corp., Tokyo, Japan) connected in series using a Waters 2690 Alliance separations module. The sample was eluted with 0.1 M $NaNO_3$ (0.7 ml/min, 60 °C). The eluted material was detected by a Waters 490E variable wavelength detector (280 nm), a DAWN-EOS multi-angle laser light scattering detector with a laser at 690 nm (Wyatt Technology Corp., Santa Barbara, CA) and a Waters 2410 refractive index monitor connected in series. The weight-average molecular weight determination was analysed using ASTRA software (v4.73.04, Wyatt Technology Corp.). The data used for analysing the molecular weight was selected based on the elution volume between 9.4 - 12.2ml of the chromatogram. An incremental refractive index (*dn/dc*) of 0.141 ml/g determined experimentally was used in the analysis.

6.2.5 Rheological Measurements

The viscosity curves of the purified mamaku polysaccharide at different concentrations were measured using a Paar Physica rheometer MCR 301 (Anton-Paar, Graz, Austria) in controlled shear rate (CSR) mode at 20.0 ±0.1°C with the cone and plate geometry (CP 40-4 and P-PTD200/56, gap=0.049 μm). The temperature of the sample was maintained using a Peltier system to an accuracy of ±0.1 °C. The samples were allowed to rest for 10 minutes after loading into the geometry prior to starting the test. This was done to reduce any effects of shear history and to allow for temperature equilibration. To obtain the plot of concentration dependence of zero shear rate viscosity, the viscosities of dilute mamaku solutions (0.01-0.1% w/w) were measured using an Ubbelohde capillary viscometer (viscometer no. 100, K59, Cannon Instrument Co., U.S.A.). The zero shear rate viscosities in the semi-dilute regime (0.6-1.4% w/w) were estimated by fitting the simplified Cross' equation $\left(\eta = \frac{\eta_0}{1+(\lambda\dot{\gamma})^{1-n}}\right)$ to the complex viscosity as a function of angular frequency (0.1 to 10 rad/s) obtained from dynamic oscillatory shear measurements at a strain amplitude of 1% (within linear viscoelastic region) as described in an earlier study (Goh, et al., 2007).

6.3 Results and Discussion

6.3.1 Purification

6.3.1.1 Ultracentrifugation

The native extract obtained after ultracentrifugation was a clear, yellowish solution as opposed to a cloudy yellowish dispersion before ultracentrifugation (Figure 6.4). The rheological properties, particularly the shear-thickening property of the sample were unaffected by ultracentrifugation. The sediment discarded after centrifugation was likely to contain a small amount of polysaccharide aggregates and other plant cell wall materials such as hemicelluloses, celluloses and lignins. It is interesting to note that the sediment was also tested negative for starch. Approximately 10% of solid material was lost after ultracentrifugation and the final yield obtained after ethanol (80% v/v) precipitation was 11.8% instead of 16.1% (w/w) (Figure 6.5). Ultracentrifugation of the hydrated native solution was included in the purification procedure to remove extraneous matter.

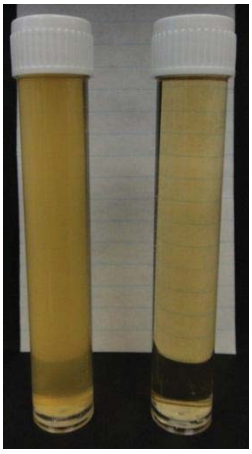

Figure 6.4 – Appearance of native mamaku solution before (left) and after (right) ultracentrifugation at 250,000g for 1 hour at 20°C

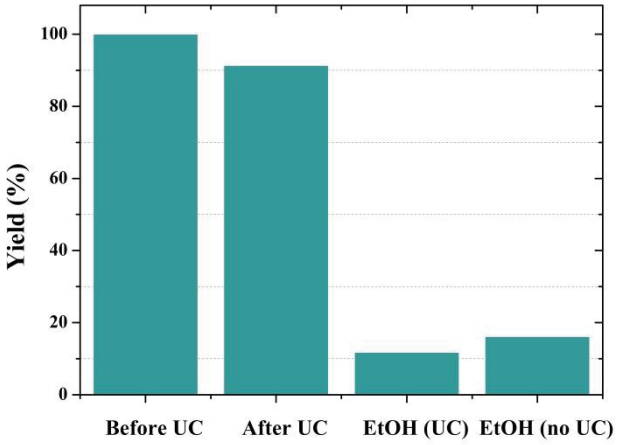

Figure 6.5 – Yield of solid material before and after ultracentrifugation (UC) and ethanol precipitation (EtOH)

6.3.1.2 Protein Removal

Two protein removal methods were compared for the purification of mamaku gum. In one of the methods, protease was used for protein depolymerisation at alkaline pH (~7.5). In the second method, denoted as the Sevag method, protein present in the extract was denatured at native pH (~5.5) using a mixture of chloroform and 1-butanol. The reaction resulted in the protein forming precipitates. The polysaccharide solution was subsequently removed from the precipitates by decantation (Figure 6.6).

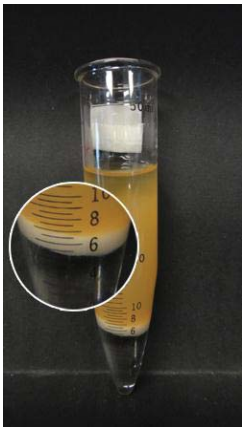

Figure 6.6 – Protein removal using Sevag reagent; top brown layer: aqueous polysaccharide phase; water-chloroform interface: denatured protein gel; bottom clear layer: chloroform phase

The protein contents before and after protein removal using both methods were determined using the Leco total combustion method (AOAC 968.06; nitrogen to protein conversion factor of 6.25) and shown in Table 6.1. The gum obtained after treatment with the Sevag reagents was observed to be more soluble in water, although the amount of protein remaining (6.3% w/w) was more than using protease (4.1% w/w). The rehydrated mamaku solution retained its rheological properties and shear-thickening characteristic after protein removal (using protease or Sevag reagent), followed by ethanol precipitation and freeze-drying of reconstituted precipitate.

Table 6.1 – Protein content of purified mamaku obtained with protein removal using protease or Sevag's reagent determined using the Leco total combustion method

	Yield (% w/w)	Protein (% w/w)	Shear-thickening
No protein removal	16.8	6.8	Yes
Protease	15.1	4.1	Yes
Sevag reagent (x1)	13.2	6.3	Yes

The protease method was able to remove more protein from the material as compared to using Sevag's reagent. However, the enzymatic method required pH adjustment as well as incubation at elevated temperatures (60°C for 30 minutes). Furthermore, commercial enzymes are often contaminated with carbohydrase, which could cleave glycosidic bonds of the polysaccharide. In this case, carbohydrases activities were unlikely because these enzymes have an optimum acidic pH, which the adjustment of pH of the polysaccharide solution to alkaline pH could suppress the carbohydrase activity (BeMiller, 2006). The enzymes are deactivated upon precipitation with 80% v/v ethanol.

On the other hand, the organic solvents used in Sevag's method may chemically modify the polysaccharide and therefore functionality. However, this has been the preferred method of protein removal in the extraction and

isolation of other plant polysaccharides as enzymes are costly (Jahanbin, Moini, Gohari, Emam-Djomeh, & Masid, 2012; Nguyen Tien, Do Truong, Nguyen Thi, Pham Le, & Nguyen Van, 2011). It is one of the mildest techniques of protein removal with minimal degradation to the polysaccharide although it may result in losses of polysaccharide material (Staub, 1971). The use of chloroform (non-polar solvent) may also help remove any residual fat lipid compounds within the material (Steve & Yolanda, 2006). Based on the advantages and limitations of each method, both methods were fairly suitable to remove protein from the mamaku polysaccharide, depending on what the factor of consideration is e.g. cost, purity, and processing time. Alternatively, protein removal could be omitted from the purification process as the amount removed was not exceptionally significant. It is also likely that the protein present were contaminants from the plant cell walls rather than proteins linked to the polysaccharide since the functional and rheological properties of the polysaccharide was not modified after the protein removal.

6.3.1.3 Ethanol Precipitation

Ethanol precipitation is one of the major techniques employed in the purification of polysaccharides. The difference in solubility of polysaccharides and other extraneous small molecular weight components in ethanol enable separation of the polymer from most small molecular weight constituents such as free sugars and salts. By adding ethanol (or other organic solvents) to water, the dielectric constant of the solvent is effectively reduced. In other words, the solvent becomes less polar and solvent-polymer interactions are weakened leading to increased probability for polymer-polymer interactions and precipitation (Smidsrod & Haug, 1967). Low molecular weight sugars and peptides, organic acids, minerals, free amino acids and pigments are extracted into the ethanol. The efficiency of ethanol precipitation is dependent on numerous factors, mainly ethanol concentration, polysaccharide concentration, type of polysaccharide *i.e.* acidic or neutral, salt concentration and cation type (Smidsrod & Haug, 1967).

The mamaku solution was subjected to ethanol precipitation to remove the high quantities of sugars (44% w/w) and minerals (18% w/w) present in the native extract (Goh, et al., 2007). Ethanol precipitation was also used to remove glucose from starch breakdown, peptide chains after protein depolymerisation with protease and to deactivate the α-amylase, amyloglucosidase and protease enzymes if they were used in prior purification steps.

The effect of number of ethanol precipitations was explored on the polysaccharide recovery and purity. Theoretically, the polysaccharide is further purified with each ethanol precipitation step (Goh, 2004). The polysaccharide solution was precipitated either once, twice or thrice with ethanol. Figure 6.7 illustrates the various fractions recoverable from varying the number of ethanol precipitation steps.

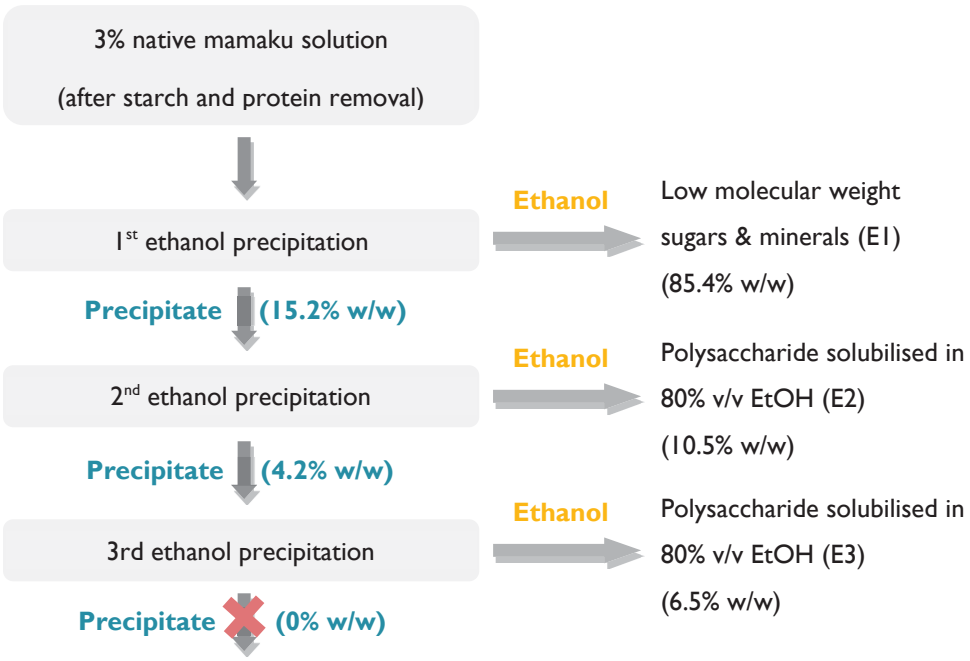

Figure 6.7 – Extraction scheme for multiple ethanol precipitation of native mamaku polysaccharide solution

The appearance of the residue obtained after the first and second ethanol precipitation steps is shown on Figure 6.8. On the first ethanol precipitation (80% w/v), long thread-like strands of yellowish-white fibrous precipitate with a substantial yield was obtained and spooled onto a glass rod. The solvent was yellowish-brown in colour, indicating that there could be some losses of materials from the extract. The solvent mixture was retained and recovered for any polysaccharide material by evaporating off the solvent. The precipitate was separated from the solvent and re-solubilised in water to make up 5% w/w solution based on wet weight of the precipitate. This solution was then subjected to a second ethanol precipitation (80% w/v). On the second ethanol precipitation, short strands of brown precipitate were obtained which could not be coiled around the glass rod. The amount of solid material recovered was also considerably less than during the first ethanol precipitation. Again, the solvent was retained and recovered for any polysaccharide material. The procedure was repeated for a third ethanol precipitation. However, no insoluble material was obtained on the third precipitation.

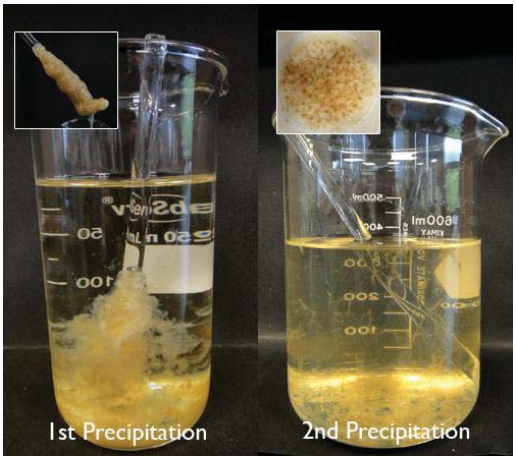

Figure 6.8 – Appearance of polysaccharide residue after first and second ethanol precipitations

The low yield of precipitate obtained on second precipitation was likely to be due to low salt concentration remaining in the material as most minerals would have been removed during the first ethanol precipitation. Solubility of neutral polysaccharides in ethanol is independent of salt concentration. However, solubility of acidic polysaccharides such as the mamaku polysaccharide (~70% uronic acid) is sensitive to the presence of ions (Smidsrod & Haug, 1967). Preliminary testing showed that adding 0.05M NaCl to the rehydrated precipitate allowed formation of the thread-like fibrous precipitate on second ethanol precipitation. The presence of salt resulted in an increased activity coefficient between the cations and the polymer, which reduced the effective charge of the polymer (Smidsrod & Haug, 1967). Likewise, when the mamaku solution is dialysed prior to ethanol precipitation, little or no precipitate was obtained. Therefore dialysis of the material should be carried out after rehydration of the precipitate before freeze-drying to remove the remaining tightly-bound cations not removable by ethanol precipitation.

The concentration of the polysaccharide solution before ethanol precipitation was also critical in determining its solubility in ethanol. Dilute polysaccharide solutions have been found to precipitate poorly (Steve & Yolanda, 2006). The residue redissolved in 60g of water was relatively dilute, with a concentration likely to be below the coil overlap concentration. At low concentrations, the polymer-polymer interaction was weak and did not result in the formation of precipitates. Polymer-solvent interactions were therefore able to overcome the polymer-polymer interactions, causing the polysaccharide to dissolve instead (Whistler, 1973). However, the polysaccharide was unable to precipitate properly when the polysaccharide solution was too concentrated (≥5% w/w). The high viscosity acts as a physical barrier to the ethanol solvent. Hence, the polymer-water interactions within the mamaku samples were not affected.

The ethanol used to precipitate the polysaccharide was retained and freeze-dried to determine the amount of solid material lost during the extraction (expressed as yield of original amount of extract). The first ethanol precipitation removed mainly sugars and minerals as yellow sugar crystals remaining after freeze-drying. Although no polysaccharide was visibly present in this fraction (E1, Figure 6.7), uronic acid (~8% w/w) was detected which could be part of the polysaccharide or existing as free acidic sugars.

On the second ethanol precipitation, the yield of alcohol-insoluble fraction (EtOH x 2) greatly decreased to 4.2% w/w and it did not exhibit shear-thickening. Instead, it was shear-thinning with a high low-shear viscosity *i.e.* ~100Pa.s at $0.1s^{-1}$ (Figure 6.9). On the other hand, the soluble fraction (E2) (recovered from ethanol after second precipitation) was shear-thickening. It is possible that alcohol-insoluble residues obtained from the second precipitation are the larger polysaccharide aggregates, or there exists shear-thinning and shear-thickening fractions within the polysaccharide which could be separately extracted based on their different solubility properties.

Overall, a single ethanol (80% w/v) precipitation would be recommended as part of the final purification procedure. The yield obtained with a single precipitation (15.2% w/w) was reasonably close to the NSP content of the native freeze dried extract *i.e.* ~10% w/w (Goh, et al., 2007). Precipitating the polysaccharide twice resulted in separation of two fractions of either different polarities or solubility, and a low yield for the alcohol-insoluble fraction (4.2% w/w). Further studies on identification of these two fractions and improving the yield would need to be carried out if two-times ethanol precipitation were to be used. For example, the ionic strength of the solution prior to the second ethanol precipitation could be adjusted to obtain maximum yield.

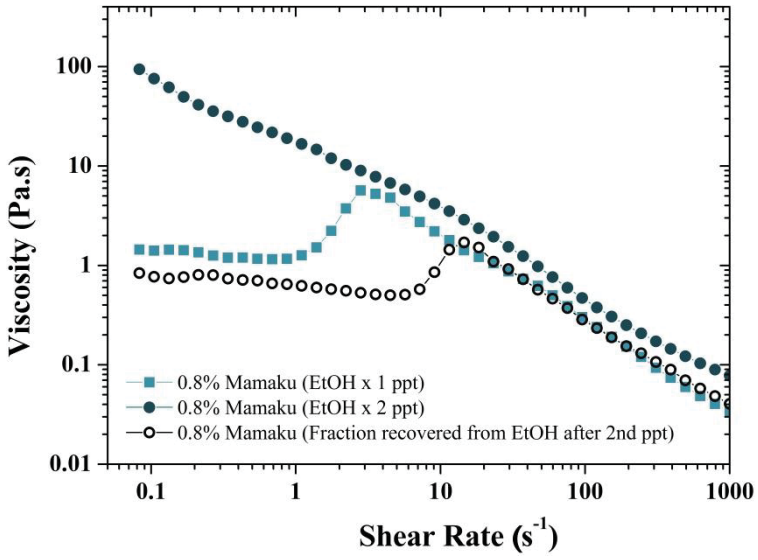

Figure 6.9 – Viscosity curves of purified mamaku solutions (0.8% w/w) with one (EtOH x 1, ■) or two (EtOH x 2, ●) ethanol precipitations, and the alcohol-soluble fraction after two precipitations (E2, ○)

The purification procedure used for subsequent composition, molecular weight, rheological and structural characterisation in this chapter was finalised as: i) ultracentrifugation of native mamaku solution at 250,000*g* for 1 hour at 20°C, ii) starch hydrolysis with α-amylase (100°C for 6 minutes) and amyloglucosidase (50°C for 30 minutes), iii) deproteinisation with Sevag's reagent (1-butanol:chloroform = 1:4 v/v) at 20°C, and iv) single precipitation with 80% v/v ethanol.

6.3.2 Composition Analysis

Table 6.2 – Comparison of chemical composition of native and purified mamaku fractions

	Native	Purified
Appearance		
Moisture (% w/w)	8.3 ± 0.03	3.0 ± 0.6
Total Carbohydrate (% w/w)	55.6	78.9
NSP (% w/w)	12.3	69.8
Uronic Acid (% w/w)	7.2	48.1
Protein (% w/w)	2.5	5.7
Ash (% w/w)	20.7 ± 0.5	12.4 ± 0.9
Starch (% w/w)	12.9	Not detected

Table 6.2 summarises the chemical composition of the mamaku polysaccharide before (native) and after purification with ultracentrifugation, starch hydrolysis, de-proteinisation and ethanol precipitation. The amount of non-starch polysaccharide present in the freeze-dried material increased from approximately 10 to 80% w/w. Protein and ash contents appeared to have increased due to the loss of material *i.e.* sugars and minerals. Based on % w/w NSP, protein content have decreased from 20.3 (2.5/12.3*100%) to 8.2% (5.7/69.8*100%) w/w, while ash content has decreased from 105 to 12.4% w/w. Starch was also completely removed after starch hydrolysis as starch was not detected in the purified polysaccharide. Therefore the purification procedure could be considered effective in removing moisture, starch and ash while retaining a high polysaccharide yield.

6.3.3 Size-Exclusion Chromatography-Multi-Angle Laser Light Scattering (SEC-MALLS) of Purified Mamaku Polysaccharide

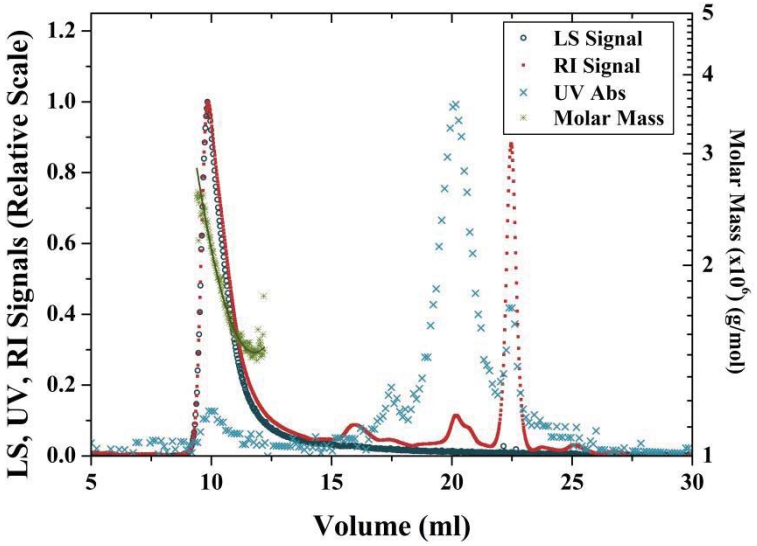

Figure 6.10 - Molecular weight analysis by size-exclusion coupled with multi-angle laser light scattering (SEC-MALLS) of purified mamaku polysaccharide

Figure 6.10 shows the chromatogram of the mamaku polysaccharide purified using the steps as described in the previous section. The chromatogram shows a single large light scattering (LS; 90°) peak overlapped with an RI signal peak detected at elution volume range of ~9-12 ml. The low UV absorbance in this peak suggested that this material is mostly polysaccharide. The weight-average molecular weight (M_w) of the purified mamaku polysaccharide was determined to be 1.944 x 10^6 Da with a low polydispersity index (M_w/M_n) of 1.034 and a Z-average RMS radius $(r_g^2)_z^{1/2}$ of 94 nm based on the Zimm model. This molecular weight is smaller than that determined previously (3.2 x 10^6 Da, polydispersity index of 1.08 and $(r_g^2)_z^{1/2}$ of 144 nm) for the native mucilage (Goh, et al., 2011). The higher molecular weight value and Z-average RMS radius could be due to the presence of aggregates in the native mucilage. These contaminants were markedly reduced in the purified samples.

6.3.4 Rheological Properties of Purified Mamaku Polysaccharide

The viscosity of the purified mamaku polysaccharide was tested at various concentrations from 0.2-1.4% w/w (Figure 6.11a). Shear-thickening occurred at a concentration above 0.3% w/w and was accompanied by a large increase in viscosity. This large increase in viscosity was most likely due to coil-overlap, where each polysaccharide molecule now interacts in close proximity within its hydrodynamic radius (Morris, et al., 1981). The onset of shear-thickening (generally at shear rates of ~$10s^{-1}$) was shifted to lower shear rates as the concentration increased. The same phenomenon was observed for the native solution, where shear thickening was seen only at concentrations above 4% w/w (Goh, et al., 2007). The viscosity of a 5% w/w native solution (dashed lines on Figure 6.11b) corresponds approximately to a 0.5% w/w purified solution and is consistent with the native mucilage containing about ~10% w/w non-starch polysaccharides. The data suggested strongly that the polysaccharide purified in the present study, is responsible for the shear-thickening behaviour of the

native mucilage. Figure 6.11b shows the zero-shear viscosities of the purified material in the dilute and semi-dilute regions. A power law equation ($y=a \cdot x^b$) was fitted to the data for each concentration regime. The exponent of concentration dependence (*b*) in the dilute and semi-dilute region is 1.6 and 3.1 respectively, similar to most other random coil polysaccharides (dilute: $C^{1.4}$; semi-dilute: $C^{3.3}$) (Morris, et al., 1981). The coil overlap concentration (the intersection between the two fit lines) was estimated as 0.35% w/w, which is in close approximation with the onset concentration for shear-thickening as inferred from the viscosity curves (Figure 6.11b).

Note: The rheological properties of the purified polysaccharide were found to be unstable with storage, with loss of shear-thickening after approximately 1.5 years. This will require further investigation which is beyond the scope of the thesis.

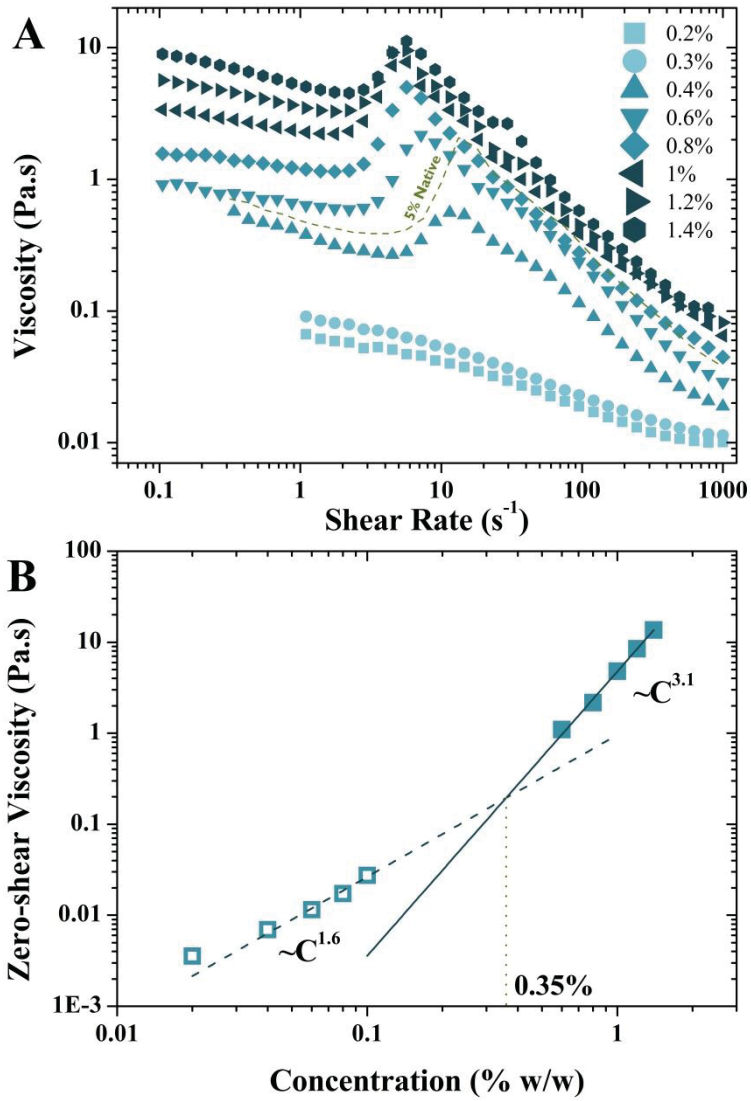

Figure 6.11 – a) Viscosity curves of purified mamaku at concentrations of 0.2-1.4% w/w; dashed lines represent viscosity of a 5% w/w native mamaku solution before purification; b) Concentration dependence of zero-shear viscosity; Unfilled symbols (□) represent viscosities measured using an Ubbelohde dilution capillary viscometer; filled symbols (■) are zero-shear viscosities in the dilute regime estimated by fitting the Cross equation to the complex viscosity curves

6.3.5 Structural Analysis

6.3.5.1 Constituent Sugar Composition

The basic structure of the purified polysaccharide was next determined by analysing its constituent sugars (monosaccharides) and the linkage type of these individual units. Detailed sequencing analysis will not be covered in the scope of this thesis.

The constituent sugar composition was determined by the three complementary methods *i.e.* i) hydrolysis by methanolic HCl/TFA and analysed by HPAEC-PAD, ii) hydrolysis by methanolic HCl/TFA and analysed by GC-MS and iii) hydrolysis by TFA and analysed by GC-MS. HPAEC-PAD is a technique used for analysing carbohydrate compositions with several advantages over the traditional GC-MS method: i) uronic acids could be determined along with neutral sugars, ii) reduction and acetylation steps not required as the sugars do not have to be in a volatile form for GC-MS and iii) better precision and efficiency (Cataldi, Campa, & De Benedetto, 2000; Davis, 1998). The results obtained from these three methods are in fairly good agreement (Table 6.3).

Table 6.3 – Constituent sugar composition of purified mamaku polysaccharide determined using HPAEC and GC-MS

Sugar	Weight % w/w[a]		
	Me-HCl/TFA		TFA
	HPAEC	GC-MS	GC-MS
Rhamnose	1.2	0.5	0.8
Fucose	0.8	0.3	0.4
Arabinose	1.8	0.8	0.9
Xylose	5.1	3.0	3.8
Mannose	12.5	12.5	6.4
Galactose	15.4	15.7	13.0
Glucose	0.1	3.8	5.1
Glucuronic acid	50.0	n.d[b]	n.d[b]
Galacturonic acid	1.8	n.d[b]	n.d[b]
Total neutral sugar	37.1	36.6	30.4
Uronic acid	51.8	53.0[c]	53.0[c]
Total sugar	88.9	89.6	83.4

a Values are the averages of duplicate analyses.
b n.d.: not determined.
c Determined colorimetrically.

In the first method, the total sugar content determined by HPAEC-PAD was 88.9% w/w, with 37.1% w/w neutral sugars composing of mostly glucuronic acid, galactose, mannose and xylose, with small amounts of other sugars (Table 6.3). In the second and third methods, analyses of monosaccharides by GC-MS, following hydrolysis of the purified mamaku sample with methanolic HCl/TFA, or TFA alone, gave neutral sugar contents

of 36.6% and 30.4%, respectively. Both analyses showed mainly galactose, mannose, glucose and xylose, although hydrolysis with TFA alone gave lower amounts of mannose and galactose than with methanolic HCl/TFA (Table 6.3). The lower yield of these sugars could be due to their linkage to uronic acids and thus remained more resistant to acid hydrolysis (Melton & Smith, 2001). The higher glucose contents observed when hydrolysates were analysed by GC-MS were probably due to the formation of glucuronolactone, which was then reduced to glucose (Wagner et al., 2008). In terms of the uronic acid content, the colorimetric (*m*-hydroxydiphenyl) analysis gave 53% w/w which is in good agreement with that determined by HPAEC (51.8%). The total sugar content, including the uronic acid determined colorimetrically, was 89.6% (methanolic HCl and TFA) and 83.4% (TFA only).

6.3.5.2 Glycosyl Linkage Analysis

After identifying the major sugar constituents in the polysaccharide, the carbon positions at which these sugars are linked at *i.e.* glycosyl linkage were analysed. Uronic acid residues were carboxyl-reduced using $NaBD_4$ and $NaBH_4$ to their respective 6,6'-dideuterio labelled neutral sugars prior to linkage analysis (Table 6.4). Carboxyl reduction is necessary to convert the carboxylic groups to their respective alcohol groups such that these groups could be hydrolysed. By using both $NaBD_4$ and $NaBH_4$ reducing agents, the extent of esterification in the uronic acid groups could be determined (Figure 6.2). The analysis of the purified mamaku polysaccharide using GC-MS showed high proportions of 4-linked methylesterified glucopyranosyl uronic acid (4-Glc*p*A), 2,3- and 2,3,4-linked mannopyranosyl (2,3- and 2,3,4-Man*p*) residues, consistent with the presence of a glucuronomannan comprising of a backbone of 4-Glc*p*A and 2-Man*p*, branched at O-3 of 45% and at both O-3 and O-4 of 53% of the Man*p* residues (Redgwell, O'Neill, Selvendran, & Parsley, 1986a, 1986b). The other major linkages detected were terminal xylopyranosyl (T-Xyl*p*), terminal galactopyranosyl (T-Gal*p*) and non-esterified 3-Glc*p*A residues. Other linkages observed (3-, 6- and 3,6-Gal*p*) were typical of type II arabinogalactans that are typically terminated variously by rhamnopyranosyl (Rha*p*), arabinofuranosyl (Ara*f*), arabinopyranosyl (Ara*p*) and Gal*p* residues (Sims & Furneaux, 2003).

The ^{13}C NMR spectrum of the purified mamaku polysaccharide showed C-1 signals from 98.9–104.0 ppm, together with a weak C-1 signal at 109.8 ppm (Figure 6.12a) and ^{1}H NMR showed H-1 signals from 4.47–5.37 ppm (Figure 6.12b). The DEPT-135 experiment showed three methylene ($-CH_2$) signals at 60.3, 62.1 and 65.9 ppm, with H-1 cross-peaks in the HSQC spectrum at 3.94/3.83, 3.77/3.64 and 4.00/3.33 ppm, respectively. The spectra were assigned on the basis of HSQC, COSY and DEPT-135 experiments and by comparison with published spectra of similar polysaccharide molecules e.g. glucuronomannans (Honda, Inaoka, Takei, Sugimura, & Otsuji, 1996; Wagner et al., 2007; Wagner, et al., 2008; Wagner et al., 2004). From both ^{13}C NMR and ^{1}H NMR spectra, signals at C-1/H-1 98.9–99.5/5.37 were assigned to α-D-Man*p* residues. C-3/H-3 signal at 83.4/3.75 was consistent with O-3 substitution of these residues as observed in the glycosyl linkage analysis (Table 6.4). Similarly, signals at C-1/H-1 102.5–102.8/4.54–4.59 were assigned to β-D-Glc*p*A residues. The presence of a carbonyl signal in the ^{13}C NMR spectrum at 171.0 ppm and absence of a signal at 175 ppm (data not shown), together with an intense *O*-methyl signal (^{13}C 54.2 ppm, ^{1}H 3.88 ppm) indicated that the Glc*p*A residues were completely esterified, agreeing with glycosyl linkage analysis which showed that nearly all of the 4-Glc*p*A residues were methylesterified. Signals at C-1/H-1 103.9/4.70 were assigned to β-D-Gal*p* residues

and the weak C-1 signal (109.8 ppm) in the ^{13}C NMR spectrum was assigned to an α-L-Ara*f* residue (Sims & Furneaux, 2003). Other anomeric signals were not assigned, but probably represent other residues (e.g. Xyl*p* and 3-Glc*p*A) observed in the glycosyl linkage analysis (Table 6.4). The methylene signal at 65.9 ppm with H-1 cross peaks at 4.00/3.33 ppm (see Figure 6.12b) was assigned to T-Xylp, which was the major xylose linkage observed (Sims & Newman, 2006). Similarly, the methylene signals at 60.3 ppm (H-1 3.94/3.83 ppm) and 62.1 (H-1 3.77/3.64) were assigned to α-D-Man*p* and β-D-Gal*p* residues, respectively. The presence of small proportions of Rha*p* and fucopyranosyl (Fuc*p*) residues observed in the linkage analysis was supported by the presence of two *C*-methyl signals (^{13}C 17.3 and 16.1 ppm, ^{1}H 1.30 and 1.26 ppm).

Based on these evidences, it is likely that the polysaccharide is a glucuronomannan since glucuronic acid and mannose were present in the largest quantities. Other sugars such as galactose and xylose were primarily terminal groups which would not be able to form the backbone.

Table 6.4 – Glycosyl linkage composition of carboxyl-reduced mamaku polysaccharide

Sugar	Deduced linkage[a]	Relative amount (mol %)[b]
Rha*p*	terminal	2.9
Fuc*p*	terminal	0.8
	2-	0.7
Ara*p*	terminal	2.3
	2-	1.0
Ara*f*	Terminal	1.0
Xyl*p*	terminal	8.9
	2-	1.8
	4-	2.8
Gal*p*	Terminal	14.8
	3-	0.6
	6-	0.9
	3,6-	1.0
Glcp	4-	1.1
Man*p*	2,3-	9.2
	2,3,4-	10.9
Glc*p*A	terminal	2.3
	3-	5.9
	4-	27.9 (100)
Other[c]		3.2

a Terminal Rhap deduced from 1,5-di-O-acetyl-6-deoxy-2,3,4-tetra-O-methylrhamnitol, etc.

b Values are the averages of duplicate determinations (value in parentheses is the degree of methylesterification).

c Comprises linkages present ⩽0.5 mol%

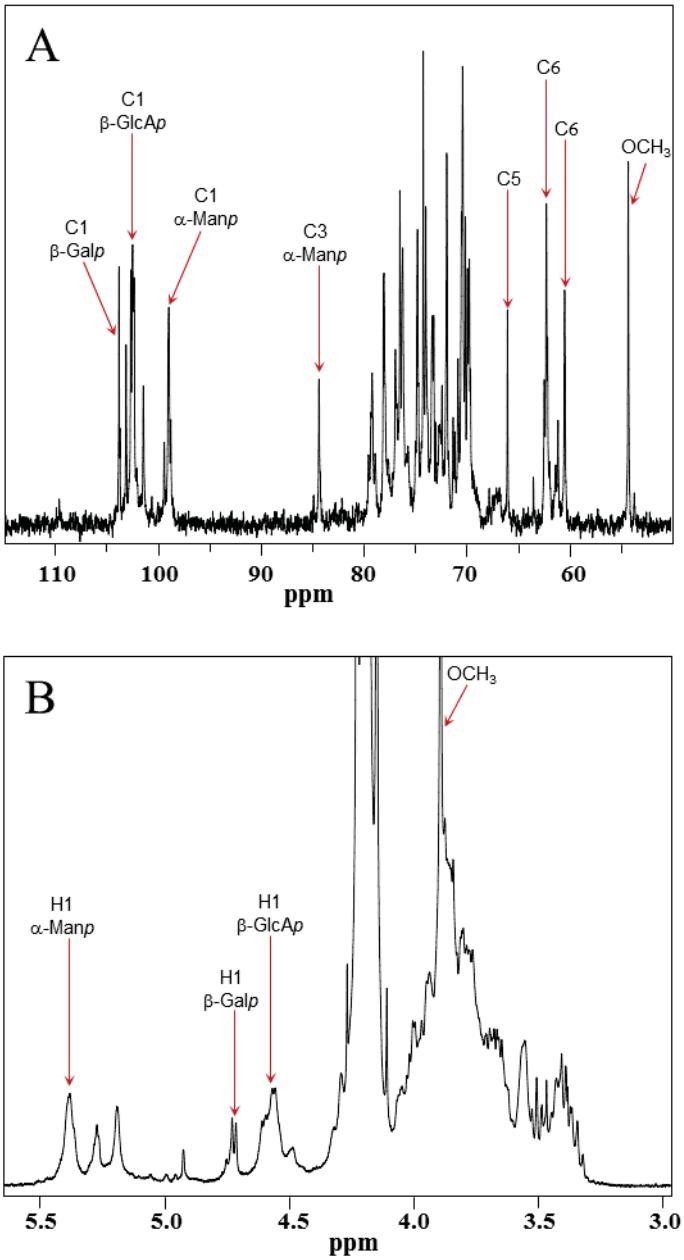

Figure 6.12 – Selected regions of the a) ^{13}C-NMR and b) ^{1}H-NMR spectra of purified mamaku polysaccharide

Glucuronomannans, comprising of a repeating backbone of -4)-β-D-Glc*p*A-(1 →2)-α-D-Man*p*-(1→- are commonly found as gum and mucilage polysaccharides. For example, glucuronomannans are components of a number of exudate gums, including gum Ghatti (G. O. Aspinall, Hirst, & Wickstrøm, 1955) and *Anogeissus leiocarpus* gum (G. O. Aspinall, Carlyle, McNab, & Rudowski, 1969), as well as gum exudates from the *Hakea* species (Eagles, Stephen, & Churms, 1993) and from *Vochysia spp*. trees (Wagner, et al., 2007; Wagner, et al., 2008; Wagner, et al., 2004). They have also been extracted from the stem pith of *Actinidia deliciosa* (kiwifruit) (Redgwell, 1983; Redgwell, et al., 1986a, 1986b), fronds of *Asplenium australasicum* fern (Lai & Liang, 2012), the mucin of *Drosera binata* (Gowda, Reuter, & Schauer, 1982) and the fruit of *Auricularia auricala* (Li et al., 2012). These polysaccharides usually have heterogeneous side-chains comprising variously of Ara*f*, Ara*p*, Gal*p*, Fuc*p* and Xyl*p* residues attached to O-3 of the backbone residues. Thus, it is probable that the purified mamaku

polysaccharide comprises a similar repeating backbone structure, but differs from most of the reported structures in that all of the Man*p* residues bear one or two side chains, and no side chain is attached to Glc*p*A residues (Figure 6.13).

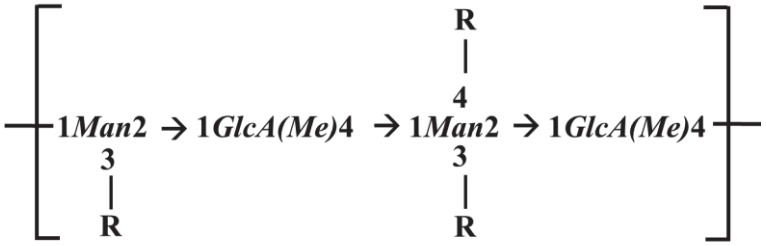

Figure 6.13 – Possible structure of mamaku polysaccharide; R = T-Xyl*p*, T-Gal*p* or T-Glc*p*A and other more complex oligosaccharides containing sugars with linkages shown in Table 6.4

The functionality of glucuronomannans in gums and mucilages may have an important role in the plants. The presence of uronic acids which forms part of the backbone of glucuronomannans could improve the solubility of the polysaccharide molecules and increase their water holding capacity due to stronger hydrogen bonds formed between the polar carboxyl groups and water (Whistler, 1973). This enables the polysaccharide to hydrate rapidly and form a protective layer on the plant when external injuries to the plant are inflicted. Besides, the mucilage may also function to store reserves of water during droughts (Clarke, Anderson, & Stone, 1979). The slimy consistency of mucilages may also act as lubrication within the plant during water transport (Zimmermann et al., 1994). However, many of the glucuronomannans found in literature have not been characterised for their rheological properties. The mucilage from *Drosera binata* (a carnivorous plant) which contains a glucuronomannan with a relatively simple structure (linear glucuronomannan backbone with small side chain residues of D-Gal*p* and D-Xyl*p*) displays complex flow mechanisms (e.g. extensional viscoelasticity, capillary thinning) in order to trap its prey (Erni, Varagnat, & McKinley, 2008; Gowda, et al., 1982). The methylesterified uronic acid groups could also serve to prevent premature cross-linking or interaction with cations until required e.g. when wounded (J. B. Kim & Carpita, 1992).

Rheological properties of polymers are largely dependent on the intra- or intermolecular interactions between chains (polymer-polymer) and solvent (polymer-water). Based on the results from Chapter 5, hydrogen bond was found to be the main intermolecular interaction responsible for shear-thickening. The carbonyl groups (-C=O) of the methylesterified and non-methylesterified Glc*p*A residues, carboxylic acid groups (-COOH) of the charged Glc*p*A, as well as the hydroxyl groups of the sugars along the backbone chain could participate in hydrogen bonding to other glucuronic acid residues, sugars or even water molecules. The resultant rheological behaviour of the purified mamaku polysaccharide would be a balance of these intra and inter molecular chain-chain and chain-solvent interactions.

6.4 Conclusion

The native mamaku extract was purified using ultracentrifugation, starch hydrolysis, de-proteinisation using Sevag's reagent and single precipitation with 80% w/v ethanol. The total non-starch polysaccharide content of the material improved from approximately 10 to 77%, with free sugars, moisture, minerals, starch and protein removed. The purified polysaccharide retained its shear-thickening property and molecular weight was not significantly affected. Structural characterisation of the purified mamaku polysaccharide molecule indicated that it is possibly a glucuronomannan backbone (methylesterified 4-Glc*p*A with 2,3- and 2,3,4-linked Man*p*) with branched sugar side-chains of galactose, arabinose, xylose, non-methylesterified glucuronic acid and other simple sugars at the O-3 and O-4 of the mannose residues. Hydrogen bond interactions may take place between the carbonyl groups (-C=O) of the methylesterified and non-methylesterified uronic acids, carboxyl groups (-COOH) of the uronic acids, as well as the hydroxyl groups of mannose (and other neutral sugars) under shear, resulting in shear-thickening.

Chapter 7 Pilot Study on Satiety Effects of Mamaku Gum in Rats

7.1 Introduction

For any polysaccharide, the ultimate aim of characterisation is to find a suitable application based on its functional properties identified. The signature feature of the mamaku gum is its shear-thickening behaviour (Chapter 4), which in addition could be manipulated to our advantage by modifying the temperature, ionic strength etc. (Chapter 5). Potentially, the mamaku gum could be used as a (food) thickener, demulcent, dysphagia aid or satiety aid.

In a recent study, the effects of mamaku and guar gums on the antral and fundic activities in the rat stomach maintained *ex vivo* were compared (Lentle, et al., 2010). The mamaku gum was reported to increase the frequency and velocity of antrocorporal contractions, and to cause variation in direction of propagation. It was likely that the shear-thickening and highly viscoelastic properties of the mamaku gum caused unusual patterns of wall tension during peristaltic compression that is not observed with guar gum and other digesta. Hence gastric emptying could be prolonged by consequent modification of the mechanics of antral contractions using mamaku gum, with subsequent gastric distension inducing satiety.

In this chapter, the study by Lentle et. al. (2010) was taken a stage further, where the mamaku gum was orally gavaged in rats to test the effects of weight loss and anorexia *in vivo*. This chapter bridges between the research (Chapters 4-6) and application domains of the mamaku polysaccharide, and provides the platform for further or larger scale studies on rats or humans. The use of mamaku to induce satiety in this study would be appropriate in face of the obesity epidemic.

The objectives of this work were to gavage the rats with mamaku gum (distilled water for control group), and use indicators such as food consumption after gavaging, weight changes, and weight of stomach contents remaining post-mortem to assess potential satiety effects. The hypothesis was that the rheological properties of the mamaku gum would delay gastric emptying, cause a reduction in food consumption, and therefore an overall weight loss. Toxicity of the mamaku gum will also be evaluated using kidney and blood samples for supporting claims of 'Generally Recognised as Safe' (GRAS) based on traditional use by the Māori people.

7.2 Materials and Methods

7.2.1 Animal Ethics

The experimental protocol was approved by the Massey University Animal Ethics Committee (Palmerston North, New Zealand; Protocol No.: 14/21). A copy of the application is listed in Appendix D.

7.2.2 Preparation of Mamaku Solution

The freeze-dried mamaku gum extract was hydrated overnight in potable distilled water to a concentration of 15.0% w/w. The solution was sterilised by heating at 100°C for approximately 3 minutes, and allowed to cool to room temperature (~20°C) prior to feeding.

7.2.3 Animals and Experimental Design

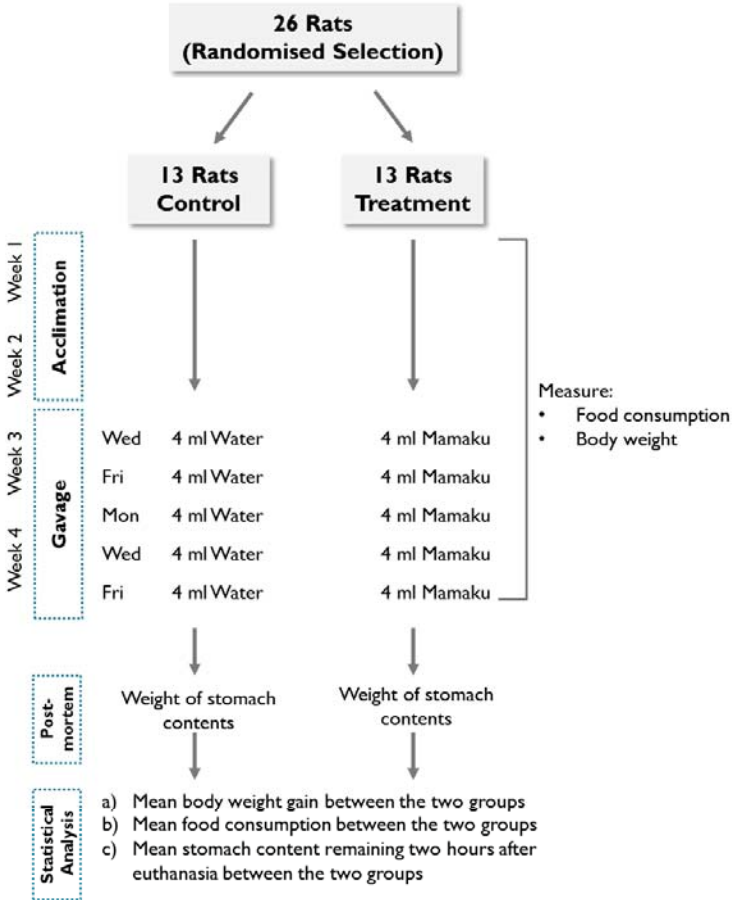

Figure 7.1 – Summary of experimental design in a flow diagram

Figure 7.1 illustrates and summarises the experimental design in a flow diagram. Twenty-six male Sprague Dawley rats (born 26-28 April 2014) were reared in the Small Animal Production Unit in Palmerston North, New Zealand. They were housed individually in wire-bottom cages in a room with a temperature of 22 ± 1°C and exposed to a 17/7 hour light-dark cycle (lights off at 1200-1900). The rats were acclimated for a period of 14 days starting from 26 May 2014 (at 4 weeks old; 100±10% g) prior to gavaging. At the end of acclimation,

thirteen rats were randomly selected (using a random number generator with Microsoft Excel) for the control group and thirteen rats for the treatment group. The rats were approximately 200g at the start of the gavaging period.

The rats in the control group were gavaged with 4ml of distilled water for the control group, and those in the treatment group were gavaged with 4ml of 15.0% w/w mamaku solution using a straight stainless steel gavage needle (size 18ga x 76mm; Instech Solomon) attached to a 5 ml syringe. Gavaging was carried out a total of 5 times for a period of two weeks on alternate weekdays (Wed, Fri, Mon, Wed and Fri). The order of each gavage was randomised to prevent any order effects. Droplet feeding was not feasible as the material is shear-thickening and could potentially result in choking of the rats. The use of a flexible cannula was attempted however it could not be executed as it could not be pushed down from the oesophagus to the stomach easily. All gavaging was performed by a skilled technician who specialised in the procedure.

Standard rat chow pellets were fed to the rats and removed from the cages at 1900 every evening, so that the rats fasted for 13 hours prior to gavage the next morning. This procedure was carried out daily throughout the experiment starting in the acclimation period so that effects of fasting on weight loss were accounted for. The rats had ad libitum access to food and water for the remaining 11 non-fasting hours. The rats' body weight and their food remaining in the hopper plus ullages were weighed at the same time every day. To account for food spillage during consumption, the ullages were collected and weighed. Moisture absorption by the rat chow was determined by weighing the difference in weight of a 200g sample at the start and at the end of the experimental period, and was found to be negligible.

The rats were euthanased two hours after the final (5^{th}) gavage by intraperitoneal phenobarbitone. Blood samples were collected from each rat via cardiac puncture. The stomachs were then excised at the division between the oesophagus and diaphragm from one end, and at the pyloric sphincter on the other end and weighed. The stomach was then cut lengthwise and weighed again after scraping and removing the contents from the stomach wall. The amount of material remaining in the stomach two hours post-gavaging was determined as the weight difference i.e.: Stomach content (g) = Weight of stomach with contents (g) – weight of stomach with contents removed (g). The kidneys and liver were removed and stored in 4% formol saline solution for histological studies to detect any cell necrosis or other pathology.

7.2.4 Statistical Analysis

Statistical programs Minitab® and Systat® were used for one-way analysis of variance (ANOVA) and repeated measures ANOVA on 1) the weight gained by the rats (g) in the control and treatment groups, 2) food consumed by the rats in the control and treatment groups and 3) weight of stomach content remaining after euthanasia of the control and treatment groups. The Kolmogrov-Smirnov (modified Lilliefors) test was performed on the data prior to ANOVA analysis to ensure the assumptions of ANOVA tests were met (*i.e.* data is normally distributed and there is equality of variance).

7.2.5 Pathology

The kidney and the liver were removed at autopsy and preserved in 4% v/v formol saline solution. Blood samples were collected via cardiac puncture and stored in serum (red) and plasma (lavender; treated with EDTA anticoagulant) vacutainers for analysis. The blood samples were allowed to clot at 4°C for two hours prior to centrifugation at 3000 rpm for 10 minutes. The supernatants of the serum and plasma tubes were transferred into 0.5ml aliquots in Eppendorf tubes and stored at -80°C prior to analysis. The blood serum, kidney and liver tissues were analysed by an accredited laboratory (New Zealand Veterinary Pathology, Massey University) for toxicity.

7.2.6 Rheological Measurements

Rheological measurements were made as described in Chapter 4 using a cone-and-plate geometry with a controlled shear rate rheometer (Paar Physica, Anton Paar, Germany) at 37°C.

7.2.7 Bomb Calorimetry

Gross energy content of the hydrated mamaku gum solution (3% w/w) was measured by bomb calorimetry analysis by an accredited laboratory (Nutrition Laboratory, Institute of Food Nutrition and Human Health, Massey University) and determined as gross energy (J/g). The gross energy content of 15% w/w solution was extrapolated from this measurement.

7.3 Results

7.3.1 Gastric Emptying

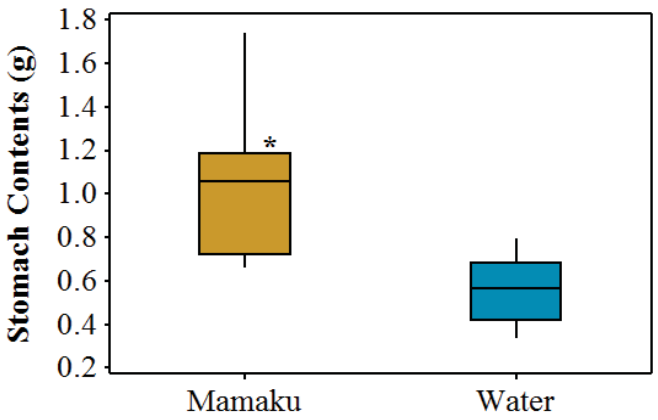

Figure 7.2 – Boxplot of stomach contents two hours after gavaging with 4ml mamaku or water; a significant difference (*) was found in the weight of contents remaining in the stomach of rats gavaged with mamaku compared with those gavaged with water; horizontal line represents the median and the box represents the interquartile ranges

The weight of the stomach contents remaining two hours after gavaging with either 4ml mamaku or 4ml distilled water were compared (Figure 7.2). The weights of the stomach contents of the rats gavaged with the mamaku gum were significantly greater than those gavaged with water (*df*, 1, 22; F = 21.6; $p<0.005$). Figure 7.3 shows the mamaku gum removed from the stomach, which appear to have been somewhat diluted by gastric juices and/or the euthanizing drug. The observations confirm that the mamaku gum persists in the stomach to delay gastric emptying up to two hours post-gavage.

Figure 7.3 – Mamaku gum removed from the stomach two hours post-gavage

7.3.2 Food Consumption

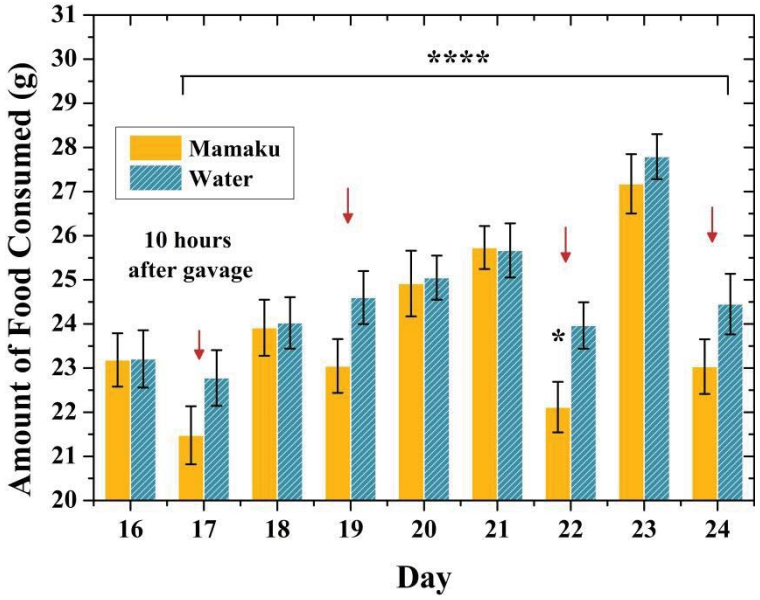

Figure 7.4 – Mean quantity of food consumed by each treatment group from day 16 to day 24; red arrows indicate days which the rats have been gavaged; significant difference (*) between groups gavaged with mamaku and water on day 22 (3rd gavage) and for all gavaging days (****) based on repeated measures ANOVA; bars represent standard error (SE) of the mean

Figure 7.4 shows the average amounts of food consumed by the two groups during the gavaging period from day 16 to day 24. In general, the rats ate less on the same day that they were gavaged (days 17, 19, 22, 24) and food consumption significantly increased the following day. The rats gavaged with mamaku ate less than the rats gavaged with distilled water on the gavaging days (indicated by red arrows). A one-way ANOVA test showed a significant overall difference on day 22 between the two groups (*df* 1, 23; F=5.6; $p<0.05$). A repeated-measures ANOVA was also tested using all gavaging days, and there was a significant difference (*df* 1, 13; F=4.5; $p<0.05$) between the two treatments. Therefore rats gavaged with mamaku consumed significantly less food than rats gavaged with distilled water on the day that they were gavaged.

7.3.3 Body Weight

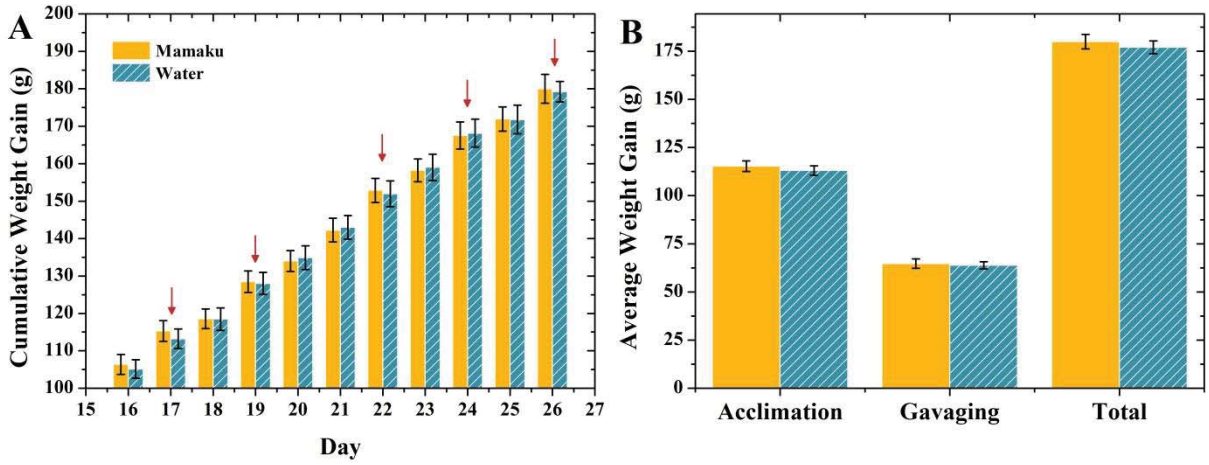

Figure 7.5 – a) Cumulative average weight gain of mamaku and water group during gavaging week (day 17-26); error bars represent SE of the mean; red arrows indicate days which the rats have been gavaged; b) Average weight gain of mamaku and water group during acclimation (day 1-16), gavaging (day 17-25), and for the entire experiment (day 1-25)

Figure 7.5a shows the cumulative mean (±SE) weight gained by the rats during the gavaging period, and Figure 7.5b shows the mean total weight (±SE) gained by the rats in the mamaku and water group during the acclimation, gavaging, and the entire experimental period. There were no significant differences between the two groups from days 17 to 26 based on repeated measures ANOVA. There were also no significant differences between the average total weight gained by the two groups during acclimation, during the gavaging weeks or for the entire experimental period. The mean weight gain dropped by approximately 45% during the gavaging period for both groups, thus showing that the act of gavaging itself had an impact on the rat weights. Gavaging is a stressful event for the rats which was likely to have contributed to the rats gaining less weight (Turner, et al., 2012).

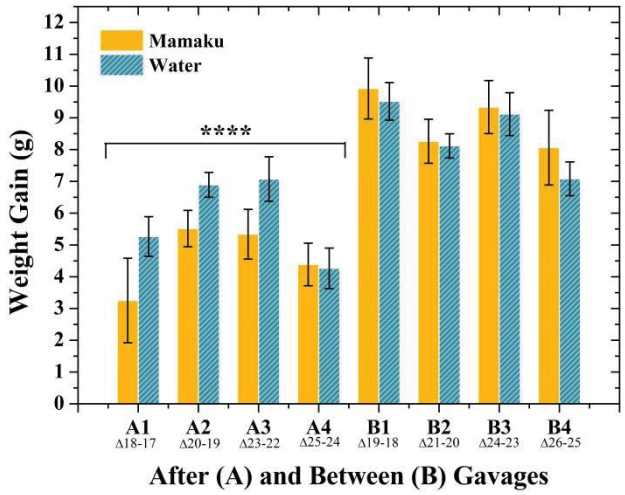

Figure 7.6 – Average weight gain after gavage (total weight change 24 hours after gavage e.g. weight difference between days 17 and 18) and between gavage (total weight change in 24 hours without gavage e.g. weight difference between days 18 and 19) gavages for mamaku and water group; significant difference (****) between groups gavaged with mamaku and water 24 hours after gavage based on repeated measures ANOVA error bars represent SE of the mean

Figure 7.6 compares the mean weight gain in the rats gavaged with mamaku or water 24 hours after being gavaged, and the subsequent 24 hours when the rats have not been gavaged. In other words, it shows the short-term loss in weight gain by the rats after gavaging, and if the effects persist over a total of 48 hours. On days 17, 19, 22, and 24 the rats were weighed and then gavaged. Therefore the weights gained *after* the first, second, third and fourth gavages are the weight differences between days 18 & 17, 20 & 19, 23 & 22 and 25 & 24, labelled A1, A2, A3 and A4 respectively. To see if the weights gained in 24 hours remained consistent, the weight difference in the subsequent 24 hours were compared, *i.e. between* gavages, or the weight differences between days 19 & 18, 21 & 20, 24 & 23 and 26 & 25, labelled B1, B2, B3 and B4 respectively.

The rats gavaged with mamaku gained significantly less weight on ANOVA on the day of the gavage (*df* 1, 22; F=5.22; $p<0.05$) than the rats gavaged with water. On the following day, the weights were not significantly different (Figure 7.6). This was consistent with their food consumption patterns, whereby the rats gavaged with mamaku ate less after gavaging and therefore gained less weight than the rats gavaged with water. Subsequently however, the rats gavaged with mamaku gained more weight than the rats gavaged with water between gavaging days (B1 to B4 of Figure 7.6), likely due to compensate eating to reduce hunger intake and weight after being gavaged. The fluctuations in weight gain after and between gavages results in an overall no significant difference in cumulative weight gain between treatments.

7.4 Discussion

7.4.1 Gastric Emptying

The weight of the contents remaining in the stomach two hours post-mortem was used as an indicator of gastric emptying in this study. There was a significant difference between the stomach content weights of rats gavaged with mamaku and with water, suggesting that mamaku gum was able to delay gastric emptying significantly longer than water. The presence of some mamaku gum in the stomach two hours post-gavage supports the hypothesis. The pH values of rat stomach with consumed food is about 3.2 (McConnell, Basit, & Murdan, 2008), which should not have any degrading effects on the polysaccharide (Matia-Merino, et al., 2012).

Gastric emptying is the onflow of chyme (food) from the stomach to the duodenum and small intestine. Figure 7.7 illustrates the gastric emptying process. The bulk of emptying results from fundal tone of the gastric fundus (1). The fundus reduces its volume with incoming digesta, and is facilitated by antral contraction waves (2) which promote flow towards the pyloric sphincter (pylorus) by minimising the pressure gradient immediately distal to the fundus (3). Thus when there is a brief opening of the pylorus, the chyme is pushed through the duodenum (4) (Lentle & Janssen, 2011). Factors governing gastric emptying include feedback from the nutrients in the small intestine, gastric volume, physical characteristics of the food (solid or liquid), and chemical composition of the food (e.g. protein or carbohydrate). Fluids are emptied more rapidly than solid foods, with emptying times as short as 12 to 15 minutes while solid meals varies from 23 to 77 minutes. (Rose, 1979). Increasing the viscosity of fluids with gums also prolonged gastric emptying times. For example, addition of guar gum to low fat soups doubled the half-emptying time of the soups (French & Read, 1994).

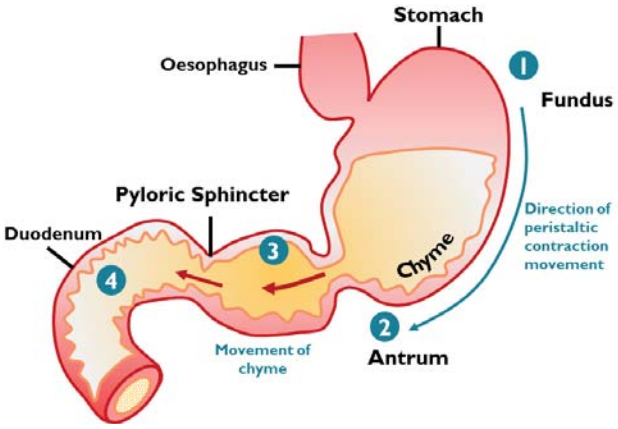

Figure 7.7 – Illustration of the gastric emptying process (adapted from Sherwood, 1993)

Polysaccharide gums typically confer satiety via its viscous consistency by delaying gastric emptying, which prolongs the satiety signals from the stomach and the physical feeling of fullness (Marciani, et al., 2001). The transit time of the meal through the small intestine may also be extended, thus increasing the period of contact between the nutrients and the small intestine epithelium (J. Slavin & Green, 2007). These polysaccharide gums are also hydrocolloids which absorb large quantities of liquid in the stomach *i.e.* gastric antrum distension, contributing to the feeling of 'bloatedness'. Efficacy of digestive enzymes is reduced in high viscosity

environments, thus delaying the breakdown of other food components for absorption (Fiszman & Varela, 2013).

It could be argued that the viscosity of the mamaku polysaccharide (e.g. 7Pa.s at $1s^{-1}$) was the main functional property responsible for the effects in gastric emptying. Guar gum, pectin and other high viscosity polysaccharides (dietary fibre) have been reported to induce satiety, reduce post-prandial consumption and/or delay gastric emptying (Davidson & Swithers, 2005; French & Read, 1994; Mattes & Rothacker, 2001; Schroeder, Marquart, & Gallaher, 2013; Tiwary, et al., 1997; Tomlin et al., 1993; Zhu, Hsu, & Hollis, 2013). The viscosities used in these studies ranged from 3.6Pa.s ($0.8s^{-1}$) to 16Pa.s. However, some studies disagree with these findings and show that guar gum does not delay gastric emptying (van Nieuwenhoven, Kovacs, Brummer, Westerterp-Plantenga, & Brouns, 2001). The difference in concentration and therefore viscosity of the guar gum used in these studies (as well as the shear rate at which these viscosities were reported at) makes a fair comparison difficult. The food mediums and quantities by which these gums were delivered were also different, further adding on to the uncertainty between comparisons.

Apart from having a high viscosity, the shear-thickening and viscoelastic properties of the mamaku gum are proposed to have contributed to gastric emptying. At a concentration of 15% w/w, the mamaku gum exhibited shear-thickening (*i.e.* increase in viscosity with increasing shear rate) properties at digestive shear rates between 1 to $10s^{-1}$ (Figure 7.8) (Lentle & Janssen, 2011). The viscosity increased from 7Pa.s at shear rate of $1s^{-1}$ to approximately 12Pa.s at $6s^{-1}$ (for comparison, the viscosity of water at room temperature is about 0.001Pa.s). Apart from increasing viscosity, the viscoelastic mamaku gum also exhibited a sharp increase in shear stresses (rotational and normal stresses) at these shear rates (see Chapter 4 and Figure 7.8). In the study by Lentle et. al. (2010), image analysis of muscular activity of the rat stomach maintained *ex vivo* showed that the origin and direction of propagation of antral contractions varied when the mamaku gum was perfused. The viscoelastic nature of the gum could cause residual stress to persist within the solution after it has been deformed by the contracting stomach wall as a result of feedback control of antral contractions via mechanoreceptors in the wall of the stomach.

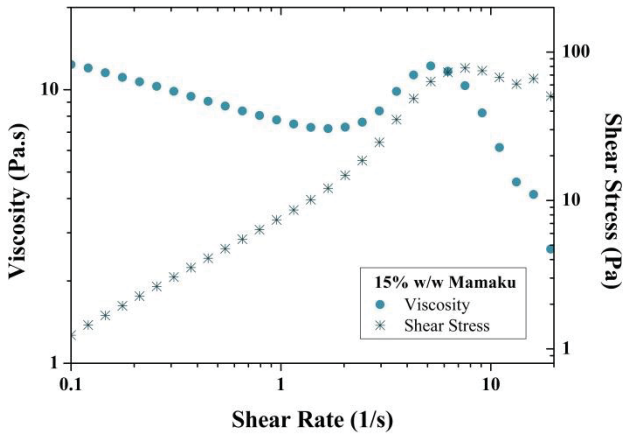

Figure 7.8 – Viscosity curve of 15% w/w mamaku solution at 37°C

In Lentle *et. al.*'s study (2010), a direct comparison was made between mamaku gum (16.4% w/w) and guar gum (1.5% w/w) perfused in the rat stomach, both at similar viscosities between 1 to $10s^{-1}$ (Figure 7.9). Unlike the

mamaku gum, guar gum (and most other polysaccharide gums) is a shear-thinning or pseudoplastic liquid which does not show any increment in viscosity or normal stresses during digestion. Characteristics of antrocorporal contractions with guar gum differed greatly from that of the mamaku gum. The frequency, amplitude and velocity of the contractions were not altered and remained the same for guar gum and saline solution.

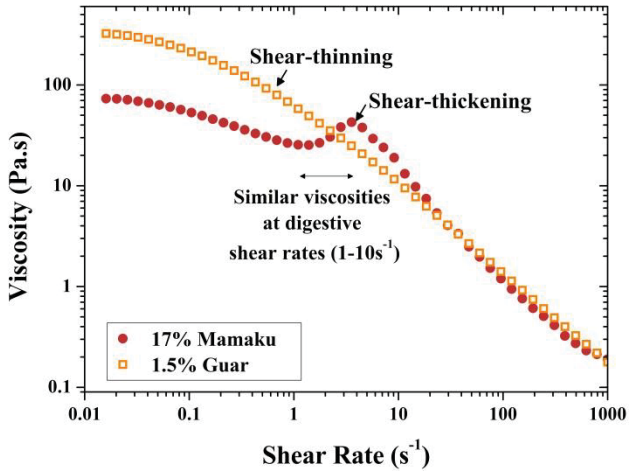

Figure 7.9 – Viscosity curves of 17% w/w mamaku gum and 1.5% w/w guar gum at 20°C

Therefore there seems to be a strong correlation between the shear-thickening or viscoelastic properties of the mamaku gum being responsible for the delayed gastric emptying in addition to the viscosity of the solution itself. It should be noted that the concentration of mamaku gum used in this study (15% w/w) was lower that the concentration used in Lentle et. al.'s (2010) study (17% w/w) due to technical issues arising during gavaging. The viscosity had to be adjusted and reduced in order to pass through the thin gavage needles smoothly in the shortest time possible, hence lowering the stress imposed on the rats. At a concentration of 17% w/w, a considerable amount of force would be required to force the solution through the syringe and the gavage needle which was not ideal for the technician. The findings from this *in vivo* study with rats therefore agreed with the *ex vivo* observations made by Lentle et. al. (2010).

Delayed gastric emptying times is correlated with satiety (French & Read, 1994; Mackie, Rafiee, Malcolm, Salt, & van Aken, 2013; Tomlin, et al., 1993), which is beneficial in situations where reducing food intake is required. Longer gastric emptying times also translates to reduced postprandial glycaemic levels by slowing down the rate of glucose onflow and absorption (Blackburn & Johnson, 1981; Marathe, Rayner, Jones, & Horowitz, 2013). This would be of significance to patients with diabetes. Nevertheless, there are still studies which do not show a correlation between delayed gastric emptying and reduced glycaemic response (Clegg & Shafat, 2014). Based on the findings from Chapter 5, a non-shear thickening mamaku gum solution either treated by heat/high pressure, or dialysed with the salts removed could possibly be used as a control for future studies. In this case, it would be clearer to identify whether it is the shear-thickening property or the viscosity of the polysaccharide which delayed gastric emptying.

7.4.2 Food Consumption

The amount of food consumed 10 hours post-gavage was significantly lesser for the rats gavaged with mamaku than the control group. This is consistent with the findings on delayed gastric emptying, which probably led to prolonged satiety and hence smaller intakes of food. Slower gastric emptying may contribute to satiety due to gastric distension (Mackie, et al., 2013; G.-J. Wang et al., 2008) *i.e.* bloatedness, delaying the delivery of nutrients into the small intestine (Clegg & Shafat, 2014) or by gastroparesis *i.e.* dysfunctional antral musculature causing nausea and vomiting (Hasler, 2008). However, this was a short-term effect whereby no significant differences in food consumption between the groups were detected on the subsequent non-gavaging days.

The act of gavaging itself may have induced stress in the rats (Okva, et al., 2006), or resulted in gastric distension with the gavage volume, which led to delayed gastric emptying (Enck, Merlin, Erckenbrecht, & Wienbeck, 1989) and/or reduction in food intake in both groups on gavaging days. Since both groups were gavaged under similar conditions, the decrease in food consumption in the mamaku group could only be attributed to presence of the gum in the stomach. No particular trend was observed with time (days), although it was expected that the effect of the gum would become more pronounced as the rats start accustoming to oral gavage.

The study showed that the effects of mamaku gum on satiety were short-term, therefore food consumption measurements should be made more frequently post-gavage e.g. hourly. Rasoamanana, Even, Darcel, Tome & Fromentin (2013) demonstrated that dietary fibre inhibited food intake in mice by increasing satiation 1 hour after intra-gastric gavage. Similar results were found by Davidson and Swithers (2005), where meal calories intake one hour after a high viscosity test meal was significantly lesser in rats. Zhu, Hsu and Hollis (2013) have also suggested shorter intervals between test meals and measurements as the postprandial satiety effects of a high viscosity test meal do not last more than 3 hours. The amounts of food consumed were not determined at short intervals in this study in order to minimise disturbances to the rats continued after gavaging. Automatic food consumption measurements would be recommended where the technology is available with the ullages accounted for as well. The prompt restoration of normal appetite also indicate that the weight loss effect does not result from the effect of an endotoxin present in the mamaku gum as this would cause ongoing suppression of appetite.

The mamaku gum (15% w/w solution) has a caloric content of 0.35 kcal/g solution as determined via bomb calorimetric analysis. This method of analysis does not provide the representative energy available to the rat gavaged with mamaku since the polysaccharide, like other dietary fibres, is most likely not digested in the gut and used as an energy source. For dietary fibres, 70% of the carbohydrate is fermented and approximately only 2 kcal of digestible energy is available per gram carbohydrate (Andrew, 2006).

7.4.3 Body Weight Gain

There were no significant differences in overall body weight gain by the rats in the two groups over the entire experimental period. However, the rate of growth slowed down dramatically for both groups during the gavaging period, presumably due to the stress caused by gavaging and the reduced food consumption. Interestingly, the overall body weight of the rats gavaged with mamaku was not lower than the rats gavaged with water, even though there was delayed gastric emptying and smaller food consumption for these rats. This was however reflected in the short term decrease in weight gain in rats after being gavaged with the mamaku. These animals were gavaged at intervals hence daily gavage would probably produce ongoing weight loss.

Changes to body weight may only surface in long term studies, whereby the duration of study is more than, for example, eight weeks (Davidson & Swithers, 2005; Pranprawit, Wolber, Heyes, Molan, & Kruger, 2013), or when the rats have been fed with the test meal on a daily basis (Faipoux et al., 2006). A significant difference in cumulative weight gain was only found during the fifth week of experiment between rats given high- and low viscosity dietary supplements (Davidson & Swithers, 2005). This current study was not carried out long-term due to limitations in gavaging for ethical reasons. It is also possible that the free sugars and/or starch present in the mamaku gum solution compensated for the decreased energy intake, resulting in no weight loss.

7.4.4 Toxicity

The rats gavaged with mamaku gum did not show any symptoms of malaise at the end of the trial. Blood, kidney and liver results for toxicity were also negative.

7.5 Conclusion

This study suggests that mamaku gum in the stomach has the potential to reduce short term food consumption by delaying gastric emptying. The shear-thickening property as well as the high viscosity of the mamaku gum was likely to play an important role in prolonging gastric emptying by modifying antrocorporal movements of the stomach. There were no significant impacts on body weight for this duration of study (4 weeks). However, given a longer experimental period (e.g. 8 weeks), there may be weight loss effects for the rats gavaged with the mamaku gum as a result of reduced food consumption over a longer period of time. No toxicity effects of the mamaku gum were found based on serum and liver tissue analyses, therefore the gum is most likely safe for consumption. Future work could include feeding for longer periods with the mamaku gum to monitor long term weight loss, gavaging with either guar gum or mamaku gum without the shear-thickening property, as well as incorporating the mamaku gum into food systems.

Acknowledgements

We would like to thank Kim Wylie, Anne Broomfield, Corrin Hulls and Juliet Cayzer for their expertise in animal care and providing technical support throughout the experiment.

Chapter 8 Overall Conclusions and Recommendations

8.1 Overall Conclusions

The polysaccharide extracted from the New Zealand black tree fern (mamaku), *Cyathea medullaris* was characterized using rheological, physico-chemical and structural analysis techniques. The results obtained from this study provided a clearer picture of the molecular parameters of the polymer as well as the possible mechanisms involved in its unique rheological properties under shear and extensional deformations. From the research, the following questions were answered:

1. What are its rheological properties under shear, strain and extension? (Chapter 4)
2. How do environmental conditions affect the rheological function of the polysaccharide? (Chapter 5)
3. What is the monosaccharide composition and structure of the polysaccharide? (Chapter 6)
4. What is the molecular origin for its rheological behaviour? What causes shear-thickening? (Chapters 4-6)
5. Can the polysaccharide be used as a suitable medium for controlling food intake? (Chapter 7)

The overall rheological behaviour of a 5% w/w mamaku polysaccharide can be described to possess Newtonian, shear-thinning, shear-thickening, anti-thixotropic, thixotropic or rheopectic properties depending on shear-history. It is also viscoelastic, strain-hardening, instantaneously strain-stiffening, highly extensional with a large Trouton ratio, rod-climbing, self-siphoning. Nonetheless, all of these properties observed were dependent on the timescale and stress (or strain) at which the material was probed.

From all the observations that were made with various rheological techniques and environmental conditions of the polysaccharide, a simple mechanism has been proposed to explain the shear-thickening, anti-thixotropy or strain-hardening properties (Figure 8.1). Under shear or extension, the polysaccharide molecules disentangle and transit from intramolecular to intermolecular interactions involving hydrogen bonding as more associative groups within the polymer chains are exposed. This proposed mechanism was consistent under different concentrations, temperatures, urea concentrations, ionic strength and pH (Figure 8.2). Structural characterisation (Figure 8.3) revealed a glucuronomannan backbone (methylesterified 4-Glc*p*A with 2,3- and 2,3,4-linked Man*p*) with branched sugar side-chains of galactose, arabinose, xylose, non-methylesterified glucuronic acid and other simple sugars at the O-3 and O-4 of the mannose residues. Given this knowledge, functional groups in the polysaccharide which could be responsible for hydrogen bonding were identified to be the hydroxyl groups of mannose along the backbone and the carbonyl/carboxylic groups of the uronic acids (Figure 8.4). Further investigation is warranted to identify the exact functional group responsible for shear-thickening.

The mamaku polysaccharide has demonstrated rheological properties which could be independently controlled based on their sensitivity to hydrogen bonding. Factors which promote or disrupt hydrogen bonding, and therefore shear-thickening, are dependent on shear rate, strain amplitude, concentration, temperature and the presence of urea (chaotropic agent). The native mamaku gum is relatively insensitive to pH and salt, which

could be advantageous when polysaccharide stability is required in extreme environments. With the removal (via dialysis) of the indigenous salt content originally present in the native fraction, the polysaccharide could become more sensitive to changes in pH and ionic strength. In addition, the type of cation (valency dependent) could also play a role in the rheological properties of the mamaku polysaccharide. Hydrogen bonds are directional, short-ranged and moderately weak. Therefore apart from the factors studied in this thesis, other factors which are able to modify the alignment and/or distance between the polysaccharides chains, as well as weaken hydrogen bonds are expected to alter the rheological properties of the polysaccharide.

Rat studies conducted showed that the mamaku gum is generally safe for consumption based on well-being of the rats during study as well as negative toxicity tested post-mortem. Interestingly, the polysaccharide showed potential short term effects on delaying gastric emptying (satiety) and thus reducing food consumption. This short study provided a unique functional benefit of the mamaku polysaccharide in human health and well-being. This study provides a platform for future work in the context of designing foods for controlling food intake.

This thesis is without a doubt incomplete in its entirety of knowledge on the polysaccharide. Nevertheless, it provides a good foundation for future research in exploiting the functionality of the biopolymer. It is envisaged that the mamaku polysaccharide will interest researchers from various fields - polymer scientists, botanists, food technologists, physiologists, chefs, dieticians etc. Perhaps eventually, the mamaku polysaccharide may come to enjoy success as a major commercial polysaccharide like xanthan gum and guar gum. In a final concluding remark, the mamaku polysaccharide is indeed a unique polysaccharide that has rheological and physico-chemical properties unlike any other polysaccharides. The potential for this polysaccharide to be used in food as well as non-food applications is diverse and unlimited.

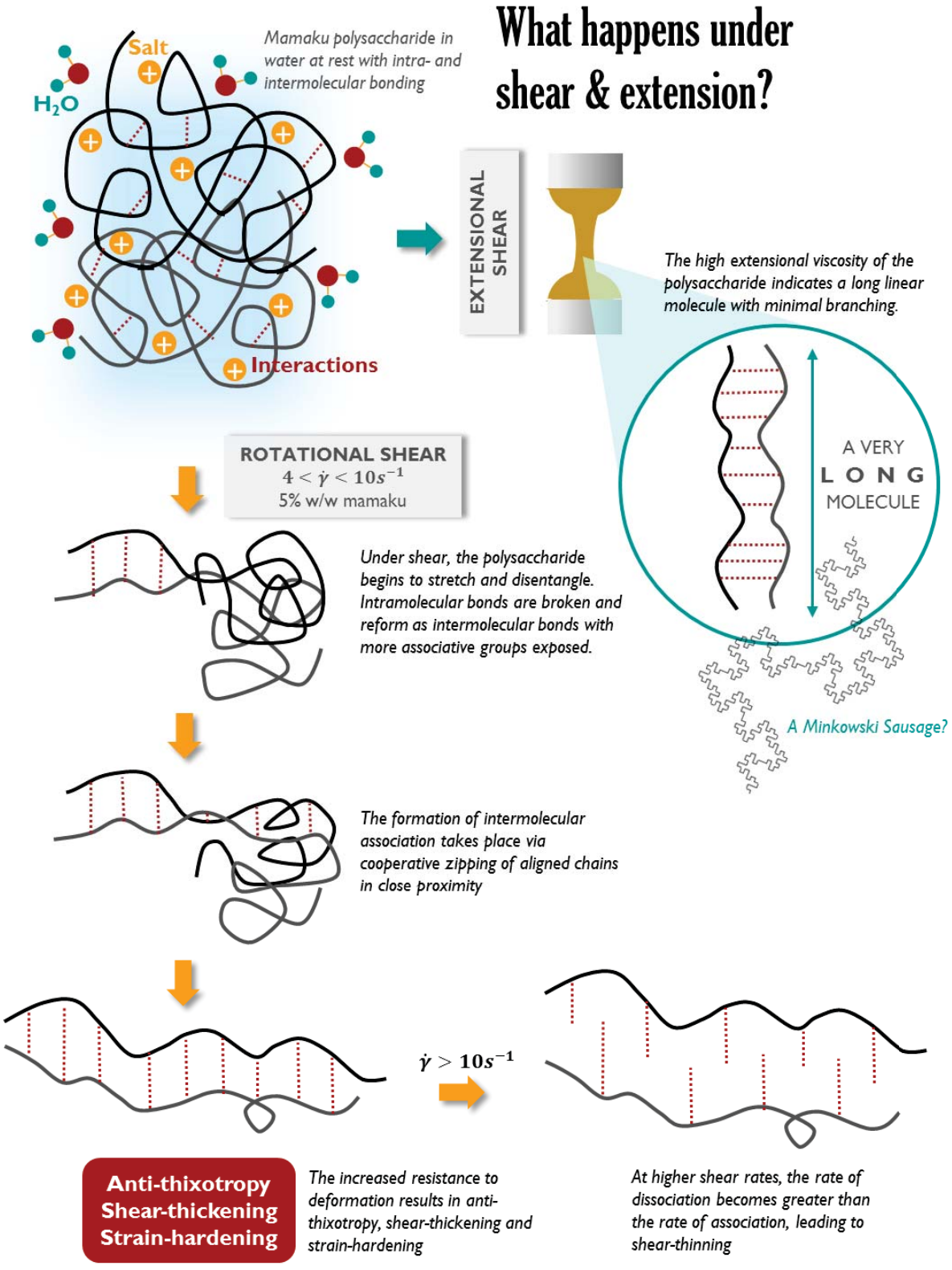

Figure 8.1 – Schematic illustration of the polysaccharide during shear and extensional deformations (dotted lines represent intermolecular hydrogen bonds)

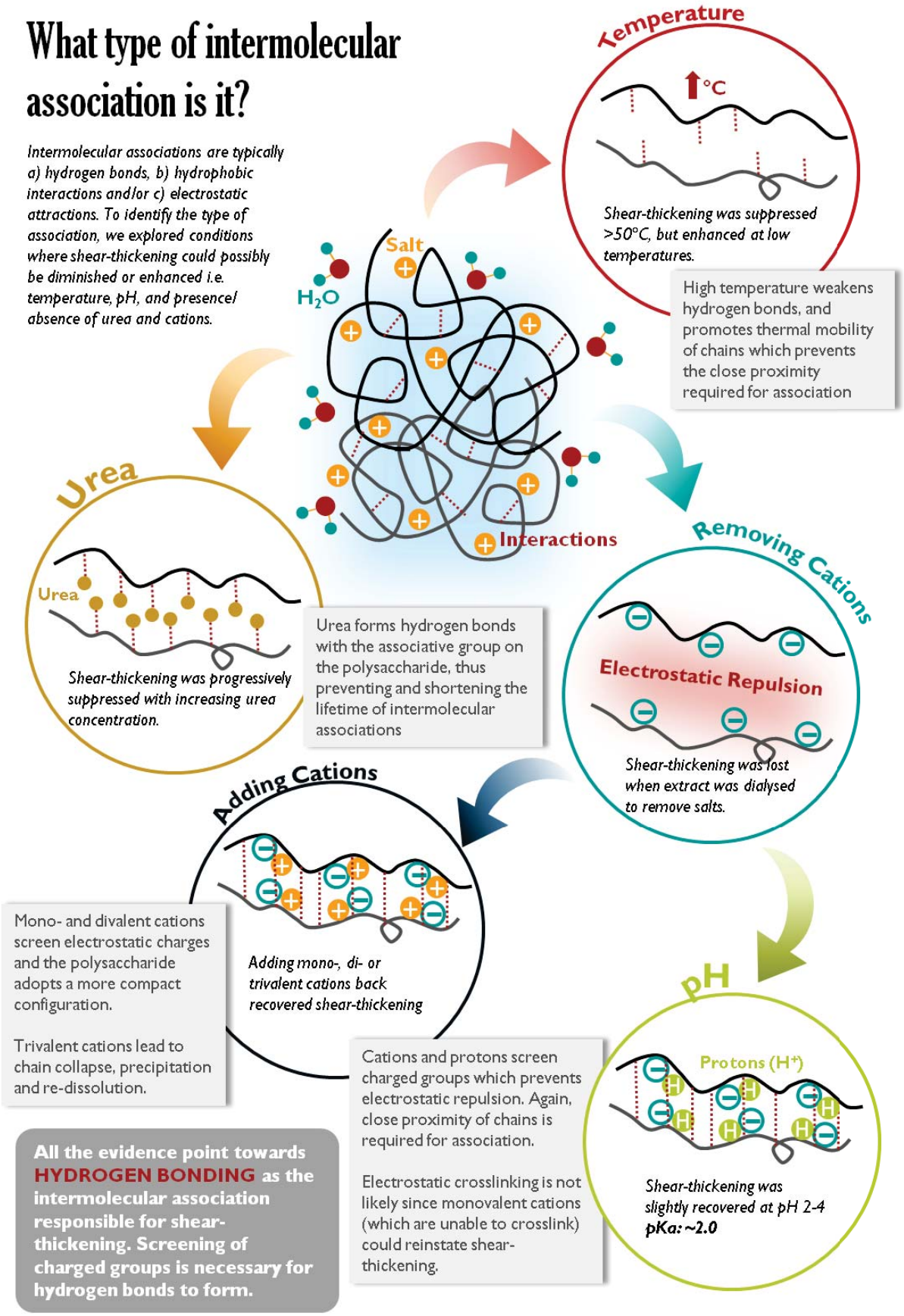

Figure 8.2 – Schematic illustration of overview of effects of temperature, urea, cations and pH on the polysaccharide during shear

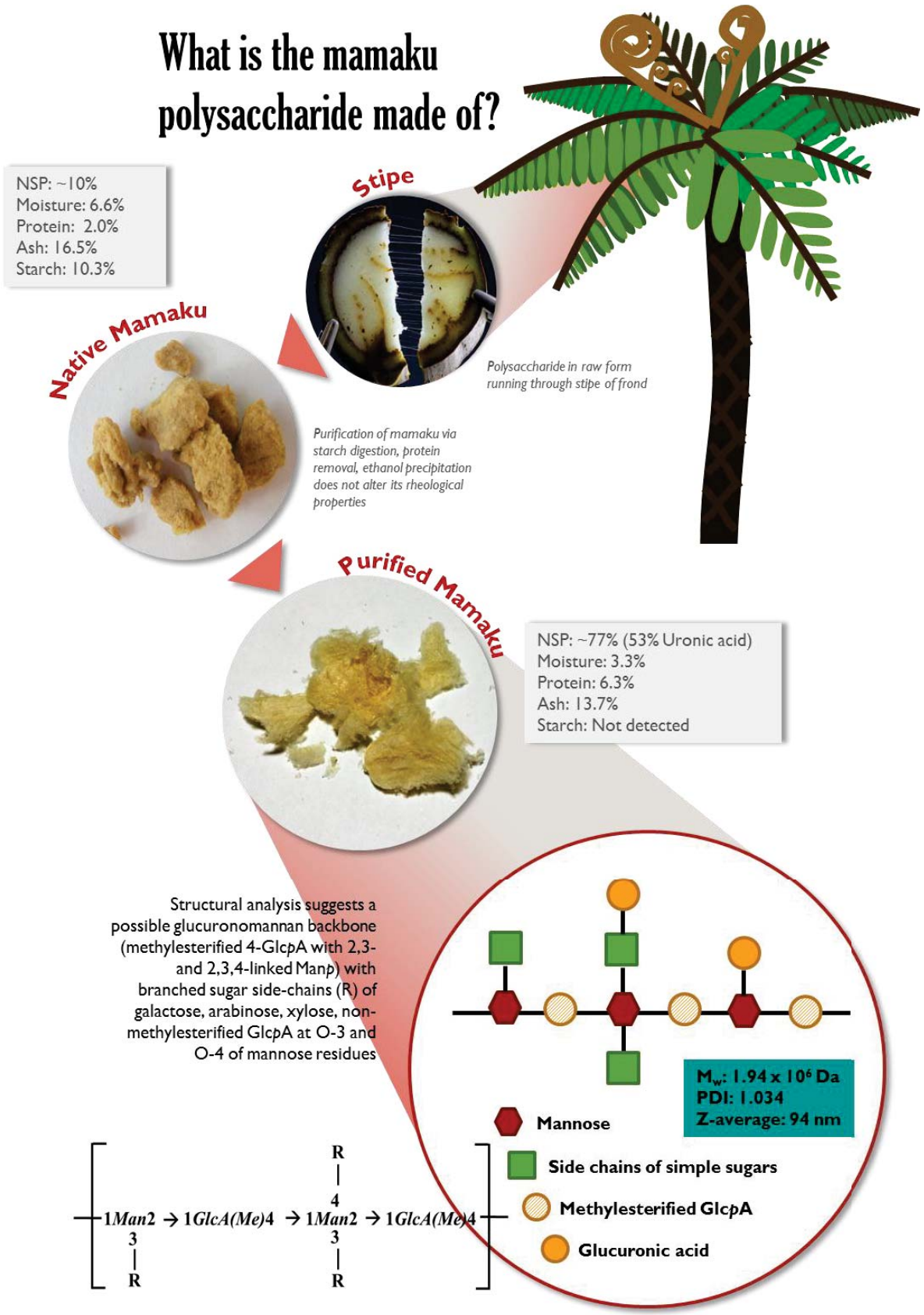

Figure 8.3 – Schematic illustration of purification and structural characterisation of the polysaccharide

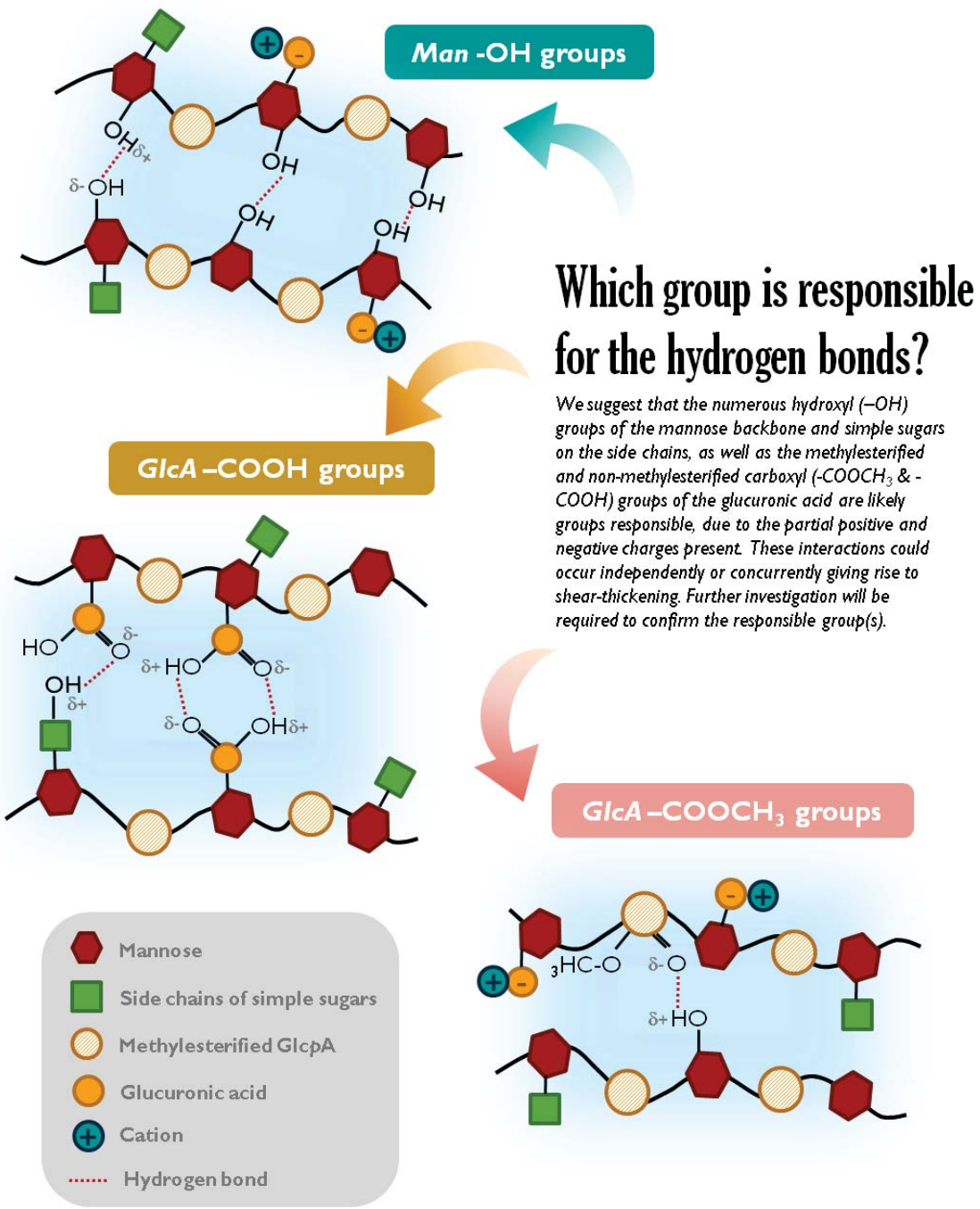

Figure 8.4 – Schematic illustration of possible hydrogen bond configurations between functional groups in the polysaccharide chain responsible for hydrogen bonding

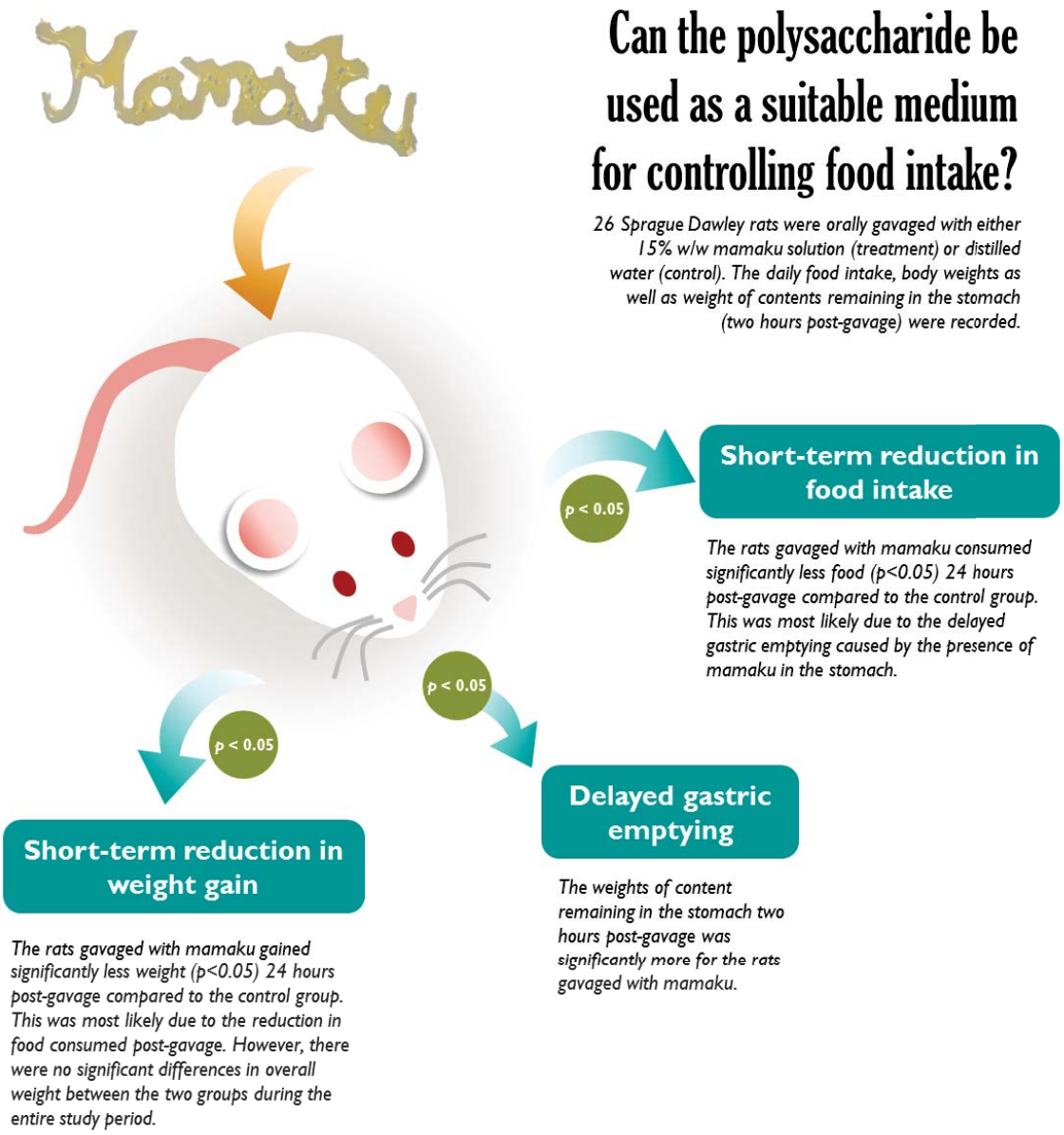

Figure 8.5 – Schematic illustration on effects of mamaku polysaccharide on the food intake, body weight and gastric emptying in rats

8.2 Recommendations

8.2.1 Future Work

1. Extraction Conditions and Optimisation

The yield and composition of the mamaku polysaccharide can vary greatly, depending on the plant condition and the parameters used in the extraction process itself. There has only been one extraction protocol used in this thesis, thus it is not known yet what the optimum conditions are e.g. for highest yield or highest uronic acid content in the polysaccharide. Plant materials may differ during growth and may be dependent on the soil and climatic conditions. It is important to understand what effects the age, climatic, soil conditions, etc. have on the functional properties of the tree fern polysaccharide. Extraction and processing conditions require further studies to obtain better yield and retain its optimal functionality. Temperature of solvent, type of solvent (e.g. water, ethanol, sodium bicarbonate), plant to solvent ratio, time of extraction, pre-processing treatments (e.g. blanching) are several factors which could be explored in future studies.

2. Further Rheological and Structural Characterisation

The rheological techniques used to characterise the mamaku polysaccharide in the thesis have given a sufficiently complete overall picture of its rheological behaviour. However, there are still other rheological techniques which could complement existing knowledge of rheological properties. For instance, controlled shear stress rheometry (instead of shear rate), stress relaxation and creep tests, steady-state extensional viscosity using the filament stretching extensional rheometer (FiSER) or optimised shape cross-slot microfluidic extensional rheometer (OSCER), and perhaps rheology coupled with another characterisation technique such as rheo-optics or rheo-NMR.

The molecular structure of the polysaccharide suggested in Chapter 6 was based on existing glucuronomannans with similar structures. However, to confirm the actual sequence and arrangement of the monosaccharides, two-dimensional nuclear magnetic resonance techniques (2D NMR) e.g. nuclear overhauser effect spectroscopy (NOESY) or correlation spectroscopy (COSY) could be employed. Preliminary 2D NMR experiments were conducted but a clear resolution of shifts was not obtained.

3. Identifying Sites Responsible for Hydrogen Bonding

The specific sites which are responsible for hydrogen bonding during shear-thickening should also be identified. The polysaccharide could be chemically modified to alter/deactivate suspected hydrogen bonding sites, and then tested for its rheology. For example, methylesterification of the glucuronic acid groups, or vice versa, de-methylesterification of the methylesterified glucuronic acid groups, or methylation of the mannose hydroxyl groups. This could potentially be quite challenging since chemical modification would change its solubility as well. Other techniques such as NMR or FTIR or solvents of differing polarities could be used.

4. Further Characterisation of Purified Fractions

In Chapter 6, a polysaccharide fraction which was highly insoluble in ethanol was found upon a second ethanol precipitation step. This fraction did not display shear-thickening characteristics while the shear-thickening fraction was then solubilised in ethanol. It is unclear whether the alcohol insoluble fraction was polysaccharide aggregates or an entirely different fraction present in small quantities. Therefore further work e.g. structural and molecular weight characterisation would be needed to identify this fraction. Furthermore, the polysaccharide material purified using the outlined steps in Chapter 6 lost its shear-thickening characteristic with storage (approximately 2 years). This could be due to ageing of the material or other mechanisms such as loss of bound water. More investigation is needed to elucidate the cause of material degradation with time.

5. *In vivo* and *In vitro* Studies

Further studies will be needed in order for the mamaku polysaccharide to be used as a satiety enhancer in humans. *In vitro* studies stimulating gastric and small intestinal digesta conditions are first recommended prior to conducting human trials (*in vivo*). For example, the breakdown of protein into peptides and amino acid could be monitored with time in the presence or absence of mamaku polysaccharide.

6. Micro-rheology of Unprocessed Mucilage

The filament strands observed within the stipe demonstrated remarkable extensional and viscoelastic properties e.g. beads-on-a-string formation when the stipe was broken and pulled apart. Visually, it resembled spider silk. This is likely to be the polysaccharide in its raw, unprocessed form. Due to the limits of small sample sizes available, micro-rheology of this raw mucilage could be performed e.g. in a μ-CaBER or OSCER to characterise its extensional properties.

7. Other Fern Polysaccharides

Mucilage from other tree ferns in the same *Cyathea* family e.g. silver tree fern (*Cyathea dealbata*) could be extracted and characterised. Similar properties may reveal a common function of these polysaccharides in tree ferns such as to support growth and extension of the frond or act as some form of stress-resistance mechanism. Conversely, the rheological properties of the mamaku gum may be unique to the black tree fern.

8. Pharmacological Activity

Polysaccharides may also exhibit pharmacological activities such as anti-oxidant, anti-bacterial, anti-cancer, anti-inflammatory, and anti-tumour etc. effects. These pharmacological activities should be investigated to fully exploit the health-related functionalities of the polysaccharide.

9. Other Characterisation Techniques

The unusual physico-chemical properties of the mamaku polysaccharide merits further exploration using other characterisation techniques. Preliminary atomic force microscopy (AFM) work was carried out to blueprint its single-molecule chain stretching profile but good adhesion to the substrate was not achieved. Isothermal

titration calorimetry could also be used to quantify enthalpy and enthalpy changes of the polysaccharide in the presence of urea, as well as further characterise its ion-binding capabilities with mono-, di- and trivalent cations. Hydrogen bonds have also recently been investigated using high pressure processing techniques.

8.2.2 Applications

A. Satiety Aid

The mamaku gum has shown promising results in Chapter 7 as a potential food medium that could help control food intake in rats. This functional advantage may be extended to humans with further research required to verify this hypothesis. Consumption of the mamaku gum at sufficient concentrations with or without accompanying food substances could delay gastric emptying and prolong the time between meals. Further work is underway on developing suitable delivery system of mamaku gum in food products either in the powder or in solution form.

B. Demulcent and Emollient

A demulcent is an agent that forms a soothing film over a mucous membrane, such as the nasal or oesophageal membrane, providing relief from pain and inflammation. Emollients are substances which soothe and soften the skin. Many plant mucilages or exudates are used as demulcents or emollients, due to their mucosal-like properties of being slimy, smooth and gel-like. Given the consistency of the mamaku polysaccharide, it would make a suitable demulcent or emollient. Furthermore, the Māori people have been known to use the mamaku gum as a demulcent over burn wounds or consumed to ease an irritated stomach.

C. Dysphagia Aid

Dysphagia is an eating or drinking disorder whereby the patients have difficulties in swallowing. One of the methods to alleviate dysphagia is to thicken the fluid, typically with starch to ease the swallowing. The shear-thickening property of the mamaku gum could be useful in this case, which provides the stress resistance during flow constriction absent in dysphagia patients. The flow properties of the mamaku gum during swallowing could be characterised using the 'Cambridge Throat' device, as constructed by Mackley, Anthony, Butler, Chapman and Vadillo of the University of Cambridge (2013).

D. Biomimetic

Hydrogen bonds are essential for maintaining biological structures, such as stabilising DNA strands and the folded protein molecule. The orchestrated hydrogen bonding in the mamaku polysaccharide under shear/stress deformation could be used as an inspiration for constructing synthetic molecules requiring shear or strain resistance via hydrogen bond associations.

E. Texture Modifier, Drag-flow Reducer and Lubricant

The highly extensional properties of the mamaku polysaccharide distinguish it from other industrial polysaccharides. Novel or existing applications could exploit these properties. For example, the polysaccharide

could be used in foods or cuisines as a textural modifier to produce new textures and mouthfeel. Drag-flow reducers are usually polymers which are soluble, flexible, extensional, linear, with high molecular weight and resistant to flow-induced shear degradation. Polymers such as guar gum, xanthan gum and polyethylene oxide have been used as drag-flow reducers, which could be replaced with the mamaku polysaccharide. Mucilages have also been used as lubricants due to its mucosal-like properties. Their ability to bind to a large number of water molecules reduces the friction coefficient between the mucilage and a surface.

References

Aitkadi, A., Carreau, P. J., & Chauveteau, G. (1987). Rheological properties of partially hydrolyzed polyacrylamide solutions. *Journal of Rheology, 31*(7), 537-561. doi: 10.1122/1.549959

Alhadithi, T. S. R., Barnes, H. A., & Walters, K. (1992). The relationship between the linear (oscillatory) and nonlinear (steady-state) flow properties of a series of polymer and colloidal systems. *Colloid and Polymer Science, 270*(1), 40-46. doi: 10.1007/bf00656927

Alistair, S., & Shirley, C. (2010). Introduction. In S. Alistair, P. Glyn & W. Peter (Eds.), *Food Polysaccharides and their Applications* (2nd ed.). Boca Raton, FL: CRC Press.

Alistair, S., Shirley, C., Peter, W., & Glyn, P. (2006). Gums and Mucilages *Food Polysaccharides and Their Applications* (pp. 455-495): CRC Press.

Andrew, C. (2006). Dietary Fiber *Food Polysaccharides and Their Applications* (pp. 629-663): CRC Press.

Anna, S. L., & McKinley, G. H. (2001). Elasto-capillary thinning and breakup of model elastic liquids. *Journal of Rheology, 45*(1), 115-138. doi: 10.1122/1.1332389

Annable, T., Buscall, R., Ettelaie, R., & Whittlestone, D. (1993). The rheology of solutions of associating polymers: Comparison of experimental behavior with transient network theory. *Journal of Rheology, 37*(4), 695-726. doi: 10.1122/1.550391

Aspinall, G. O. (1982). *The Polysaccharides* (Vol. 1). New York: Academic Press.

Aspinall, G. O., Carlyle, J. J., McNab, J. M., & Rudowski, A. (1969). Anogeissus leiocarpus gum. Part II. Fractionation of the gum and partial hydrolysis of leiocarpan A. *Journal of the Chemical Society C: Organic*(5), 840-845.

Aspinall, G. O., Hirst, E. L., & Wickstrøm, A. (1955). Gum ghatti (Indian gum). The composition of the gum and the structure of two aldobiouronic acids derived from it. *Journal of the Chemical Society (Resumed)*, 1160-1165.

Athanasiadis, T., Beule, A. G., Robinson, B. H., Robinson, S. R., Shi, Z., & Wormald, P. J. (2008). Effects of a novel chitosan gel on mucosal wound healing following endoscopic sinus surgery in a sheep model of chronic rhinosinusitis. *Laryngoscope, 118*(6), 1088-1094.

Aubry, T., & Moan, M. (1994). Rheological behaviour of a hydrophobically associating water-soluble polymer. *Journal of Rheology, 38*(6), 1681-1692. doi: 10.1122/1.550566

Avachat, A. M., Dash, R. R., & Shrotriya, S. N. (2011). Recent investigations of plant based natural gums, mucilages and resins in novel drug delivery systems. *Indian Journal of Pharmaceutical Education and Research, 45*(1), 86-99.

Bagley, E. B., & Dintzis, F. R. (1999). Shear thickening and flow induced structures in foods and biopolymer systems. In D. D. K. D.A. Siginer & R. P. Chhabra (Eds.), *Rheology Series* (Vol. Volume 8, pp. 63-86): Elsevier.

Balci, M. (2005). *Basic 1H- and 13C-NMR Spectroscopy*. Amsterdam: Elsevier.

Baljon-Haakman, A. R. C., & Witten, T. A. (1992). Architecture-controlled interaction between associating polymers. *Macromolecules, 25*(11), 2969-2976.

Ballard, M. J., Buscall, R., & Waite, F. A. (1988). The theory of shear-thickening polymer solutions. *Polymer, 29*(7), 1287-1293.

Barnes, H. A., Hutton, J. F., & Walters, K. (1989). *An Introduction to Rheology*. Amsterdam: Elsevier Science.

Bellisle, F., & Blundell, J. E. (2013). Satiation, satiety: concepts and organisation of behaviour. In J. E. Blundell & F. Bellisle (Eds.), *Satiation, Satiety and the Control of Food Intake : Theory and Practice*. Oxford, Philadelphia: Woodhead Pub.

BeMiller, J. (2006). Gums and Hydrocolloids *Carbohydrates in Food, Second Edition* (pp. 209-231): CRC Press.

Bender, J., & Wagner, N. J. (1996). Reversible shear thickening in monodisperse and bidisperse colloidal dispersions. *Journal of Rheology, 40*(5), 899-916.

Bhardwaj, A., Miller, E., & Rothstein, J. P. (2007). Filament stretching and capillary breakup extensional rheometry measurements of viscoelastic wormlike micelle solutions. *Journal of Rheology, 51*(4), 693-719. doi: 10.1122/1.2718974

Blackburn, N. A., & Johnson, I. T. (1981). The effect of guar gum on the viscosity of the gastrointestinal contents and on glucose uptake from the perfused jejunum in the rat. *British Journal of Nutrition, 46*(2), 239-246. doi: 10.1079/bjn19810029

Blumenkrantz, N., & Asboe Hansen, G. (1973). New method for quantitative determination of uronic acids. *Analytical Biochemistry, 54*(2), 484-489. doi: 10.1016/0003-2697(73)90377-1

Boger, D. V., & Walters, K. (1993). *Rheological phenomena in focus*. Amsterdam: Elsevier.

Bourbon, A. I., Pinheiro, A. C., Ribeiro, C., Miranda, C., Maia, J. M., Teixeira, J. A., & Vicente, A. A. (2010). Characterization of galactomannans extracted from seeds of Gleditsia triacanthos and Sophora japonica through shear and extensional rheology: Comparison with guar gum and locust bean gum. *Food Hydrocolloids, 24*(2-3), 184-192. doi: 10.1016/j.foodhyd.2009.09.004

Briscoe, B., Luckham, P., & Zhu, S. (1996). Rheological study of poly(ethylene oxide) in aqueous salt solutions at high temperature and pressure. *Macromolecules, 29*(19), 6208-6211. doi: 10.1021/ma960667z

Briscoe, B., Luckham, P., & Zhu, S. (1998). Rheological properties of poly(ethylene oxide) aqueous solutions. *Journal of Applied Polymer Science, 70*(3), 419-429.

Briscoe, B., Luckham, P., & Zhu, S. (2000). The effects of hydrogen bonding upon the viscosity of aqueous poly(vinyl alcohol) solutions. *Polymer, 41*(10), 3851-3860. doi: 10.1016/s0032-3861(99)00550-9

Brooker, S. G., Cambie, R. C., & Cooper, R. C. (1987). *New Zealand medicinal plants*. Auckland: Reeds Books.

Brown, A. P., Dinger, N., & Levine, B. S. (2000). Stress produced by gavage administration in the rat. *Contemporary Topics in Laboratory Animal Science, 39*(1), 17-21.

Broze, G., Jerome, R., Teyssie, P., & Marco, C. (1983). Halato-telechelic polymers 6. Viscoelastic properites of solutions of alkaline-earth alpha,omega-dicarboxylatopolybutadiene. *Macromolecules, 16*(6), 996-1000. doi: 10.1021/ma00240a033

Bull, L. S., & Pitts, G. C. (1971). Gastric capacity and energy absorption in the force-fed rat. *Journal of Nutrition, 101*(5), 593-&.

Burckbuchler, V., Kjøniksen, A. L., Galant, C., Lund, R., Amiel, C., Knudsen, K. D., & Nyström, B. (2006). Rheological and structural characterization of the interactions between cyclodextrin compounds and hydrophobically modified alginate. *Biomacromolecules, 7*(6), 1871-1878.

Carriere, C. J., & Inglett, G. E. (1998). Solution viscoelastic properties of OATRIM-10 and cooked oat bran. *Cereal Chemistry, 75*(3), 354-359.

Cataldi, T. R. I., Campa, C., & De Benedetto, G. E. (2000). Carbohydrate analysis by high-performance anion-exchange chromatography with pulsed amperometric detection: The potential is still growing. *Fresenius' Journal of Analytical Chemistry, 368*(8), 739-758. doi: 10.1007/s002160000588

Chaffey, C. E. (1977). Mechanisms and equations for shear thinning and thickening in dispersions. *Colloid and Polymer Science Kolloid Zeitschrift & Zeitschrift für Polymere, 255*(7), 691-698.

Chan, S., Chen, J., Ettelaie, R., Law, Z., Alevisopoulos, S., Day, E., & Smith, S. (2007). Study of the shear and extensional rheology of casein, waxy maize starch and their mixtures. *Food Hydrocolloids, 21*(5/6), 716-725.

Chassenieux, C., Nicolai, T., & Benyahia, L. (2011). Rheology of associative polymer solutions. *Current Opinion in Colloid and Interface Science, 16*(1), 18-26.

Cheng, H. N., & Neiss, T. G. (2012). Solution NMR Spectroscopy of Food Polysaccharides. *Polymer Reviews, 52*(2), 81-114. doi: 10.1080/15583724.2012.668154

Cho, J., Heuzey, M. C., Begin, A., & Carreau, P. J. (2006). Effect of urea on solution behavior and heat-induced gelation of chitosan-beta-glycerophosphate. *Carbohydrate Polymers, 63*(4), 507-518. doi: 10.1016/j.carbpol.2005.10.013

Choi, H., Mitchell, J. R., Gaddipati, S. R., Hill, S. E., & Wolf, B. (2014). Shear rheology and filament stretching behaviour of xanthan gum and carboxymethyl cellulose solution in presence of saliva. *Food Hydrocolloids, 40*, 71-75.

Ciucanu, I., & Kerek, F. (1984). A simple and rapid method for the permethylation of carbohydrates. *Carbohydrate research, 131*(2), 209-217. doi: 10.1016/0008-6215(84)85242-8

Clarke, A. E., Anderson, R. L., & Stone, B. A. (1979). Form and function of arabinogalactans and arabinogalactan-proteins. *Phytochemistry, 18*(4), 521-540.

Clasen, C., Plog, J. P., Kulicke, W. M., Owens, M., Macosko, C., Scriven, L. E., . . . McKinley, G. H. (2006). How dilute are dilute solutions in extensional flows? *Journal of Rheology, 50*(6), 849-881. doi: 10.1122/1.2357595

Clegg, M. E., & Shafat, A. (2014). The effect of agar jelly on energy expenditure, appetite, gastric emptying and glycaemic response. *European Journal of Nutrition, 53*(2), 533-539. doi: 10.1007/s00394-013-0559-x

Cleland, R. (1971). Cell wall extension. *Annual Review of Plant Physiology, 22*, 197-&. doi: 10.1146/annurev.pp.22.060171.001213

Clifford, S. C., Arndt, S. K., Popp, M., & Jones, H. G. (2002). Mucilages and polysaccharides in Ziziphus species (Rhamnaceae): Localization, composition and physiological roles during drought-stress. *Journal of experimental botany, 53*(366), 131-138.

Cox, W. P., & Merz, E. H. (1958). Correlation of dynamic and steady flow viscosities. *Journal of Polymer Science, 28*(118), 619-622. doi: 10.1002/pol.1958.1202811812

Crowe, A. (2004). *A field guide to the native edible plants of New Zealand*. Birkenhead, Auckland: Godwit.

Crowe, A. (2009). *Which native fern? New Zealand native ferns - a simple guide to their identification, ecology and uses*. Auckland: Penguin Books.

Cui, S. W. (2005). Structural Analysis of Polysaccharides *Food Carbohydrates*: CRC Press.
Davidson, T. L., & Swithers, S. E. (2005). Food viscosity influences caloric intake compensation and body weight in rats. *Obesity Research, 13*(3), 537-544. doi: 10.1038/oby.2005.57
Davis, M. W. (1998). A Rapid Modified Method for Compositional Carbohydrate Analysis of Lignocellulosics by High pH Anion-Exchange Chromatography with Pulsed Amperometric Detection (HPAEC/PAD). *Journal of Wood Chemistry and Technology, 18*(2), 235-252. doi: 10.1080/02773819809349579
De Dier, R., Mathues, W., & Clasen, C. (2013). Extensional Flow and Relaxation of Semi-dilute Solutions of Schizophyllan. *Macromolecular Materials and Engineering, 298*(9), 944-953. doi: 10.1002/mame.201200359
de Graaf, C., Blom, W. A. M., Smeets, P. A. M., Stafleu, A., & Hendriks, H. F. J. (2004). Biomarkers of satiation and satiety. *American Journal of Clinical Nutrition, 79*(6), 946-961.
de Kruif, C. G., Weinbreck, F., & de Vries, R. (2004). Complex coacervation of proteins and anionic polysaccharides. *Current Opinion in Colloid & Interface Science, 9*(5), 340-349. doi: 10.1016/j.cocis.2004.09.006
Dealy, J., & Plazek, D. (2009). Time-temperature superposition - a users guide. *Rheology Bulletin, 78*.
DeSesso, J. M., & Jacobson, C. F. (2001). Anatomical and physiological parameters affecting gastrointestinal absorption in humans and rats. *Food and Chemical Toxicology, 39*(3), 209-228. doi: 10.1016/s0278-6915(00)00136-8
Deshpande, A. (2010). Oscillatory shear rheology for probing nonlinear viscoelasticity of complex fluids: large amplitude oscillatory shear In A. Deshpande, M. J. Krishnan & P. B. Kumar (Eds.), *Rheology of Complex Fluids*: Springer.
Dobrynin, A. V., Colby, R. H., & Rubinstein, M. (1995). Scaling theory of polyelectrolyte solutions. *Macromolecules, 28*(6), 1859-1871. doi: 10.1021/ma00110a021
Dogan, H., & Kokini, J. L. (2006). Rheological Properties of Food. In D. R. Heldman, D. B. Lund & C. Sabliov (Eds.), *Handbook of Food Engineering* (2nd ed.): CRC Press.
Doi, M., & Edwards, S. F. (1988). *The theory of polymer dynamics*: Oxford University Press.
Dong, X., Li, L., Xu, J., & Guo, X. (2011). Rheological behavior of PMVE-MA aqueous solution with metallic cations. *Frontiers of Chemical Engineering in China, 5*(1), 126-130.
Dormidontova, E. E. (2002). Role of competitive PEO-water and water-water hydrogen bonding in aqueous solution PEO behavior. *Macromolecules, 35*(3), 987-1001. doi: 10.1021/ma010804e
Dougherty, R. C. (1998). Temperature and pressure dependence of hydrogen bond strength: A perturbation molecular orbital approach. *Journal of Chemical Physics, 109*(17), 7372-7378. doi: 10.1063/1.477343
Dubois, M., Gilles, K. A., Hamilton, J. K., Rebers, P. A., & Smith, F. (1956). Colorimetric method for determination of sugars and related substances. *Analytical Chemistry, 28*(3), 350-356.
Duxenneuner, M. R., Fischer, P., Windhab, E. J., & Cooper-White, J. J. (2008). Extensional Properties of Hydroxypropyl Ether Guar Gum Solutions. *Biomacromolecules, 9*(11), 2989-2996. doi: 10.1021/bm800553v
Eagles, P. F. K., Stephen, A. M., & Churms, S. C. (1993). Molecular structures of gum exudates from Hakea species. *Phytochemistry, 34*(3), 709-713.
Edmond-Ghanem, M., Han, R. M., Classen, B., Quetin-Leclerq, J., Mahy, G., Ruan, C. J., . . . Lutts, S. (2010). Mucilage and polysaccharides in the halophyte plant species Kosteletzkya virginica: Localization and composition in relation to salt stress. *Journal of Plant Physiology, 167*(5), 382-392.
Edwards, B. J., Keffer, D. J., & Reneau, C. W. (2002). An examination of the shear-thickening behavior of high molecular weight polymers dissolved in low-viscosity newtonian solvents. *Journal of Applied Polymer Science, 85*(8), 1714-1735. doi: 10.1002/app.10807
Enck, P., Merlin, V., Erckenbrecht, J. F., & Wienbeck, M. (1989). Stress effects on gastrointestinal transit in the rat. *Gut, 30*(4), 455-459. doi: 10.1136/gut.30.4.455
Englyst, H. N., Quigley, M. E., Hudson, G. J., & Cummings, J. H. (1992). Determination of dietary fiber as nonstarch polysaccharides by gas-liquid-chromatography. *Analyst, 117*(11), 1707-1714. doi: 10.1039/an9921701707
Erk, K. A., Henderson, K. J., & Shull, K. R. (2010). Strain Stiffening in Synthetic and Biopolymer Networks. *Biomacromolecules, 11*(5), 1358-1363. doi: 10.1021/bm100136y
Erni, P., Varagnat, M., & McKinley, G. H. (2008). Little shop of horrors: Rheology of the mucilage of Drosera sp., a carnivorous plant. In A. Co, L. G. Leal, R. H. Colby & A. J. Giacomin (Eds.), *Xvth International Congress on Rheology - the Society of Rheology 80th Annual Meeting, Pts 1 and 2* (Vol. 1027, pp. 579-581).
Ewoldt, R. H., Clasen, C., Hosoi, A. E., & McKinley, G. H. (2007). Rheological fingerprinting of gastropod pedal mucus and synthetic complex fluids for biomimicking adhesive locomotion. *Soft Matter, 3*(5), 634-643. doi: 10.1039/b615546d
Ewoldt, R. H., Hosoi, A. E., & McKinley, G. H. (2008a). New measures for characterizing nonlinear viscoelasticity in large amplitude oscillatory shear. *Journal of Rheology, 52*(6), 1427-1458.

Ewoldt, R. H., Hosoi, A. E., & McKinley, G. H. (2008b). An ontology for large amplitude oscillatory shear flow. In A. Co, L. G. Leal, R. H. Colby & A. J. Giacomin (Eds.), *Xvth International Congress on Rheology - the Society of Rheology 80th Annual Meeting, Pts 1 and 2* (Vol. 1027, pp. 1135-1137).

Ewoldt, R. H., Hosoi, A. E., & McKinley, G. H. (2009). Nonlinear viscoelastic biomaterials: Meaningful characterization and engineering inspiration. *Integrative and Comparative Biology, 49*(1), 40-50.

Ewoldt, R. H., Winter, P., Maxey, J., & McKinley, G. H. (2010). Large amplitude oscillatory shear of pseudoplastic and elastoviscoplastic materials. *Rheologica Acta, 49*(2), 191-212.

Faipoux, R., Tome, D., Bensaid, A., Morens, C., Oriol, E., Bonnano, L. M., & Fromentin, G. (2006). Yeast proteins enhance satiety in rats. *Journal of Nutrition, 136*(9), 2350-2356.

Farhoosh, R., & Riazi, A. (2007). A compositional study on two current types of salep in Iran and their rheological properties as a function of concentration and temperature. *Food Hydrocolloids, 21*(4), 660-666.

Feng, Y., Grassl, B., Billon, L., Khoukh, A., & François, J. (2002). Effects of NaCl on steady rheological behaviour in aqueous solutions of hydrophobically modified polyacrylamide and its partially hydrolyzed analogues prepared by post-modification. *Polymer International, 51*(10), 939-947.

Fiszman, S., & Varela, P. (2013). The role of gums in satiety/satiation. A review. *Food Hydrocolloids, 32*(1), 147-154. doi: 10.1016/j.foodhyd.2012.12.010

Foster, T. (2008). *Plant heritage New Zealand: te whakapapa o nga rakua: interpreting the species features of native plants*. North Shore: Raupo.

French, S. J., & Read, N. W. (1994). Effect of guar gum on hunger and satiety after meals of differing fat content - relationship with gastric emptying. *American Journal of Clinical Nutrition, 59*(1), 87-91.

Galindo-Rosales, F. J., Rubio-Hernández, F. J., & Sevilla, A. (2011). An apparent viscosity function for shear thickening fluids. *Journal of Non-Newtonian Fluid Mechanics, 166*(5-6), 321-325.

Galindo-Rosales, F. J., Rubio-Hernández, F. J., Sevilla, A., & Ewoldt, R. H. (2011). How Dr. Malcom M. Cross may have tackled the development of " An apparent viscosity function for shear thickening fluids". *Journal of Non-Newtonian Fluid Mechanics, 166*(23-24), 1421-1424.

Gao, H. W., Yang, R. J., He, J. Y., & Yang, L. (2010). Rheological Behaviors of PVA/H2O Solutions of High-Polymer Concentration. *Journal of Applied Polymer Science, 116*(3), 1459-1466. doi: 10.1002/app.31677

Geng, M., Xu, M., Xiao, H., Wang, H., He, L., Zhao, Z., & Yu, M. (2011). Protective role of mucilage against Al toxicity to root apex of pea (Pisum sativum). *Acta Physiologiae Plantarum*, 1-6.

Goh, K. K. T. (2004). *Isolation and characterisation of bacterial exopolysaccharides produced by Lactobacillus delbrueckii subsp. bulgaricus NCFB 2483 and Sphingomonas elodea ATCC 31461e.* Massey University, Palmerston North.

Goh, K. K. T., Matia-Merino, L., Hall, C. E., Moughan, P. J., & Singh, H. (2007). Complex rheological properties of a water-soluble extract from the fronds of the black tree fern, Cyathea medullaris. *Biomacromolecules, 8*(11), 3414-3421. doi: 10.1021/bm7005328

Goh, K. K. T., Matia-Merino, L., Pinder, D. N., Saavedra, C., & Singh, H. (2011). Molecular characteristics of a novel water-soluble polysaccharide from the New Zealand black tree fern (Cyathea medullaris). *Food Hydrocolloids, 25*(3), 286-292. doi: 10.1016/j.foodhyd.2010.06.005

Gowda, D. C., Reuter, G., & Schauer, R. (1982). Structural features of an acidic polysaccharide from the mucin of Drosera binata. *Phytochemistry, 21*(9), 2297-2300.

Graessley, W. W. (1980). Polymer chain dimensions and the dependence of viscoelastic properties on concentration, molecular weight and solvent power. *Polymer, 21*(3), 258-262.

Grant, G. T., Morris, E. R., Rees, D. A., Smith, P. J. C., & Thom, D. (1973). Biological interactions between polysaccharides and divalent cations - egg-box model. *Febs Letters, 32*(1), 195-198. doi: 10.1016/0014-5793(73)80770-7

Green, M. S., & Tobolsky, A. V. (1946). A new approach to the theory of relaxing polymeric media. *Journal of Chemical Physics, 14*(2), 80-92. doi: 10.1063/1.1724109

Grosberg, A. Y., Nguyen, T. T., & Shklovskii, B. I. (2002). Colloquium: The physics of charge inversion in chemical and biological systems. *Reviews of Modern Physics, 74*(2), 329-345. doi: 10.1103/RevModPhys.74.329

Gunasekaran, S., & Ak, M. M. (2000). Dynamic oscillatory shear testing of foods - selected applications. *Trends in Food Science & Technology, 11*(3), 115-127. doi: 10.1016/s0924-2244(00)00058-3

Hammes, G. G., & Swann, J. C. (1967). Influence of denaturing agents on solvent structure. *Biochemistry, 6*(6), 1591-&. doi: 10.1021/bi00858a004

Hasler, W. L. (2008). Gastroparesis--current concepts and considerations. *Medscape journal of medicine, 10*(1), 16-16.

Haward, S. J., Odell, J. A., Berry, M., & Hall, T. (2011). Extensional rheology of human saliva. *Rheologica Acta, 50*(11-12), 869-879. doi: 10.1007/s00397-010-0494-1

Haward, S. J., Sharma, V., Butts, C. P., McKinley, G. H., & Rahatekar, S. S. (2012). Shear and Extensional Rheology of Cellulose/Ionic Liquid Solutions. *Biomacromolecules, 13*(5), 1688-1699. doi: 10.1021/bm300407q

Higgs, P. G., & Ball, R. C. (1989). Formation of gels and complexes by pairwise interacting polymers. *Journal De Physique, 50*(21), 3285-3308. doi: 10.1051/jphys:0198900500210328500

Hoad, C. L., Rayment, P., Spiller, R. C., Marciani, L., Alonso, B. D., Traynor, C., . . . Gowland, P. A. (2004). In vivo imaging of intragastric gelation and its effect on satiety in humans. *Journal of Nutrition, 134*(9), 2293-2300.

Honda, Y., Inaoka, H., Takei, A., Sugimura, Y., & Otsuji, K. (1996). Extracellular polysaccharides produced by tuberose callus. *Phytochemistry, 41*(6), 1517-1521.

Hsiao, P. Y. (2006). Chain morphology, swelling exponent, persistence length, like-charge attraction, and charge distribution around a chain in polyelectrolyte solutions: Effects of salt concentration and ion size studied by molecular dynamics simulations. *Macromolecules, 39*(20), 7125-7137. doi: Ma0609782

10.1021/ma0609782

Hsiao, P. Y. (2008). Overcharging, charge inversion, and reentrant condensation: Using highly charged polyelectrolytes in tetravalent salt solutions as an example of study. *Journal of Physical Chemistry B, 112*(25), 7347-7350. doi: 10.1021/jp800331b

Hsiao, P. Y., & Luijten, E. (2006). Salt-induced collapse and reexpansion of highly charged flexible polyelectrolytes. *Physical Review Letters, 97*(14).

Hu, Y., Wang, S. Q., & Jamieson, A. M. (1995). Rheological and rheooptical studies of shear-thickening polyacrylamide solutions. *Macromolecules, 28*(6), 1847-1853.

Huggins, M. L. (1942). The viscosity of dilute solutions of long-chain molecules. IV. Dependence on concentration. *Journal of the American Chemical Society, 64*, 2716-2718. doi: 10.1021/ja01263a056

Hwang, J. W., & Kokini, J. L. (1991). Structure and rheological function of side branches of carbohydrate polymers. *Journal of Texture Studies, 22*(2), 123-167. doi: 10.1111/j.1745-4603.1991.tb00011.x

Hyun, K., Kim, S. H., Ahn, K. H., & Lee, S. J. (2002). Large amplitude oscillatory shear as a way to classify the complex fluids. *Journal of Non-Newtonian Fluid Mechanics, 107*(1-3), 51-65.

Indei, T., Koga, T., & Tanaka, F. (2005). Theory of shear-thickening in transient networks of associating polymers. *Macromolecular Rapid Communications, 26*(9), 701-706.

Israelachvili, J. N. (2011). *Intermolecular and surface forces* (3rd ed.): Acedemic Press.

Izydorczyk, M. (2005). Understanding the chemistry of food carbohydrates *Food carbohydrates*: CRC Press.

Jacques, L., & Jean-Louis, D. (2004). Rheological Behavior of Polysaccharides Aqueous Systems *Polysaccharides*: CRC Press.

Jahanbin, K., Moini, S., Gohari, A. R., Emam-Djomeh, Z., & Masid, P. (2012). Isolation, purification and characterization of a new gum from Acanthophyllum bracteatum roots. *Food Hydrocolloids, 27*(1), 14-21. doi: 10.1016/j.foodhyd.2011.09.007

Jaishankar, A., & McKinley, G. H. (2013). Power-law rheology in the bulk and at the interface: quasi-properties and fractional constitutive equations. *Proceedings of the Royal Society a-Mathematical Physical and Engineering Sciences, 469*(2149).

James, D. F., & Sridhar, T. (1995). Molecular conformation during steady state measurements of extensional viscosity. *Journal of Rheology, 39*(4), 713-724. doi: 10.1122/1.550653

Jan, J.-S., & Breedveld, V. (2008). Microrheological study of polyelectrolyte collapse and reexpansion in the presence of multivalent counterions. *Macromolecules, 41*(17), 6517-6522. doi: 10.1021/ma8002714

Jani, G. K., Shah, D. P., Prajapatia, V. D., & Jain, V. C. (2009). Gums and mucilages: Versatile excipients for pharmaceutical formulations. *Asian Journal of Pharmaceutical Sciences, 4*(5), 309-323.

Japper-Jaafar, A., Escudier, M. P., & Poole, R. J. (2009). Turbulent pipe flow of a drag-reducing rigid "rod-like" polymer solution. *Journal of Non-Newtonian Fluid Mechanics, 161*(1-3), 86-93. doi: 10.1016/j.jnnfm.2009.04.008

Jiang, W., Sun, Y., Xu, Y., Peng, C., Gong, X., & Zhang, Z. (2010). Shear-thickening behavior of polymethylmethacrylate particles suspensions in glycerine-water mixtures. *Rheologica Acta, 49*(11), 1157-1163.

Jin, L., Shangguan, Y., Ye, T., Yang, H., An, Q., & Zheng, Q. (2013). Shear induced self-thickening in chitosan-grafted polyacrylamide aqueous solution. *Soft Matter, 9*(6), 1835-1843. doi: 10.1039/c2sm27404c

Jonsson, H. (2010). *Exploring the structure of oligo- and polysaccharides.* Stockholm University, Stockholm, Sweden.

Karazhiyan, H., Razavi, S. M. A., Phillips, G. O., Fang, Y., Al-Assaf, S., Nishinari, K., & Farhoosh, R. (2009). Rheological properties of Lepidium sativum seed extract as a function of concentration, temperature and time. *Food Hydrocolloids, 23*(8), 2062-2068. doi: 10.1016/j.foodhyd.2009.03.019

Kaur, L., Singh, J., & Singh, H. (2009). Characterization of gum ghatti (Anogeissus latifolia): A structural and rheological approach. *Journal of Food Science, 74*(6), E328-E332.

Kheirandish, S., Guybaidullin, I., Wohlleben, W., & Willenbacher, N. (2008). Shear and elongational flow behavior of acrylic thickener solutions Part I: Effect of intermolecular aggregation. *Rheologica Acta, 47*(9), 999-1013. doi: 10.1007/s00397-008-0292-1

Kim, J. B., & Carpita, N. C. (1992). Changes in esterification of the uronic acid groups of cell wall polysaccharides during elongation of maize coleoptiles. *Plant Physiology, 98*(2), 646-653. doi: 10.1104/pp.98.2.646

Kim, S., Willett, J. L., Carriere, C. J., & Felker, F. C. (2002). Shear-thickening and shear-induced pattern formation in starch solutions. *Carbohydrate Polymers, 47*(4), 347-356.

Kinraide, T. B., Parker, D. R., & Zobel, R. W. (2005). Organic acid secretion as a mechanism of aluminium resistance: A model incorporating the root cortex, epidermis, and the external unstirred layer. *Journal of experimental botany, 56*(417), 1853-1865.

Kishbaugh, A. J., & McHugh, A. J. (1993). A rheo-optical study of shear-thickening and structure formation in polymer solutions. Part II: Light scattering analysis. *Rheologica Acta, 32*(2), 115-131.

Kjoniksen, A. L., Hiorth, M., & Nystrom, B. (2005). Association under shear flow in aqueous solutions of pectin. *European Polymer Journal, 41*(4), 761-770. doi: 10.1016/j.eurpolymj.2004.11.006

Kjøniksen, A. L., Hiorth, M., & Nyström, B. (2005). Association under shear flow in aqueous solutions of pectin. *European Polymer Journal, 41*(4), 761-770.

Kjøniksen, A. L., Hiorth, M., Roots, J., & Nyström, B. (2003). Shear-induced association and gelation of aqueous solutions of pectin. *Journal of Physical Chemistry B, 107*(26), 6324-6328.

Koga, T., & Tanaka, F. (2005). Molecular origin of shear thickening in transient polymer networks: a molecular dynamics study. *The European physical journal. E, Soft matter, 17*(2), 115-118. doi: 10.1140/epje/i2005-10010-2

Koga, T., & Tanaka, F. (2010). Theoretical predictions on normal stresses under shear flow in transient networks of telechelic associating polymers. *Macromolecules, 43*(6), 3052-3060.

Koliandris, A.-L. (2010). *Flow behaviour of biopolymer solutions and effect on saltiness perception.* University of Nottingham, Loughborough.

Kosvintsev, S. R., Riande, E., Velarde, M. G., & Guzman, J. (2001). Rheological behaviour of solutions of poly(2-hydroxyethyl methacrylamide) in glycerine. *Polymer, 42*(17), 7395-7401. doi: 10.1016/s0032-3861(01)00195-1

Kozu, H., Kobayashi, I., Nakajima, M., Uemura, K., Sato, S., & Ichikawa, S. (2010). Analysis of Flow Phenomena in Gastric Contents Induced by Human Gastric Peristalsis Using CFD. *Food Biophysics, 5*(4), 330-336. doi: 10.1007/s11483-010-9183-y

Kraemer, E. O. (1938). Molecular weights of celluloses. *Industrial and Engineering Chemistry, 30*, 1200-1203. doi: 10.1021/ie50346a023

Kulicke, W.-M., & Clasen, C. (2004). *Viscosimetry of Polymers and Polyelectrolytes*. Berlin: Springer.

Kurniawan, N. A., Wong, L. H., & Rajagopalan, R. (2012). Early Stiffening and Softening of Collagen: Interplay of Deformation Mechanisms in Biopolymer Networks. *Biomacromolecules, 13*(3), 691-698. doi: 10.1021/bm2015812

Lacombe, C., & Essabbah, H. (1981). Comparative haemorheology of pathological blood. *Scandinavian Journal of Clinical & Laboratory Investigation, 41*(s156), 249-250. doi: doi:10.3109/00365518109097478

Lai, L. S., & Liang, H. Y. (2012). Chemical compositions and some physical properties of the water and alkali-extracted mucilage from the young fronds of Asplenium australasicum (J. Sm.) Hook. *Food Hydrocolloids, 26*(2), 344-349.

Lapasin, R., & Pricl, S. (1999). *Rheology of industrial polysaccharides*. Britain: Blackie Academic & Professional.

Laufer, Z., Jalink, H. L., & Staverma.Aj. (1973). Time-dependence of shear and normal stresses of polystyrene and poly(ethylene oxide) solutions. *Journal of Polymer Science Part a-Polymer Chemistry, 11*(11), 3005-3015. doi: 10.1002/pol.1973.170111119

Leibler, L., Rubinstein, M., & Colby, R. H. (1991). Dynamics of reversible networks. *Macromolecules, 24*(16), 4701-4707.

Lele, A. K., & Mashelkar, R. A. (1998). Energetically crosslinked transient network (ECTN) model: implications in transient shear and elongation flows. *Journal of Non-Newtonian Fluid Mechanics, 75*(1), 99-115. doi: 10.1016/s0377-0257(97)00070-0

Lentle, R. G., & Janssen, P. W. M. (2011). *The Physical Processes of Digestion*: Springer.

Lentle, R. G., Janssen, P. W. M., Goh, K., Chambers, P., & Hulls, C. (2010). Quantification of the effects of the volume and viscosity of gastric contents on antral and fundic activity in the rat stomach maintained ex vivo. *Digestive Diseases and Sciences, 55*(12), 3349-3360.

Lewandowska, K. (2007). Comparative studies of rheological properties of polyacrylamide and partially hydrolyzed polyacrylamide solutions. *Journal of Applied Polymer Science, 103*(4), 2235-2241. doi: 10.1002/app.25247

Li, Z., Jiang, D., Bi, H., Liu, D., Jang, S., & Zhou, Y. (2012). Preparation of a Novel Glucuronomannan from Auricularia auricala and its Immunological Activity. *Natural Product Communications, 7*(11), 1507-1510.

Liang, R. F., & Mackley, M. R. (1994). Rheological characterization of the time and strain dependence of polyisobutylene solutions. *Journal of Non-Newtonian Fluid Mechanics, 52*(3), 387-405. doi: 10.1016/0377-0257(94)85031-3

Lin, K. Y., Daniel, J. R., & Whistler, R. L. (1994). Structure of chia seed polysaccharide exudate. *Carbohydrate Polymers, 23*(1), 13-18.

Liu, S., Ghosh, K., & Muthukumar, M. (2003). Polyelectrolyte solutions with added salt: A simulation study. *Journal of Chemical Physics, 119*(3), 1813-1823. doi: 10.1063/1.1580109

Ma, L. L., Xu, J. Y., Coulombe, P. A., & Wirtz, D. (1999). Keratin filament suspensions show unique micromechanical properties. *Journal of Biological Chemistry, 274*(27), 19145-19151. doi: 10.1074/jbc.274.27.19145

Ma, S. X., & Cooper, S. L. (2001). Shear thickening in aqueous solutions of hydrocarbon end-capped poly(ethylene oxide). *Macromolecules, 34*(10), 3294-3301.

Mackie, A. R., Rafiee, H., Malcolm, P., Salt, L., & van Aken, G. (2013). Specific food structures supress appetite through reduced gastric emptying rate. *American Journal of Physiology-Gastrointestinal and Liver Physiology, 304*(11), G1038-G1043. doi: 10.1152/ajpgi.00060.2013

Mackley, M. R., Tock, C., Anthony, R., Butler, S. A., Chapman, G., & Vadillo, D. C. (2013). The rheology and processing behavior of starch and gum-based dysphagia thickeners. *Journal of Rheology, 57*(6), 1533-1553. doi: 10.1122/1.4820494

Macosko, C. W. (1994). *Rheology principles, measurements and applications*: VCH Publishers.

Maleki, A., Kjoniksen, A.-L., & Nystrom, B. (2007). Anomalous viscosity behavior in aqueous solutions of hyaluronic acid. *Polymer Bulletin, 59*(2), 217-226. doi: 10.1007/s00289-007-0760-2

Malkin, A. Y., & Isayev, A. I. (2012). *Rheology: concepts, methods and applications*. Toronto: ChemTec Pub.

Marathe, C. S., Rayner, C. K., Jones, K. L., & Horowitz, M. (2013). Relationships Between Gastric Emptying, Postprandial Glycemia, and Incretin Hormones. *Diabetes Care, 36*(5), 1396-1405. doi: 10.2337/dc12-1609

Marciani, L., Gowland, P. A., Spiller, R. C., Manoj, P., Moore, R. J., Young, P., & Fillery-Travis, A. J. (2001). Effect of meal viscosity and nutrients on satiety, intragastric dilution, and emptying assessed by MRI. *American Journal of Physiology-Gastrointestinal and Liver Physiology, 280*(6), G1227-G1233.

Marcus, Y. (1988). Ionic radii in aqueous solutions. *Chemical Reviews, 88*(8), 1475-1498. doi: 10.1021/cr00090a003

Marrucci, G., Bhargava, S., & Cooper, S. L. (1993). Models of shear-thickening behavior in physically cross-linked networks. *Macromolecules, 26*(24), 6483-6488.

Marvelys, L., Maritza, M., Lilian, S., Depintogladys, L., & Julio, H. (2006). Structural elucidation of the polysaccharide from Sterculia apetala gum by a combination of chemical methods and NMR spectroscopy. *Food Hydrocolloids, 20*(6), 908-913. doi: 10.1016/j.foodhyd.2005.09.005

Matia-Merino, L., Goh, K. K. T., & Singh, H. (2012). A natural shear-thickening water-soluble polymer from the fronds of the black tree fern, Cyathea medullaris: Influence of salt, pH and temperature. *Carbohydrate Polymers, 87*(1), 131-138. doi: 10.1016/j.carbpol.2011.07.027

Mattes, R. D., & Rothacker, D. (2001). Beverage viscosity is inversely related to postprandial hunger in humans. *Physiology & Behavior, 74*(4-5), 551-557. doi: 10.1016/s0031-9384(01)00597-2

McConnell, E. L., Basit, A. W., & Murdan, S. (2008). Measurements of rat and mouse gastrointestinal pH fluid and lymphoid tissue, and implications for in-vivo experiments. *Journal of Pharmacy and Pharmacology, 60*(1), 63-70. doi: 10.1211/jpp.60.1.0008

McIntyre, K. (2001). Rodent gavage technique concerns: Avoiding excess mortality. *Contemporary Topics in Laboratory Animal Science, 40*(4), 7-7.

McKinley, G. H., & Sridhar, T. (2002). Filament-stretching rheometry of complex fluids. *Annual Review of Fluid Mechanics, 34*, 375-415. doi: 10.1146/annurev.fluid.34.083001.125207

Melton, L. D., & Smith, B. G. (2001). Isolation of Plant Cell Walls and Fractionation of Cell Wall Polysaccharides *Current Protocols in Food Analytical Chemistry*: John Wiley & Sons, Inc.

Mezger, T. G. (2011). *The Rheology Handbook* (3rd ed.). Hanover: Vincentz Network.

Michael, G., & Reid, J. G. (2006). Galactomannans and Other Cell Wall Storage Polysaccharides in Seeds *Food Polysaccharides and Their Applications* (pp. 181-215): CRC Press.

Mirhosseini, H., & Amid, B. T. (2012). A review study on chemical composition and molecular structure of newly plant gum exudates and seed gums. *Food Research International, 46*(1), 387-398.

Miri, T. (2010). Viscosity and Oscillatory Rheology. In I. T. Norton, F. Spyropoulos & P. Cox (Eds.), *Practical Food Rheology - An Interpretive Approach*: John Wiley & Sons.

Morris, E. R. (1989). Polysaccharide solution properties: origin, rheological and characterization and implications for food systems. In R. P. Millane, J. BeMiller & R. Chandrasekaran (Eds.), *Frontiers in carbohydrate research, 1: Food applications* (pp. 132-163). London: Elsevier applied science.

Morris, E. R., Cutler, A. N., Ross-Murphy, S. B., Rees, D. A., & Price, J. (1981). Concentration and shear rate dependence of viscosity in random coil polysaccharide solutions. *Carbohydrate Polymers, 1*(1), 5-21. doi: 10.1016/0144-8617(81)90011-4

Mucha, M. (1998). Rheological properties of chitosan blends with poly(ethylene oxide) and poly(vinyl alcohol) in solution. *Reactive & Functional Polymers, 38*(1), 19-25. doi: 10.1016/s1381-5148(98)00028-5

Munoz, M. E., & Santamaria, A. (2003). Enhancement of the first normal stress coefficient and dynamic moduli during shear thickening of a polymer solution. *Journal of Rheology, 47*(4), 1041-1050.

Nahar, N., Hazra, B. K., Mosihuzzaman, M., Mahbubur Rahman, M., & Andersson, R. (1994). Structural studies of a mucilage from Abroma augusta root bark. *Carbohydrate Polymers, 24*(4), 277-280.

Neelamegam, R., Shankar, V., & Das, D. (2013). Suppression of purely elastic instabilities in the torsional flow of viscoelastic fluid past a soft solid. *Physics of Fluids, 25*(12). doi: 10.1063/1.4840195

Nep, E. I., & Conway, B. R. (2010). Characterization of Grewia Gum, a potential pharmaceutical excipient. *Journal of Excipients and Food Chemicals, 1*(1), 30-40.

Nguyen Tien, A., Do Truong, T., Nguyen Thi, D., Pham Le, D., & Nguyen Van, D. (2011). Isolation and characteristics of polysaccharide from Amorphophallus corrugatus in Vietnam. *Carbohydrate Polymers, 84*(1), 64-68. doi: 10.1016/j.carbpol.2010.10.074

Nguyen, T. T., Rouzina, I., & Shklovskii, B. I. (2000). Reentrant condensation of DNA induced by multivalent counterions. *Journal of Chemical Physics, 112*(5), 2562-2568. doi: 10.1063/1.480819

Nightingale, E. R. (1959). Phenomenological theory of ion solvation - effective radii of hydrated ions. *Journal of Physical Chemistry, 63*(9), 1381-1387. doi: 10.1021/j150579a011

Niklas, K. K., & Spatz, H.-C. (2012). *Plant Physics*. Chicago: University of Chicago Press.

Nwokocha, L. M., & Williams, P. A. (2012). Rheological characterization of the galactomannan from Leucaena leucocephala seed. *Carbohydrate Polymers, 90*(2), 833-838. doi: 10.1016/j.carbpol.2012.06.008

Nystrom, B., Kjoniksen, A.-L., Beheshti, N., Zhu, K., & Knudsen, K. D. (2009). Rheological and structural aspects on association of hydrophobically modified polysaccharides. *Soft Matter, 5*(7), 1328-1339. doi: 10.1039/b817349d

Oakenfull, D. (1998). Polysaccharide molecular structures. In R. Walter (Ed.), *Polysaccharide association structures in food*. New York: Marcel Dekker.

Oakenfull, D., & Fenwick, D. E. (1977). Thermodynamics and mechanism of hydrophobic interaction. *Australian Journal of Chemistry, 30*(4), 741-752.

Oakenfull, D., & Scott, A. (1984). Hydrophobic interaction in the gelation of high methoxyl pectins. *Journal of Food Science, 49*(4), 1093-1098. doi: 10.1111/j.1365-2621.1984.tb10401.x

Oakley, J. G., Giacomin, A. J., & Yosick, J. A. (1998). Molecular origins of nonlinear viscoelasticity. *Mikrochimica Acta, 130*(1-2), 1-28. doi: 10.1007/bf01254586

Oelschlaeger, C., Coelho, M. C. P., & Willenbacher, N. (2013). Chain Flexibility and Dynamics of Polysaccharide Hyaluronan in Entangled Solutions: A High Frequency Rheology and Diffusing Wave Spectroscopy Study. *Biomacromolecules, 14*(10), 3689-3696. doi: 10.1021/bm4010436

Okva, K., Tamoseviciute, E., Ciziute, A., Pokk, P., Ruksenas, O., & Nevalainen, T. (2006). Refinements for intragastric gavage in rats. *Scandinavian Journal of Laboratory Animal Science, 33*(4), 243-252.

Olvera De La Cruz, M., Belloni, L., Delsanti, M., Dalbiez, J. P., Spalla, O., & Drifford, M. (1995). Precipitation of highly charged polyelectrolyte solutions in the presence of multivalent salts. *The Journal of Chemical Physics, 103*(13), 5781-5791.

Padmanabhan, M. (2010). Extensional rheology. In D. R. Heldman (Ed.), *Encyclopaedia of agricultural, food and biological engineering*. Boca Raton, FL: CRC Press.

Paeschke, T. M., & Aimutis, W. R. (2011). *Nondigestible Carbohydrates and Digestive Health*: John Wiley & Sons.

Pellens, L., Corrales, R. G., & Mewis, J. (2004). General nonlinear rheological behavior of associative polymers. *Journal of Rheology, 48*(2), 379-393.

Pendrill, R., Sawen, E., & Widmalm, G. (2013). Conformation and Dynamics at a Flexible Glycosidic Linkage Revealed by NMR Spectroscopy and Molecular Dynamics Simulations: Analysis of beta-L-Fucp-(1 -> 6)-alpha-D-Glcp-OMe in Water Solution. *Journal of Physical Chemistry B, 117*(47), 14709-14722. doi: 10.1021/jp409985h

Perlin, A. S., & Casu, B. (1982). Spectroscopic Methods. In G. O. Aspinall (Ed.), *The Polysaccharides* (pp. 133-191). New York: Academic Press.

Pettolino, F. A., Walsh, C., Fincher, G. B., & Bacic, A. (2012). Determining the polysaccharide composition of plant cell walls. *Nature Protocols, 7*(9), 1590-1607. doi: 10.1038/nprot.2012.081

Pieter, W. (2003). *Physical chemistry in foods*. New York: Marcel Dekker Inc.

Porter, R. S., & Johnson, J. F. (1966). Entanglement concept in polymer systems. *Chemical Reviews, 66*(1), 1-&. doi: 10.1021/cr60239a001

Pranprawit, A., Wolber, F. M., Heyes, J. A., Molan, A. L., & Kruger, M. C. (2013). Short-term and long-term effects of excessive consumption of saturated fats and/or sucrose on metabolic variables in Sprague Dawley rats: a pilot study. *Journal of the Science of Food and Agriculture, 93*(13), 3191-3197. doi: 10.1002/jsfa.6240

Pu, Q., Ng, S., Mok, V., & Chen, S. B. (2004). Ion bridging effects on the electroviscosity of flexible polyelectrolytes. *Journal of Physical Chemistry B, 108*(37), 14124-14129. doi: 10.1021/jp0486200

Raghavan, S. R., & Khan, S. A. (1997). Shear-thickening response of fumed silica suspensions under steady and oscillatory shear. *Journal of Colloid and Interface Science, 185*(1), 57-67. doi: 10.1006/jcis.1996.4581

Rao, M., & Silva, J. L. d. (2006). Pectins *Food Polysaccharides and Their Applications* (pp. 353-411): CRC Press.

Rasoamanana, R., Even, P. C., Darcel, N., Tome, D., & Fromentin, G. (2013). Dietary fibers reduce food intake by satiation without conditioned taste aversion in mice. *Physiology & Behavior, 110*, 13-19. doi: 10.1016/j.physbeh.2012.12.008

Razavi, S. M. A., Taheri, H., & Sanchez, R. (2013). Viscoelastic Characterization of Sage Seed Gum. *International Journal of Food Properties, 16*(7), 1604-1619. doi: 10.1080/10942912.2011.604888

Reddy, K., Mohan, G. K., Satla, S., & Gaikwad, S. (2011). Natural polysaccharides: Versatile excipients for controlled drug delivery systems. *Asian Journal of Pharmaceutical Sciences, 6*(6), 275-286.

Redgwell, R. J. (1983). Composition of Actinidia mucilage. *Phytochemistry, 22*(4), 951-956.

Redgwell, R. J., O'Neill, M. A., Selvendran, R. R., & Parsley, K. J. (1986a). Structural features of the mucilage from the stem pith of kiwifruit (acitinidia deliciosa): part II, structure of the neutral oligosaccharides. *Carbohydrate research, 153*(1), 107-118.

Redgwell, R. J., O'Neill, M. A., Selvendran, R. R., & Parsley, K. J. (1986b). Structural features of the mucilage from the stem pith of kiwifruit (actinidia deliciosa): part I, structure of the inner core. *Carbohydrate research, 153*(1), 97-106.

Rendleman, J. A. (1978a). Metal-polysaccharide complexes part I. *Food Chemistry, 3*(1), 47-79. doi: 10.1016/0308-8146(78)90047-x

Rendleman, J. A. (1978b). Metal-polysaccharide complexes part II. *Food Chemistry, 3*(2), 127-162. doi: 10.1016/0308-8146(78)90031-6

Rigaud, D., Paycha, F., Meulemans, A., Merrouche, M., & Mignon, M. (1998). Effect of psyllium on gastric emptying, hunger feeling and food intake in normal volunteers: a double blind study. *European Journal of Clinical Nutrition, 52*(4), 239-245. doi: 10.1038/sj.ejcn.1600518

Rinaudo, M. (2009). Polyelectrolyte properties of a plant and animal polysaccharide. *Structural Chemistry, 20*(2), 277-289. doi: 10.1007/s11224-009-9426-z

Rivero, D., Gouveia, L. M., Mueller, A. J., & Saez, A. E. (2012). Shear-thickening behavior of high molecular weight poly(ethylene oxide) solutions. *Rheologica Acta, 51*(1), 13-20. doi: 10.1007/s00397-011-0569-7

Rochefort, W. E., & Middleman, S. (1987). Rheology of xanthan gum - salt, temperature and strain effects in oscillatory and steady shear experiments. *Journal of Rheology, 31*(4), 337-369. doi: 10.1122/1.549953

Rodd, L. E., Scott, T. P., Cooper-White, J. J., & McKinley, G. H. (2005). Capillary break-up rheometry of low-viscosity elastic fluids. *Applied Rheology, 15*(1), 12-27.

Rose, E. F. (1979). Factors influencing gastric emptying *Journal of Forensic Sciences, 24*(1), 200-206.

Rossky, P. J. (2008). Protein denaturation by urea: Slash and bond. *Proceedings of the National Academy of Sciences of the United States of America, 105*(44), 16825-16826. doi: 10.1073/pnas.0809224105

Sabatié, J., Choplin, L., Paul, F., & Monsan, P. (1986). Shear-induced structure in enzymatically-synthesized dextran solutions. *Rheologica Acta, 25*(3), 287-295.

Savins, J. G. (1968). Shear thickening phenomena in poly(vinyl)alcohol-borate complexes. *Rheologica Acta, 7*(1), 87-93.

Schroeder, N., Marquart, L. F., & Gallaher, D. D. (2013). The Role of Viscosity and Fermentability of Dietary Fibers on Satiety- and Adiposity-Related Hormones in Rats. *Nutrients, 5*(6), 2093-2113. doi: 10.3390/nu5062093

Semmrich, C., Larsen, R. J., & Bausch, A. R. (2008). Nonlinear mechanics of entangled F-actin solutions. *Soft Matter, 4*(8), 1675-1680. doi: 10.1039/b800989a

Serge, P., & Karim, M. (2004). Conformations, Structures, and Morphologies of Celluloses *Polysaccharides*: CRC Press.

Shaw, M. T. (2012). *Introduction to polymer rheology*. New Jersey: John Wiley and Sons.

Sherwood, L. (1993). *Human physiology : from cells to systems*. Minneapolis: West Pub. Co.

Sim, H. G., Ahn, K. H., & Lee, S. J. (2003). Large amplitude oscillatory shear behavior of complex fluids investigated by a network model: a guideline for classification. *Journal of Non-Newtonian Fluid Mechanics, 112*(2-3), 237-250. doi: 10.1016/s0377-0257(03)00102-2

Sims, I. M., & Bacic, A. (1995). Extracellular polysaccharides from suspension cultures of Nicotiana plumbaginifolia. *Phytochemistry, 38*(6), 1397-1405.
Sims, I. M., & Furneaux, R. H. (2003). Structure of the exudate gum from Meryta sinclairii. *Carbohydrate Polymers, 52*(4), 423-431.
Sims, I. M., & Newman, R. (2006). Structural studies of acidic xylans exuded from leaves of the monocotyledonous plants Phormium tenax and Phormium cookianum. *Carbohydrate Polymers, 63*(3), 379-384. doi: 10.1016/j.carbpol.2005.09.021
Slavin, J., & Green, H. (2007). Dietary fibre and satiety. *Nutrition Bulletin, 32*(Suppl.1), 32-42. doi: 10.1111/j.1467-3010.2007.00603.x
Slavin, J. L., Savarino, V., Paredes-Diaz, A., & Fotopoulos, G. (2009). A Review of the Role of Soluble Fiber in Health with Specific Reference to Wheat Dextrin. *Journal of International Medical Research, 37*(1), 1-17.
Smidsrod, O., & Haug, A. (1967). Precipitation of acidic polysaccharides by salts in ethanol-water mixtures. *Journal of Polymer Science Part C-Polymer Symposium*(16PC), 1587-&.
Smith, D. E., & Chu, S. (1998). Response of flexible polymers to a sudden elongational flow. *Science, 281*(5381), 1335-1340. doi: 10.1126/science.281.5381.1335
Smolka, L. B., & Belmonte, A. (2006). Charge screening effects on filament dynamics in xanthan gum solutions. *Journal of Non-Newtonian Fluid Mechanics, 137*(1-3), 103-109. doi: 10.1016/j.jnnfm.2006.01.012
Solah, V. A., Kerr, D. A., Adikara, C. D., Meng, X., Binns, C. W., Zhu, K., . . . Prince, R. L. (2010). Differences in satiety effects of alginate- and whey protein-based foods. *Appetite, 54*(3), 485-491. doi: 10.1016/j.appet.2010.01.019
Song, K. W., Kuk, H. Y., & Chang, G. S. (2006). Rheology of concentrated xanthan gum solutions: Oscillatory shear flow behavior. *Korea-Australia Rheology Journal, 18*(2), 67-81.
Staub, A. M. (1971). Removal of proteins. In R. L. Whistler (Ed.), *Methods in Carbohydrate Chemistry* (Vol. 5). New York: Academic Press.
Stelter, M., Brenn, G., Yarin, A. L., Singh, R. P., & Durst, F. (2002). Investigation of the elongational behavior of polymer solutions by means of an elongational rheometer. *Journal of Rheology (1978-present), 46*(2), 507-527.
Stern, J. S., & Kazaks, A. (2009). *Obesity: A Reference Handbook*: ABC-CLIO.
Steve, C., & Qi, W. (2005a). Understanding the Conformation of Polysaccharides *Food Carbohydrates*: CRC Press.
Steve, C., & Qi, W. (2005b). Understanding the Physical Properties of Food Polysaccharides *Food Carbohydrates*: CRC Press.
Steve, C., & Yolanda, B. (2006). Detection and Determination of Polysaccharides in Foods *Food Polysaccharides and Their Applications* (pp. 675-712): CRC Press.
Storm, C., Pastore, J. J., MacKintosh, F. C., Lubensky, T. C., & Janmey, P. A. (2005). Nonlinear elasticity in biological gels. *Nature, 435*(7039), 191-194. doi: 10.1038/nature03521
Suzuki, S., Uneyama, T., & Watanabe, H. (2013). Concentration Dependence of Nonlinear Rheological Properties of Hydrophobically Modified Ethoxylated Urethane Aqueous Solutions. *Macromolecules, 46*(9), 3497-3504. doi: 10.1021/ma400429y
Tam, K. C., Jenkins, R. D., Winnik, M. A., & Bassett, D. R. (1998). A structural model of hydrophobically modified urethane-ethoxylate (HEUR) associative polymers in shear flows. *Macromolecules, 31*(13), 4149-4159.
Tan, H., Tam, K. C., & Jenkins, R. D. (2001). Network structure of a model HASE polymer in semidilute salt solutions. *Journal of Applied Polymer Science, 79*(8), 1486-1496. doi: 10.1002/1097-4628(20010222)79:8<1486::aid-app160>3.3.co;2-#
Tan, H., Tam, K. C., Tirtaatmadja, V., Jenkins, R. D., & Bassett, D. R. (2000). Extensional properties of model hydrophobically modified alkali-soluble associative (HASE) polymer solutions. *Journal of Non-Newtonian Fluid Mechanics, 92*(2-3), 167-185. doi: 10.1016/s0377-0257(00)00093-8
Tanaka, F., & Edwards, S. F. (1992). Viscoelastic properties of physically cross-linked networks. Transient network theory. *Macromolecules, 25*(5), 1516-1523.
TAPPI. (1985). *TAPPI standards method T 249 cm-85, carbohydrate composition of extractive-free wood and wood pulp by gas-liquid chromatography*.
Tepale, N., Macias, E. R., Bautista, F., Puig, J. E., Manero, O., Gradzielski, M., & Escalante, J. I. (2011). Effects of electrolyte concentration and counterion valence on the microstructural flow regimes in dilute cetyltrimethylammonium tosylate micellar solutions. *Journal of Colloid and Interface Science, 363*(2), 595-600. doi: 10.1016/j.jcis.2011.07.051
Tirtaatmadja, V., McKinley, G. H., & Cooper-White, J. J. (2006). Drop formation and breakup of low viscosity elastic fluids: Effects of molecular weight and concentration. *Physics of Fluids, 18*(4).

Tirtaatmadja, V., Tam, K. C., & Jenkins, R. D. (1997). Superposition of oscillations on steady shear flow as a technique for investigating the structure of associative polymers. *Macromolecules, 30*(5), 1426-1433. doi: 10.1021/ma960098v

Tiwary, C. M., Ward, J. A., & Jackson, B. A. (1997). Effect of pectin on satiety in healthy US Army adults. *Journal of the American College of Nutrition, 16*(5), 423-428.

Tomlin, J., Brown, N., Ellis, A., Carlsson, A., Bogentoft, C., & Read, N. W. (1993). The effect of liquid fiber on gastric emptying in the rat and humans and the distribution of small-intestinal contents in the rat. *Gut, 34*(9), 1177-1181. doi: 10.1136/gut.34.9.1177

Trinh, K. T., & Trinh, B. (2009). *Practical rheology with special references to food*. Palmerston North: Institute of Food, Nutrition and Human Health, Massey University.

Tripathi, A., Tam, K. C., & McKinley, G. H. (2006). Rheology and dynamics of associative polymers in shear and extension: Theory and experiments. *Macromolecules, 39*(5), 1981-1999.

Tung, S.-H., & Raghavan, S. R. (2008). Strain-stiffening response in transient networks formed by reverse wormlike micelles. *Langmuir, 24*(16), 8405-8408. doi: 10.1021/la704045t

Turner, P. V., Vaughn, E., Sunohara-Neilson, J., Ovari, J., & Leri, F. (2012). Oral Gavage in Rats: Animal Welfare Evaluation. *Journal of the American Association for Laboratory Animal Science, 51*(1), 25-30.

Van Egmond, J. W. (1998). Shear-thickening in suspensions, associating polymers, worm-like micelles, and poor polymer solutions. *Current Opinion in Colloid and Interface Science, 3*(4), 385-390.

van Nieuwenhoven, M. A., Kovacs, E. M., Brummer, R. J. M., Westerterp-Plantenga, M. S., & Brouns, F. (2001). The effect of different dosages of guar gum on gastric emptying and small intestinal transit of a consumed semisolid meal. *Journal of the American College of Nutrition, 20*(1), 87-91.

Vasudevan, M., Shen, A., Khomami, B., & Sureshkumar, R. (2008). Self-similar shear thickening behavior in CTAB/NaSal surfactant solutions. *Journal of Rheology, 52*(2), 527-550. doi: 10.1122/1.2833594

Vijayanathan, V., Thomas, T., & Thomas, T. J. (2002). DNA nanoparticles and development of DNA delivery vehicles for gene therapy. *Biochemistry, 41*(48), 14085-14094. doi: 10.1021/bi0203987

Vrblac, M., & Sostar Turk, S. (2000). Mixed synthetic and polysaccharide thickeners in reactive printing. *Mesanice polisaharidno/sinteticnih gostil v reaktivnem tisku, 43*(1-2), 13-20.

Wagner, R., Simas, F. F., Pereira, G. C. Z., Angeli, A., Brito, J. O., Woranovicz-Barreira, S. M., . . . Gorin, P. A. J. (2007). Structure of a glycoglucuronomannan from the gum exudate of Vochysia tucanorum (family Vochysiaceae). *Carbohydrate Polymers, 69*(3), 512-521. doi: 10.1016/j.carbpol.2007.01.005

Wagner, R., Simas, F. F., Sassaki, G. L., Iacomini, M., da Silva, M. A., & Gorin, P. A. J. (2008). A high-viscosity glycoglucuronomannan from the gum exudate of Vochysia thyrsoidea: Comparison with those of other Vochysia spp. *Carbohydrate Polymers, 72*(3), 382-389. doi: 10.1016/j.carbpol.2007.09.005

Wagner, R., Woranovicz-Barreira, S. M., Iacomini, M., Delgobo, C. L., Pimentel, N. M., & Gorin, P. A. J. (2004). Structure of a glycoglucuronomannan from the low-viscosity gum of Vochysia lehmannii. *Carbohydrate Polymers, 57*(3), 269-275. doi: 10.1016/j.carbpol.2004.05.004

Walter, R. (1997). Isolation, purification and characterization. In S. Taylor (Ed.), *Polysaccharide dispersions - chemistry and technology in food*: Academic Press.

Walter, R. (1998). Origin of Polysaccharide Supramolecular Assemblies. In R. Walter (Ed.), *Polysaccharide Association Structures in Food*: CRC Press.

Wang, G.-J., Tomasi, D., Backus, W., Wang, R., Telang, F., Geliebter, A., . . . Volkow, N. D. (2008). Gastric distention activates satiety circuitry in the human brain. *NeuroImage, 39*(4), 1824-1831. doi: 10.1016/j.neuroimage.2007.11.008

Wang, S. Q. (1992). Transient network theory for shear-thickening fluids and physically cross-linked systems. *Macromolecules, 25*(25), 7003-7010.

Watanabe, T., Misawa, S., Hiradate, S., & Osaki, M. (2008). Root mucilage enhances aluminum accumulation in Melastoma malabathricum, an aluminum accumulator. *Plant Signaling and Behavior, 3*(8), 603-605.

Waynforth, H. B., & Flecknell, P. A. (1992). *Experimental and surgical technique in the rat* (2nd ed.). London: Academic Press.

Western, T. L. (2012). The sticky tale of seed coat mucilages: Production, genetics, and role in seed germination and dispersal. *Seed Science Research, 22*(1), 1-25.

Whistler, R. L. (1973). Solubility of polysaccharides and their behavior in solution. *Advances in Chemistry Series*(117), 242-255.

Whitten, K. W., Davis, R. E., Stanley, G. G., & Peck, L. M. (2006). *Chemistry* (8th ed.). Belmont, CA, USA: Thomson Brooks/Cole.

Williams, P. A., & Phillips, G. O. (2009). Introduction to food hydrocolloids. In G. O. Phillips & P. A. Williams (Eds.), *Handbook of hydrocolloids* (2nd ed.). Cambridge, UK: Woodhead Publishing Limited.

Witten Jr, T. A., & Cohen, M. H. (1985). Cross-linking in shear-thickening ionomers. *Macromolecules, 18*(10), 1915-1918.

Wyatt, N. B., Gunther, C. M., & Liberatore, M. W. (2011). Increasing viscosity in entangled polyelectrolyte solutions by the addition of salt. *Polymer, 52*(11), 2437-2444. doi: 10.1016/j.polymer.2011.03.053

Wyatt, N. B., & Liberatore, M. W. (2010). The effect of counterion size and valency on the increase in viscosity in polyelectrolyte solutions. *Soft Matter, 6*(14), 3346-3352.

Xu, D., & Craig, S. L. (2011). Strain Hardening and Strain Softening of Reversibly Cross-Linked Supramolecular Polymer Networks. *Macromolecules, 44*(18), 7478-7488. doi: 10.1021/ma201386t

Xu, X., Liu, W., & Zhang, L. (2006). Rheological behavior of Aeromonas gum in aqueous solutions. *Food Hydrocolloids, 20*(5), 723-729. doi: 10.1016/j.foodhyd.2005.06.012

Yalpani, M., Hall, L. D., Tung, M. A., & Brooks, D. E. (1983). Unusual rheology of a branched, water-soluble chitosan derivative. *Nature, 302*(5911), 812-814.

Zaccheus, M. (2012). *Structural and Conformational Studies of Oligo- and Polysaccharides.* Stockholm University, Stockholm, Sweden.

Zhu, Y., Hsu, W. H., & Hollis, J. H. (2013). The Impact of Food Viscosity on Eating Rate, Subjective Appetite, Glycemic Response and Gastric Emptying Rate. *PLoS One, 8*(6).

Zimmermann, U., Zhu, J. J., Meinzer, F. C., Goldstein, G., Schneider, H., Zimmermann, G., . . . Haase, A. (1994). High molecular weight organic compounds in the xylem sap of mangroves - implications for long-distance water transport. *Botanica Acta, 107*(4), 218-229.

Appendix

Appendix A Supplementary Information for Chapter 4

Shear-Dependent Viscosity

The viscosity curve of shear-thickening mamaku gum solutions were fitted using the empirical Cross' equation for shear-thickening fluids (Equation A1). The predicted viscosity values were very close to the actual viscosity curve (Figure A1). The model was fitted with input parameters γ_{crit}, η_{crit}, $\dot{\gamma}_{max}$ and η_{max} to obtain output parameters of time ($\lambda_{I\text{-}III}$) and viscosity ($\eta_{0,I\text{-}III}$) constants (Table A1). These constants would allow us to compare the shear-thickening characteristics of the mamaku gum to other shear-thickening polymers in a quantitative manner.

$$\eta(\dot{\gamma})=\begin{cases}\eta_I\ (\dot{\gamma})=\eta_c+\dfrac{\eta_0-\eta_c}{1+\left[\lambda_I\left(\dfrac{\dot{\gamma}^2}{\dot{\gamma}_c\text{-}\dot{\gamma}}\right)\right]^{\eta_I}} & \text{for } \dot{\gamma}\le\dot{\gamma}_c \\ \eta_{II}\ (\dot{\gamma})=\eta_{max}+\dfrac{\eta_c-\eta_{max}}{1+\left[\lambda_{II}\left(\dfrac{\dot{\gamma}\text{-}\dot{\gamma}_c}{\dot{\gamma}_{max}\text{-}\dot{\gamma}}\right)\right]^{\eta_{II}}} & \text{for } \dot{\gamma}_c<\dot{\gamma}\le\dot{\gamma}_{max} \\ \eta_{III}(\dot{\gamma})=\dfrac{\eta_{max}}{1+[\lambda_{III}(\dot{\gamma}\text{-}\dot{\gamma}_{max})]^{\eta_{III}}} & \text{for } \dot{\gamma}_{max}<\dot{\gamma}\end{cases}$$

Equation A1

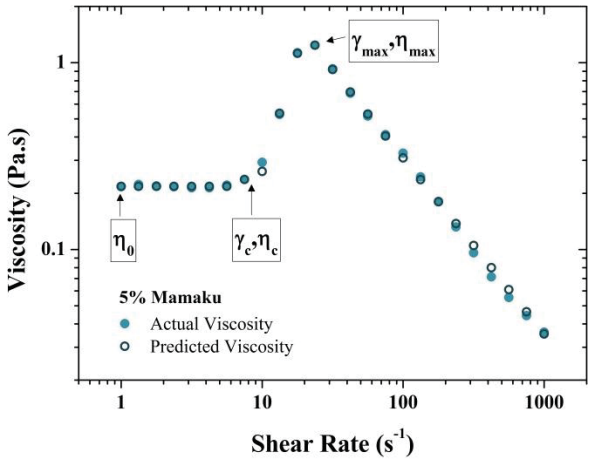

Figure A1 – Actual and predicted viscosity curves of 5% w/w mamaku using the Cross' equation for shear-thickening fluids

Table A1 – Fitting parameters used in Cross' equation for shear-thickening fluids on 5% w/w mamaku

Critical shear rate	γ_{crit}	7.5
Critical viscosity	η_{crit}	0.237
Zero shear viscosity	η_0	0.199
Shear rate at max. viscosity	γ_{max}	23.7
Maximum viscosity	η_{max}	1.24
Time constant I	λ_I	0.520
Time constant II	λ_{II}	0.088
Time constant III	λ_{III}	0.042
Viscosity constant I	η_I	0.000
Viscosity constant II	η_{II}	2.010
Viscosity constant III	η_{III}	0.952

The evolution of viscosity vs. shear stress shows that the critical stress at network rupture increases with concentration (Figure A2). For 2.5% w/w mamaku, the critical stress is approximately 8 Pa and the critical stress at twice the concentration (5% w/w) is almost ten times larger (~80 Pa). The total number of associative groups increases with concentration, therefore strengthening the network which requires larger stresses for disruption.

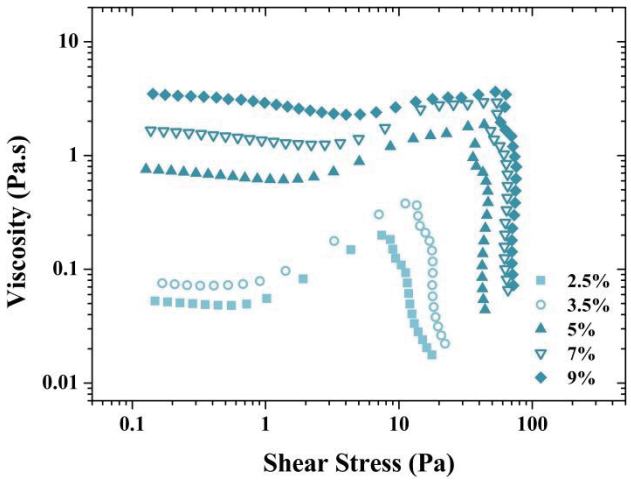

Figure A2 – Viscosity vs. shear stress for 2.5, 3.5, 5, 7 and 9% w/w mamaku

Large Amplitude Oscillatory Shear

Large amplitude oscillatory shear of 1% w/w guar gum (Figure A3) and 1% w/w xanthan gum (Figure A4) shows strain-softening and weak strain overshoot behaviours respectively. Their amplitude sweep shows distinctively different viscoelastic properties from the mamaku gum even at similar elasticity (G') values (~10 Pa). Their elastic Lissajous plots showed intracycle strain-softening with ellipsoidal (guar, Figure A5) or rectangular with rounded corners shapes (xanthan, Figure A6) which are typical of pseudoplastic polysaccharides.

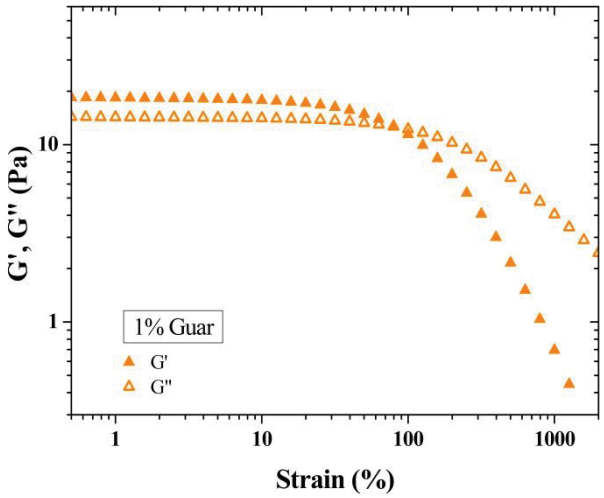

Figure A3 – Amplitude sweep of 1% w/w guar gum at ω=10 rad/s, 20°C

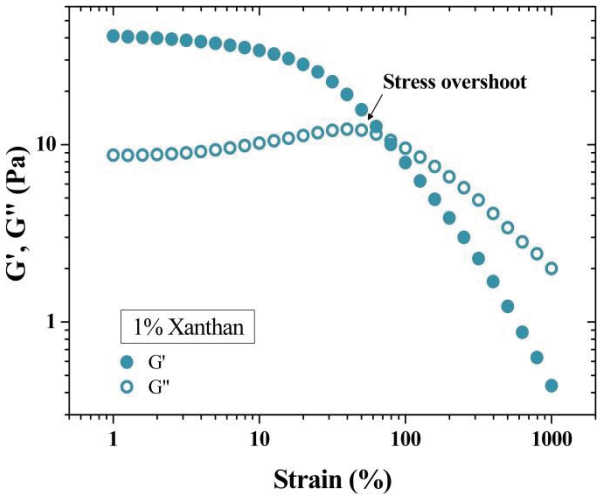

Figure A4 - Amplitude sweep of 1% w/w xanthan gum at ω=10 rad/s, 20°C

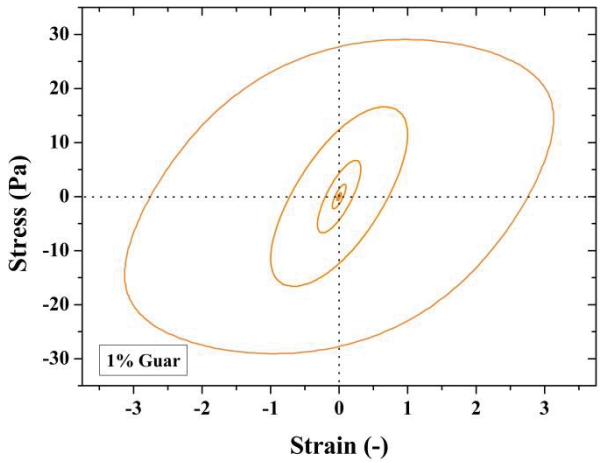

Figure A5 – Elastic Lissajous plots of 1% w/w guar gum

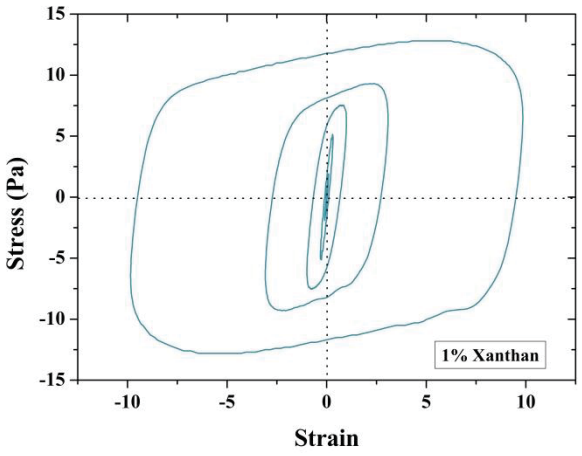

Figure A6 – Elastic Lissajous plots of 1% w/w guar gum

Appendix B Supplementary Information for Chapter 5

Effect of Temperature

Using 30 minutes as fixed heat treatment duration, the polysaccharide was able to retain its shear-thickening behaviour up to temperatures of 80°C. Above 80°C, the decrease in viscosity and extent of shear-thickening became more evident as the associations in the material become permanently lost (Figure B1). Prolonging the heat treatment duration from 30 to 60 minutes at 80°C also caused a reduction in viscosity and a loss of shear-thickening. In other words, the mamaku polysaccharide would be able to withstand heat processes such as pasteurisation (72°C for 15 seconds) without causing permanent loss of shear-thickening.

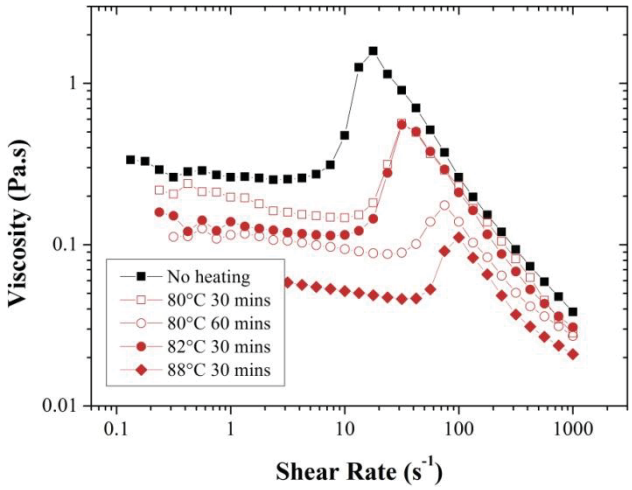

Figure B1 – Viscosity curves for 5% w/w mamaku heat treated at various times and temperature at 20°C

The critical stress at network rupture with increasing temperature appears to be fairly constant ~20-30 Pa (Figure B2). Therefore the total number of associations contributing to the overall network strength does not change with temperature. Increasing temperature shortens the lifetime of the associations by promoting thermal mobility.

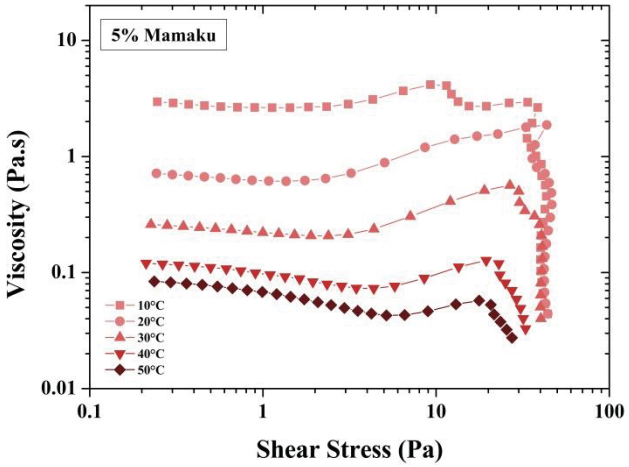

Figure B2 - Viscosity vs. shear stress for 5% w/w mamaku at 10-50°C

Effect of Urea

Similarly for urea, the critical stress at network rupture with increasing temperature appears to be fairly constant ~20-30 Pa for the same mamaku concentration (Figure B3). Likewise, the total number of associations contributing to the overall network strength does not change with addition of urea. Increasing urea concentration shortens the lifetime of the associations due to competition for binding by urea molecules.

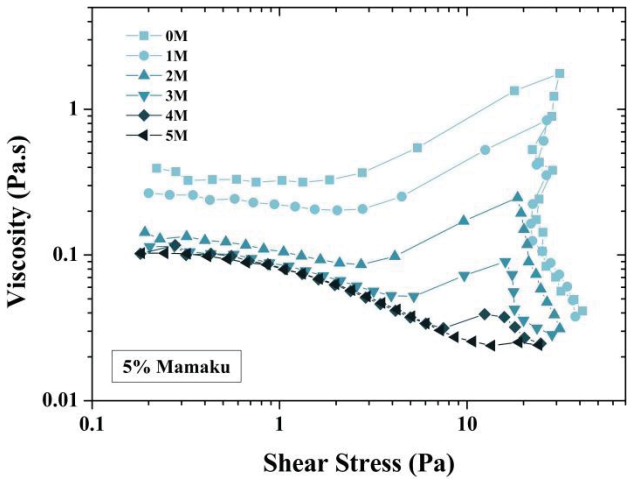

Figure B3 - Viscosity vs. shear stress for 5% w/w mamaku with 0-5M urea

LAOS was also used to characterise the effect of urea on the nonlinear rheological properties of the mamaku polysaccharide. Amplitude sweeps of 5% w/w mamaku with increasing urea concentration show a loss of elasticity as characterised by the decrease in G' from 1-10,000% γ_0 (Figure B4a). However, for G", the trend was dependent on the strain value (Figure B4b). In the linear to strain-softening regions ($\leq\gamma_{crit}$), there was an increase in energy dissipated (G") with urea. In the nonlinear or strain-hardening region, G" decreased with more urea. This suggests that the addition of urea promotes flow in the linear and strain-softening region by disrupting intra- and intermolecular associations resulting in disentanglement. Exceeding the critical strain, intermolecular associations with longer lifetimes at lower urea concentrations formed, which require more energy to disrupt. Hence a shift in G" trend in the nonlinear region was observed.

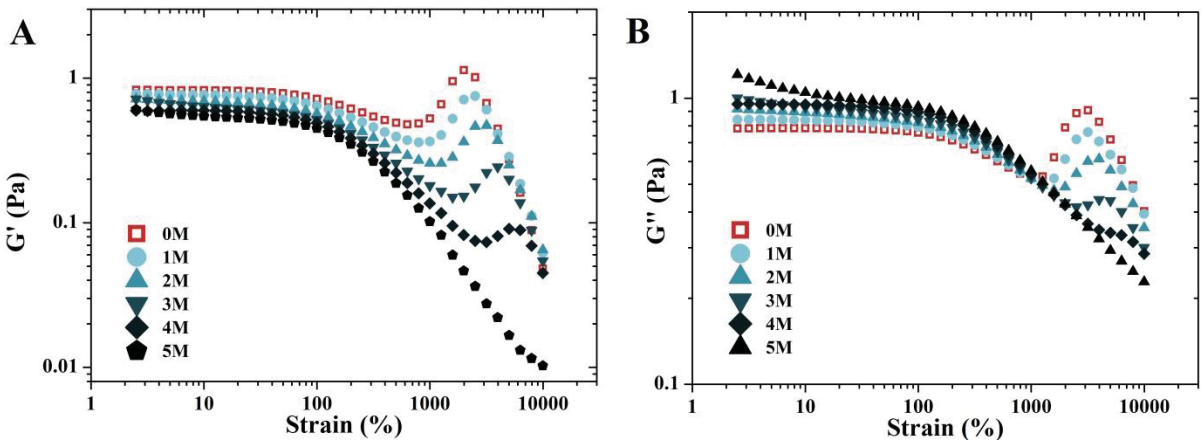

Figure B4 – Amplitude sweep *i.e.* a) G' and b) G" with strain of 5% w/w mamaku, ω=10rad/s, 20°C

The extensional relaxation times (λ_E) of 2.5, 5 and 7% w/w mamaku at various urea concentrations were calculated from their diameter-time profiles and normalised by the relaxation time at 0M urea (λ_{E0}) (Figure B5). A master curve of normalised relaxation times with urea concentration was obtained which was independent of mamaku concentration.

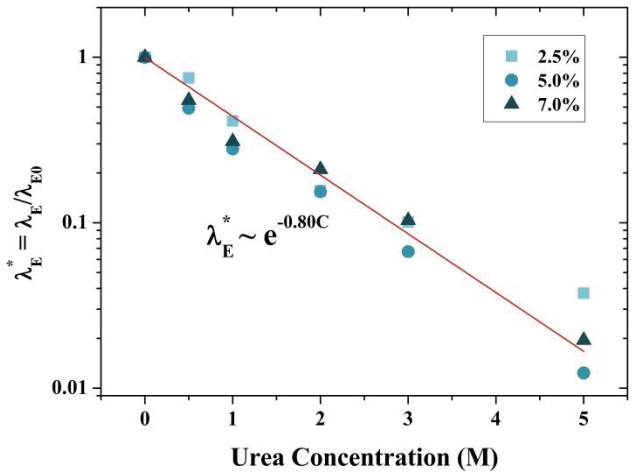

Figure B5 – Normalised extensional relaxation times with increasing urea concentration in 2.5, 5 and 7% w/w mamaku solutions

Effect of Ionic Strength

The activation energies at η_{crit} and η_{max} were obtained at different ionic strengths using either NaCl or $CaCl_2$ salts in 5% w/w dialysed mamaku (Figure B6). As mentioned in the main discussion, the interactions were not cation-specific and more dependent on final ionic strength. With increasing ionic strength, the activation energy decreases for both η_{crit} and η_{max}, and activation energy for $\eta_{max} > \eta_{crit}$. These are consistent with the trends observed for the native mamaku. At higher ionic strengths, more charges are screened and the polysaccharide adopts a more compact configuration. The polysaccharide then occupies less hydrodynamic space in solution, forming denser entanglement and association network during shear-thickening. Therefore it is postulated at higher ionic strengths, the chains would be more resistant to thermal mobility with increasing temperature, and thus activation energies are smaller.

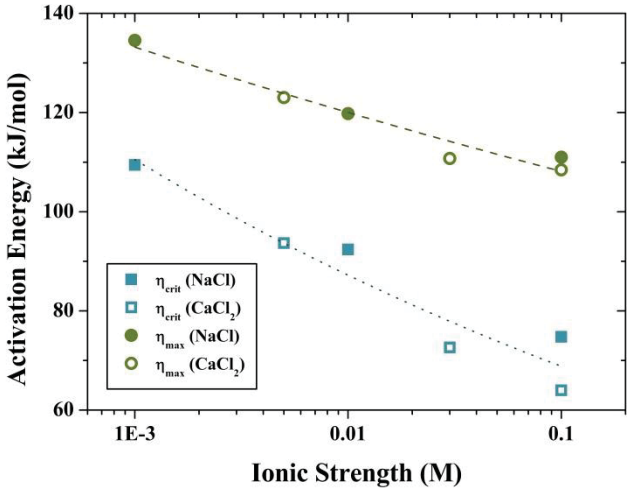

Figure B6 – Activation energies of dialysed 5% w/w mamaku at η_{crit} and η_{max} with various ionic strengths (based on concentrations of NaCl and $CaCl_2$)

Appendix C ^{1}H and ^{13}C NMR Chemical Shift Assignments

Table C1 – ^{1}H NMR chemical shift assignments of glucuronomannans from literature

Chemical Shift (ppm)	Assignment	Reference
4.65	β-glucuronic acid	(Redgwell, et al., 1986b)
4.71	H1 GlcA	(Nahar, Hazra, Mosihuzzaman, Mahbubur Rahman, & Andersson, 1994)
3.5	H2 GlcA	
3.52	H3 GlcA	
3.61	H4 GlcA	
3.8	H5 GlcA	
5.44	H1 -->2)-α-D-Manp-(1-->	(Wagner, et al., 2007)
4.18	H2 -->2)- α-D-Manp-(1-->	
3.89	H3 -->2)- α-D-Manp-(1-->	
3.73	H4 -->2)- α-D-Manp-(1-->	
3.89	H5 -->2)- α-D-Manp-(1-->	
3.84	H6 -->2)- α-D-Manp-(1-->	
4.53	H1 -->4)- β-D-GlcA-(1-->	
3.44	H2 -->4)- β-D-GlcA-(1-->	
3.73	H3 -->4)- β-D-GlcA-(1-->	
3.84	H4 -->4)- β-D-GlcA-(1-->	
3.57	H5 -->4)- β-D-GlcA-(1-->	
-	H6 -->4)- β-D-GlcA-(1-->	
4.49	β-D-Gal	(Honda, et al., 1996)
4.57	β-D-GlcA	
5.35	α-D-Man	
5.45	α-L-Ara	

Table C2 – ^{13}C NMR chemical shift assignments of glucuronomannans from literature

Chemical Shift (ppm)	Assignment	Reference
174.9	C6 α-D-glcA(1-->	(Lin, Daniel, & Whistler, 1994)
98.7	C1 α-D-glcA(1-->	
82.3	C4 4-O-methylglcA	
73.5	C3 α-D-glcA	
71.8	C2 α-D-glcA(1-->	
70.5	C5 α-D-glcA(1-->	
60.8	MeO-4-glcA	
104.44/103.68	C1 β-D-GlcA(1-->	(Marvelys, Maritza, Lilian, Depintogladys, & Julio, 2006)
75.85/75.40	C2 β-D-GlcA(1-->	
76.26/76.02	C3 β-D-GlcA(1-->	
73.54	C4 β-D-GlcA(1-->	
76.69/76.86	C5 β-D-GlcA(1-->	
475.72/176.11	C6 β-D-GlcA(1-->	
99.66/99.74	C1 4-O-Me-α-D-GlcA(1-->	
72.26/72.61	C2 4-O-Me-α-D-GlcA(1-->	
73.54	C3 4-O-Me-α-D-GlcA(1-->	
82.32/82.75	C4 4-O-Me-α-D-GlcA(1-->	
70.07/70.65	C5 4-O-Me-α-D-GlcA(1-->	
59.84/59.66	C6 4-O-Me-α-D-GlcA(1-->	
98.4	C1 -->2)- α-D-Manp-(1-->	(Wagner, et al., 2007)
77.8	C2 -->2)- α-D-Manp-(1-->	
69.7	C3 -->2)- α-D-Manp-(1-->	
67	C4 -->2)- α-D-Manp-(1-->	
72.9	C5 -->2)- α-D-Manp-(1-->	
60.6	C6 -->2)- α-D-Manp-(1-->	
101.6	C1 -->4)- β-D-GlcA-(1-->	
72.9	C2 -->4)- β-D-GlcA-(1-->	
76.6	C3 -->4)- β-D-GlcA-(1-->	
77.1	C4 -->4)- β-D-GlcA-(1-->	
77	C5 -->4)- β-D-GlcA-(1-->	
174.8	C6 -->4)- β-D-GlcA-(1-->	
173.5	C6-Glucuronomannan	(Sims & Bacic, 1995)
103.3	C1-GlcpA	
100.4	C1-Manp	
174.8	GlcA	(Honda, et al., 1996)
170.9	Esterified GlcA	
108.8	α-arabinofuranosyl	
103.9	β-D-galactosyl	
102.5	β-D-glucuronosyl acid	
98.9	α-D-mannosyl	
54.4	Partially methoxylated GlcA	

Appendix D Animal Ethics Applications

Animal Ethics Application No. 14/21

AEC/17 (Amended 01/14)

Massey University
Animal Ethics Committee

To: The Secretary
Animal Ethics Committee
Research Ethics Office
Room 1.25
Courtyard Complex
Manawatu Campus PN221

Please provide one original single-sided application plus 14 copies
Application due Wednesday of week prior to meeting

APPLICATION FOR APPROVAL OF PROPOSED RESEARCH, TESTING OR TEACHING PROCEDURES USING LIVE ANIMALS

1. CHIEF APPLICANT: *(Staff Member only)*

(a) **Name** Lara Matia-Merino
Qualifications MSc (FoodSci), PhD (Food Colloids)
Position Senior Lecturer in Food Technology
Inst/Sch/Dept IFNHH

2. OTHER APPLICANTS: *(refer Code of Ethical Conduct, Item 3.2, for those who should be listed)*

(a) **Name** May Wee Sui Mei
Qualifications Bachelor in Food Technology (Hons)
Position PhD Student (Food Technology)

(b) **Name** Professor Roger Lentle
Qualifications PhD MB BS LRCP MRCS
Position Professor of Digestive Biomechanics

(c) **Name** Kim Wylie
Qualifications Diploma in Veterinary Nursing
Position Technical Officer

(d) **Name** Corrin Hulls
Qualifications BSc
Position Technical Officer

(e) **Name** Anne Broomfield
Qualifications NZVACAT, NZCS
Position Technical Officer

(f) **Name**
Qualifications
Position

3. DETAILS OF PROJECT:

(a)	**Title** *(maximum 20 words)*	Pilot study of satiety effects of Mamaku gum extract **(re-submission)**	
(b)	**Type of project**	**Research**	☑
		Testing	☐
		Teaching	☐
		Paper Number(s):	
(c)	**Commercial sensitivity status**	**No**	☑
		Yes	☐
(d)	**Does the project involve use of native species?**	**No**	☑
		Yes	☐
	If yes:		
	Has DoC approval been:	**Sought but not yet granted**	☐
		Granted	☐
		Permit Number(s):	
	Māori consultation: *(must be by applicant(s) directly with iwi)*	**Has been undertaken**	☐
		Is currently being undertaken	☐
	(For guidance, click here)	**The project is approved by iwi*:** Yes ☐ No ☐ *(*Please refer to guidance opposite)*	

4. JUSTIFICATION OF PROJECT:

(a) **What are the expected benefits of the proposed work and how will the new knowledge be communicated to others?** *(Benefits may include improved basic knowledge, improved animal health, teaching)*

This project is a joint undertaking between the Physiology and Food Technology departments of IFNHH. It was originally conceived two years ago but there have been a series of delays occasioned by ethical problems. Hence the MUAEC originally queried whether a rat of the size proposed could be gavaged with 4ml volume. A series of trials established that this would not cause any distress to the animal. Subsequently there was discussion as to which type of gavaging device should be used, Hence whilst a veterinarian stated that a plastic flexible device was likely to be less distressing for the animal our staff who have a cumulative experience of over 20years feel that a plastic device was more difficult to use. A steel gavage needle will be used for the following reasons. The plastic gavage device is flexible but has a small cross sectional area of edge. Hence the operator cannot feel the force that is being applied and the risk of inadvertent perforation is high. The metal gavage needle is rigid but blunt ended with a large rounded cross sectional area of

edge. Hence the operator can feel the force that is being applied and the risk of inadvertent perforation is low.

Mamaku gum is a traditional food used by Maori as an anorexiant (Brooker, Cambie, & Cooper, 1987; Crowe, 2004) and has been shown to exhibit unusual flow properties i.e. shear thickening at shear rates that are found in the mammalian stomach (Goh, et al., 2007). Further, the digesta group in IFNHH have recently found that administration of mamaku gum directly into the cavity of a living rat stomach maintained in vitro alters the pattern of intrinsic mobility (Lentle, et al., 2010). This alteration causes the direction of antrocorporal peristaltic contractions to reverse bringing about gastric distension and satiety.

The proposed experiment is a pilot study that seeks to determine whether mamaku gum can reduce food intake and induce weight loss in adult (6 weeks old; approximately 200g body weight) male Sprague Dawley rats which would indicate that it would be worthwhile to proceed to a series of larger trials designed to research its use as a possible non pharmacological i.e. fluid mechanical gastric anorexiant. Such an agent would have application in the treatment of human obesity. It also seeks to pilot whether there is any accompanying toxicity.

A previous trial with three male Sprague Dawley rats (protocol no. 12/102) was successfully conducted in February 2013. The rats did not show adverse reactions to the gavaged gum and had showed gastric retention of the gum in the stomach two hours post-gavage.

This work will be part of PhD student May Wee's thesis.

(b) **Why is it necessary to use animals for this activity?** *(The term "animal" is defined in the Code of Ethical Conduct, Item 10)*

Mamaku gum is a traditional food used by Maori as an anorexiant (Brooker, et al., 1987; Crowe, 2004) and has been shown to exhibit unusual flow properties i.e. shear thickening at shear rates that are found in the mammalian stomach (Goh, et al., 2007). Further, the digesta group in IFNHH have recently found that administration of mamaku gum directly into the cavity of a living rat stomach maintained in vitro alters the pattern of intrinsic mobility (Lentle, et al., 2010). Whilst mamaku gum is still being consumed as a traditional food, no data are available regarding any untoward effects thus it currently does not meet requirements to be categorised as a GRAS food ingredient. (Generally Recognised As Safe). The initial toxicological studies (liver function tests kidney and liver histology plus behavioural assessment) will allow us to determine whether any gross toxicity exists and will enable more formal trials to be appropriately designed. Further formal toxicological trials will be required before the food can be certified as safe in this regard. Until these are done we cannot conduct a human trial.

5. **DESCRIPTION OF PROCEDURES AND MANIPULATIONS:** *("Manipulation" is defined in the*

Code of Ethical Conduct, Item 10)

(a) **Give a brief description of your trial design/teaching demonstration.** *(One or two paragraphs) (For complex protocols, it may be beneficial to provide information as a timeline or in tabulated form)*

Twenty-eight 120±20% gram adult male Sprague Dawley rats will be acclimated in shoebox cages with false-bottom wires at SAPU for 2 weeks prior to the commencement of the study. Two of these rats are used as overall experimental controls and will not be subjected to gavaging. The remaining twenty-six rats will be inspected and weighed daily gavaged with 4ml of treatment solution on alternate week days to a total of 5 gavages (a number previously negotiated with MUAEC) and euthanased 2 hours after the final gavage.. The rats will be fasted 14 hours prior to gavaging and they will receive mamaku gum (4ml or 50% of their stomach volume). The rats will be fed ad libitum however, 14 hours prior to gavaging, the chow will be removed from the cages to stop further food consumption. A weighed quantity of chow (~200 grams) is being given each morning. The residual chow and any ullages (orts) will be collected and weighed each evening after gavaging the rats.

After euthanasia under anaesthesia with ACP-ketamine-xylazine mix each rat will be weighed, abdomen will be opened and the stomach removed and weighed. The stomach will then be opened, the contents removed and the wall of the stomach weighed again. During the course of the experiment any rat discovered to be unwell or to have significantly reduced mobility or to refuse chow will be euthanased. Should more than 1 rat of each treatment group become unwell during the trial it will be terminated and all animals euthanased.

(b) **Describe the statistical methods that you will use to analyse these data.**

Twenty-eight rats will be used. This is a pilot study. No data are available for power analyses.

(c) **Provide justification for the group sizes that you propose.**

Ten rats for each treatment group with three additional rats in the event of loss of rats. Two additional rats will be used as an overall control without gavage treatment.

(d) **Describe the manipulations to be performed on the animals.**

Gavage of 4ml of mamaku solution with a steel gavage needle. This will be only carried out by an experienced operator Kim Wylie.

Note it is not possible to use techniques of pharyngeal delivery where the animal is obliged to sip. This is on account of the rheological properties of the mamaku gum that cause it to exhibit high cohesion behaviour e.g. rod climbing. Hence the first part of any dose in the pharynx will draw the subsequent part of the dose behind it causing it to linger in the pharynx. The large dose in the pharynx the greater difficulty in swallowing (shear thickening behaviour). Hence it is likely the animals would asphyxiate.

(e) **How will the proposed manipulation affect the well-being of the animals?**

The animals will be mildly distressed for a short time at approximately the level experienced during endoscopy of conscious human subjects.

(f) **Describe any restraint applied to the animals.**

Manual restraint by the animals body being firmly wrapped in a towel or scruffed

6. CARE OF ANIMALS:

(a) **What access will the animals have to water?**

Available ad libitum throughout experiment.

(b) **Describe the feeding regimen for the animals.**

The rats will be gavaged with control or treatment solutions (4ml) on alternate week days (5 gavages total). Standard rat chow will be accessible ad libitum for 9.5 hours (from 8.30 a.m. to 7 p.m.) during the dark period of the light/dark cycle.

(c) **From where will the animals be sourced?** *(Refer Code of Ethical Conduct, Item 2.15) (Where animals are personally owned, consent forms must be obtained)*

Small Animal Production Unit (SAPU)

(d) **Where will the animals be kept throughout the study period?**

Massey University's small animal production unit

(e) **Who is responsible for the routine care and health surveillance of the animals?**

Kim Wylie and May Wee (routine care)

(f) **If the Chief Applicant is unavailable, who will make decisions if emergency care is required?**

Kim Wylie

7. FATE OF ANIMALS:

Note: If any animal is either euthanased or dies due to the unexpected side effects of approved manipulations, the animal should be subjected to a post-mortem examination by an experienced person. The results of the post-mortem must be communicated to the Massey University Animal Ethics Committee along with any modifications put in place to minimise the occurrence of similar events to other animals.

(a) **What will happen to the animals at the completion of the study?**

They will be euthanased.

(b) **Will any animals be euthanased, either as part of the** **No** ☐

study, or in the event of untoward outcomes? **Yes** ☑

If yes:

Applicants must be familiar with the resource material on supporting staff involved with animal euthanasia at the following link:
http://www.massey.ac.nz/massey/staffroom/national-shared-services/health-safety/for-managers/responding-to-stress-complaint.cfm

The Chief Applicant must also confirm that he/she understands his/her obligations in regard to discussing the availability of this material with all people listed on the application on a per-project basis. ☑ *Tick Box*

Describe the euthanasia method you will use.

Euthanasia following anaesthesia with intraperitoneal ACP-ketamine-xylazine mix. Under the surgical (or deeper) plane of anaesthesia induced by the anaesthetic combination, and the thorax will be opened (to stop lungs from inflating). These procedures will be carried out by Anne Broomfield who is experienced in this respect.

(c) What level of losses do you expect to occur during this work and how will you investigate any unexpected deaths? *(refer Code of Ethical Conduct, Items 2.20-2.22)*

No losses are expected as a result of treatment solution except due to perforation of oesophagus during gavage. The rats will be dissected and perforations on the oesophagus and stomach lining will be examined.

8. ALLEVIATION OF IMPACT OF MANIPULATIONS:

(a) What features of the manipulations minimise their impact on the animals?

The short duration of gavaging as performed by a highly skilled technician experience in using steel feeding needles, performing gavage only five times for each animal, and performing euthanasia under sedation.

(b) If blood samples are to be collected, stipulate volume per sample and frequency of sampling.

Blood will be collected by cardiac puncture after the rat is anaesthetised.

(c) Stipulate the use (and dose rate and route of administration) of any anaesthesia, analgesia, sedative, tranquilliser or other pharmacological agent applied to reduce the impact of manipulations on the animals.

ACP 2mg/ml (2 parts) will be mixed with ketamine 100 mg/ml (5 parts), xylazine 100mg/ml (1 part) and sterile water (2 parts). This mix will be administered intraperitoneally at a dose rate of 0.12ml/100g of rat.

(d) **What frequency of monitoring is to be maintained?**

Daily

(e) **What advice regarding identification of any expected adverse effects will be given to staff responsible for the ongoing care of the animals?**

The health status of the rats will be assessed using a rat health score checksheet. Fur smoothness, eye redness, posture, spontaneous activity/inquisitiveness, respiration frequency and characteristics faecal characteristics will be monitored and scored daily. Any deviation in the behaviour of a rat from normal will be reported to Kim Wylie, who will make a judgement as to whether the animal will be euthanased or examined by a veterinarian. The experiment will be terminated should one rat from a gavaged treatment group have an overall score of $\geq$12 points on the health checksheet on a particular day.

9. EXPERIENCE OF APPLICANTS:

(a) **What is the experience of the applicants with the techniques being used in this project?**

Kim Wylie and Anne Broomfield have extensive experience with the gavaging, anaesthesia and euthanasia of rats having conducted numerous such manipulations on rats.

(b) **If an applicant is using a technique with which he/she has no previous experience, what training will be provided?**

May will be trained in feed renewal and weighing procedures and in the identification of any signs of distress by Kim

(c) **List the people providing professional services and the services provided.** *(refer Code of Ethical Conduct, Item 3.2) (These personnel need not be applicants)*

Dr Juliet Cayzer

Appendix E Flowchart of Various Mamaku Fractions and Usages

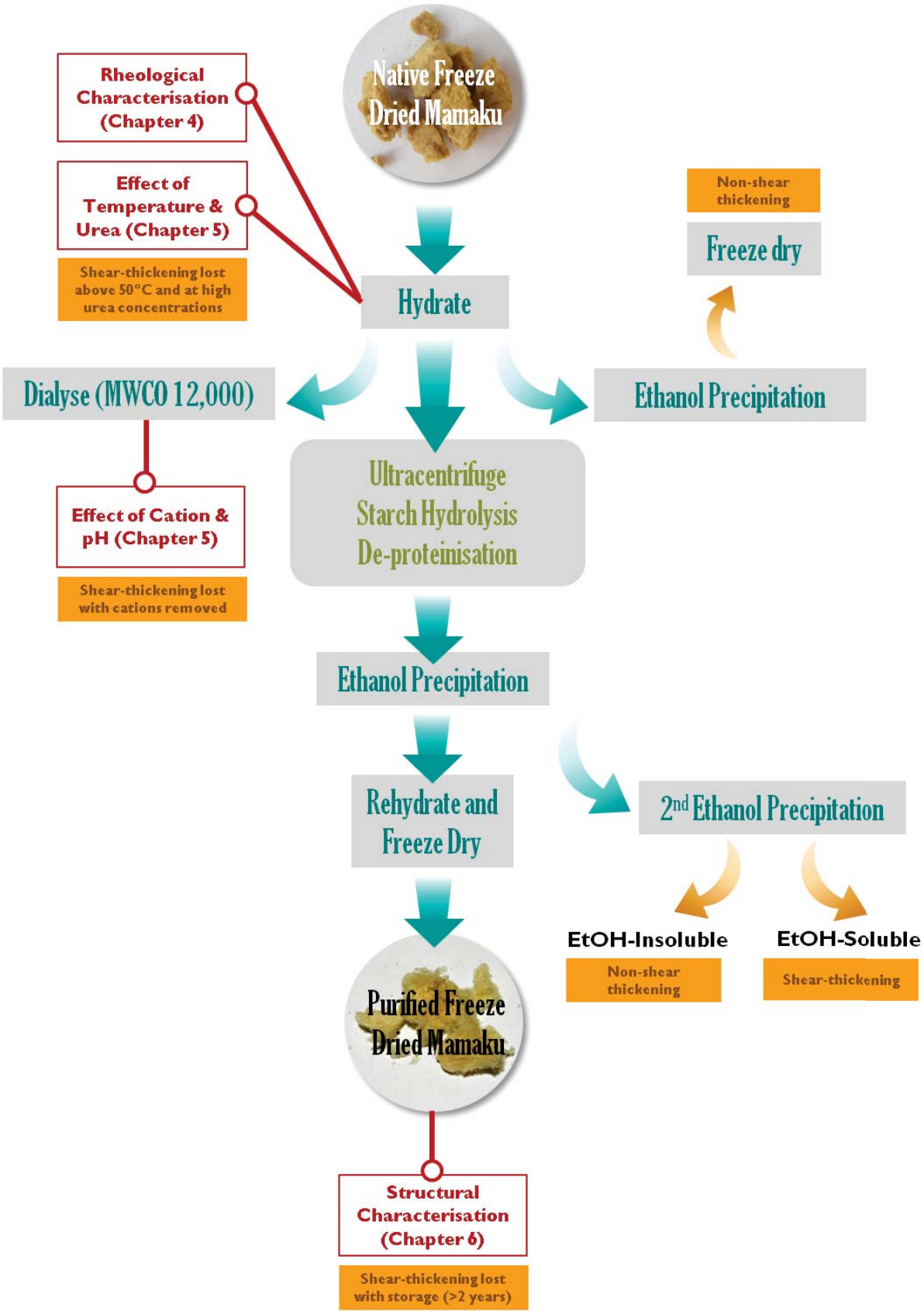

DRC 16

MASSEY UNIVERSITY
GRADUATE RESEARCH SCHOOL

STATEMENT OF CONTRIBUTION
TO DOCTORAL THESIS CONTAINING PUBLICATIONS

(To appear at the end of each thesis chapter/section/appendix submitted as an article/paper or collected as an appendix at the end of the thesis)

We, the candidate and the candidate's Principal Supervisor, certify that all co-authors have consented to their work being included in the thesis and they have accepted the candidate's contribution as indicated below in the *Statement of Originality*.

Name of Candidate: May Wee Sui Mei

Name/Title of Principal Supervisor: Dr. Lara Matia-Merino

Name of Published Research Output and full reference:

Wee, May Sui Mei, Matia-Merino, Lara, Carnachan, Susan. M. , Sims, I. M., & Goh, K.T.T. (2014). Structure of a Shear-thickening Polysaccharide Extracted from New Zealand Black Tree Fern, Cyathea medullaris. International journal of biological macromolecules, 70(0), 86-91.

In which Chapter is the Published Work: Chapter 6

Please indicate either:

- The percentage of the Published Work that was contributed by the candidate: 75%

  and / or

- Describe the contribution that the candidate has made to the Published Work:

  The candidate has carried out experimental work by herself under the guidance of experienced researchers from Callaghan Innovation. The interpretation of experimental results were done together with these researchers.

May Wee — Candidate's Signature — 16 Nov 2014 — Date

Lara Matia-Merino — Principal Supervisor's signature — 17 Nov 2014 — Date

GRS Version 3– 16 September 2011

DRC 16

MASSEY UNIVERSITY
GRADUATE RESEARCH SCHOOL

STATEMENT OF CONTRIBUTION TO DOCTORAL THESIS CONTAINING PUBLICATIONS

(To appear at the end of each thesis chapter/section/appendix submitted as an article/paper or collected as an appendix at the end of the thesis)

We, the candidate and the candidate's Principal Supervisor, certify that all co-authors have consented to their work being included in the thesis and they have accepted the candidate's contribution as indicated below in the *Statement of Originality*.

Name of Candidate: May Wee Sui Mei

Name/Title of Principal Supervisor: Dr. Lara Matia-Merino

Name of Published Research Output and full reference:

Wee, M.S.M., Matia-Merino, L., Goh, K.K.T (2015). Time and shear-history dependence of rheological properties of a water soluble extract from the fronds of the black tree fern, Cyathea medullaris. Journal of Rheology, 59, 365.

In which Chapter is the Published Work: Chapter 4

Please indicate either:

- The percentage of the Published Work that was contributed by the candidate: 92%

  and / or

- Describe the contribution that the candidate has made to the Published Work:

  The experimental work and writing were carried out fully by the candidate with input from the supervisors on the draft version.

May Wee — Digitally signed by May Wee DN: cn=May Wee, o=Massey University, ou=IFNHH, email=s.m.wee@massey.ac.nz, c=NZ Date: 2015.03.19 13:14:09 +13'00'

Candidate's Signature

19/03/15

Date

Lara Matia-Merino — Digitally signed by Lara Matia-Merino DN: cn=Lara Matia-Merino, o, ou=IFNHH, email=l.matia-merino@massey.ac.nz, c=NZ Date: 2015.03.19 13:22:22 +13'00'

Principal Supervisor's signature

19/03/15

Date

DRC 16

MASSEY UNIVERSITY
GRADUATE RESEARCH SCHOOL

STATEMENT OF CONTRIBUTION TO DOCTORAL THESIS CONTAINING PUBLICATIONS

(To appear at the end of each thesis chapter/section/appendix submitted as an article/paper or collected as an appendix at the end of the thesis)

We, the candidate and the candidate's Principal Supervisor, certify that all co-authors have consented to their work being included in the thesis and they have accepted the candidate's contribution as indicated below in the *Statement of Originality*.

Name of Candidate: May Wee Sui Mei

Name/Title of Principal Supervisor: Dr. Lara Matia-Merino

Name of Published Research Output and full reference:

Jaishankar, A., Wee, M., Matia-Merino, L., Goh, K., & McKinley, G.H. (2015). Probing hydrogen bond interactions in a shear thickening polysaccharide using nonlinear shear and extensional rheology. Carbohydrate Polymers, 123, 136-145.

In which Chapter is the Published Work: Chapter 4

Please indicate either:

- The percentage of the Published Work that was contributed by the candidate: 35%

  and / or

- Describe the contribution that the candidate has made to the Published Work:

  The candidate has run experiments with the main author and analysed data independently for the chapter. Discussions in the chapter were altered to suit the flow of the thesis better.

May Wee — Digitally signed by May Wee DN: cn=May Wee, o=Massey University, ou=IFNHH, email=s.m.wee@massey.ac.nz, c=NZ Date: 2015.03.19 13:10:13 +13'00'

Candidate's Signature — 19/03/2015 — Date

Lara Matia-Merino — Digitally signed by Lara Matia-Merino DN: cn=Lara Matia-Merino, o, ou=IFNHH, email=l.matia-merino@massey.ac.nz, c=NZ Date: 2015.03.19 13:21:11 +13'00'

Principal Supervisor's signature — 19/03/2015 — Date